Universidad de Alcalá

Programa de Doctorado en Electrónica: Sistemas Electrónicos Avanzados. Sistemas Inteligentes

# Contributions to physical exercises monitoring with inertial measurement units

Ph.D. Thesis Presented by

**Sara García de Villa**

2022

Universidad de Alcalá

Programa de Doctorado en Electrónica: Sistemas Electrónicos Avanzados. Sistemas Inteligentes

# Contributions to physical exercises monitoring with inertial measurement units

Ph.D. Thesis Presented by

**Sara García de Villa**

Advisors

**Dr. Juan Jesús García Domíngez**
**Dr. Ana Jiménez Martín**

Alcalá de Henares, 2022

*"Tanta vida"*

# Agradecimientos

Los primeros a los que quiero y debo dedicar esta tesis es a mi madre, mi padre y mi hermana. Gracias por acompañarme en este viaje, cada uno a vuestra manera, pero sin faltar el desearnos "Buenos días" y "Buenas noches". Hermana, seguro que eres la persona que más se alegra de que termine esta etapa. Los días que te he dado cobijo han sido un respiro. Gracias por siempre entender esta etapa como un "PFC" muy largo y todo lo que conlleva. Mamá, gracias por siempre estar y soportarnos, en todos los sentidos, tanto a mi hermana como a mí. Es todo un privilegio tener una madre que controle tantos temas y nos ayude tanto en todo. Papá, siempre has estado para mis dudas, desde lejos o encuarentenados en unas navidades que iban a durar tres días y duraron más de treinta. Valoro mucho que, aunque empieces respondiendo lo primero que "ya no te acuerdas de la teoría de lo que le estoy preguntando", después acabes peleando con lo que haga falta y explicándomelo.

No me gustaría posponer los agradecimientos a mis tutores, Ana y Juan Jesús. Agradezco mucho que me propusieseis empezar este camino y el apoyo al recorrerlo. No ha sido fácil. He aprendido mucho con vosotros. Al resto de profesores de depeca, gracias a los que me habéis ayudado de forma directa y los que me habéis sugerido cambios o ideas sobre esta tesis, pero, sobre todo, gracias por poner en valor el trabajo de los becarios dedicándoles vuestro tiempo.

En este pequeño parrafito quiero agradecer a todas las personas que se han prestado para que las grabe en las campañas de medida. Literalmente, sin vosotros, esto no habría sido posible. Espero que el rato de actividad física os despejase el día que os grabé.

I also want to thank the DLR for inviting me to work with them and help me with the experiments. I was pretty sure that it was going to be difficult to find people to enroll in my experiments and you surprised me for the better. Special thanks to Dina and Estefania for hosting me so well and teaching me everything that can be taught in three months.

A la familia más cercana. Todas las que me habéis preguntado y animado en esta etapa, aunque tardase en dar señales de estar viva, gracias. Muchas gracias abuela por asegurarme tantas veces que ya tenía que quedar poco. Igual han pasado tres años desde la

primera vez que quedaba poco, pero ya sí que ha sido verdad.

A Lea y Lis no puedo no agradecerles su apoyo en este viaje. Lea, siempre recordaré el día que me trajisteis a Alcalá por primera vez y me animaste a empezar este camino. Bien hecho. Has formado parte de él desde el minuto cero, entendiéndome cada una de las veces de los millones de veces que me he saturado. A Lis, que llegaste cuando aún no sabía todo lo que iba a implicar este viaje. Puede que hayas sido la mayor alegría de esta etapa. Gracias por alegrarme tantos días. Seguramente seas la persona que más me ha hecho desconectar en los momentos más difíciles de la tesis.

A todas las viejas amistades que han compartido un rato conmigo durante estos años. A las chicas, Claudia, Iris y Lau, que, aunque estemos en la etapa más compleja, en diferentes países, opositando, viviendo una pandemia, en una cuarentena eterna, estáis. Sin duda, tengo que agradecer a Iris que compartamos ciudad y, gracias a ello, nunca me falte familia a distancia de un paseo. A Javier, "Puenca", le deberíamos dedicar los logros de nuestra vida muchas personas. No conozco a nadie que cuide sus amistades tanto como tú. Somos unas afortunadas de tenerte.

A las y los que han aparecido en los últimos cuatro años. A los que me habéis aconsejado tanto sobre la tesis estando varios pasos por delante, Miguel, Sara y Elena. Imagino que sabéis lo tranquilizador que es escuchar un "es normal". Gracias, pero sobre todo gracias por los ratos que no han ido de esto, que han ido de Sevilla, o Demandafolk, o Tempranillo. En esto último sin duda también merecen mención Irene y Miguel -el otro Miguel.

A los compañeros de la etapa universitaria que mantengo en mi vida, especialmente María, Jesús y Roque. Los tres formáis mis mejores recuerdos de la primera parte de esta larga etapa. María, menos mal que nos embarcamos juntas en la aventura de ir a Valencia. Puede que uno de los mejores años de mi vida haya sido viviendo allí. Roque, las charlas sobre la tesis han sido un placer, casi tanto como lo fueron todos los ratos que disfrutamos en terrazas, el Jonny o preparando exámenes en el pueblo donde éramos tan eficientes que el estudio era lo que menos tiempo ocupaba. Jesús, agradezco cada rato sacando adelante trabajos y exámenes, explicándonos lo que entendíamos a medias cada uno para llegar a entender el temario completo, atravesando rápidamente CIU y compartiendo el viaje de metro, descubriendo el nuevo -ya viejo- disco de Extremoduro que siempre me recordará a ti y, por supuesto, consiguiendo nuestro ECTS en la Semana del Vino, esa gran suerte de ser de la UPM.

De mis compañeros, Rubén y Fran, compañeros de laboratorio de los inicios, más que agradeceros, os pido perdón por lo que habéis tenido que aguantar. Rubén, menos mal que nos embarcamos en la impresión de "bracitos". Fran V. el tiempo que coincidimos en la UAH fue muy divertido y un poco de aire fresco cuando podía poco más. A los que faltan del O22 y O31, a todos muchas gracias por compartir este camino. Los que estáis al principio o a mitad del recorrido de la tesis, deciros que intentéis disfrutar

lo que se pueda y sobrellevéis lo mejor posible lo que no. Todo llega. Sin duda, la persona que tiene mención especial, ya que tendría un hueco en varios párrafos de estos agradecimientos, es Elena. He tenido una gran suerte de ser tu compañera y vivir esta etapa contigo. Eres una máquina en todo lo que te propones y también eres una de las mejores personas que conozco. Agradezco a la vida que seas mi amiga.

Por último, porque no podría ser el primero, pero también merece una posición destacable como la que tiene en mi vida, muchas gracias a David Casillas. Sin ti no habría llegado al final del camino. Gracias por escuchar tantos "ya no puedo más" y seguir aquí. Esta es la segunda tesis que cerramos siendo el "equipo L". Gracias por todas las dudas resueltas, por todos tus sermoncitos de señor de cien años y por todo lo que me apoyas. Sobre todo, gracias por tu compañía todos los días, eres un soporte vital, desde el primer café de la mañana que cualquiera que me conozca sabe que yo no preparo. También en la etapa de la cuarentena, en la que me ayudaste a sacar mi primer artículo a pesar de toda la ansiedad que me rodeaba. Eres el mayor regalo que me llevo de haber venido a Alcalá.

# Resumen

La monitorización de movimientos trata de obtener información sobre la ejecución de los mismos. Esta información es esencial en múltiples aplicaciones, incluidas las clínicas, para medir la evolución de los pacientes, valorar posibles patologías, tanto motoras, como cognitivas, y para el seguimiento de terapias físicas. En estas últimas, la monitorización tiene un doble objetivo: asegurar la corrección en la ejecución de movimientos y mejorar la adherencia a los programas prescritos por el facultativo. Ambos objetivos son esenciales para lograr los beneficios asociados a las terapias físicas. Para lograr esta monitorización de forma remota y poco intrusiva, se necesitan recursos tecnológicos como los ampliamente utilizados sensores inerciales, habitualmente integrados dentro de los conocidos *wearables*.

Este trabajo se centra en las soluciones basadas en sistemas inerciales para la monitorización de rutinas de terapias físicas. Sin embargo, los resultados de este trabajo no son excluyentes de dicho ámbito, pudiendo aplicarse en monitorización de movimientos con diferentes propósitos, intentando suplir las necesidades de los sistemas de monitorización encontrados en la literatura.

En la revisión de las propuestas previas para la monitorización remota de rutinas de rehabilitación se han encontrado dos enfoques principales. El primero se basa en el análisis de movimientos, en el que se estiman parámetros cinemáticos, y el segundo se centra en la caracterización cualitativa de los mismos. A partir de esta diferenciación, se han identificado las limitaciones de cada uno de los enfoques desarrollando contribuciones en ambos sentidos.

Respecto al primer enfoque, centrado en el análisis de movimientos para la estimación de parámetros cinemáticos, se ha encontrado un parámetro anatómico requerido en diversos métodos propuestos en la literatura. Dicho parámetro consiste en la posición de las articulaciones respecto de los sensores y, en ocasiones, también se requiere la longitud de los segmentos anatómicos. La determinación de estos parámetros internos es compleja y se suele realizar en entornos controlados con sistemas ópticos o mediante palpación de marcas anatómicas por personal especializado. Sin embargo, hay pocos trabajos en la literatura que determinen estos parámetros anatómicos mediante sensores inerciales.

En este trabajo se introduce un algoritmo para esta calibración anatómica, basado en la determinación del punto de aceleración nula presente en las articulaciones fijas. El método propuesto emplea un sensor inercial por articulación para simplificar la complejidad frente a usar varios de ellos. Puesto que la posición relativa de este punto puede variar por movimientos del tejido blando o el movimiento articular, se estima mediante mínimos cuadrados el punto medio de aceleración nula para el movimiento de calibración. Este algoritmo está adaptado a los movimientos lentos que se dan en los miembros inferiores para cumplir con la requerida estabilización de las articulaciones. Además, se puede aplicar tanto a centros como a ejes articulares, aunque estos últimos presentan una determinación más compleja. Puesto que se trata de la calibración de un sistema tan complejo como es el cuerpo humano, también se evalúan diferentes movimientos y su relación con la precisión del sistema.

Esta tesis además propone un segundo método de calibración más versátil, que se adapta al característico tejido blando asociado al cuerpo humano. Este método emplea las medidas de un sensor inercial como entradas en un filtro de Kalman extendido. La propuesta se prueba tanto en datos sintéticos como en el escenario real de la determinación del centro de rotación de la cadera. En simulación se alcanza una precisión del 3 % y en el escenario real, donde la referencia se obtiene con un sistema óptico de alta precisión, del 10 %. De esta forma se propone un algoritmo novedoso que localiza las articulaciones de forma adaptativa al movimiento de los tejidos con resultados dentro del estado del arte.

Por otro lado, este trabajo se centra en otra de las limitaciones del análisis de movimientos que es la falta de datos comunes para la evaluación de los algoritmos y el desarrollo de nuevas propuestas. Para ello, se diseña y se crea una base de datos pública centrada en movimientos habituales en rutinas físicas. En su diseño se tiene en cuenta la calibración articular que suele plantearse para la monitorización de los parámetros cinemáticos, realizando movimientos funcionales para la misma. Se monitorizan ejercicios de miembros inferiores y superiores ejecutados de forma correcta e incorrecta por 30 voluntarios de ambos sexos y con un amplio rango de edades. Puesto que uno de los principales objetivos a cumplir por esta base de datos es la validación de algoritmos basados en sistemas inerciales, está grabada con cuatro sensores inerciales, e incluyendo un sistema de referencia de alta precisión basado en cámaras de infrarrojos. Además, los movimientos grabados se encuentran etiquetados acorde a su caracterización, la cual se basa en el tipo de ejercicio realizado y la calidad de los mismos. Se proporciona un total de 7 076 ficheros de datos cinemáticos inerciales con una referencia de alta precisión, caracterizados de forma completa, junto con una función para su procesamiento automático. Esta base de datos ya es pública en Zenodo, disponible para su uso por parte de la comunidad científica.

Finalmente, se estudia el segundo enfoque de monitorización de rutinas físicas, cuyo

objetivo es la determinación de información cualitativa de su ejecución. Este trabajo contribuye a la caracterización de los movimientos como el conjunto de su reconocimiento y la evaluación, que comúnmente se han estudiado de forma separada. Con este objetivo, se proponen tres sistemas de clasificación que emplean las medidas de cuatro sensores inerciales. Las propuestas difieren en la distribución de datos y, por tanto, el nivel de detalle en las salidas del sistema. Para realizar las clasificaciones propuestas, se evalúan seis algoritmos de *machine learning* con el fin de determinar el más adecuado en cada una de ellas. Los algoritmos evaluados son *Support Vector Machines*, *Decision Trees*, *Random Forest*, *K Nearest Neighbors*, *Extreme Learning Machines* and *Multi-Layer Perceptron*. Las propuestas dan lugar a una exactitud, valor F1, precisión y sensibilidad por encima del 88 %. Además, se consigue un sistema con una exactitud del 95 % en la caracterización cualitativa completa de los movimientos, que reconoce el movimiento realizado y evalúa la exactitud en su ejecución. Cabe destacar que el algoritmo que siempre reporta las mejores métricas es *Support Vector Machines* de entre todos los evaluados. El clasificador propuesto que obtiene los mejores resultados es el dividido en dos etapas, que primero reconoce y después evalúa los ejercicios, frente a los que realizan ambas tareas en una única clasificación.

De nuestro trabajo, se puede concluir que los sistemas inerciales son adecuados para la monitorización de los ejercicios físicos de forma remota. Por un lado, son adecuados para la calibración de las articulaciones humanas necesaria para diversos métodos de análisis de movimientos, empleando un sensor inercial por articulación. Estos sensores permiten obtener la estimación de una localización media de las articulaciones, así como la longitud media de los segmentos anatómicos. Asimismo, se pueden localizar los centros articulares en escenarios en los que se producen movimientos de los sensores relativos a las articulaciones, asociados al movimiento de los tejidos blandos. Por otro lado, con la algoritmia propuesta se puede lograr una caracterización completa de los ejercicios físicos realizados utilizando cuatro sensores inerciales. De esta forma, se puede obtener información anatómica, así como información cuantitativa y cualitativa sobre la ejecución de las terapias físicas mediante el uso de sensores inerciales.

# Abstract

This thesis is framed in the field of remote motion monitoring, which aims to obtain information about the execution of movements. This information is essential in many applications, including the clinical ones, to measure the evolution of patients, to assess possible pathologies, such as motor or cognitive ones, and to follow up physical therapies. The monitoring of physical therapies has twofold purpose: to ensure the correct execution of movements and to improve adherence to the programs. Both purposes are essential to achieve the benefits associated with physical therapies. To accomplish this monitoring in a remote and non-intrusive way, technological resources such as the well-known inertial sensors are needed, which are commonly integrated into the so-called wearables.

This work focuses on inertial-based solutions for monitoring physical therapy routines. However, the results of this work are not exclusive of this field, being able to be applied in other fields that require a motion monitoring. This work is intended to meet the needs of the monitoring systems found in the literature.

In the review of previous proposals for remote monitoring of rehabilitation routines, we found two different main approaches. The first one is based on the analysis of movements, which estimates kinematic parameters, and the second one focuses on the qualitative characterization of the movements. From this differentiation, we identify and contribute to the limitations of each approach.

With regard to the motion analysis for the estimation of kinematic parameters, we found an anatomical parameter required in various methods proposed in the literature. This parameter consists in the position of the joints with respect to the sensors, and sometimes these methods also require the length of the anatomical segments. The determination of these internal parameters is complex and is usually performed in controlled environments with optical systems or through palpation of anatomical landmarks by trained personnel. There is a lack of algorithms that determine these anatomical parameters using inertial sensors.

This work introduces an algorithm for this anatomical calibration, which is based on the determination of the point of zero acceleration present in fixed joints. We use one inertial sensor per joint in order to simplify the complexity of algorithms versus using

more than one. Since the relative position of this point may vary due to soft tissue movements or joint motion, the mean null acceleration point for the calibration motion is estimated by least squares. This algorithm is adapted to slow movements occurring in the lower-limbs to meet the required joint stabilization. Moreover, it can be applied to both joint centers and axes, although the latter is more complex to determine. Since we are dealing with the calibration of a system as complex as the human body, we evaluate different movements and their relation to the accuracy of the proposed system.

This thesis also proposes a second, more versatile calibration method, which is adapted to the characteristic soft tissue associated with the human body. This method is based on the measurements of one inertial sensors used as inputs of an extended Kalman filter. We test the proposal both in synthetic data and in the real scenario of hip center of rotation determination. In simulations it provides an accuracy of 3 % and in the real scenario, where the reference is obtained with a high precision optical system, the accuracy is 10 %. In this way, we propose a novel algorithm that localizes the joints adaptively to the motion of the tissues.

In addition, this work addresses another limitation of motion analysis which is the lack of common datasets for the evaluation of algorithms and for the development of new proposals of motion monitoring methods. For this purpose, we design and create a public database focused on common movements in rehabilitation routines. Its design takes into account the joint calibration that is usually considered for the monitoring of joint parameters, performing functional movements for it. We monitor lower and upper limb exercises correctly and incorrectly performed by 30 volunteers of both sexes and a wide range of ages. One of the main objectives to be fulfilled by this database is the validation of algorithms based on inertial systems. Thus, it is recorded by using four inertial systems placed on different body limbs and including a highly accurate reference system based on infrared cameras. In addition, the recorded movements are labeled according to their characterization, which is based on the type of exercise performed and their quality. We provide a total of 7 076 files of inertial kinematic data with a high-precision reference, characterized with respect to the kind of performed motion and their correctness in performance, together with a function for automatic processing.

Finally, we focus on the analysis of the second approach of monitoring physical routines, whose objective is to obtain qualitative information of their execution. This work contributes to the characterization of movements including their recognition and evaluation, which are usually studied separately. We propose three classification systems which use four inertial sensors. The proposals differ in the distribution of data and, therefore, the level of detail in the system outputs. We evaluate six machine learning techniques for the proposed classification systems in order to determine the most suitable for each of them: Support Vector Machines, Decision Trees, Random Forest,

K Nearest Neighbors, Extreme Learning Machines and Multi-Layer Perceptron. The proposals result in accuracy, F1-value, precision and sensitivity above the 88 %. Furthermore, we achieve a system with an accuracy of 95 % in the complete qualitative characterization of the motions, which recognizes the performed motion and evaluates the correctness of its performance. It is worth highlighting that the highest metrics are always obtained with Support Vector Machines, among all the methods evaluated. The proposed classifier that provides the highest metrics is the one divided into two stages, that first recognizes the exercises and then evaluates them, compared with the other proposals that perform both tasks in one single-stage classification.

From our work, it can be concluded that inertial systems are appropriate for remote physical exercise monitoring. On the one hand, they are suitable for the calibration of human joints necessary for various methods of motion analysis using one inertial sensor per joint. These sensors allow to obtain the estimation of an average joint location as well as the average length of anatomical segments. Also, joint centers can be located in scenarios where joint-related sensor movements occur, associated with soft tissue movement. On the other hand, a complete characterization of the physical exercises performed can be achieved with four inertial sensors and the appropriate algorithms. In this way, anatomical information can be obtained, as well as quantitative and qualitative information on the execution of physical therapies through the use of inertial sensors.

# Contents

# List of Figures

# List of Tables

# Glossary and Acronyms

## List of mathematical symbols

| | |
|---|---|
| $X^k$ | Magnitude $X$ at a time instant $k$ (superscript) |
| $X_I$ | Magnitude $X$ measured by sensor I (subscript) |
| $X_r$ | Reference value of $X$ |
| $\hat{X}$ | Predicted value of the magnitude $X$ |
| $R$ | Generic rotation matrix |
| $C$ | Direction Cosine Matrix |
| $\boldsymbol{\omega}$ | Turn rate |
| $\boldsymbol{\omega}_Z$ | Turn rate of the rigid-solid body Z |
| $\omega_A$ | Turn rate over axis A |
| $\dot{\boldsymbol{\omega}}$ | Turn rate derivative |
| $\dot{\boldsymbol{\omega}}_Z$ | Turn rate derivative of the rigid-solid body Z |
| $\boldsymbol{f}$ | Specific force (linear acceleration with the gravity influence) |
| $\boldsymbol{v}$ | Linear speed |
| $\boldsymbol{a}$ | Linear acceleration |
| $a_A$ | Linear acceleration over axis A |
| $\boldsymbol{a}_Z$ | Linear acceleration |
| **OB** | Generic direction vector from O to B |
| $\Delta OB$ | Distance error in the estimation of **OB** |
| $M$ | Matrix of turn rate and angular accelerations to determine **OB** |
| $B$ | Pseudo-inverse of $M$ obtained by SVD |
| $d_A$ | Length of segment A |
| $\Delta d_A$ | Error in the estimation of the length of segment A |
| $\boldsymbol{r}$ | Generic direction vector variable |
| $\|\|\Delta \boldsymbol{r}\|\|$ | Euclidean norm of the vector difference between the reference $\boldsymbol{r}_r$ and its estimation $\boldsymbol{r}$ |
| $\Delta\|\|\boldsymbol{r}\|\|$ | Difference between norms of $\boldsymbol{r}_r$ and $\boldsymbol{r}$ |
| $\gamma$ | Deviation angle between $\boldsymbol{r}_r$ and $\boldsymbol{r}$ |
| $\boldsymbol{g}$ | Gravity vector |
| acc | Accuracy |
| prec | Precision |

| | |
|---|---|
| sens | Sensitivity |
| F1 | F1-Score |
| spec | Specificity |
| $P$ | Positives |
| $N$ | Negatives |
| $TP$ | True positives |
| $TN$ | True negatives |
| $FP$ | False positives |
| $FN$ | False negatives |

# List of acronyms

| | |
|---|---|
| 1Re-2Ev | first, Recognition and, second, Evaluation method in two-stage method |
| ANN | Artificial Neural Network |
| AOR | Axis of Rotation |
| ArVE | Adaptive r Vector Estimator |
| ArVE$_d$ | Adaptive r Vector Estimator considering the derivative of $r$ in the state vector |
| C | Correct (performance) |
| COR | Center of Rotation |
| DOF | Degree of Freedom |
| DT | Decision Trees |
| EAH | Extension of Arms over Head |
| EFE | Elbox Flex-Extension |
| EKF | Extended Kalman Filter |
| ELM | Extreme Learning Machine |
| FFT | Fast Fourier Transform |
| GAT | Gait |
| GHT | Gait with Heel-Tiptoe |
| GIS | Gait describing the $\infty$ Symbol |
| HAA | Hip Abduction/Adduction |
| HA(A)L/R | Hip Abduction/Adduction with the Left or Right leg |
| HCR | Hip Crosses exercise |
| HCS | Hip Circles exercise |
| IMU | Inertial Measurement Unit |
| INP | Inverse Pendulum |
| KF | Kalman Filter |
| KFE | Knee Flex-Extension |
| KF(E)L/R | Knee Flex-Extension with the Left or Right leg |

| | |
|---|---|
| KNN | K-Nearest Neighbors |
| LDA | Linear Discriminant Analysis |
| LOSO | Leave-One-Subject-Out (cross-validation) |
| ML | Machine Learning |
| MLP | Multi-Layer Perceptron |
| MoCap | Motion Capture |
| MrVS | Mean r Vector Estimator |
| $NAP_f$ | Null Acceleration Point with a low-pass filter with a cut-off frequency of $f$ Hz |
| $NAP_\omega$ | Null Acceleration Point using signals with a turn rate over $0.5\,\mathrm{rad/s}$ |
| NB | Naive Bayes |
| OBJ | Object (in optical systems) |
| PCA | Principal Component Analysis |
| PHYTMO | PHYsical Therapy MOnitoring (database) |
| ReEv | Recognition and Evaluation method in a row |
| ReC-V | Recognition of Correct repetitions method and elimination of the Wrong ones |
| RF | Random Forest |
| ROM | Range of Motion |
| sEMG | Surface Electromyography |
| SKT | Skeleton (in optical systems) |
| SQT | Squats |
| SQZ | Hands Squeezing a clothing |
| STA | Soft Tissue Artifacts |
| SVD | Singular Value Decomposition |
| $SVM_X$ | Support Vector Machines with a kernel X |
| UKF | *unscented* Kalman Filter |
| UT | *unscented* transform |
| W | Wrong (performance) |
| WL | Wrong performance of Lower-limb exercises |
| WU | Wrong performance of Upper-limb exercises |

# Chapter 1

# Introduction

Physical therapies are a crucial step in the recovery path of different surgical procedures, as cardiac surgery or hip replacement after falls, and in treatments of diseases or injuries. The recent example of the physical rehabilitation for the hospitalized people due to the corona-virus disease (Covid-19) is just one of the most currently known cases.

Those therapies are also needed for the active prevention of diseases, focused on taking care of health before the illness appears [Xu17]. Illness prevention is specially important in older people, since in the absence of adequate physical activity (PA) or exercise, the aging process is associated with premature and excessive appearance of diseases and dysfunctions [Izq21]. Exercise is a type of PA, which is planned, structured and repetitive, and is aimed to improve or maintain one or more components of physical fitness. PA and exercise have proved to be preventive measures in conjunction with other lifestyle factors, improving the elder frailty parameters and their functional capacity [Izq20, Izq18, Fra19]. Long-term (over one year) physical exercise interventions have been associated with a lower risk of falls, improving muscle strength, balance, physical and cognitive functions [Sou19]. Thus, an appropriate exercise prescription should be included in all health-care recommendations for the elderly.

The exercise monitoring is crucial to give proper recommendations according to the patient's health progression [Com15, Fra19], improving their adherence to the therapy [W B13] and assuring the correctness of motions through a continuous and immediate feedback [Zha16, Llo15]. If patients do the exercises on their own, data about routines are subjective and depend on the information provided by patients, who commonly overestimate their training sessions [Suc57]. Furthermore, the information given to physicians by patients does not include descriptions of the performance of exercises, as the range of motions (ROM) or the speed of movements, required to make a proper evaluation of their performance. Then, physical therapies and their guidance are established in hospitals and rehabilitation centers where the health-care staff su-

pervises the patients, as illustrated in Figure 1.1-left. Supervisors assess the physical therapy, monitoring motion parameters such as the performance quality, the range of motions or the number of repetitions. This approach, established in health-care centers, implies economic challenges associated to infrastructure and personnel [Sah19].

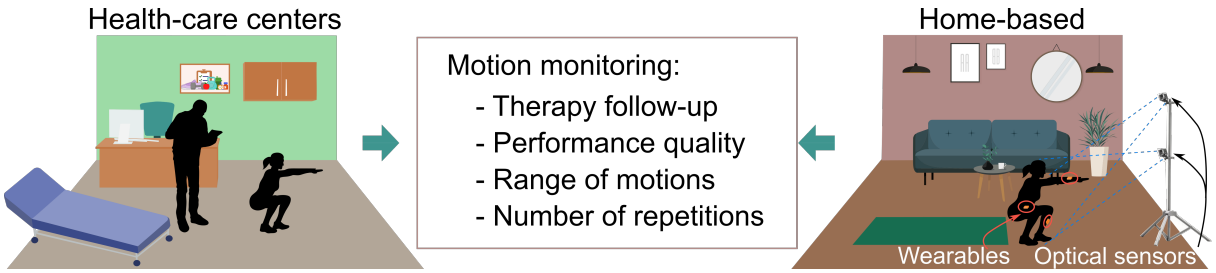


**Figure 1.1:** The two main different types of motion monitoring: *(left)* human-based in health-care centers and *(right)* home-based relying on technology; and some of the parameters to obtain. Graphics are from Vecteezy [Vec22].

One alternative is the home-based monitoring of therapies, as virtual coaches, which are a more reliable option for long-term therapies than what would be a human-based therapy. Information about the exercises performance can be obtained from home using motion monitoring technologies (as the optical sensors or wearables shown in Figure 1.1-right). With this approach, physical therapies can be easily fit in daily routines, being remotely guided by a physician [Dom19]. In this way, the monitoring technologies allow to obtain the therapy monitoring by health-care personnel without the need of patients attending the hospital, increasing also their independence. Furthermore, the remote monitoring give more representative measurements of the patients' activities [Man17, Vie17] and keep patients active over the long term, increasing their adherence to physical therapies [Ben11].

A useful monitoring has to be designed considering all the parameters required to evaluate the patients' health [Kay17] and the application to supervise it. There are several differences between a simple steps counter and a complete remote motion monitoring system, as a virtual coach, especially regarding the outputs to be obtained and their potential uses [Sah19]. The system that works as a virtual coach has to perform three main tasks: to analyze the human motions, i.e. to determine rotation joint angles; to monitor physical activity, evaluating the performance of the exercises and to provide feedback to patients [Kyr20a].

Systems used to analyze motions in non-controlled and non-supervised environments have to prove being reliable. Video-based technologies and sensor platforms are options for this monitoring, being the optical systems considered the *gold standard* [Che14]. However, both technologies are limited to those places where the systems are installed [Dom19, Vig19] and video-based technologies usually entail occlusions and patients' privacy concerns [Kom19a, Zih16].

Portable sensors, such as Inertial Measurement Units (IMUs), have increased their use during the last decade because of its low economical and processing costs, and its everywhere usable potential [Lop16]. IMUs include gyroscopes and accelerometers and, sometimes, magnetometers, as shown in Figure 1.2-left. These sensors measure motions in terms of turn rate, specific force, which is the linear acceleration with the influence of the gravity acceleration, and magnetic field, respectively. In this way, IMUs provide the raw data of these magnitudes and, through sensor fusion algorithms, they can estimate and provide their 3D orientation, expressed in Euler angles (see Figure 1.2-right) or quaternions, among others.

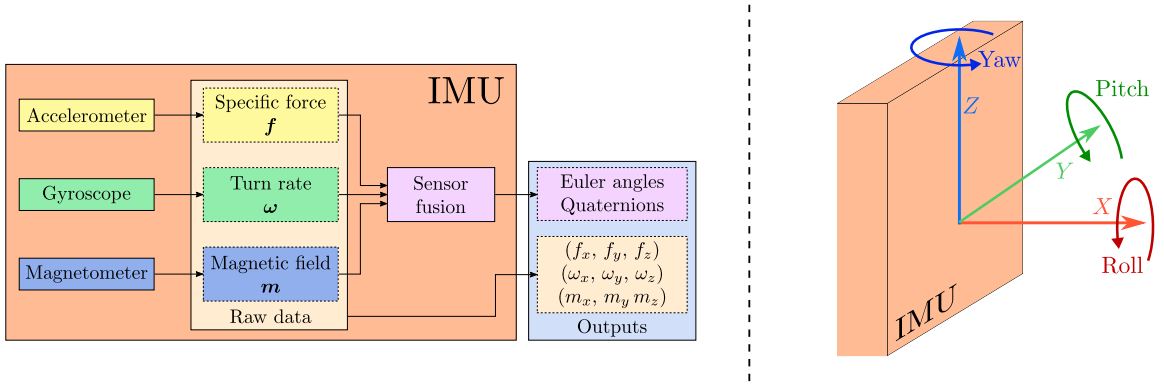


**Figure 1.2:** Functioning diagram of IMUs with their sensors, including the magnetometer, measurements and outputs (left). Euler angles to express the orientation of an IMU in the 3D space (right).

To get reliable information to obtain details about the performance of motions, these magnitudes, the specific force, turn rate and magnetic field, can be translated into clinically interpretative data for physicians, as ROM. Also, using the inertial measurements, motions can be identified or evaluated without estimating the kinematics parameters [Zha20b, Pre20, Bav19, Whe16, Kia17, Per19, Gig14, Hua16b].

In order to develop an inertial-based virtual coach system, it is necessary to understand the requirements and challenges of this remote motion monitoring application. These requirements and challenges are reviewed in the next section.

## 1.1 Challenges of Remote Motion Monitoring

This section presents the main challenges for remote human motion monitoring of physical therapies. The challenges can be divided into two groups: first, those aimed at obtaining relevant monitoring parameters, as rotation angles or limb displacement; and second, those that characterize these motions to translate the kinematic parameters into qualitative data, such as which exercise is being performed and its correctness.

With regard to the gathering of relevant motion monitoring parameters, referred in the following as motion analysis, the main challenge is the estimation of the joint angles from data provided by IMUs. The inertial-based angle estimation entails accumulated errors, which are mainly caused by the bias in the gyroscope, that has to be corrected in order to obtain reliable measurements of joint angles. Accelerometers are used to have a reference with respect to the gravity vector. In the case of Euler angles, the determination of roll and pitch angles (angles with respect to the horizontal plane, see Figure 1.2) can be corrected by this direct relationship to gravity. However, the third angle, yaw, cannot be accurately estimated in this way since it is parallel to the gravity vector.

There are different proposals to correct the accumulated error in the estimation of joint angles, such as those based on machine learning algorithms (ML) or biomechanical models. Biomechanical models, that exploit the human constraints to fuse information from IMUs, are one of the most used and most promising approaches to reduce this error associated to the drift. Several solutions have been proposed in the literature, such as limiting the estimated values to the anatomical ROM or exploiting the characteristics of the movement.

IMU-based systems that rely on these biomechanical constraints commonly require anatomical parameters for their implementation. Most of the algorithms that aim to calibrate sensor to joints focus only on the identification of axes of rotation of joints with respect to the axes of IMUs, as in [Mul17c, Cut08, Fav09]. However, the location of the center of rotation (COR) or axis of rotation (AOR) of joints with respect to the IMUs, i.e. a sensor-joint calibration, and the segment lengths are also frequently needed, as described in [Cra18]. The determination of these joints is the second challenge approached in this work. In inertial systems, the COR is determined through the oriented vector $\boldsymbol{r}$, defined from the IMU accelerometers to the COR of joints. The motion analysis and, specially, the joint angle calculation, is highly sensitive to the accuracy in this sensor-joint calibration by the estimation of the $\boldsymbol{r}$ vector [Bon15].

The location of joints are commonly determined through the palpation of external anatomic marks or by using optical systems [Bon15, Jou18, El 15]. Both systems need expert hands to place markers and are limited to controlled environments. Thus, biomechanically constrained inertial methods use external information different from the data obtained through IMUs, such as the position of markers obtained by the optical system. It limits the every-where utilization of the inertial motion analysis systems based on biomechanical models. As an alternative, different works arose to develop IMU-based algorithms that determine the $\boldsymbol{r}$ vector, being focused on the estimation of an average IMU-joint vector or of an adaptive vector at each time instant. These algorithms mainly differ in the consideration of negligible soft tissue artifacts (STA) when a complete motion is considered and, as a consequence, the IMU-joint vector is

averaged, as in [Cra16, Cra17, See12, McG13], or when STA is considered in the estimation [Fri18a, Fri18b].

For the evaluation of exercises, we need to translate from quantitative parameters of the performance, as the motion measurements obtained by IMUs, to qualitative data. Data from inertial sensors have been also used to detect and classify activities. These sensors are an alternative for motion monitoring since they have been proved to be reliable enough for joint motion monitoring [Zih16]. In this way, IMUs have been used in human applications for motion monitoring [Lin13], functional evaluation of joints [Kia16] and with respect to the study of activities performance, to their recognition or evaluation [Zha20b, Pre20, Bav19, Whe16, Kia17, Per19, Gig14, Hua16b]. However, during a remote physical therapy monitoring, we do not have information of which exercise is being performed and the correctness of the exercise can differ between exercises or repetitions. For an ideal motion monitoring system, we should consider both tasks, the recognition and evaluation, together as a complex challenge. In addition, the combination of the recognition and evaluation of exercises makes these tasks more complicated. On the one hand, gathering correct and wrong repetitions of the performed exercises means a high variability of performances during the exercise recognition. On the other hand, in order to evaluate an exercise, it has to be according to the motions that define it, so its evaluation relies on the correct recognition of motions. Errors in the recognition stage condition or entail errors in the exercises evaluation.

According to the aforementioned challenges, we can distinguish three main issues with respect to the remote physical therapy monitoring: motion analysis, sensor-joints calibration and exercises evaluation; as summarized in Figure 1.3. The motion analysis refers to the objective study of the parameters of motions. The approach to calibration in this work is focused on the estimation of CORs and AORs of human joints. Finally, the evaluation refers to determine how accurate an exercise is being performed, according to its description.

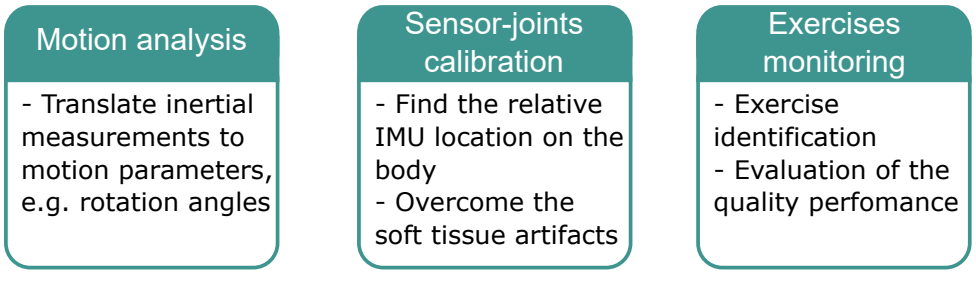


**Figure 1.3:** Three main challenges with regard to the remote motion monitoring for the follow-up of physical therapies.

Due to the potential uses and current limitations of using IMUs for remote motion monitoring, the main objective of this thesis is to study the theoretical basis for that

possible use. Next section introduces the objectives of this work, together with its research questions.

## 1.2 Objectives

The overall research objective of this thesis is human motion monitoring by means of inertial sensors, focused on physical therapies. This work aims at contributing to the objective monitoring of motion parameters through the estimation of limb joints location with inertial sensors. One IMU per joint will be used and the averaged and adaptive positioning of joints will be studied. Furthermore, the information of four IMUs will be fused in order to identify and evaluate prescribed motions.

In this way, we have the following research goals:

- Research goal 1: determine and overcome the main weaknesses of the biomechanical model-based motion monitoring systems. This work focuses on two of them: the positioning of the inertial sensors with respect to the centers and axes of joints, and the variability in the data commonly used for the evaluation of biomechanical models. With regard to the first weakness, the main goal is to develop an accurate alternative to estimate the position of the inertial sensors with respect to the center of axis of joints. The proposals must be validated by comparing with an accurate optical system, in terms of vector distance and deviation angle. For the second limitation, we aim to create a generic database of upper-and lower-limb motions recorded with inertial sensors and a reference system.

- Research goal 2: investigate and implement ML methods aimed at identifying and evaluating prescribed motions. The objective is that these methods rely only on the information of IMUs placed at the upper-or lower-limbs. To do so, we plan on studying different proposals for this two-fold objective, which will be evaluated and compared with the known characteristics of motions, i.e. the performed motion and its correctness.

## 1.3 Thesis Background

This thesis describes an original work carried out at the GEINTRA Research Group of the University of Alcalá (UAH), in the topic of ambient monitoring for independent living. It has been developed under the auspices of the research projects Frailcheck (ref. SBPLY/17/ 180501/000392, supported by Junta de Comunidades de Castilla La Mancha) and MICROCEBUS (ref. RTI2018-095168-B-C51, funded by Spanish Ministry

of Science, Innovation and Universities). It has also been economically supported by the Youth Employment Program (ref. PEJ-2017-AI/TIC-7372 and PEJ-2020-PRE/TIC-17000) and by the mobility program of the University of Alcalá. One three-month research stay was carried out thanks to the mobility program, at the German Aerospace Centre (Deutsches Zentrum für Luft- und Raumfahrt, DLR), in Munich.

The aim of the FrailCheck project was to design, develop and validate a system to aid the assessment of frailty, and one of the goals of the MICROCEBUS project was to develop an unobtrusive tool for people monitoring, by keeping track of the daily routines of dependent people, either elderly or people with intellectual disabilities. This thesis has contributed to both projects in the tasks of people activity monitoring based on IMUs. Specifically, it focuses on the monitoring of physical routines, which are essential to maintain a healthy life.

The development of this work requires different material resources. We need inertial sensors in order to test the proposals of this work, but we also need a reference system to validate them. The *gold standard* system is the one based on stereo-photogrametry, which provides the 3D coordinates of points of objects. This system uses at least two infrared cameras to obtain the coordinates in the 3D space by triangulation. During the research stay in the DLR, we used their stereophotogrammetry system (Vicon [Vic20]), based on twelve infrared cameras to record the ground truth of our measurements. In addition, the DLR has an inertial system with three available high-end IMUs (Xsens [Xse20]), whose wireless communication allows to export data for analysis in external computer programs. With both systems, the IMU signals and their reference orientations and locations, thigh and shin positioning was recorded with four and five markers, respectively.

Besides, the University of Alcalá acquired a stereophotogrammetric motion capture system based on eight infrared cameras (Optitrack [Opt20]) through the MICROCEBUS project. This system was installed in the motion capture laboratory of the Polytechnic School of the UAH (MoCap laboratory). In addition, medium-high range IMUs, the NGIMU of the X-io brand [xio21], were purchased. Therefore, from this moment on, the measurement campaigns required for the development of this thesis were carried out in the MoCap laboratory, recruiting volunteers in the university environment. Thus, the data used in this thesis were obtained in that laboratory.

This work contributes to maintaining people's health by monitoring their movements. Therefore, its development requires kinematic data from people, which had to be recorded. We have the approval for the development of this thesis of the Ethics Committee of the University of Alcalá (CEID/2021/5/125). Recordings dated prior to that approval were carried out under the approval of the Ethics Committee of the Guadalajara University Hospital (Institutional Review Board No.2018.22.PR, protocol version V.1. as of 12/21/2020). The two corresponding approval reports are in Appendix B.

## 1.4 Contributions

This thesis has four main contributions:

1. We study the approaches to track the joint angles using inertial sensors for human motion monitoring. We focus on the biomechanical model-based solutions and one of their main limitations. This limitation consists in the location of the joint center, required for the sensor fusion with those models. Thus, we provide in-depth solutions of locating the human lower-limb joints with respect to an IMU system. We evaluate an inertial method for the complete characterization of lower-limbs. The proposal is aimed at obtaining two key parameters in the development of biomechanical models, the segment lengths and the location of joints with respect to the IMU sensors. During the analysis, we also study the relationship between different calibration motions and the accuracy achieved by the calibration method proposed. The results of this work have produced two conference papers in the *XXV Seminario Anual de Automática Electrónica Industrial e Instrumentación (Annual Seminar on Industrial Electronic Automatics and Instrumentation)* and in the *2019 International Conference on Indoor Positioning and Indoor Navigation*.

2. We deal with one of the main problems associated to the human joint positioning with IMU systems: the STA. We focus on the STA that affect to the human joint determination, specifically, using inertial sensors. As in the first contribution, we aim at locating the joints center with respect to the IMU accelerometer. We denote the directed vector from the IMU accelerometer to the joint COR as $\boldsymbol{r}$. We propose an initial method, called *ArVE*, from adaptive $\boldsymbol{r}$ vector estimator and its improvement, called $ArVE_d$, that considers the derivative of $\boldsymbol{r}$ in the state vector. These methods are based on different EKFs that allow to obtain one vector per sample. We prove that $\text{ArVE}_d$ outperforms ArVE and the state-of-the-art methods that average the $\boldsymbol{r}$ vector and do not adapt to its changes. We find that our proposal obtains an accurate estimation of CORs in a 1-cm radius sphere. In the real scenario, errors are always under the 10 % of the reference vector, obtained using a 3D optical system. This research line has resulted in one journal paper in *IEEE Transactions on Instrumentation and Measurements* and two conference papers in the *2020 IEEE International Symposium on Medical Measurements and Applications* and *XXVII Seminario Anual de Automática Electrónica Industrial e Instrumentación (Annual Seminar on Industrial Electronic Automatics and Instrumentation)*.

3. For the evaluation and optimization of human motion algorithms, it is necessary to count on particular datasets adapted to the exercises to be analyzed. Recent research efforts have focused on the creation of datasets by using different sensory systems, but none contains labeled physical therapy exercises with a ground

truth from a reference system. Therefore, we design and create a database of the monitoring and evaluation of the performance of prescribed physical therapy exercises through inertial portable sensors to contribute to the research. We ensure the variability of participants recording the motion of thirty volunteers between 20 and 69 years old. Furthermore, the motions recorded vary in their performance quality so we provide a diverse variability of motions. The sensory system consists of four IMUs and one highly accurate optical system. Files are labeled according to the performed motion and its quality. In this way, we provide a total amount of 7 076 files that can be used to study inertial-based motion monitoring algorithms, such as ML applications of classification purposes, i.e. motion recognition. These data are publicly available at Zenodo [Zen20] and the data descriptor is aimed at being a journal paper currently under review in *Scientific Data*.

4. Finally, we evaluate another approach, different from the human motion analysis, for inertial motion monitoring. This second approach is focused on obtaining qualitative information about the motion performance. We study different approaches for the identification and evaluation of prescribed exercises using supervised ML methods. With this approach, our goal is to contribute to the development of virtual coaches for the remote qualification of motions during physical therapies, obtaining information of which exercise is being performed and its quality. We propose and evaluate three different approaches and their potential applications, assessed through leave-one-subject-out validation to study the evaluation of motions performed by new subjects. We study different ML algorithms and their performance to provide insights about the optimal one in this application. This research has produced two conference papers in the *2021 IEEE International Symposium on Medical Measurements and Applications* and *XXVIII Seminario Anual de Automática Electrónica Industrial e Instrumentación (Annual Seminar on Industrial Electronic Automatics and Instrumentation)* and one journal paper currently under review in *Expert Systems with Applications*.

### 1.4.1 List of Publications

The list of publications up to date is composed of the following journal and conference publications:

- **S. García-de-Villa**, A. Jiménez-Martín and J. J. García-Domínguez, "'Novel IMU-based Adaptive Estimator of the Center of Rotation of Joints for Movement Analysis"'. *IEEE Transactions on Instrumentation and Measurement* Vol. 80, pp.1-11, 2021, Art no. 40511, doi:10.1109/TIM.2021.3073688. (Q1 JCR)

- **Sara García-de-Villa,** Ana Jiménez-Martín and Juan Jesús García-Domínguez, 'A database of physical therapy exercises with variability of execution collected by wearable sensors'. *Scientific Data.* **Under review**. July. 2021. (Q1 JCR).

- **Sara García-de-Villa,** David Casillas-Perez, Ana Jiménez-Martín and Juan Jesús García-Domínguez, 'Simultaneous Exercise Recognition and Evaluation in Prescribed Routines: Approach to Virtual Coaches'. *Expert Systems with Applications.* **Under review**. November. 2021. (Q1 JCR).

- **Sara García de Villa**, Ana Jiménez Martín, Juan Jesús García Domínguez, 'A Biomechanical Model Implementation for Upper-Limbs Rehabilitation Monitoring Using IMUs'. *VII International Work-Conference on Bioinformatics and Biomedical Engineering (IWBBIO'19)* Granada, Spain. May 2019. (International). doi:10.1007/978-3-030-17935-9_32

- **Sara García de Villa**, Ana Jiménez Martín, Juan Jesús García Domínguez, 'Implementation of a lower-limb model for monitoring exercises in rehabilitation'. *2019 IEEE International Symposium on Medical Measurements and Applications (MeMeA'19)* Istambul, Turkey. July 2019. (International). doi:10.1109/MeMeA.2019.8802221. *High Quality Paper: Travel Award*

- **Sara García de Villa**, Estefania Munoz Diaz, Dina Bousdar Ahmed, Ana Jiménez Martín, Juan Jesús García Domínguez, 'IMU-based Characterization of the Leg for the Implementation of Biomechanical Models'. *2019 International Conference on Indoor Positioning and Indoor Navigation (IPIN'19)* Pisa, Italy. October 2019. (International). doi:10.1109/IPIN.2019.8911818.

- **Sara García de Villa**, Ana Jiménez Martín, Juan Jesús García Domínguez, 'Adaptive IMU-based Calibration of the Center of Joints for Movement Analysis: One Case Study'. *2020 IEEE International Symposium on Medical Measurements and Applications (MeMeA'20)* Bari, Italy. *Online*. Jun 2020. (International). doi:10.1109/MeMeA49120.2020.9137135.

- **Sara García de Villa**, Andrea Martínez Parra, Ana Jiménez Martín, Juan Jesús García Domínguez, David Casillas-Pérez, 'ML algorithms for the assessment of prescribed physical exercises'. *2021 IEEE International Symposium on Medical Measurements and Applications (MeMeA'21)* Neuchâtel, Switzerland. *Online*. Jun 2021. (International). doi:10.1109/MeMeA52024.2021.9478725

- **Sara García de Villa**, Ana Jiménez Martín, Juan Jesús García Domínguez, Álvaro Page del Pozo, 'Estimacion de centros y ejes de rotacion mediantes ensores inerciales'. *XXV Seminario Anual de Automática Electrónica Industrial e Instrumentación*

*(SAAEI'18)* Barcelona, Spain. July 2018. (National).
ISBN: 978-84-947311-4-3

- **Sara García de Villa**, Ana Jiménez Martín, Juan Jesús García Domínguez, 'Implementación de un modelo biomecánico para el análisis de movimientos con sensores inerciales'. *XXVI Seminario Anual de Automática Electrónica Industrial e Instrumentación (SAAEI'19)* Córdoba, Spain. July 2019. (National).
ISBN: 978-84-17171-50-6

- **Sara García de Villa**, Ana Jiménez Martín, Juan Jesús García Domínguez, 'Calibración adaptativa de los centros articularespara el análisis de movimientos con IMUs'. *XXVII Seminario Anual de Automática Electrónica Industrial e Instrumentación (SAAEI'20)* Ciudad Real, Spain. *Online*. September 2020. (National).
ISBN: 978-84-122260-2-7

- **Sara García de Villa**, Andrea Martínez Parra, Ana Jiménez Martín, Juan Jesús García Domínguez, David Casillas-Pérez, 'Evaluación de ejercicios físicos pautados mediante algoritmos de Machine Learning'. *XXVIII Seminario Anual de Automática Electrónica Industrial e Instrumentación (SAAEI'21)* Ciudad Real, Spain. *Online*. July 2021. (National).
ISBN: 978-84-123292-2-3

- Alberto García, Cristina Losada, **Sara García**, Ana Jiménez, J. Jesús García, 'Contactless real-time analysis of elderly people posture for sleep disorders evaluation'. *2018 International Conference on Indoor Positioning and Indoor Navigation (IPIN'18)* Nantes, France. September 2018. (International)

- Ana Jiménez Martín, Alejandro Cuevas Notario, J. Jesús García Domínguez, **Sara García de Villa**, Miguel A. Herrero Ramiro, 'Data Fusion for Improving Sleep Apnoea Detection from Single-lead ECG Derived Respiration'. *VII International Work-Conference on Bioinformatics and Biomedical Engineering (IWBBIO'19)* Granada, Spain. May 2019. (International). doi:10.1007/978-3-030-17935-9_5

- Ismael Miranda Gordo, Ana Jiménez Martín, David Gualda Gómez, Juan Jesús García Domínguez, **Sara García de Villa**, 'Symbolic localization of institutionalized patients for detection of daily living activities'. *2020 IEEE International Symposium on Medical Measurements and Applications (MeMeA'20)* Bari, Italy. *Online*. Jun 2020. (International). doi:10.1109/MeMeA49120.2020.9137208.

- Juan Jesús García Domínguez, Ana Jiménez Martín, José M. Villadangos Carrizo, Sergio Lluva Plaza, Sergio Humanes Lopez, Sergio Martín Serrano, **Sara García de Villa**, 'Portable System for the Functional Assessment of Older Adults'. *2020 IEEE International Symposium on Medical Measurements and Applications (MeMeA*

*'20)* Bari, Italy. *Online*. Jun 2020. (International). / doi:10.1109/MeMeA49120.2020.9137311

- Ana Jiménez Martín, Ismael Miranda Gordo, David Gualda Gómez, **Sara García de Villa**, Sergio Lluva Plaza, Juan Jesús García Domínguez, 'BLE-based approach for detecting daily routine changes'. *2021 IEEE International Symposium on Medical Measurements and Applications (MeMeA'21)* Neuchâtel, Switzerland. *Online*. Jun 2021. (International). doi:10.1109/MeMeA52024.2021.9478752

- Alberto García Merino, Cristina Losada Gutiérrez, **Sara García de Villa**, Ana Jiménez Martín, Juan Jesús García Domínguez, 'Análisis postural sin contacto y en tiempo real de personas ancianas para la evaluación de trastornos del sueño'. *XXV Seminario Anual de Automática Electrónica Industrial e Instrumentación (SAAEI '18)* Barcelona, Spain. July 2018. (National).
ISBN: 978-84-947311-4-3

- Ismael Miranda, Juan Jesús García, Ana Jiménez, David Gualda, **Sara García**, 'Localización simbólica de pacientes institucionalizados para la detección de actividades de la vida diaria'. *XXVII Seminario Anual de Automática Electrónica Industrial e Instrumentación (SAAEI'20)* Ciudad Real, Spain. *Online*. September 2020. (National).
ISBN: 978-84-122260-2-7

- Ismael Miranda Gordo, Ana Jiménez Martín, David Gualda Gómez, **Sara García de Villa**, Sergio Lluva Plaza, Juan Jesús García Domínguez, 'Detección de cambios en la rutina diaria a través de localización BLE'. *XXVIII Seminario Anual de Automática Electrónica Industrial e Instrumentación (SAAEI'21)* Ciudad Real, Spain. *Online*. July 2021. (National).
ISBN: 978-84-123292-2-3

Furthermore, a database, called PHYTMO, is published at Zenodo and its data descriptor is included in Chapter 5:

- **Sara García-de-Villa**, Ana Jiménez-Martín and Juan Jesús García-Domínguez, 'A database of physical therapy exercises with variability of execution collected by wearable sensors'. *Zenodo* July. 2021. doi:10.5281/zenodo.5052756

## 1.5 Outline

The aforementioned contributions are given in separate chapters which are self-contained and follow a paper structure. The chapters are organized as follows:

- Chapter 2 reviews the state-of-the-art of the problem of human motion monitoring. We focus on the use of inertial systems for this aim. We study two main approaches. Firstly, the monitoring of joint angles through the use of biomechanical models, focusing on their limitation of locating the human joints. And secondly, the identification and evaluation of prescribed motions.
- Chapter 3 includes the contributions in the human lower-limb calibration with IMUs. We propose and evaluate the proposals in the estimation of directed IMU-joint vectors, the segment length and the joint axis orientation with respect the inertial sensors.
- Chapter 4 describes a new algorithm proposed in this thesis, called ArVE$_d$, aimed at obtaining IMU-joint vectors in scenarios as human legs, where STA occur.
- Chapter 5 is the data descriptor of the database physical therapy exercises with variability of execution. This chapter details the content and structure of the data.
- Chapter 6 includes an in-depth study of the identification of prescribed motions and their evaluation. We detail and evaluate different ML algorithms for its application in the field of virtual coaches.
- Chapter 7 summarizes the contributions of this thesis and the proposed future research lines.
- Appendix A details the mathematical frame in which this thesis has been developed.
- Appendix B includes the approval reports of the ethics committees required for this study.

# Chapter 2

# State of the Art

This chapter reviews the previous works related to physical exercises monitoring. We first give insight about the technologies that have been used with this goal. We analyze their advantages and drawbacks, and discuss the selection of IMUs as technological alternative for this work. Then, we provide a detailed survey of the state-of-the-art methods for human motion analysis based on IMUs, studying the different approaches and their limitations.

## 2.1 Technological Solutions

For the human motion monitoring and analysis, we count on different measurement systems with multiple technological basis. Since our objective is to monitor human motions during the performance of different movements described on a specific way, we focus on systems that do not interfere with the motion performance. It implies that we discard sensing devices based on exoskeletons from the beginning. The rest of existing motion capture systems can be categorized according to whether or not they are vision-based.

The most widely used system is based on optical capture with passive markers [Che14]. A minimum of two infrared cameras emit radiation subsequently detected after its reflection on the markers, which are positioned at anatomical points of interest on the subject or other significant points even on external objects. In this way, the system provides the positions of these markers in the 3D space, obtained by geometrical relationships. The inverse system has also been developed, in which the markers emit infrared radiation to a fixed external integrated measuring unit composed of photosensitive cells. The measurement units detect the radiation and infer the different angles at which the markers are oriented. These optical systems are considered the *gold standard* since they provide highly accurate measurements, about 1 mm accuracy

in 3D positioning of markers.

However, despite their remarkable accuracy in a laboratory setup, they require long installation time, a high-performance processing platform, a controlled and constrained environment with appropriate lighting conditions, and suffer from occlusions [Dom19, Vig19]. In addition, another major constraint is that they entail patient privacy concerns [Kom19a, Zih16]. As a continuous monitoring system has to be usable in the home environment and portable to other locations, it has to be easily deployable and user-friendly. Therefore, the restrictions of optical systems make them impractical for continuous monitoring.

In addition to the vision-based systems, there are those based on electromagnetic fields [Che14]. An antenna creates the magnetic field and sensors made of coils disturb it, so the position can be inferred from these disturbances. These systems are no limited to the vision zones of the receivers and they can reach a position accuracy over 1.5 mm. However, the measurements obtained by these systems are affected by metallic objects and electromagnetic distortions of the environment.

Another technological alternative are the IMUs, which contain at least two sensors: gyroscopes and accelerometers, and frequently include magnetometers. Compared to other non-invasive sensory systems used for motion assessment, IMUs are small, light-weight and portable, which are crucial requirements for user-friendly monitoring technologies. Furthermore, due to their low latencies, wide sampling rates and small size, they are a good choice for ambulatory capture systems. Thus, IMUs allow measurements in various environments, both in daily life and in controlled tests in laboratories, and for long duration, which is an advantage over other types of human movement monitoring sensors.

They have been used in many works to assess movement characteristics [Vie17, Dor19, Mun20b, Rap21, Abb18, Dua20, Abb17, Naz21b], e.g., obtaining the rotation angles with an accuracy over 5 °, or to obtain a recognition or evaluation of motions [Zha20a, Pre20, Whe16, Kia17, Gig14, Hua16a], for example evaluating single leg squats, between correct or wrong, with an accuracy over 94 % [Kia17].

Due to its versatility and ease of use, in this work we use IMUs as the technological alternative to carry out the analysis of movements and their qualitative assessment.

## 2.2 IMUs for Human Motion Monitoring

IMUs allow two main alternatives for motion monitoring: the first alternative consists in the estimation of kinematic parameters, which is known as *human motion analysis*, and the second alternative deals with the *qualification of movements*, which refers to the recognition and evaluation of motions, avoiding the prior estimation of kinematic

parameters, and consequently, its limitations. This work studies both alternatives: section 2.2.1 provides an overview of the application of IMUs in the human motion analysis field in order to introduce the main limitations associated to this approach, and section 2.2.3 focuses on the different proposals that use the data from IMUs to recognize or evaluate motions. With regard to the limitations in the algorithms for human motion analysis, some of them, such as biomechanical models, require anatomic information as the location of CORs and AORs. Therefore, we analyze the methods in the literature focused on the determination of these locations in section 2.2.2. Finally, we perform an in-depth study of the data availability for the development of new IMU-based methods for physical therapy monitoring in section 2.2.4. We summarize the state-of-the-art topics and their main features and limitations in Figure 2.1.

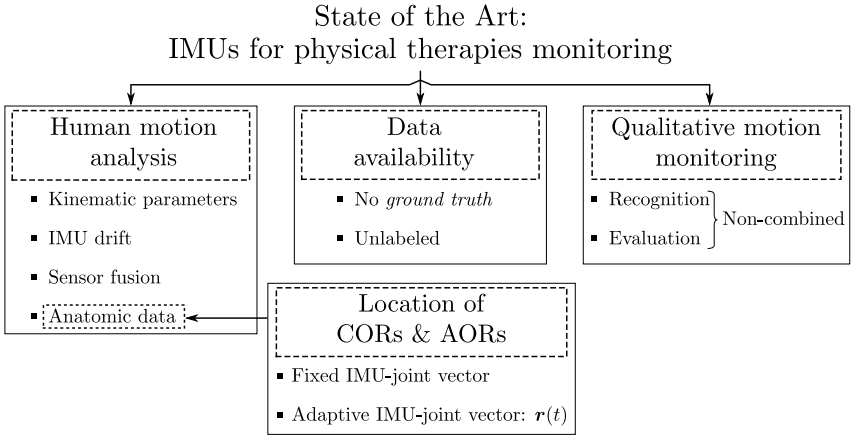


**Figure 2.1:** State of the Art scheme of the approaches for physical therapies monitoring by using IMUs.

### 2.2.1 IMUs for Human Motion Analysis

IMUs measure movements in terms of turn rate, specific force, i.e. linear acceleration under the influence of gravity, and in some occasions, magnetic field. However, the human motion analysis involves the estimation of their kinematic parameters, such as rotation angles or displacement of limbs. The rotation angles are more frequently used because they can be standardized and compared among subjects more directly than linear magnitudes, that require normalization with anatomical parameters of subjects as height or segment lengths.

Different methods have been proposed to estimate the rotation parameters using measurements from IMUs. The information from the IMU sensors are used separately through the integration of data from gyroscopes, or by observation of vectors, as gravity in the accelerometer data or the magnetic field in magnetometers. The integration of the turn rate alone entails errors in the estimations of kinematic parameters due to the accumulated error [All18, Mul17b]. Conversely, accelerometers are more frequently

used because they allow us to obtain a direct observation of their absolute reference, the gravity vector [Lai17, Gho20, Lim20, Zeh21, Zhe21]. However, this gravity observation is only possible when accelerometers are static, e.g., stance phase during gait strides. Magnetometers are sensitive to magnetic disturbances in the environment. As a consequence, only a few studies use this sensor separately [Wat21, Fri14].

Another approach is to gather the measurements of these sensors in different combinations of two or three of them with different algorithms, such as sensor fusion filters or ML methods. Sensor fusion techniques are useful methods to overcome the individual limitations of each of them. Most of studies that fuse data from various sensors combine gyroscopes and accelerometers to obtain kinematic parameters [Mun21, Mol18, All17a, Yin21, Cho18, Liu20, Lig20, Mun20a, Tha21, Jou19, Dor20, Che20, Fal20, Wey20, Men19, Jou20, Dor19, Mun20b, Rap21, Lee21, Xu18, Kit19, Lin13, Fas18, May20, Her21, Mun20c, Vil17, Jou18, Alv17, Ali17, Lia21, Sha17, Din20, Sha21, Kum18, Sal20, Fig20] or both sensors with magnetometers [Naz21a, Abb18, Dua20, Abb17, Naz21b, McG18, Fei21, Con21, Sy21b, Sy21a, Atr18, Wan17, But19, Sai20, Yan21, Fou17, Pat18, Wou19, Nag21]. Few studies fuse the accelerometer and magnetometer data [Zab15, Liu10] and even fewer use the gyroscope and magnetometer data [But21].

The sensor fusion technique most used for the inertial motion analysis is based on the Kalman Filter (KF), which is closely followed by ML techniques. In the following sections we provide an analysis of the KFs and ML methods for the motion monitoring proposed in the last five years. This analysis includes the basis of the main approaches, such as the commonly sensors used and anatomical units measured. Finally, we give insights about the accuracy of each technique and identify their limitations.

#### Bayesian Filters for Motion Analysis

The Bayesian filters used in the motion analysis field are the KFs and their variations, Extended Kalman Filter (EKF) and *Unscented* Kalman Filter (UKF), and the three of them have proven to behave similarly in the estimation of kinematic parameters [Ali17]. The problem formulation of these filters consists in the identification of the corresponding estimations through measurements observed over time that contain statistical noise and inaccuracies, see Appendix A.3. KFs are used to fuse gyroscopes with accelerometers and both with magnetometers, being the last one the most recent trend despite of the magnetometer sensitivity to electromagnetic disturbances.

KFs have been used to estimate the position of lower-limb joints (hip, knee and/or ankle) [All17a, McG18, Xu18, Lin12, But19, May20, Jou18, Sai20, Sy21b, Sy21a] and the upper-limb joints (shoulder, elbow, forearm, twist of hand, wrist and/or fingers) [Kit19, Atr18, Ali17]. Less works focus on body segments of limbs, such as legs [Naz21b, Naz21a, Sy21b], feet [Naz21b, Naz21a] or arms [Liu20, Alv17, Dua20]. Finally, only a

few of them study the motion of complex structures such as head, neck and scapula, or back, trunk and torso [Pat18, Alv17].

KFs present the advantage of allowing us to add constraints during the sensor fusion. We can find biomechanical *hard* constraints relative to the human body, such as limitation of ROM to those values anatomically possible [Dua20, Lin13] constraining the motion to less DOF, only those main directions of motions of each joint [Sy21a, Sy21b, Ali17, Jou18, McG18], and *soft* constraints, such as the relationship between the gyroscope and accelerometer measurements through the distances between sensors and joints [Ali17, Jou18, Lin13, Atr18, Kit19, Xu18, All17a].

However, the hard constraints are commonly designed for healthy people and can limit their use for the diagnosis of diseases. Regarding the soft constraints, they often require the knowledge of the location of IMUs with respect to the anatomical joints and, in some occasions, of the segment lengths. There is a lack of inertial-based methods for the joint location, so this information is commonly obtained from external sensors, which is incompatible with an IMU-based remote motion analysis. For that reason, we analyze the inertial systems for joint location in section 2.2.2.

Other possible constraints are related to the performed motion, e.g. simplification of the measurements of a motion to a plane because most of the motion occurs in that plane [Alv17], imposing a zero velocity update when monitoring repetitive motions with stops [Sy21a, Sy21b], or exploiting the pseudo-periodicity of repetitive motions in which we know a posture is repeated [Jou18].

These constraints limit the information that can be obtained from one motion, since the kinematic parameters out of the plane are dismissed. The problem of its application to a remote monitoring of motions is that inaccuracies of the motions can be not detected if they are out of the main DOFs of the prescribed motion.

These proposals are mainly validated with a highly accurate optical system and the reported errors are in the same range of values: between $0.01\,^\circ$ and $10\,^\circ$, although complex joints such as hip present errors over $15\,^\circ$ [Sy21a]. However, the comparison among them is hardly fair since the different studies test the methods in different databases, created specifically for each of these studies.

There are a low amount of publicly available data and, frequently, the number of volunteers is limited to the characteristics of the study. Most of studies test their proposals on less than 15 volunteers, and almost half of them studies are tested on only one volunteer. Furthermore, the lack of available data limits the development and validation of new proposals.

**ML Methods for Motion Analysis**

ML methods are a heterogeneous group of algorithms whose aim is to extract knowledge from data and infer mathematical models, as detailed in depth in Appendix A.4. In the motion analysis field, the objective is to obtain kinematic parameters from models based on inertial data. The ML methods that have been used are, in descending order of use: Long Short-Term Memory (LSTM), Artificial Neural Networks (ANN), Convolutional Neural Networks (CNN), generic Recurrent Neural Networks (RNN), Nonlinear AutoRegressive network with eXogenous inputs (NARX), Decision Trees (DT), Support Vector Machines (SVM) and Multi-Layer Perceptron (MLP).

These algorithms allow the fusion of sensor data in more different combinations than the Bayesian filters introduced above. Despite most proposals combine gyroscopes and accelerometers [Dor20, Mun20b, Mun20c, Fig20, Her21, Mun20a, Lia21, Tha21, Lee21, Sha21, Mun21, Rap21], other works use these sensors together with magnetometers [Wou19, Alc17, Nag21] or only accelerometers [Gho20, Lim20, Zhe21]. However, some authors have proved that not using acceleration as input improves the accuracy of the estimations because the acceleration varies depending on the location of the sensors on the body [But21].

These proposals are oriented to the estimation of the lower-limbs and the full body kinematics, in contrast to Bayesian filters that also consider the upper-limbs separately. Another difference with Bayesian filters is that these algorithms commonly do not include biomechanical constraints. Only a few works include the information about the length of limbs [Mun20c], the simplification of motions to a plane [Alc17] or the reduction of DOF of joints [Lee21]. However, learning from data includes only anatomically possible values, so ML algorithms learn about the possible estimations, constraining their values.

One of the main characteristics of these methods is the need of enough data to train and validate the algorithms. Most of the proposed models use stereophotogrammetric data for training the models [Dor19, Mun20b, Mun20c, Her21, Mun20a, But21, Sha21, Rap21]. Another alternative is the use of highly accurate inertial systems to train and validate the proposals [Wou19, Zhe21, Alc17, Lia21, Lee21]. In order to achieve a more robust training for the models, different data augmentation techniques have been used, such as adding zero mean white Gaussian noise [But21], simulating data of a sensor on specific locations [Mun20b, Mun20c] or using data from simulation software, e.g. Opensim [Sha21].

With regard to the reported accuracy of the ML-based motion analysis systems, it is similar than the accuracy reported by Bayesian filters. However, ML-based algorithms study more subjects than the proposals based on Bayesian filters because of the need of enough data to train the models, although they combine real and simulated data.

Again, the comparison between methods is unfair because different data are used to evaluate each study. Furthermore, the amount of studies that require data augmentation highlights the lack of data available for the development of ML algorithms for the estimation of kinematic parameters.

### 2.2.2 Estimation of locations of joint CORs and AORs

Some inertial-based systems aim at estimating kinematic parameters considering soft constraints, which require personalized anatomical parameters. The accuracy in the estimations of the kinematic parameters is highly sensitive to the accuracy of the anatomical parameters. These parameters include COR and AOR of joints, which are needed to establish the anatomic frame of body segments [Cra16]. Different works focus on the location of the COR of human joints, since the determination of an internal point of the body, as this center, is not trivial. The most accurate approaches to determine the position and location of IMUs with respect to anatomical CORs or joint axes orientation are based on X-ray or magnetic resonance image, but both approaches are high priced, invasive and, ultimately, impractical [Cra17]. Therefore, CORs in the motion analysis field are commonly determined through palpation of external anatomic landmarks by expert therapists or by the use of optical systems [Bon15, Jou18, El 15]. Optical systems use sphere-fitting approaches to find the radius that best fits a trajectory described by optical markers [Hua00, Ehr06, De 14]. Both, the palpation and the optical systems need expert hands to place markers and are limited to controlled environments. These methods entail the use of external information different from the obtained through IMUs, such as the position of markers from the optical system. The use of external sensors limits the ubiquitous utilization of the inertial motion analysis systems based on biomechanical models and increases their costs.

As an alternative, there are different proposals of IMU-based algorithms to determine this location as the IMU-joint positioning vector [See12, Cra16, Fri18a, Mul17a]. We can find two main approaches to estimate the location of joints, the determination of an average IMU-joint vector and the estimation of an adaptive vector at each time instant. They differ in the consideration of the soft tissue artifacts (STA), that is a consequence of the movement of soft tissue layers (muscle, tendon and dermis) between bones and the skin surface. The former approaches model the human body segments as rigid-bodies, assuming that obtaining an average IMU-joint vector, the STA of the motion are compensated and, as a consequence, eliminated. Conversely, the latter approaches take into account the possible variation in the IMU-joint vector caused by STA.

With regard to the methods to obtain an average IMU-joint vector, the AOR location of knees can be estimated by using two IMUs [See12]. Firstly, they assume that the acceleration suffered by both sensors can be related to the joint centers' acceleration

through the acceleration of the sensors around this center. This relationship can be expressed as:

$$\begin{aligned} &\left\| \boldsymbol{a}_A - \Gamma_{S_A}(\mathbf{OA}) \right\| - \left\| \boldsymbol{a}_B - \Gamma_{S_B}(\mathbf{OB}) \right\| = 0, \\ &\Gamma_{S_P}(\mathbf{OP}) := \dot{\boldsymbol{\omega}}_P + \boldsymbol{\omega}_P \times (\boldsymbol{\omega}_P \times \mathbf{OP}), \ P = A, B, \end{aligned} \tag{2.1}$$

where subindex $P = A, B$ discerns the two IMUs located at points $A$ or $B$. The turn rate and angular acceleration of the rigid-solids measured by the IMUs are $\boldsymbol{\omega}$ and $\dot{\boldsymbol{\omega}}$. Vector **OP** is the generic direction vector from O, which refers to the COR, to P, referred to any other arbitrary point of bodies. Their corresponding linear accelerations are $\boldsymbol{a}_O$ and $\boldsymbol{a}_P$, respectively, with $P = A, B$. Notice that $\boldsymbol{\omega}$ and $\dot{\boldsymbol{\omega}}$ of each sensor are distinguished with subindex $P$ in order to identify the corresponding IMU, but these magnitudes are common for the complete rigid-solid. Secondly, since any point of a joint AOR fulfills (2.1), they select the estimation to the point that is the closest to the sensors. The proposal consists in the solution of (2.1) by a Gauss-Newton method, which is tested by adding different levels of signal-to-noise ratio in [See12]. The following work by Seel et al. applies the same method on human gait scenario, but no conclusions on the accuracy in the 3D joint location estimates are given [See14].

This inertial method uses two IMUs per joint, but in a practical way, the employment of more than one IMUs per joint increases the complexity of using inertial systems. Also, one-IMU algorithms have shown a better accuracy than methods that use data from two devices when one of the segments of the joint remains still [Fri18a, Cra17], as in some physical therapy exercises. Therefore, in the following, we focus on the methods that only use one IMU per joint.

McGinnis and Perkins proposed an algorithm based on one IMU and exploiting the relationship between linear acceleration and turn rate in rigid solids [McG13]. The algorithm is based on solving (2.2),

$$\boldsymbol{a}_B = \boldsymbol{a}_O + \dot{\boldsymbol{\omega}} \times \mathbf{OB} + \boldsymbol{\omega} \times (\boldsymbol{\omega} \times \mathbf{OB}) \tag{2.2}$$

that is the equation of accelerations of a rigid-solid body moving in the 3D space. In order to obtain $\boldsymbol{a}_B$ from the specific force measured by IMUs, which is influenced by the gravity force, the vector $\boldsymbol{g}$ is summed to the measurement. The algorithm is aimed at obtaining the location of fixed COR and in this scenario $\boldsymbol{a}_O = 0$. In this way, (2.2) can be rearranged as follows:

$$\boldsymbol{a}_B = \begin{pmatrix} -\omega_y^2 - \omega_z^2 & -\dot{\omega}_z + \omega_x\omega_y & \dot{\omega}_y + \omega_x\omega_z \\ \dot{\omega}_z + \omega_x\omega_y & -\omega_x^2 - \omega_z^2 & -\dot{\omega}_x + \omega_y\omega_z \\ -\dot{\omega}_y + \omega_x\omega_z & \dot{\omega}_x + \omega_y\omega_z & -\omega_x^2 - \omega_y^2 \end{pmatrix} \mathbf{OB}, \tag{2.3}$$

so after the analytic derivation of the turn rate $\boldsymbol{\omega}$, the only unknown parameter is **OB**. *Prior* to this differentiation, the turn rate is filtered with a decimated wavelet denoising approach. The use of a least squares approach to solve (2.3) by employing various

samples gives an error of 3.1 mm in tests with a mechanical analogue of the hip joint performing a determined joint motion (with a specific trajectory, range and velocity).

This method provides an accuracy of 2 mm in a mechanical joint [Cra16], where the method shows dependence on the velocity of motion during tests. This study reports an impact of the angular velocity on the COR identification and non-critical relations with the type and ranges of motion. This algorithm applied on the glen-humeral joint estimation scenario provides an accuracy of 21 mm compared with magnetic resonance images [Cra17]. It was concluded that the location of fixed CORs is more accurate using the information of one IMU in the algorithm of [Cra16] than using data from two IMUs due to the small amplitude of the signals recorded by the IMU placed on the fixed segment and the difficulty related to its tracking. Olsson and Halvorsen [Ols17] tested the same proposal in the case of moving CORs in mechanical simulations, studying different methodologies of solving (2.2). However, the accuracy of this approach on the real scenario of human joints is not reported.

The algorithms explained above obtain a mean value of the IMU-joint vector (**OB**) for each test, averaging the STA. However, the least squares method used in previous proposals (such as [McG13, Cra16, Cra17]) shows no robustness to outliers that may occur as a consequence of STA [Ols17]. Furthermore, the STA can introduce significant errors in the location of the center of joints when assuming an average value of the IMU-joint vector [Fri18a].

To overcome this limitation associated with the STA, Frick and Rahmatalla propose a method to obtain an adaptive IMU-joint vector, $\boldsymbol{r}^k$, at each time instant $k$ with one device attached to a hinge joint [Fri18a]. They use (2.2), but considering that IMUs measure specific force, so they solve the following:

$$\left\| \boldsymbol{f}_A^k + \dot{\boldsymbol{\omega}}^k \times \boldsymbol{r}^k + \boldsymbol{\omega}^k \times \left( \boldsymbol{\omega}^k \times \boldsymbol{r}^k \right) \right\| - \|\boldsymbol{g}\| = 0, \tag{2.4}$$

at each time instant with a gradient descent algorithm. Where $\boldsymbol{f}_A$ refers to the specific force experienced by the IMU, the $\boldsymbol{g}$ vector refers to the gravity force, whose norm is $9.8\,\mathrm{m/s^2}$, and "$\|\cdot\|$" denotes the Euclidean norm. This approach requires its initialization which was only evaluated by using the complete test data with a duration around 25 s in order to find the global minimum instead a local one. Also, prior to apply (2.4), they low-pass filter signals from IMUs and make an analytic differentiation based on a spline conversion of the measured turn rate $\boldsymbol{\omega}$ to obtain the angular acceleration $\dot{\boldsymbol{\omega}}$. This proposal is tested with synthetic data from a 2D-pendulum simulating STA with an attached spring and reports errors of 7.53 mm. In [Fri18b], the algorithm is evaluated with a mechanical hinge joint in which the effect of STA is replicated with the IMU placed on a piece of raw meat. The authors provide results on synthetic data, where the errors range from 10.8 mm to 21.4 mm on the highest STA scenarios. Unfortunately, this algorithm has not been tested on the real scenario of human joints.

Figure 2.2 shows an overview of the approaches for the estimation of the location of CORs with vectors **OB** and $\boldsymbol{r}$, by using one IMU. This overview provides the relationship between the mechanical formulation and the mathematical methods used for their resolution with the different works in the literature and their outcomes.

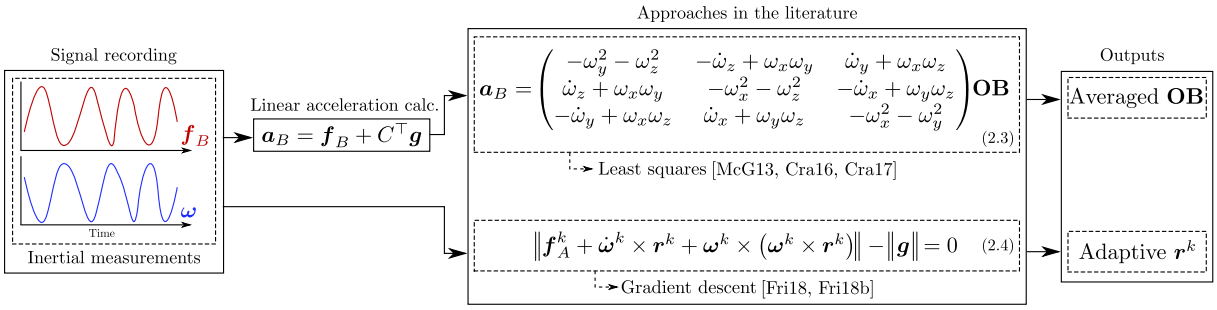


**Figure 2.2:** Overview of the the state-of-the-art methods to locate CORs by using one IMU per joint. After the signal recording, the approaches that obtain one averaged IMU-joint vector, eliminate the gravity influence of the measured specific force by the projection of $\boldsymbol{g}$, for example with the direction cosine matrix [Tit04], $C$, and then obtain the vector by least squares. Conversely, methods that obtain an adaptive IMU-joint vector use directly the IMU measurements through a gradient descent algorithm.

### 2.2.3 IMUs for Qualitative Motion Monitoring

This section focuses on the second approach for human motion monitoring using IMUs, which are based on obtaining qualitative information of the performance of prescribed exercises, instead of the kinematic parameters.

The efficacy of physical programs relies on the patient's adherence and the correct performance of the prescribed routines. Therefore, there is a need for a systematic monitoring of their execution. Recent research has explored the application of technological advances in physical routines monitoring. Video-based and portable technologies are the main alternatives proposed for exercises monitoring [Cus19]. However, as previously mentioned, video technologies are limited to those places where the systems are installed, suffer occlusions and entail patients' privacy concerns [Kom19a, Zih16]. These limitations are overcome by portable technologies as IMUs.

For a practical characterization of physical routines, recent works have investigated the feasibility of IMUs to provide accurate recognition and evaluation of exercises in different human motion fields, as sports and rehabilitation [Cus19, Cam18].

Regarding the recognition of the performed exercise or motion, Zhao and Chen recognized four basketball motions using four IMUs placed on the upper-limbs [Zha20b]. They used the mean, variance and absolute value of the maximum fast Fourier transform (FFT) coefficient of each second of the turn rate and specific force signals. They

tested combinations of these features and the features obtained with principal component analysis (PCA) as different possible inputs of SVMs with Gaussian kernel. The results, obtained with four-fold cross-validation, proved that the PCA features provided the highest accuracy, 96 %.

Also focused on the upper-limbs, but directly related to rehabilitation, Bavan et al. recognized three shoulder rehabilitation motions performed by patients with subacromial shoulder pain [Bav19]. They used only one IMU on the arm that recorded the turn rate, specific force and magnetic field, which were segmented by selecting unique data segments through a peak analysis function. This study evaluated nine time domain features (mean, root mean square, standard deviation, variance, range, inter-quartile range, percentiles and vector pair Pearson correlation coefficients) and four frequency domain features (maximum frequency component, mean frequency component, energy spectral density, entropy and kurtosis). Four ML algorithms (DT, SVM, KNN and RF) were evaluated using a ten-fold cross-validation and obtained an accuracy over 90 %. However, when they used a leave-one-subject-out (LOSO) cross-validation with the best algorithm (RF), the accuracy decreased to a maximum of 80 %.

More complex motions that included the complete body have been analyzed using five IMUs placed on the upper-and lower-limbs and one on the trunk of one side of the body [Pre20]. The motions of study were clean and jerk, box jump, American swing and burpees, and they also took into account and classified the transition intervals when no exercise was being performed. Nine time domain features (mean, standard deviation, root mean square, mean absolute deviation, maximum, minimum, kurtosis, skewness and quartiles) and seven frequency domain features (mean, power, higher frequency, lower frequency, median frequency, mean frequency and spectral entropy) were the inputs for the SVM and KNN algorithms. They evaluated different SVM and KNN kernels and sliding window sizes until 600 ms. They found that the cubic kernel SVM with 600 ms window length obtained the best results for the five-fold cross-validation, with an average accuracy of 99.1 %. With a LOSO cross-validation, this algorithm obtained an average accuracy of 97.6 %.

On the other hand, for the exercises evaluation, the performance of a variety of exercises have been individually assessed. The lunge exercise has been evaluated using five IMUs on the lumbar spine and lower-limbs [Whe16]. They used sixteen features per signal (signal peak, valley, range, mean, standard deviation, skewness, kurtosis, signal energy, level crossing rate, variance, first and third quartiles, median and the variance of both the approximate and detailed wavelet coefficients). The binary classification between correct and incorrect performances was evaluated using RF and achieved an accuracy of 90 %. They also analyzed the classification of the specific deviations, as external rotation of foots or short or long starting stances, and found an accuracy around 70 %. Similarly, the single-leg squats exercise has been evaluated using three IMUs on

the low back and on one leg [Kia17]. They used an extended Kalman filter with a biomechanical model proposed in [Lin13] to estimate the human pose. As in [Whe16], signals were segmented into exercises repetitions, but in this case only time domain features are used (root mean square, standard deviation, variance, mean, mean absolute deviation, skewness, kurtosis, range, minimum, and maximum). They used a LOSO cross-validation for the binary classification between correct and wrong performances, and they reported an accuracy of 90 % with Naive Bayes (NB), closely followed by SVM, which obtained 89 % of accuracy.

A variety of exercises have been individually evaluated in other studies, based on the knowledge of the type of exercise executed. In [Gig14], they used a logistic regression to individually classify between correct and incorrect variations of seven leg exercises. Ten features (mean, standard deviation, skewness, kurtosis, signal energy, level crossing rate, signal range, first and third quartiles and the variance of the wavelet coefficients) were obtained from the measured turn rate, specific force and from the estimated acceleration magnitude and orientation angles, pitch and roll. They monitored the motions with three IMUs placed on the thigh, shin and foot and reported an accuracy between 81 and 83 %.

Using the same placement of IMUs on legs, in [Hua16a], more ML algorithms were applied to evaluate a set of seven leg rehabilitation exercises in order to study the optimal IMU placement and combination. In that work, they evaluated logistic regression, together with DT, MLP, SVM, RF and Adaboost classifiers, which combine different ML algorithms to improve their final classifications, and averaged the metrics reported by all the methods. They segmented signals into exercises repetitions and obtained ten time domain features (mean, standard deviation, skewness, kurtosis, maximum, minimum, range, first and third quartiles and cross-correlation), sixteen coefficients of the FFT as frequency domain features and thirty-two wavelet coefficients as time-frequency features. They obtained an averaged accuracy for all the classifiers between 78 % and 97 % in the exercises evaluation.

More recently, four different knee rehabilitation exercises have been evaluated [Bev18]. To do so, they used a single inertial sensor placed on the shin that measured the turn rate and specific force, and they estimated the turn rate magnitude and the pitch and roll angles. They segmented the exercises repetitions and obtained fifteen time domain features (mean, median, standard deviation, variance, range, kurtosis, skewness, maximum, minimum, positive mean, negative mean, sum of absolute differences, first and third quartiles, and the correlation index between pitch and roll signals) and twenty-five frequency domain features (energy, energy ratio, energy average, harmonic ratio, energy entropy, and the first 20 coefficients of the FFT). They achieved a binary classification using RF and DT with accuracies that ranged between 88 % and 97 %.

IMUs have also been used for the upper-limb exercises evaluation. Pereira et al. com-

bined two inertial sensors with sEMG sensors to supervise two upper-limb exercises and one lower-limb exercise [Per19]. The inertial sensors were placed on the arm in all exercises whereas the sEMG sensors were placed according to the exercises on the back or lower-limbs. Three statistical features (skewness, kurtosis and histogram) and nine time domain features (mean, median, maximum, minimum, variance, temporal centroid, standard deviation, root mean square, and auto correlation) were used. Feature selection was based on the study of their correlations. They carried out the exercises evaluation with DT, KNN, SVM and RF and obtained an accuracy about 92 % with all the classifiers.

With respect to the gait assessment, in [Alc17], they studied the quality of gait in order to classify 30 volunteers as healthy or unhealthy. They used seven IMUs placed on the lower-limbs and the lumbar zone to record the turn rate and specific force and fuse their signals to estimate the joint angles through an EKF. They used nine features (motion intensity, peak asymmetry factor, step period, stride period, regularity, sum of power spectral density, spectral entropy, sum signal-to-noise-modulation-ratio and wavelet entropy) for the classification. They applied a Linear Discriminant Analysis (LDA), PCA and NB to obtain accuracies of 100 %, 86 % and 100 %, respectively.

As can be inferred, there is a great diversity of algorithms used in the exercise recognition and evaluation. Although, according to [Cam18, Cus19], the most promising algorithms for these objectives are SVM, RF, KNN and ANN. A variety of features are also extracted from the IMU signals, although the most common are the statistical features in the time domain, such as mean, standard deviation and maximum and minimum of signals. In addition, signal segmentation is approached from two main perspectives: window-based and repetition-based. Repetition-based segmentation involves further signal processing to detect the start and end of repetitions, and window-based segmentation involves determining the most appropriate window size. In the methods found in the literature, window sizes go up to 6 s, although in [Ban14b] the window interval of $1 - 2$ s was shown to be the best trade-off solution between accuracy and speed of activity recognition.

This review of the methods focused on a qualitative motion monitoring highlights the need of studying the recognition and evaluation of exercises as a single and complex task, specially for the monitoring of prescribed routines related to health. Virtual coaches, aimed for being used in unsupervised environments, are required to provide a complete characterization of the executed routines. Therefore, it is important to find the most suitable approach for this complex characterization.

### 2.2.4 Available Datasets for Motion Analysis and Monitoring

One of the limitations detected in the inertial monitoring systems analyzed in this review is the lack of data to jointly validate or compare the proposed algorithms, as well as for the development and validation of new proposals. Data are needed for both IMU-based monitoring approaches addressed in this work: the estimation of kinematic parameters and the qualification of the performance of prescribed exercises.

Recent research works have focused on the creation of datasets by using different sensory systems. Video-based and portable technologies are the main alternatives in the monitoring of human activities [Cus19]. The existing physical exercises databases aimed for physical therapies are recorded with optical systems, such as three-dimensional systems and RGB together with depth sensors [Vak18], or only with the RGB-depth systems [Ar14]. The use of solely optical systems implies a limitation for the physical therapies that can only be performed in controlled environments where no occlusions occur. However, as aforementioned, video-based technologies entail occlusions and patients' privacy concerns [Kom19b, Zih16].

Conversely, portable systems, such as IMUs, are becoming increasingly popular because of its practicality and its everywhere usable potential [Lop16]. IMU-based databases of human motion monitoring commonly focus on the study and assessment of gait [Luo20] or activities of daily living [Sau18].

Existing inertial databases related with the human motion monitoring commonly study walk patterns and variations [Luo20, Len19, Kwo19], activities of daily living [Acc18, Rod19, Jar19, Rei12] or are specific for different sports, such as football [Fin19] or karate [Szc21], but few data of prescribed exercises are publicly available. However, as they do not cover the need for physical exercises monitoring, there is still a lack of available data for the monitoring of commonly prescribed routines.

## 2.3 Relationship with our Work

To conclude, there are still challenges to overcome to achieve remote IMU-based monitoring of exercise routines. The most important limitations that are identified along this review of the State of the Art can be summarized as follows:

- the IMU-joint calibration of legs to obtain the parameters required in motion analysis algorithms,

- the adaptation of these algorithms to STA scenarios, which are the most realistic in the human body,

- the lack of available data to validate and compare new motion monitoring proposals,
- the complete characterization of the performed motions in a remote monitoring of physical therapies.

As seen in this section, different approaches have tried to address these challenges. In this work, we provide different alternative IMU-based solutions by the combination of just gyroscopes and accelerometers.

# Chapter 3

# IMU-based Characterization of Joints

One of the objectives of this thesis is to obtain a complete leg characterization, which is a key requirement in multiple applications of human motion analysis. CORs and AORs are two parameters commonly needed in the development of inertial monitoring systems based on biomechanical models, designed to reduce the drift associated to inertial systems, as expounded in section 2.2.1. The gold standard method to characterize limbs uses stereophotogrammetric measurements, but their limitations of costs and controlled environments make them impractical. Therefore, inertial systems aimed at characterizing limbs are needed, as discussed in section 2.2.2.

This chapter focuses on the inertial characterization of joints applied to lower-limbs. We extend and validate an IMU-based leg characterization method for its use on the estimation of axes and introduce a method to obtain two parameters of legs commonly required by biomechanical models of lower-limbs: the location of joint centers and axes, and the segment lengths.

To do so, we make use of the null acceleration point in rotation centers and axes in joints and the trigonometric relations between them. We implement four different versions of the proposed method, which are compared using a stereophotogrammetric system as reference. We validate the method with four volunteers by doing five exercises, so we also analyze the influence of motions in the determination of the location of joints.

The main outcome of this chapter is a validated method for a complete characterization of lower-limbs. We provide the accuracy of the proposal, as well as the best motions to obtain the highest accuracy and the most suitable signal processing approach for the calibration of legs.

## 3.1 Proposed Method

In this section, we detail the algorithm for characterizing leg joints. The characterization consist of two main steps: determination of the joints rotation centers and axes, and estimation of the length of the leg segments. We first detail the method to determine the location of CORs and AORs in legs using one IMU per joint. Then, since we obtain the length of leg segments by trigonometric relations, we explain the procedure for the alignment of their frames. Finally, we detail all the positioning vectors and segment lengths obtained for the lower-limbs.

### 3.1.1 Center and Axis Determination

The goal of the proposed method is to determine the rotation centers and axes of joints. The algorithm is based on the relationship between the linear acceleration of two arbitrary points O and B of a rigid body during free motion, which has been previously introduced in section 2.2.2, but repeated in (3.1) for clarity.

$$\boldsymbol{a}_B = \boldsymbol{a}_O + \dot{\boldsymbol{\omega}} \times \mathbf{OB} + \boldsymbol{\omega} \times (\boldsymbol{\omega} \times \mathbf{OB}) \tag{3.1}$$

We define point O as the rotation center or axis, depending on the case, and B as the origin of the sensor frame. The linear acceleration of two points O and B on a rigid body, $\boldsymbol{a}_O$ and $\boldsymbol{a}_B$, are related by means of the turn rate $\boldsymbol{\omega}$, the angular acceleration $\dot{\boldsymbol{\omega}}$ and the distance vector between these points **OB**, see Figure 3.1. Notice that the linear accelerations are applied in specific points but the turn rate and the angular acceleration are referred to the body. Angular magnitudes are common for each point of the body, but linear magnitudes depend on the distance from the point to the center of rotation.

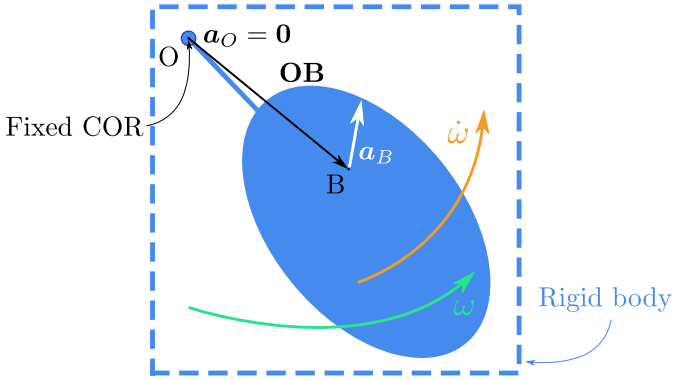


**Figure 3.1:** Rigid body moving in the three-dimensional space around a fixed COR (O), with turn rate $\boldsymbol{\omega}$ and angular acceleration $\dot{\boldsymbol{\omega}}$. O is the fixed COR and B represents any other arbitrary point of this body. Their linear accelerations are $\boldsymbol{a}_O$ and $\boldsymbol{a}_B$, respectively. The director vector of our interest in this chapter is **OB**.

Vector $\boldsymbol{\omega}$ is the turn rate measured by the IMU gyroscope. We calculate the angular acceleration $\dot{\boldsymbol{\omega}}$ as the three-points derivative of the measured turn rate $\boldsymbol{\omega}$. Since IMUs measure the specific force $\boldsymbol{f}_B$ and (3.1) requires the linear acceleration $\boldsymbol{a}_B$, the gravitational acceleration $\boldsymbol{g}$ must be subtracted from the measurements. To model the gravity influence and subtract it, we obtain the IMU orientation with respect to the gravity vector.

We use the attitude tracking algorithm detailed in [Dia19] to estimate the IMU orientation. This algorithm estimates the Euler angles using the measurements of the gyroscopes with a gravity update that corrects the estimation of the roll and pitch angles. The Euler angles are translated to the direction cosine matrix, $C$, to make transformations from the sensor frame, which moves with the IMUs, to the global frame, which is fixed. In this way, the gravity force is subtracted from the measurements as follows:

$$\boldsymbol{a}_B = \boldsymbol{f}_B + C^\top \boldsymbol{g}, \tag{3.2}$$

where the gravity vector $\boldsymbol{g}$ is defined as $-9.8\mathbf{k}\,\mathrm{m/s^2}$, being $\mathbf{k}$ the vertical vector that points upwards in the global frame.

The magnetometer is not used, as proposed in [Cra16], because its measurements can be distorted by magnetic disturbances, that are more or less significant depending on the environment and we aim to develop an everywhere-usable method. Besides, since $\boldsymbol{g}$ is vertical, the rotation angle over the $\mathbf{k}$ axis, also vertical, can have errors because it does not affect the result of the rotation of $\boldsymbol{g}$ to project it into the IMU frame.

The linear acceleration $\boldsymbol{a}_B$ in the sensor is obtained from (3.2) and the linear acceleration of the rotation center or axis, $\boldsymbol{a}_O$, is assumed zero. Thus, expanding the cross products and collecting the obtained elements by the **OB** components, we can rearrange (3.1) as the following linear equation:

$$\boldsymbol{a}_B = M\mathbf{OB}, \tag{3.3}$$

where:

$$M = \begin{pmatrix} -\omega_y^2 - \omega_z^2 & -\dot{\omega}_z + \omega_x\omega_y & \dot{\omega}_y + \omega_x\omega_z \\ \dot{\omega}_z + \omega_x\omega_y & -\omega_x^2 - \omega_z^2 & -\dot{\omega}_x + \omega_y\omega_z \\ -\dot{\omega}_y + \omega_x\omega_z & \dot{\omega}_x + \omega_y\omega_z & -\omega_x^2 - \omega_y^2 \end{pmatrix}. \tag{3.4}$$

When (3.3) is applied to determine axes positions, the system is indeterminate. That occurs when the body rotates over a single axis, over parallel axes or if the algorithm is employed in real-time applications for axis determination. In the above-mentioned situations, the matrix $M$ becomes singular and there is not a unique solution, each point of the rotation axis fulfills (3.3).

As a solution, we obtain the Moore-Penrose pseudo-inverse $B$ of the matrix $M$ [Pen55]. Moore-Penrose pseudo-inverse $B$ is obtained by singular value decomposition (SVD)

of the matrix $M$ as follows:

$$B = VS^{-1}U, \tag{3.5}$$

where matrices $V$ and $U$ contain the right and left singular vectors and matrix $S$ the singular values of the matrix $M$. In this way, we ensure to obtain a unique solution to the system. The solution corresponds to the vector **OB** with the lowest norm that fulfills (3.3).

Furthermore, we use SVD because it provides more relevant information about the AOR than their location. The singular vectors of a system describing motion provide the directions of this motion ordered by the amount of movement or variance in these directions (for more details about SVD, see Appendix A.2). In the scenario of determining an AOR, there is no motion in the direction of this axis. As a consequence, the direction associated to the smallest eigenvalue, which has to be almost null, is the direction of the AOR. In this way, we can obtain the direction of the AOR by obtaining the SVD of $M$ and determining the direction associated to the smallest eigenvalue. We tested this approach of SVD for the determination of the direction of AORs in a mechanical hinge in [Gar18]. We found deviation angles between the estimated direction AORs and the reference of $0.5\,^{\circ}$ using one IMU per segment. In this way, using SVD we completely characterize the two kind of joints considered in this work, spherical and hinge joints.

### 3.1.2 Leg Characterization

We determine the positioning vector **OB** from each IMU to each leg joint center and axis using (3.3). The vectors needed to characterize a leg using IMUs are depicted in Figure 3.2. The vectors that we obtain directly from (3.3) are **TH**, **SH**, **SK** and **SA**. The combination of those vectors with the knowledge about the leg structure allows us to characterize the lower-limbs obtaining their lengths and all their distance vectors.

We obtain an average vector assuming that the location of CORs and AORs with respect to the IMUs remains constant. However, the human body presents mobile AORs, as the one in knees, whose relative location changes along motions. We evaluate the error associated to this assumption in [Gar18] in synthetic data and found an error between 0.33 and 0.49 radius of joint units, that increases with the increment of the joint range of motion. Since this error is of the order of millimeters and occurs in the estimation of a value of several tens of centimeters, it is an error about 1%, in other words, an acceptable error for this application.

Using the positioning vectors obtained by $\text{IMU}_\text{S}$, we estimate the positioning vector of the thigh **HK** and the shin **KA**. The vector **HK** is defined from the hip center H to the knee axis K, and the vector associated to the shin, **KA**, goes from the knee axis K to the

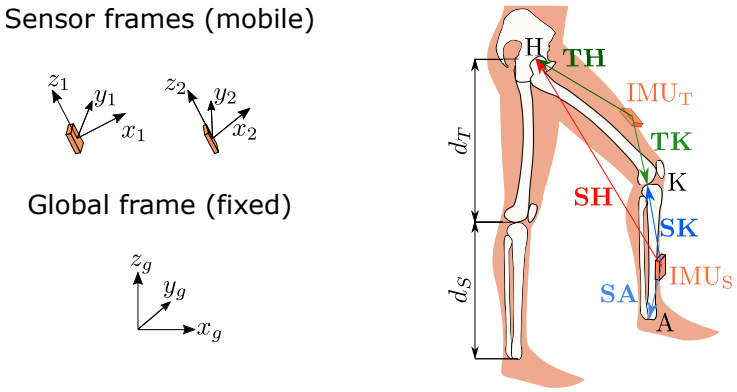


**Figure 3.2:** Left: sensor and global frames. Global frame is fixed but sensor frames depends on the sensor position. Right: illustration of a leg with the estimated vectors. The vectors **TH** and **TK** begin in the accelerometer of the IMU placed on the thigh $IMU_T$ and end in the hip center H and knee axis K, respectively. The vectors **SH**, **SK** and **SA** begin in the accelerometer of the IMU placed on the shin $IMU_S$ and end in the hip center H, knee axis K and ankle center A, respectively. $d_T$ and $d_S$ refers to the thigh and shin lengths.

ankle center A. In this way, vectors **HK** and **KA** are obtained using:

$$\begin{aligned} \mathbf{HK} &= \mathbf{HS} - \mathbf{KS} \\ \mathbf{KA} &= \mathbf{KS} - \mathbf{AS} \end{aligned}. \tag{3.6}$$

The Euclidean norms of vectors **HK** and **KA** correspond to the thigh and shin lengths, $d_T$ and $d_S$, see Figure 3.2.

The vector **TK** cannot be directly obtained due to the difficulty of movements with thigh movement keeping the knee still. The estimation of the vector **TK** is carried out by means of trigonometric relations as follows:

$$\mathbf{TK} = \mathbf{TH} + \mathbf{HK}. \tag{3.7}$$

### 3.1.3 Frames Alignment

The IMU measurements and the distance vectors are expressed in the respective sensor frame, see Figure 3.2. Even if the sensors are carefully placed, it is unlikely that they are aligned. In order to calculate parameters based on trigonometric relationships, distance vectors must be expressed in the same reference frame, aligned frames or axis deviations must be known. We choose to transform the vectors into a common reference frame, composed of the X', Y' and Z' axes, to simplify equations.

We use the hip flex-extension movement, see Figure 3.3, to define the direction of Y' axis in this common frame. We define the direction vector $\mathbf{y'}_s$ of Y' axis as the normalized mean of the turn rate $\boldsymbol{\omega}$ measured during the hip flex-extension motion in one direction. The direction vector of the Z' axis, $\mathbf{z'}_s$, is established parallel to the gravity

vector $\boldsymbol{g}$ measured in standing position. The gravity vector $\boldsymbol{g}$ is never parallel to vector $\mathbf{y'}_s$ to due to the hip flex-extension exercise specifications. The direction vector of X' axis, $\mathbf{x'}_s$, is obtained as the cross product between $\mathbf{y'}_s$ and $\mathbf{z'}_s$. To ensure an orthogonal frame, the direction vector of Y' axis, $\mathbf{y'}_s$, is calculated again as the cross product between the direction vectors $\mathbf{z'}_s$ and $\mathbf{x'}_s$. Thus, we transform the measurements from each sensor frame to the common frame as:

$$\mathbf{v}_c = \left[\mathbf{x'}_s\mathbf{y'}_s\mathbf{z'}_s\right]\mathbf{v}_s, \tag{3.8}$$

where $\mathbf{x'}_s$, $\mathbf{y'}_s$ and $\mathbf{z'}_s$ are expressed in coordinates of the sensor frame. Vectors $\mathbf{v}_c$ and $\mathbf{v}_s$ are the coordinates of vector $\mathbf{v}$ with respect to the common frame and the sensor frame, respectively.

### 3.1.4 Signal Processing

The proposed method requires that CORs or AORs remain still during the motion so $\boldsymbol{a}_O = \mathbf{0}$ and (3.1) can be rearranged as (3.3). The only option to accomplish this requirement in the calibration of legs is performing slow motions, since fast ones entail trunk instability. However, to obtain the highest accuracy by using (3.3) to determine CORs, movements have to be executed with a turn rate above 2.5 rad/s [Cra16]. An existent approach is to dismiss the signal intervals when the measured turn rate norm does not exceed 0.5 rad/s [Cra17], but this thresholding implies a data loss between 20 % and 60 % depending of the exercise requirements.

As an alternative we propose the adjustment of the method in order to use (3.3) even with slow motions, which are characteristic of lower-limb calibration motions. The adaptation, hereafter named $\text{NAP}_f$, is based on signal preprocessing. We low-pass filter the signals with a 7-order Butterworth filter with delay correction. Due to the movement slowness, we assess the algorithm performance using the low cutoff frequencies: 3, 7 and 15 Hz. We use our implementation of the proposal [Cra17] as a benchmark and we name it $\text{NAP}_\omega$.

## 3.2 Experimental Results

In this section, we describe the measurement campaign, the performed exercises and the results obtained. The measurement campaign is detailed in terms of the studied population characteristics, the employed systems and the algorithms involved in the measurements. Also, we present and discuss the accuracy of the $\text{NAP}_\omega$ and $\text{NAP}_f$ algorithms.

### 3.2.1 Measurement Campaign

We recorded the data of these experiments in the DLR (German Aerospace Center) during a research stay, as detailed in section 1.3. We used the Mw inertial sensors from Xsens [Xse20], and the Vicon motion capture system [Vic20] as *gold standard* to validate our proposals. Both inertial and optical measurements were recorded at a sampling rate of 100 Hz. The Vicon system provided the position and orientation of IMUs and the position of each marker used to capture the IMUs. We used these data to determine the CORs and AORs of leg joints by means of the algorithm presented in [Ehr06].

Four volunteers from the DLR staff participated in the study. Their average height was $167 \pm 2$ cm. The volunteers performed the exercises detailed in section 3.2.2. The volunteers were equipped with two IMUs placed on the thigh and shin, see Figure 3.2. Four passive reflectors were also located on the thigh and five passive reflectors on the shin.

### 3.2.2 Exercises

The volunteers performed 5 exercises to estimate the location of the different leg centers and axes. The exercises are classified according to the joint whose location is estimated: hip, knee or ankle.

During the hip exercises, the volunteers remained in standing position and their backs rested on a stable surface. The foot of the non-instrumented leg was fixed on the floor and the instrumented leg moved remaining straight. The hip center H was determined with respect to both sensors $\text{IMU}_\text{T}$ and $\text{IMU}_\text{S}$. We evaluated the performance of the algorithm in the hip center H doing 2 exercises: leg crosses, labeled as cross; and leg circles, labeled as circle. The cross and circle movements are depicted in Figure 3.3. The exercises were performed by the instrumented leg as follows:

- Cross: the series consisted in a hip flex-extension cycle followed by a hip abduction and adduction cycle. The cross movement was repeated 10 times.
- Circle: the movement mixed circular movements over the inclination around 20 ° with rotations on the leg internal and external rotation axis. Each volunteer repeated the circle movement 10 times.

To locate the knee axis K with respect to the $\text{IMU}_\text{S}$, the volunteers performed knee flex-extensions. The volunteers remained sitting on a stable surface to do knee bending. The non-instrumented leg was still and the instrumented leg moves. The instrumented leg moved forward 10 times from the vertical position of the shin to an inclination around 20 °, see Figure 3.3.

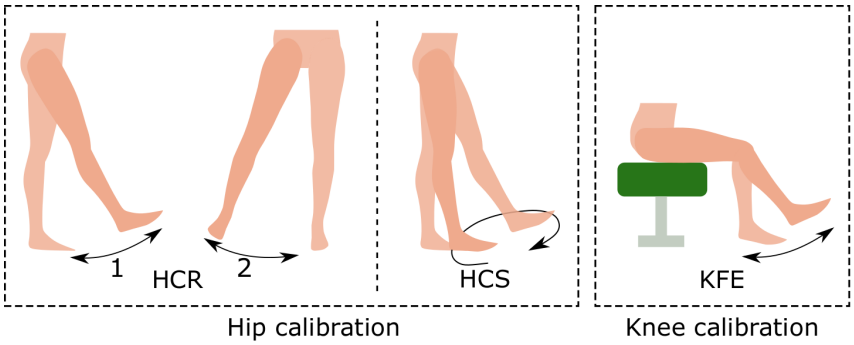


**Figure 3.3:** Calibration exercises for hip and knee. HCR and HCS are the exercises cross and circle. Both cross and circle are referred to exercises of hip center H location. The knee bending (KFE) is the motion carried out to determine the knee axis K location.

Finally, the volunteers performed two exercises to locate the ankle center with respect to the $IMU_S$: squats and inverse pendulum, illustrated in Figure 3.4. The volunteers began in standing position for both exercises. The squats and pendulum motions are detailed below:

- Squats: the volunteer flexed both knees and hip with the feet fixed on the floor and moved back to the initial position. The movement was repeated 10 times.
- Pendulum: the instrumented leg foot remained fixed and the body moved around. The non-instrumented leg motions were free. The body moves 10 times in forward-backward directions with slight deviations.

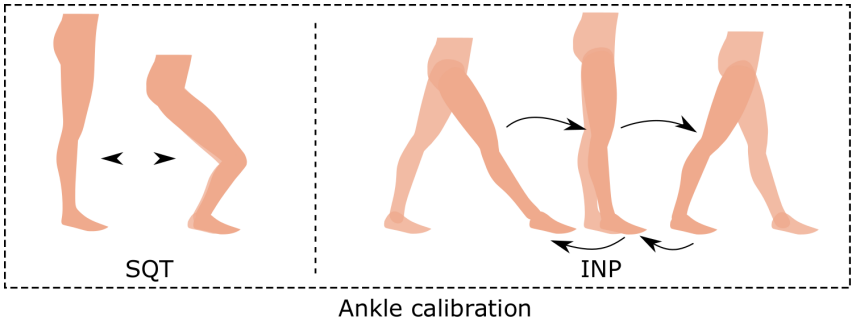


**Figure 3.4:** Ankle calibration exercises for ankle center A location. The exercise squats is labeled with SQT and the exercise pendulum with INP.

### 3.2.3 Evaluation

#### Direct calculation vectors

We establish the reference vectors $\mathbf{TH}_r$, $\mathbf{SH}_r$, $\mathbf{SK}_r$ and $\mathbf{SA}_r$, see Figure 3.2, as the positioning vectors obtained by the stereophotogrammetric system. We obtain the reference vectors from the exercises that had the lowest number of occlusions. Thus, the

exercises used to determine the reference measurements are circle, knee bending and pendulum, see Figure 3.3 and Figure 3.4. The reference vector norms $TH_r$, $SH_r$, $SK_r$ and $SA_r$ are shown in Table 3.1 as mean and standard deviation for each volunteer and the average values.

**Table 3.1:** Reference vector norm for each volunteer (mm) and average norms.

| | Volunteer 1 | Volunteer 2 | Volunteer 3 | Volunteer 4 | Average |
|---|---|---|---|---|---|
| $TH_r$ (mm) | $166 \pm 4$ | $223 \pm 6$ | $170 \pm 5$ | $233 \pm 7$ | $198 \pm 11$ |
| $SH_r$ (mm) | $573 \pm 5$ | $515 \pm 17$ | $538 \pm 11$ | $541 \pm 9$ | $542 \pm 23$ |
| $SK_r$ (mm) | $214 \pm 3$ | $183 \pm 3$ | $166 \pm 3$ | $210 \pm 4$ | $193 \pm 7$ |
| $SA_r$ (mm) | $177 \pm 2$ | $216 \pm 4$ | $265 \pm 3$ | $210 \pm 4$ | $217 \pm 7$ |

We evaluate the accuracy of the $NAP_\omega$ and $NAP_f$ algorithms. Our error metric is the norm of the average distance vector between the vectors estimated by each algorithm to the reference vector. We note the variations in the $NAP_f$ algorithm as the cutoff frequency used to filter the signal, e.g. label "fc=3Hz" corresponds to the $NAP_f$ algorithm error using low-pass filtered signals with a cutoff frequency of 3 Hz. The results are sorted by exercises in order to assess the most suitable movement for each application.

We name the error in the hip center H calibration referred to the $IMU_T$ as $\Delta TH$. Table 3.2 and Figure 3.5 present $\Delta TH$ for the exercise cross, and Table 3.3 and Figure 3.6 correspond to the same error, $\Delta TH$, for the exercise circle. The averaged $\Delta TH$ using $NAP_\omega$ is over 80 mm for both evaluated exercises. This error decreases with the signal filtering until 20 mm for cross exercise and 22 mm for circle exercise with the lowest cutoff frequency. Thus, the $NAP_f$ algorithm is the most accurate to obtain vector **TH** performing these motions. With regard to the exercise discrimination, $\Delta TH$ varies less than 10 mm between exercises cross and circle for all volunteers. Since both exercises present similar accuracy, they are equally suitable to estimate the **TH** vector.

**Table 3.2:** $\Delta TH$ error for the exercise cross (mm).

| | Volunteer 1 | Volunteer 2 | Volunteer 3 | Volunteer 4 | Average |
|---|---|---|---|---|---|
| $NAP_\omega$ | $85 \pm 4$ | $87 \pm 4$ | $100 \pm 5$ | $102 \pm 6$ | $93 \pm 10$ |
| fc=3Hz | $\mathbf{35 \pm 4}$ | $\mathbf{12 \pm 4}$ | $\mathbf{22 \pm 6}$ | $\mathbf{16 \pm 7}$ | $\mathbf{21 \pm 11}$ |
| fc=7Hz | $47 \pm 4$ | $35 \pm 4$ | $39 \pm 5$ | $21 \pm 5$ | $35 \pm 9$ |
| fc=15Hz | $81 \pm 4$ | $76 \pm 4$ | $95 \pm 5$ | $94 \pm 3$ | $86 \pm 8$ |

The accuracy in the hip center H calibration referred to the $IMU_S$ is assessed in terms of $\Delta SH$ error. Table 3.4 and Figure 3.7 show the error $\Delta SH$ for the exercise cross, and Table 3.5 and Figure 3.8 for the exercise circle. As in the previous case, the average error from the $NAP_\omega$ algorithm is higher than the obtained using $NAP_f$, and the lower the

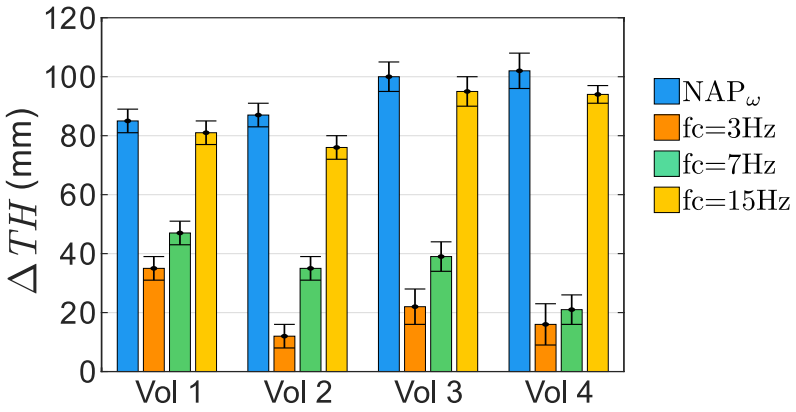


**Figure 3.5:** Bar chart of $\Delta TH$ for each volunteer (Vol $1-4$) and algorithm for the exercise cross. The error $\Delta TH$ is associated to the director vector from the IMU$_\mathrm{T}$ to the hip (H).

**Table 3.3:** $\Delta TH$ error for the exercise circle (mm).

| | Volunteer 1 | Volunteer 2 | Volunteer 3 | Volunteer 4 | Average |
|---|---|---|---|---|---|
| NAP$_\omega$ | $70 \pm 3$ | $61 \pm 6$ | $98 \pm 4$ | $97 \pm 9$ | $81 \pm 12$ |
| fc=3Hz | $\mathbf{19 \pm 6}$ | $\mathbf{13 \pm 5}$ | $\mathbf{20 \pm 3}$ | $25 \pm 4$ | $\mathbf{19 \pm 9}$ |
| fc=7Hz | $25 \pm 4$ | $34 \pm 6$ | $36 \pm 3$ | $\mathbf{18 \pm 4}$ | $28 \pm 9$ |
| fc=15Hz | $66 \pm 3$ | $57 \pm 6$ | $90 \pm 3$ | $87 \pm 5$ | $75 \pm 9$ |

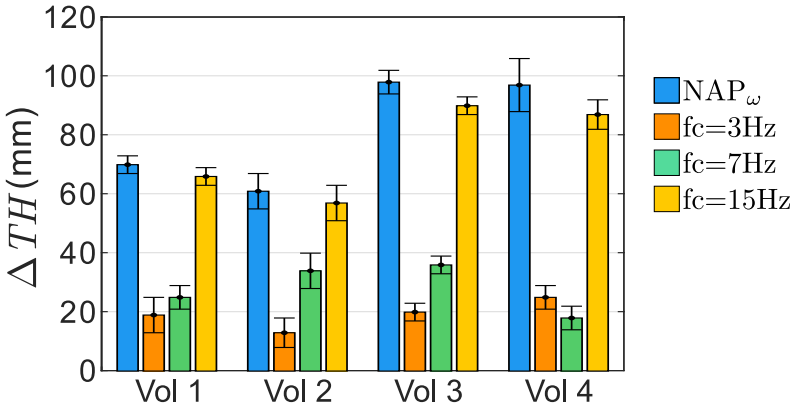


**Figure 3.6:** Bar chart of $\Delta TH$ for each volunteer (Vol $1-4$) and algorithm for the exercise circle. The error $\Delta TH$ is associated to the director vector from the IMU$_\mathrm{T}$ to the hip (H).

cutoff frequency is, the smaller $\Delta SH$. The average error reduction is over 50 mm for the evaluated exercises comparing $\text{NAP}_\omega$ algorithm with $\text{NAP}_f$ using a cutoff frequency of 3 Hz. Furthermore, the error $\Delta SH$ decreases in the exercise circle versus the exercise cross. We obtain an average $\Delta SH$ error of 67 mm for the exercise cross and 36 mm for the exercise circle. The error $\Delta SH$ is over 31 mm smaller in the exercise circle than in the exercise cross. The main reason of the error associated to the exercise cross is the loss of stiffness in the knee when performing the leg flex-extension movement. Conversely, volunteers keep the leg stiffness to perform leg circles for the exercise circle. Therefore, the movement of cross has to be dismissed for the estimation of vector **SH**.

**Table 3.4:** $\Delta SH$ error for the exercise cross (mm).

| | Volunteer 1 | Volunteer 2 | Volunteer 3 | Volunteer 4 | Average |
|---|---|---|---|---|---|
| $\text{NAP}_\omega$ | $92 \pm 5$ | $58 \pm 12$ | $162 \pm 11$ | $156 \pm 10$ | $117 \pm 20$ |
| fc=3Hz | $\mathbf{39 \pm 5}$ | $\mathbf{25 \pm 6}$ | $\mathbf{43 \pm 10}$ | $\mathbf{91 \pm 9}$ | $\mathbf{49 \pm 16}$ |
| fc=7Hz | $56 \pm 5$ | $38 \pm 11$ | $105 \pm 11$ | $132 \pm 10$ | $83 \pm 19$ |
| fc=15Hz | $83 \pm 5$ | $4.9 \pm 12$ | $151 \pm 11$ | $151 \pm 9$ | $108 \pm 19$ |

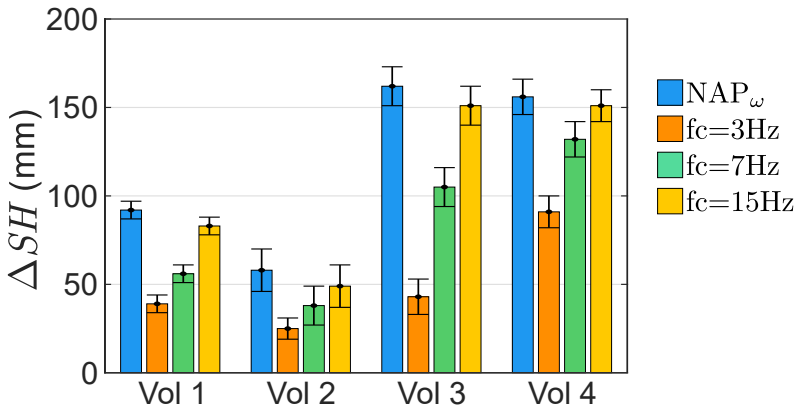


**Figure 3.7:** Bar chart of $\Delta SH$ for each volunteer (Vol $1-4$) and algorithm for the exercise cross. NAP$\omega$ corresponds to the algorithm from [Cra18]. The error $\Delta SH$ is associated to the director vector from the $\text{IMU}_\text{S}$ to the hip (H).

**Table 3.5:** $\Delta SH$ error for the exercise circle (mm).

| | Volunteer 1 | Volunteer 2 | Volunteer 3 | Volunteer 4 | Average |
|---|---|---|---|---|---|
| $\text{NAP}_\omega$ | $95 \pm 10$ | $37 \pm 8$ | $106 \pm 16$ | $107 \pm 11$ | $86 \pm 23$ |
| fc=3Hz | $\mathbf{35 \pm 6}$ | $\mathbf{18 \pm 8}$ | $\mathbf{32 \pm 10}$ | $\mathbf{44 \pm 10}$ | $\mathbf{32 \pm 14}$ |
| fc=7Hz | $53 \pm 7$ | $24 \pm 8$ | $61 \pm 14$ | $60 \pm 11$ | $49 \pm 21$ |
| fc=15Hz | $83 \pm 10$ | $31 \pm 8$ | $99 \pm 16$ | $96 \pm 11$ | $77 \pm 23$ |

We name $\Delta SK$ to the errors for the knee axis K calibration referred to the $\text{IMU}_\text{S}$. Table 3.6 and Figure 3.9 present the error $\Delta SK$. The error $\Delta SK$ presents a higher reduction

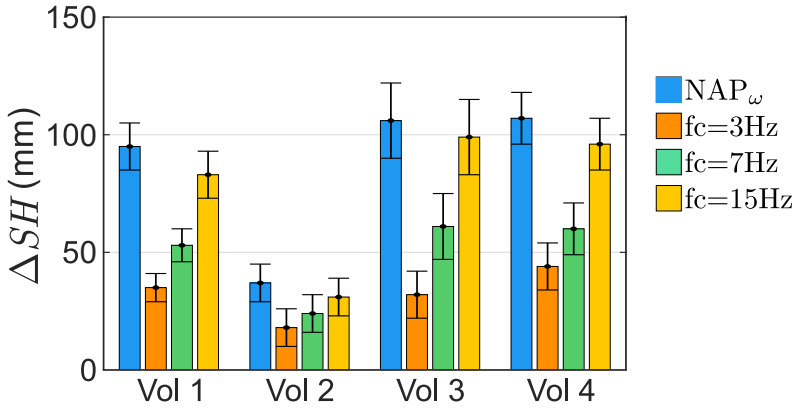


**Figure 3.8:** Bar chart of $\Delta SH$ for each volunteer (Vol $1-4$) and algorithm for the exercise circle. The error $\Delta SH$ is associated to the director vector from the IMU$_S$ to the hip (H).

as the lower cutoff frequency is for all volunteers but volunteer 3. However, the error $\Delta SK$ varies in 1 mm using the lowest cutoff frequency versus the most accurate method so this variation is negligible. The error $\Delta SK$ average improves using the NAP$_f$ algorithm with the lowest cutoff frequency versus the NAP$_\omega$ in 25 mm. The error $\Delta SK$ from the NAP$_f$ algorithm with the lowest cutoff is 9 % of SK$_r$. The error $\Delta SK$ is mostly caused by the assumption that the rotation axis has null linear acceleration, when it does not occur at the knee joint. The error is proportional to the rotation amplitude. However, since the shin lengths are around 350 to 450 mm in adults, a 20 mm error represents an accuracy of 5 % in shin characterization. In this way, the proposed method is highly accurate for the knee calibration.

**Table 3.6:** $\Delta SK$ error for the exercise knee bending (mm).

| | Volunteer 1 | Volunteer 2 | Volunteer 3 | Volunteer 4 | Average |
|---|---|---|---|---|---|
| NAP$_\omega$ | $67 \pm 3$ | $55 \pm 2$ | $27 \pm 3$ | $27 \pm 3$ | $44 \pm 6$ |
| fc=3Hz | $\mathbf{16 \pm 3}$ | $\mathbf{12 \pm 3}$ | $22 \pm 4$ | $\mathbf{26 \pm 2}$ | $\mathbf{19 \pm 6}$ |
| fc=7Hz | $30 \pm 3$ | $56 \pm 3$ | $\mathbf{21 \pm 2}$ | $29 \pm 2$ | $34 \pm 5$ |
| fc=15Hz | $71 \pm 3$ | $55 \pm 2$ | $26 \pm 2$ | $27 \pm 2$ | $45 \pm 4$ |

$\Delta SA$ notes the errors obtained in the ankle center A calibration referred to the IMU$_S$. The error $\Delta SA$ is presented in Table 3.7 and Figure 3.10 for the exercise squat, and Table 3.8 and Figure 3.11 for the exercise pendulum. For the squats exercise case, the NAP$_f$ accuracy does not improve with low cutoff frequencies in every case. The error $\Delta SA$ does not improve in this case because the volunteers can do the exercise squat faster than the other exercises. Even so, the average error $\Delta SA$ decreases 3 and 12 mm for the exercise squats and pendulum, respectively, using the NAP$_f$ algorithm with a cutoff frequency of 3 Hz versus using the NAP$_\omega$. Besides, the average error $\Delta SA$ for squat exercise is 25 mm and 19 mm for the exercise pendulum using the NAP$_f$ algorithm, so the error decreases an average of 6 mm between the two exercises. As there

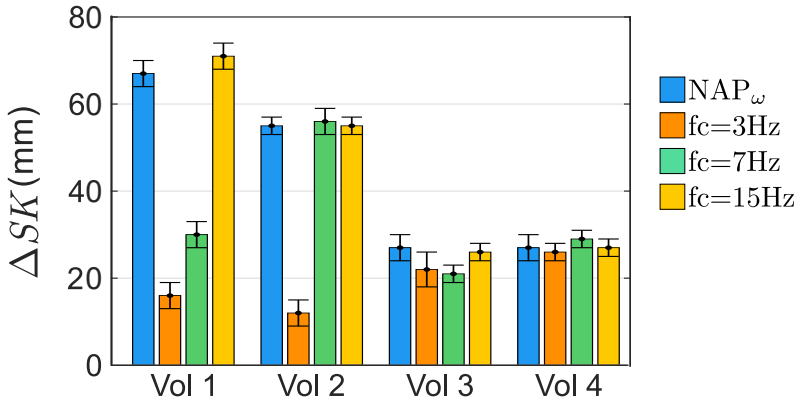


**Figure 3.9:** Bar chart of $\Delta SK$ for each volunteer (Vol $1-4$) and algorithm for the knee bending. The error $\Delta SK$ is associated to the director vector from the IMU$_S$ to the knee (K).

is no significant difference in errors, we cannot conclude there is a most suitable procedure. However, since the error $\Delta SA$ decreases by the low-pass filter for the exercise pendulum, this exercise should be performed in a leg calibration procedure. The same as the previous case, an error around 20 mm is a high accuracy for shin characterization so the proposed method is suitable for this application.

**Table 3.7:** $\Delta SA$ error for the exercise squats (mm).

| | Volunteer 1 | Volunteer 2 | Volunteer 3 | Volunteer 4 | Average |
|---|---|---|---|---|---|
| NAP$_\omega$ | $30 \pm 2$ | $\mathbf{18 \pm 2}$ | $38 \pm 2$ | $27 \pm 4$ | $28 \pm 5$ |
| fc=3Hz | $\mathbf{27 \pm 2}$ | $19 \pm 3$ | $33 \pm 5$ | $21 \pm 3$ | $25 \pm 7$ |
| fc=7Hz | $29 \pm 2$ | $18 \pm 3$ | $24 \pm 4$ | $14 \pm 3$ | $\mathbf{21 \pm 6}$ |
| fc=15Hz | $31 \pm 2$ | $19 \pm 2$ | $\mathbf{22 \pm 4}$ | $\mathbf{13 \pm 3}$ | $\mathbf{21 \pm 6}$ |

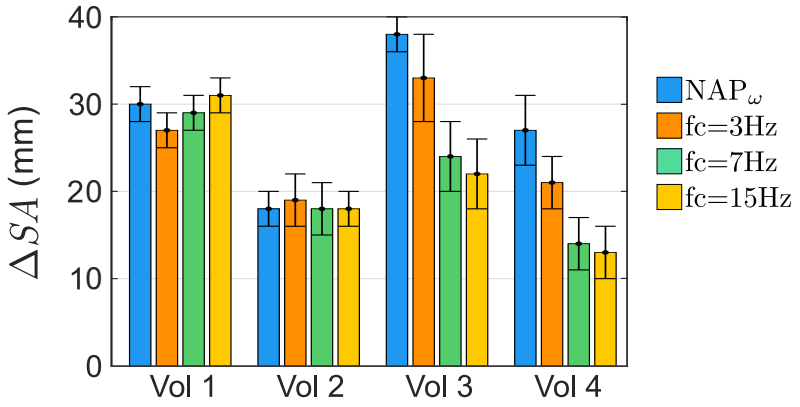


**Figure 3.10:** Bar chart of $\Delta SA$ for each volunteer (Vol $1-4$) and algorithm for the exercise squats. The error $\Delta SA$ is associated to the director vector from the IMU$_S$ to the ankle (A).

The highest accuracy for the joint axes and centers determination with the proposed algorithm NAP$_f$ is achieved with a 3 Hz low-pass filter. Furthermore, based on the evaluation of exercises, we can conclude that by doing circle, knee bending and pen-

**Table 3.8:** $\Delta SA$ error for the exercise pendulum (mm).

| | Volunteer 1 | Volunteer 2 | Volunteer 3 | Volunteer 4 | Average |
|---|---|---|---|---|---|
| $\text{NAP}_\omega$ | $34 \pm 2$ | $22 \pm 3$ | $41 \pm 3$ | $27 \pm 2$ | $31 \pm 5$ |
| fc=3Hz | $\mathbf{27 \pm 2}$ | $\mathbf{20 \pm 4}$ | $\mathbf{19 \pm 3}$ | $\mathbf{9 \pm 2}$ | $\mathbf{19 \pm 6}$ |
| fc=7Hz | $30 \pm 2$ | $22 \pm 4$ | $26 \pm 3$ | $15 \pm 3$ | $23 \pm 6$ |
| fc=15Hz | $37 \pm 2$ | $23 \pm 3$ | $29 \pm 3$ | $20 \pm 3$ | $27 \pm 6$ |

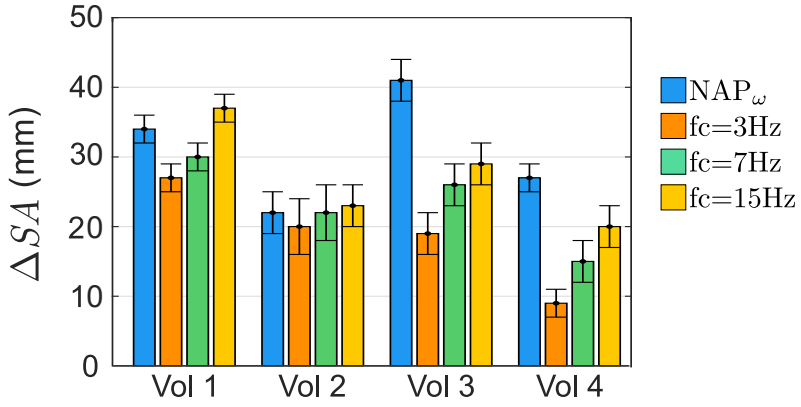


**Figure 3.11:** Bar chart of $\Delta SA$ for each volunteer (Vol $1-4$) and algorithm for the exercise pendulum. The error $\Delta SK$ is associated to the director vector from the $\text{IMU}_\text{S}$ to the knee (K).

dulum exercises, we achieve a calibration of leg vectors with an accuracy around 8 % using the $\text{NAP}_f$.

### Vector obtained from trigonometric relationships

For the estimation of the vector **TK**, we use the results from the circle exercise. As we previously mentioned, the hip center H calibration from $\text{IMU}_\text{S}$ (vector **SH**) is more accurate doing circle exercise than if the volunteer does the exercise cross. We obtain the vector **TK** using (3.7) to relate **TH** and **HK**. We define the error $\Delta TK$ as the norm of the distance vector between the **TK** from the proposed system and the mean of the reference vector $\mathbf{TK}_r$. Since we achieve the best accuracy of the $\text{NAP}_f$ algorithm using a cutoff frequency of 3 Hz, we use this value henceforth. We present error $\Delta TK$ in Table 3.9 and Figure 3.12.

**Table 3.9:** $\Delta TK$ error for the exercise circle (mm).

| | Volunteer 1 | Volunteer 2 | Volunteer 3 | Volunteer 4 | Average |
|---|---|---|---|---|---|
| $\text{NAP}_\omega$ | **45** | **92** | 66 | **38** | 60 |
| fc=3Hz | 58 | 94 | **34** | 44 | **57** |

The error $\Delta TK$ is higher than previous errors for the shortest vectors ($\Delta TH$, $\Delta SK$ and $\Delta SA$) due to the errors propagation. A high $\Delta TK$ is expected since we obtain vector

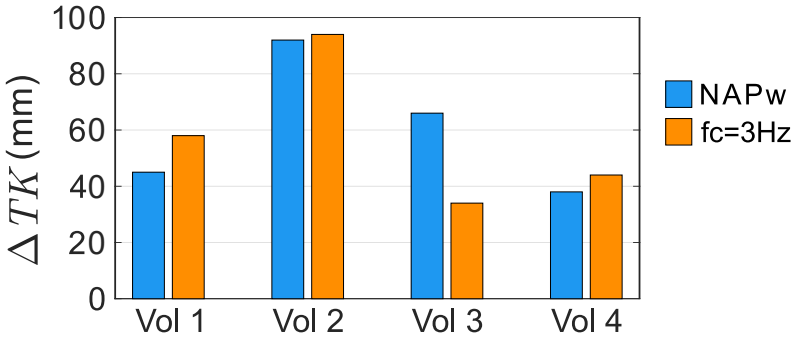


**Figure 3.12:** Bar chart of $\Delta TK$ for each volunteer (Vol $1-4$) and algorithm for the exercise circle. We use the algorithm NAP$_f$ with a cutoff frequency of 3 Hz.

**TK** using vectors **TH**, **SK** and **SH**. In this way, the errors $\Delta TH$, $\Delta SK$ and $\Delta SH$ affect the estimation of vector **TK**. In any case, as in the previous estimations, the algorithm NAP$_f$ is more accurate than the algorithm NAP$_\omega$ as expected from the noise reduction without compromising the amount of data under consideration.

### Segment lengths

The reference measurements for the thigh and shin lengths ($d_{Tr}$ and $d_{Sr}$) obtained from the optical system are shown in Table 3.10. The reference lengths $d_{Tr}$ and $d_{Sr}$ are obtained using the results of the exercise with least occlusions in the reference system for each volunteer.

**Table 3.10:** Reference measurements for $d_T$ and $d_S$ (mm).

| | Volunteer 1 | Volunteer 2 | Volunteer 3 | Volunteer 4 | Average |
|---|---|---|---|---|---|
| $d_{Tr}$ | 388 | 390 | 407 | 391 | 394 |
| $d_{Sr}$ | 383 | 381 | 419 | 392 | 394 |

The error in the segment length estimations is defined as the absolute difference between the reference length $d_{Tr}$ or $d_{Sr}$ and the estimated length $d_T$ or $d_S$. We assess the estimated lengths obtained by the NAP$_\omega$ and NAP$_f$ algorithms. As in the previous case, the NAP$_f$ algorithm is used with a cutoff frequency of 3 Hz, because it provides the best results. The error $\Delta d_T$ for the thigh length $d_T$ estimation is shown in Table 3.11 and Figure 3.13. The error $\Delta d_S$ for the shin length $d_S$ estimation is shown in Table 3.12 and Figure 3.14 and Table 3.13 and Figure 3.15. Since there is no difference in the proposed system accuracy doing the squats or pendulum exercises, both exercises are evaluated for the $d_S$ estimation.

The errors $\Delta d_T$ and $\Delta d_S$ decrease using the NAP$_f$ algorithm versus the NAP$_\omega$ algorithm for each volunteer but volunteer 1 in error $\Delta d_S$. The average errors $\Delta d_T$ and $\Delta d_S$ are around 10 and 20 mm smaller with the NAP$_f$ algorithm. In this way, the NAP$_f$

**Table 3.11:** Error $\Delta d_T$ (mm) for the exercise circle.

| | Volunteer 1 | Volunteer 2 | Volunteer 3 | Volunteer 4 | Average |
|---|---|---|---|---|---|
| $\text{NAP}_\omega$ | 63 | 34 | 75 | 93 | 66 |
| fc=3Hz | **13** | **7** | **9** | **31** | **15** |

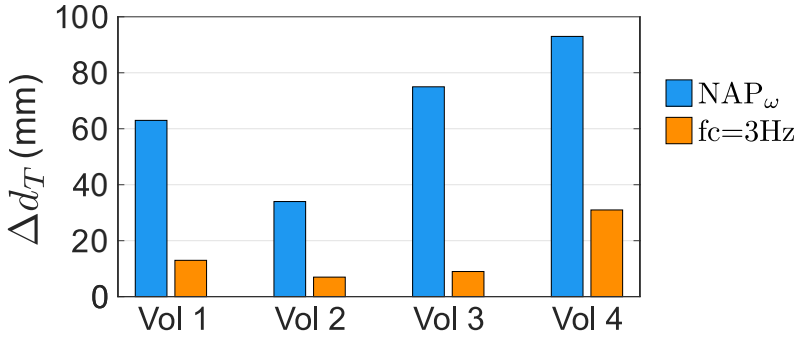


**Figure 3.13:** Bar chart of $\Delta d_T$ for each volunteer (Vol $1-4$) and algorithm. We use the algorithm $\text{NAP}_f$ with a cutoff frequency of 3 Hz.

**Table 3.12:** Error $\Delta d_S$ for squats exercise (mm).

| | Volunteer 1 | Volunteer 2 | Volunteer 3 | Volunteer 4 | Average |
|---|---|---|---|---|---|
| $\text{NAP}_\omega$ | **5** | 24 | 63 | 22 | 29 |
| fc=3Hz | 20 | **4** | **6** | **19** | **12** |

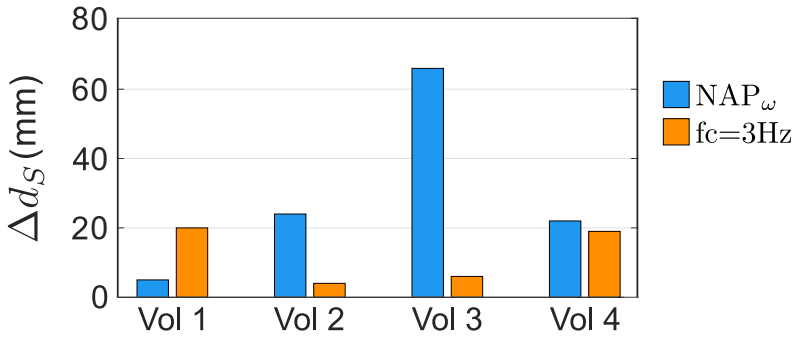


**Figure 3.14:** Bar chart of $\Delta d_S$ for each volunteer (Vol $1-4$) and algorithm for the exercise squats. We use the algorithm $\text{NAP}_f$ with a cutoff frequency of 3 Hz.

**Table 3.13:** Error $\Delta d_S$ for pendulum exercise (mm).

| | Volunteer 1 | Volunteer 2 | Volunteer 3 | Volunteer 4 | Average |
|---|---|---|---|---|---|
| $\text{NAP}_\omega$ | **10** | 23 | 63 | 40 | 32 |
| fc=3Hz | 28 | **11** | **15** | **18** | **18** |

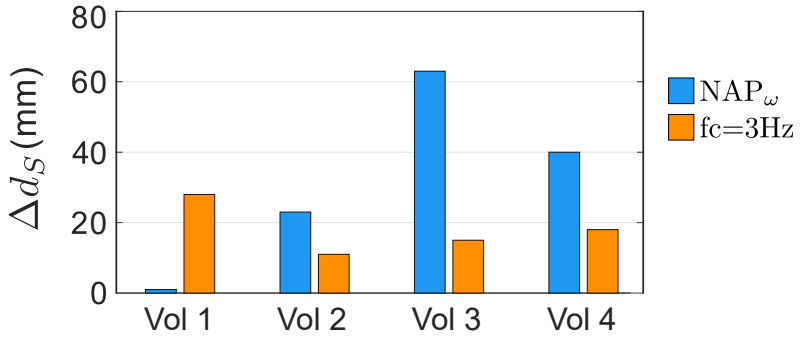


**Figure 3.15:** Bar chart of $\Delta d_S$ for each volunteer (Vol $1-4$) and algorithm for the exercise pendulum. We use the algorithm NAP$_f$ with a cutoff frequency of 3 Hz.

algorithm improves the accuracy of the NAP$_\omega$ algorithm.

However, both NAP$_\omega$ and NAP$_f$ methods achieve precise estimations of the leg segment lengths. The average error $\Delta d_S$ is 29 mm using NAP$_\omega$ and of 12 mm using NAP$_f$ for the squat exercise. Likewise, the average error $\Delta d_S$ is 32 mm using NAP$_\omega$ and of 18 mm using NAP$_f$ for the pendulum exercise.

As anticipated, the errors obtained with the NAP$_\omega$ algorithm are higher than reported in [Cra17] and [Cra18] using our implementation of the algorithm. The main reason is the slowness in the leg movements. Due to this slowness, we obtain the most accurate results using a low-pass filter with the lowest evaluated cutoff frequency, which is 3 Hz.

## 3.3 Conclusions

We develop an accurate IMU-based method for leg characterization based on finding of the location of the null acceleration point in joints. The proposal is adapted to slow movements by a signal preprocessing based on low-pass filtering. The proposed method solves the linear acceleration relationship in a rigid body equation using the Moore-Penrose pseudo-inverse to adapt its use for rotation axes allowing us to obtain the direction vector of AORs. In this way, the proposal is suitable for the determination of spherical joints and the characterization of hinge joints in terms of joint location and estimation of the orientation of the joint axis. The method shows the most accurate results by using the lowest cutoff frequency tested (3 Hz) because of the slowness in the evaluated leg movements. Our method achieves an average error of 8 % for the leg joint centers and axis determination, and of 4 % for the leg length estimation. We prove that the error in leg characterization depends on the performed exercises. The circle, knee bending and pendulum exercises improve the method accuracy. Although this work focuses on lower limbs, the results can be extrapolated to upper limbs where the movements do not present these restrictions of slow speed or almost strict axes of rotation such as the knee. Finally, results confirm that our proposal improves the

performance of the state-of-the-art methods that use only one IMU in the lower-limbs scenario.

The contents of this chapter has been published in two conference publications [Gar18, Gar19].

# Chapter 4

# Adaptive IMU-Joint Center Estimator Method

As derived from Chapter 3, we can obtain average vectors to determine the location of CORs with respect to the IMUs. When we obtain these vectors, we assume that the STA affecting the estimations are eliminated averaging over long tests. However, this approach can lead to errors on scenarios with STA [Ols17, Fri18a] as exposed in section 2.2.2. In order to overcome this limitation, we propose in this chapter a novel estimator of direction vectors that adapts to variations in the relative positions of IMUs. Since the distance to this center commonly varies during the joint motion due to STA, our approach is aimed at adapting to these small variations when the COR is fixed, as hip joints during some specific rehabilitation motions. The IMU-joint vector is named **OB** in Chapter 3 because both points were assumed fixed, so we rename it $\boldsymbol{r}$ in this case that the IMU is expected to suffer STA.

Our proposal is called $ArVE_d$, that stands for Adaptive $\boldsymbol{r}$ Vector Estimator. This algorithm is based on the method ArVE introduced in [Gar20a]. To the best of our knowledge, ArVE is the first real-time estimator of the IMU-joint center vector based on one IMU. Previous works are off-line and require a complete measurement batch to be solved and most of them are not tested on the real scenario.

Therefore, the main goal of this chapter is to introduce $\text{ArVE}_d$ and demonstrate its suitability to estimate the location of CORs of fixed human joints with one IMU, assuming that the IMU undergoes STA during motions. To evaluate its performance, we compare $\text{ArVE}_d$ with the approach described in [Cra16], used as a reference to estimate an average $\boldsymbol{r}$, hereinafter $MrVS$, that stands for Mean $\boldsymbol{r}$ Vector least-Squares-based estimator. We perform this evaluation through different experiments, including synthetic and real data.

## 4.1 Proposed Algorithm

The main goal of our proposal is to obtain the location of the COR as an adaptive IMU-joint vector, $\boldsymbol{r} = [r_x, r_y, r_z]^\top$, defined from the accelerometer to this COR in the sensor frame. We aim at estimating $\boldsymbol{r}$ with one IMU by using the measures of turn rate $\boldsymbol{\omega}_I$ and specific force $\boldsymbol{f}_{A,I}$, that is the linear acceleration $\boldsymbol{a}_A$ influenced by the gravity acceleration $\boldsymbol{g}$. Subindex $I$ indicates the measurements obtained directly from the IMU in its reference system. We obtain the IMU-joint vector $\boldsymbol{r}$ on the basis of the equation of accelerations of a rigid-solid body moving in the 3D space (4.1).

$$\boldsymbol{a}_0^k = \boldsymbol{a}_A^k + \dot{\boldsymbol{\omega}}^k \times \boldsymbol{r}^k + \boldsymbol{\omega}_I^k \times \left(\boldsymbol{\omega}_I^k \times \boldsymbol{r}^k\right), \tag{4.1}$$

Where $\boldsymbol{a}_0^k$ and $\boldsymbol{a}_A^k$ are the linear accelerations in the COR and the IMU, respectively, $\boldsymbol{\omega}_I^k$ is the turn rate of the rigid-solid body and $\dot{\boldsymbol{\omega}}^k$ is its first-order derivative. As the aim is to estimate the location of fixed CORs, we assume $\boldsymbol{a}_0^k$ negligible. All parameters are expressed in the sensor frame. Superscript $k$ denotes the time instant of parameters. Rigid-solid bodies present a constant $\boldsymbol{r}$ vector, but in this study we focus on human bodies in which STA modify $\boldsymbol{r}^k$ at each time $k$. Besides, using (4.1) to estimate an adaptive $\boldsymbol{r}^k$, we assume negligible the linear acceleration caused by STA.

Figure 4.1 depicts the relation of these magnitudes measured with one IMU and the estimation of the COR. This figure shows the global frame with the subscript $g$ and the sensor frame, which is attached to the IMU.

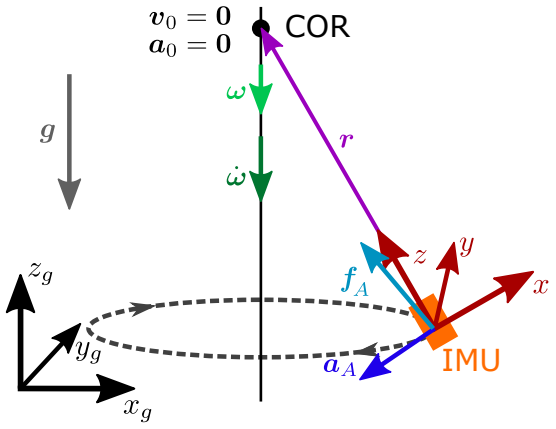


**Figure 4.1:** Scheme of the relationship between the magnitudes in (4.1). The rigid-solid body moves with turn rate $\boldsymbol{\omega}_I$ and angular acceleration $\dot{\boldsymbol{\omega}}$, whereas the IMU suffers a linear acceleration $\boldsymbol{a}_A$, but it measures the specific force $\boldsymbol{f}_{A,I}$. The specific force $\boldsymbol{f}_{A,I}$ is the result of $\boldsymbol{a}_A - \boldsymbol{g}$ both expressed in the sensor frame. Conversely, the linear velocity of CORs is $\boldsymbol{v}_0 = \boldsymbol{0}$ by definition and as it is fixed, its linear acceleration $\boldsymbol{a}_0$ is also equal to zero.

To obtain $\boldsymbol{r}^k$ with (4.1), the linear acceleration $\boldsymbol{a}_A^k$ is required. As IMUs provide the specific force $\boldsymbol{f}_{A,I}^k$ undergone by the accelerometer, we obtain $\boldsymbol{a}_A^k$ correcting the effect

of the gravity through the projection of the gravity vector $\boldsymbol{g}$ into the frame of IMUs as follows:

$$\boldsymbol{a}_A^k = \boldsymbol{f}_{A,I}^k + (C^k)^\top \boldsymbol{g}, \tag{4.2}$$

where $C^k$ is the *Direction Cosine Matrix* that relates the global frame with the sensor frame and $\boldsymbol{g}$ is the gravity vector defined downwards in the global frame with a value of $9.8\,\mathrm{m/s^2}$. We do not use the direct measures of orientation with respect to the global frame in order to provide an algorithm usable with any generic IMU. We calculate the transformation matrix $C$ fusing the measures of turn rate $\boldsymbol{\omega}_I^k$ and specific force $\boldsymbol{f}_{A,I}^k$ of the IMU using the algorithm introduced in [Dia19]. This algorithm estimates through an UKF (more details about UKFs are included in Appendix A.3.3) the Euler angles of the IMU from the measures of turn rate $\boldsymbol{\omega}_I^k$ and updates these estimations with the specific force $\boldsymbol{f}_{A,I}^k$ measured in those moments when its norm is close to the gravity vector norm.

In this chapter, we evaluate three different ways to estimate $\boldsymbol{r}$: ArVE$_d$ estimates a dynamic $\boldsymbol{r}^k$ at each time $k$ and MrVS obtains, on the one hand, an averaged $\boldsymbol{r}$ for complete tests and, on the other hand, a dynamic $\boldsymbol{r}_n^k$ for a determined number of samples $n$ with an overlap of $n-1$ samples between consecutive estimations of $\boldsymbol{r}_n^k$. These methods are explained in the following two sub-sections: ArVE$_d$ in section 4.1.1 and MrVS in section 4.1.2.

### 4.1.1 Proposed algorithm: ArVE$_d$

We propose ArVE$_d$ to estimate $\boldsymbol{r}^k$ at each time instant based on the assumption of fixed CORs using an EKF (for more details about EKFs, see Appendix A.3.2). Figure 4.2 depicts the two stages of ArVE$_d$ at each time $k$: an initial stage to obtain the linear acceleration $\boldsymbol{a}_A^k$ followed by the second stage that consists in an EKF to determine $\boldsymbol{r}^k$. The EKF fuses the measured turn rate $\boldsymbol{\omega}_I^k$ and the calculated linear acceleration $\boldsymbol{a}_A^k$.

Figure 4.2 shows also the two steps of this EKF. The proposed EKF minimizes the prediction error of the state vector $\boldsymbol{x}^k$, composed of the searched oriented vector $\boldsymbol{r}^k$, its first-order derivative $\dot{\boldsymbol{r}}^k$, the turn rate $\boldsymbol{\omega}^k$ and the angular acceleration $\dot{\boldsymbol{\omega}}^k$, given the measurements from the IMU.

In the estimation step of the EKF, we assume $\hat{\dot{\boldsymbol{r}}}^k$ and $\hat{\dot{\boldsymbol{\omega}}}^k$ constant, whereas $\hat{\boldsymbol{r}}^k$ and $\hat{\boldsymbol{\omega}}^k$ are the integral at each time of these terms. Thus, the estate vector $\hat{\boldsymbol{x}}^k$ is estimated at each time $k$ as follows:

$$\begin{cases} \hat{\boldsymbol{r}}^k = \boldsymbol{r}^{k-1} + \hat{\dot{\boldsymbol{r}}}^k \Delta t \\ \hat{\dot{\boldsymbol{r}}}^k = \dot{\boldsymbol{r}}^{k-1} \\ \hat{\boldsymbol{\omega}}^k = \boldsymbol{\omega}^{k-1} + \hat{\dot{\boldsymbol{\omega}}}^k \Delta t \\ \hat{\dot{\boldsymbol{\omega}}}^k = \dot{\boldsymbol{\omega}}^{k-1} \end{cases} \tag{4.3}$$

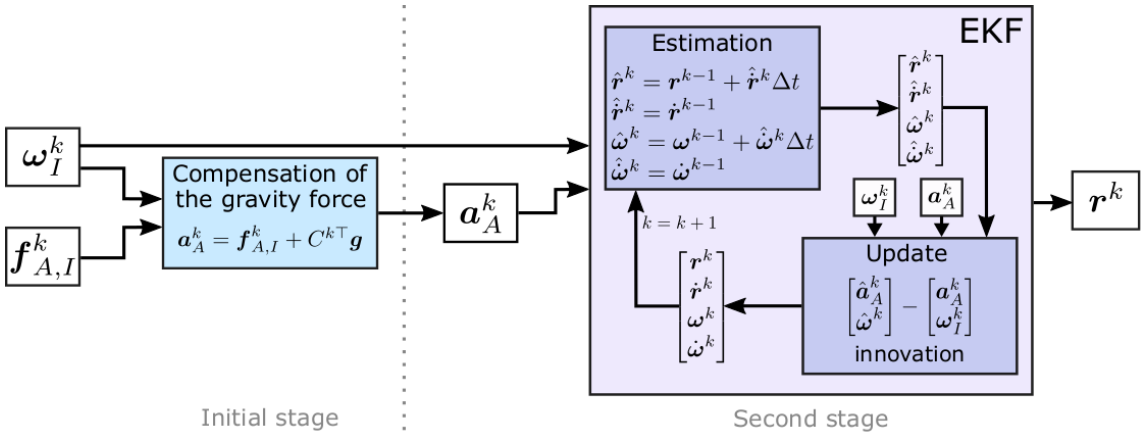


**Figure 4.2:** Flowchart to obtain the adaptive $\boldsymbol{r}^k$ at each time instant. In the initial stage, we fuse the IMU measurements of turn rate $\boldsymbol{\omega}_I^k$ and specific force $\boldsymbol{f}_{A,I}^k$ using the UKF introduced in [Dia19] to obtain the linear acceleration $\boldsymbol{a}_A^k$. In the second stage, we obtain $\boldsymbol{r}^k$ with this signal of linear acceleration combined with the turn rate through the EKF.

The observations consist of the measured turn rate $\boldsymbol{\omega}_I^k$ and the linear acceleration $\boldsymbol{a}_A^k$ obtained in the initial stage of ArVE$_d$. ArVE$_d$ then updates the estimations exploiting the relationship between the estimations and the estimated linear acceleration $\hat{\boldsymbol{a}}_A^k$, using (4.4), and the direct relation between the estimated turn rate $\hat{\boldsymbol{\omega}}^k$ and the measured one $\boldsymbol{\omega}_I^k$.

$$\hat{\boldsymbol{a}}_A^k = -\hat{\dot{\boldsymbol{\omega}}}^k \times \hat{\boldsymbol{r}}^k - \hat{\boldsymbol{\omega}}^k \times (\hat{\boldsymbol{\omega}}^k \times \hat{\boldsymbol{r}}^k) \tag{4.4}$$

The linear acceleration $\boldsymbol{a}_A^k$ and the turn rate $\boldsymbol{\omega}_I^k$ are then used to obtain the innovation of the EKF to update the estimations at each time $k$.

Considering $\boldsymbol{\omega}^k$ and $\dot{\boldsymbol{\omega}}^k$ in the state vector, we obtain an estimation of $\dot{\boldsymbol{\omega}}^k$ using the raw data from gyroscopes, facilitating the generalized use of the algorithm. Since EKFs minimize the variance of the estimation error, noisy data from IMUs do not require an initial signal filtering and avoid the post-processing suggested in [Fri18a]. Notice also that $\dot{\boldsymbol{r}}^k$ is not related to any measured magnitude, so it is not directly updated, but used as a parameter of adjustment of the EKF. The use of the derivative of $\boldsymbol{r}$ in the state vector of the EKF is one of the main differences between ArVE$_d$ and ArVE, our initial approach proposed in [Gar20a], differentiated with the subindex $d$.

The parameters of the covariance matrix of the process in the EKF are set according to [Cer03]. We select a constant value of covariance for each kind of tests, with synthetic and real data, indicated in section 4.2.3 and section 4.3.1, respectively, together with the explanation of the estimation of the estimation-error covariance matrix and the covariance matrix of the measurement noise.

### 4.1.2 MrVS

The original approach of MrVS proposed in [Cra17] is previously introduced in Chapter 3, but we summarize it in the following for clarity. MrVS uses the complete several-second long signals of tests of the measured turn rate $\boldsymbol{\omega}_I$ and the linear acceleration $\boldsymbol{a}_A$ obtained from the measured specific force $\boldsymbol{f}_{A,I}$, and it also requires computing $\dot{\boldsymbol{\omega}}$. This parameter is obtained by discrete derivative of the turn rate $\boldsymbol{\omega}_I$ measured with the IMU. Since $\boldsymbol{a}_0$ is negligible in fixed CORs, the only unknown term in (4.1) is $\boldsymbol{r}$, so it can be rearranged as follows:

$$\boldsymbol{a}_A = M\boldsymbol{r}, \tag{4.5}$$

where

$$M = \begin{pmatrix} -\omega_y^2 - \omega_z^2 & -\dot{\omega}_z + \omega_x\omega_y & \dot{\omega}_y + \omega_x\omega_z \\ \dot{\omega}_z + \omega_x\omega_y & -\omega_x^2 - \omega_z^2 & -\dot{\omega}_x + \omega_y\omega_z \\ -\dot{\omega}_y + \omega_x\omega_z & \dot{\omega}_x + \omega_y\omega_z & -\omega_x^2 - \omega_y^2 \end{pmatrix}, \tag{4.6}$$

is the matrix introduced in [Cra16]. Variables $\omega_x$, $\omega_y$ and $\omega_z$ are the components of the measured turn rate $\boldsymbol{\omega}_I$. In both (4.5) and (4.6), the vector $\boldsymbol{a}_A$ and the matrix $M$ symbolize a set of temporal measurements of the corresponding parameters, so no superscript $k$ is used. An averaged $\boldsymbol{r}$ is obtained solving (4.6) with least squares for complete tests.

When we work with several-second long IMU signals to obtain an average $\boldsymbol{r}$, the $M$ matrix from MrVS has full rank on the scenario of CORs of ball joints, as hips. However, when we look for an adaptive calculation of $\boldsymbol{r}$, uncertainties appear in (4.5) when $\boldsymbol{\omega}$ is negligible. In these points, $M$ becomes antisymmetric, so its determinant is zero and the system is undetermined. Therefore, MrVS cannot be implemented in real-time applications in a straightforward way to obtain one vector per sample. Thus, we test two approaches of MrVS: obtaining an averaged $\boldsymbol{r}$ for the complete test as proposed in [Cra17] and estimating an adaptive $\boldsymbol{r}_n^k$ in a sliding window with an $n$ number of samples.

## 4.2 Experiments on synthetic data

We carry out two experiments with synthetic data to test the performance of ArVE$_d$ and MrVS. The experiments simulate the motion of a pendulum moving in circles from a fixed ball joint. This pendulum imitates a limb carrying out circles from a fixed COR, as a leg moving from the hip. The first experiment consists in an IMU moving around a fixed COR with a constant $\boldsymbol{r}$ vector to assess the accuracy of the evaluated systems in the ideal case. The second experiment imitates the motion of an IMU around a fixed COR with variations of $\boldsymbol{r}$ over the test caused by simulated STA that involve small

translations of the IMU. In this experiment, we study the error caused by assuming a constant $\boldsymbol{r}$ whereas it varies over time.

The experiments with synthetic data are presented in four sub-sections. We describe the spherical pendulum simulated to obtain the synthetic data in section 4.2.1 and detail the metrics used to evaluate the inertial-based methods in section 4.2.2. Then, section 4.2.3 and section 4.2.4 introduce the results for these experiments carried out on synthetic data.

### 4.2.1 Simulation of a spherical pendulum

We simulate the movement of a spherical pendulum rotating in the 3D space during 10 s, around a fixed COR and around the main axis of the pendulum. The pendulum describes an ellipse with two main rotations around the $x$ and $y$ axes of the simulated IMU, and a partial rotation around its $z$ axis, combining the three motions around the three IMU axes. The amplitudes of the movements around the $x$, $y$ and $z$ axes are 17 °, 9 ° and 3 °, respectively, and the motion of the pendulum around the $x$ and $y$ axes lasts 1 s; and 1.5 s around the $z$ axis. The parameters of the simulated motions are set according to the motions observed during the lower-limb calibration observed in [Gar19], as we do in the simulations reported in [Gar20a]. Figure 4.3 depicts these axes of the IMU together with a scheme of its motion.

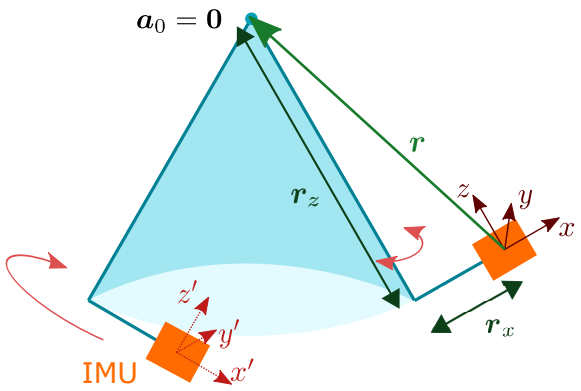


**Figure 4.3:** Scheme of the pendulum designed for simulations. The IMU (orange box) moves around the COR and its coordinate system moves with the device from positions of the initial $x$, $y$ and $z$ to each corresponding $x'$, $y'$ and $z'$. The $r_y$ component would be parallel to the drawing. In the first experiment, $\boldsymbol{r}$ remains constant and, in the second one, its coordinates change over time.

We establish $\boldsymbol{r}$ considering the most likely configuration on the real scenario, where the IMU is placed over the thigh and not in contact with the femur. In the simulation, a displacement between the main axis of the pendulum and the origin of coordinates of IMUs is taken into account and the IMU axes are misaligned with $\boldsymbol{r}$, as shown in

Figure 4.3. The $r_x$, $r_y$ and $r_z$ components are $-60$, 20, and 200 mm, respectively, so the norm of the vector is 209.8 mm.

The inertial data are simulated at a sampling rate of 100 Hz. In both experiments, we add a Gaussian noise in the simulated turn rate $\boldsymbol{\omega}_I$ and specific force $\boldsymbol{f}_{A,I}$ according to the specifications of the *MTw Awinda* sensors from *Xsens* [Xse20], since we use these sensors in the real data experiments. The standard deviation of noise in the measurements of gyroscope of turn rate $\boldsymbol{\omega}$ is $0.0017\,^\circ/\mathrm{s}$, and in the specific force $\boldsymbol{f}_A$ from the accelerometer is $0.02\,\mathrm{m/s^2}$. Bias is not considered since simulations and tests are short enough in time to be affected by it, as done in [Fri18a] and because the estimation of $\boldsymbol{r}$ does not include integration, so its estimations are insensitive to bias, according to [See12]. In order to provide more significant results than in our previous work [Gar20a], we carry out 100 tests for each experiment.

On both scenarios we set the observation noise, $R$, equally since it depends on the noise of the simulated sensors, but we adjust the estimate covariance, $P$, and the process covariance, $Q$, for each scenario.

### 4.2.2 Metrics and errors

We quantify the accuracy of the proposals using three different metrics:

1. The Euclidean norm of the vector difference between the reference $\boldsymbol{r}_r$ vector and the estimated $\boldsymbol{r}$ using the measurements from IMUs, noted with $\|\Delta\boldsymbol{r}\|$. In order to consider one method competitive for its use in orientation tracking, we define the upper limit of $\|\Delta\boldsymbol{r}\|$ in the 10 % of the Euclidean norm of $\boldsymbol{r}_r$, because in [Bon15] it is reported that errors over this 10 % double errors in estimations of the orientation of limbs.

2. The difference between the norms of $\boldsymbol{r}_r$ and $\boldsymbol{r}$, defined as $\Delta\|\boldsymbol{r}\|$.

3. The deviation angle, $\gamma$, between $\boldsymbol{r}_r$ and $\boldsymbol{r}$.

We consider these three metrics because each considered error has a source related with the different parameters in (4.1). The difference of norms $\Delta\|\boldsymbol{r}\|$ is mainly caused by errors in the determination of $\dot{\boldsymbol{\omega}}$. The deviation angle $\gamma$ is mostly affected by the accuracy of the measured linear acceleration $\boldsymbol{a}_{A,I}$ and turn rate $\boldsymbol{\omega}_I$. Finally, $\|\Delta\boldsymbol{r}\|$ is affected by both the difference between norms and the deviation angle.

### 4.2.3 Results on a constant IMU-joint vector

Using the experiments of a simulated 3D pendulum with a constant IMU-joint vector detailed in section 4.2.1, we evaluate the accuracy of MrVS and ArVE$_d$ to obtain an $\boldsymbol{r}$

per window and per sample, respectively.

We assess the proposal of MrVS in a sliding window as an alternative to estimate a variable $\boldsymbol{r}$ vector. We test different window sizes in order to study the accuracy obtained with each considered number of samples $n$. The evaluated window sizes are from $n = 5$ until $n = 100$ samples, increasing 5 samples between tests. We stop at 100 samples since it would average the STA of a complete cycle in the simulations. Windows slide 1 sample to obtain each $\boldsymbol{r}$, so they overlap $n - 1$ samples. Since the norm of the reference vector is 209.8 mm, we define the upper limit in 20 mm, which is the 10 % of the vector norm. The resulting average $\|\Delta\boldsymbol{r}\|$ of each test is depicted in Figure 4.4.

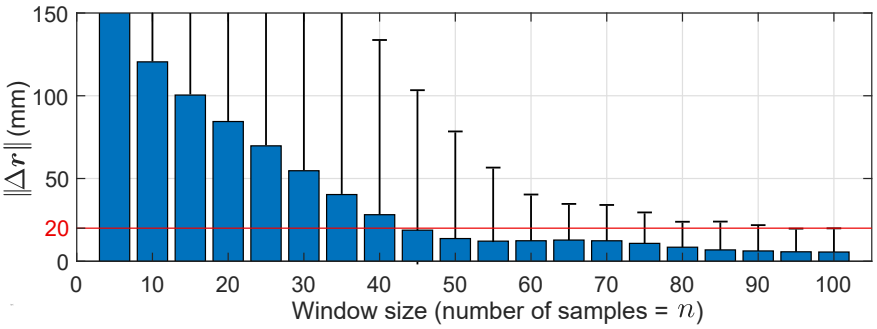


**Figure 4.4:** Average and maximum $\|\Delta\boldsymbol{r}\|$ of the 100 tests carried out with our proposal of MrVS in a sliding window with the corresponding window size used to estimate $\boldsymbol{r} = [200, 20, -60]^\top$ mm. The horizontal red line depicts the upper limit.

Results in Figure 4.4 show that the errors reduce as the number of samples increases, reaching an error smaller than 10 mm from the window size of $n = 80$ samples. The maximum errors also decrease when increasing of $n$, obtaining bearable error values under the upper limit with $n = 90$ samples. However, using 95 samples, the information of almost 1 s is averaged, which reduces the sensitivity to changes in $\boldsymbol{r}$.

The use of $n = 45$ samples in each window is a trade-off solution between the $n$ number of samples and the averaged $\|\Delta\boldsymbol{r}\|$ error. In this case, the average error is 17.6 mm, which is lower than the upper limit of 20 mm. Nevertheless, maximum errors are larger than 100 mm.

Figure 4.5 a) shows the results of MrVS with a sliding window size of 45 samples over the initial 2.5 s of the constant $\boldsymbol{r}$ test. The purple circles point out the intervals where errors of MrVS increase when the norm of $\boldsymbol{\omega}$ is negligible. The required number of samples to obtain an accurate estimation of the IMU-joint vector is too long to estimate a variable vector, so MrVS is not able to adapt to variations in the IMU-joint vector.

Conversely, we use ArVE$_d$ to combine the information of the IMU signals at each time instant, avoiding the inversion of the system matrix and the calculation of $\dot{\boldsymbol{\omega}}$. Figure 4.5 b) shows the resulting $\boldsymbol{r}$ vector when using ArVE$_d$ with an initial $\boldsymbol{r}_0$ composed

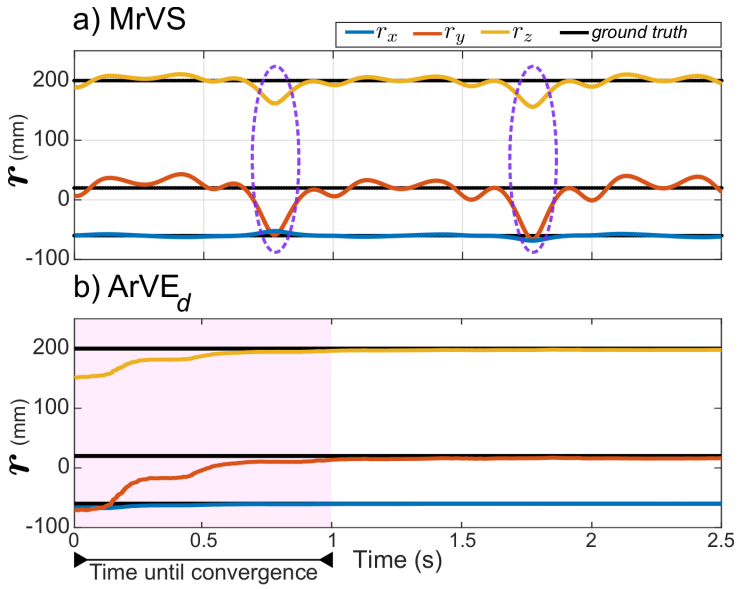


**Figure 4.5:** Results on the fixed $\boldsymbol{r}$ scenario, in which the ground truth is depicted in black. a) Vector $\boldsymbol{r}_n^k$ obtained using MrVS in a sliding window of $n = 45$ samples. b) Resulting $\boldsymbol{r}^k$ using ArVE$_d$ and setting the initial $\boldsymbol{r}_0 = [0\,,0\,,0]^\top$ in the EKF. During the first second the estimations are inaccurate, until the filter convergence. After this transitory time, estimations, depicted in blue, red and yellow, are similar to the ground truth.

of zeros. In this particular case, the EKF takes one second to converge. After this transitory time, the estimations do not suffer from miscalculations even when $\boldsymbol{\omega}$ is close to zero. We can conclude that ArVE$_d$ provides stable estimations even in the intervals where MrVS was not able to provide an accurate result, highlighted with pink circles.

Apart from the parameters of covariance in the EKF, the performance of ArVE$_d$ depends on the initial state vector, so we test the proposed method with different $\boldsymbol{r}_0$ vectors. We calculate an $\boldsymbol{r}_0$ as an average vector similarly than in MrVS, by using (4.5) with the initial samples of tests. We use from 20 until 140 samples to estimate this $\boldsymbol{r}_0$, increasing 20 samples between tests. We repeat 100 times every test to evaluate the accuracy of ArVE$_d$ with each initial vector through the metrics introduced in section 4.2.2. Figure 4.6 depicts the average of errors, together with their maximum and minimum errors.

Figure 4.6 shows the evaluated errors and their range of values decrease as the number of samples considered to estimate $\boldsymbol{r}_0$ increases. These errors become stable when we obtain $\boldsymbol{r}_0$ with 60 samples. From this number of samples, $\|\Delta\boldsymbol{r}\|$ is around 2 mm, so using more than these 60 samples (that means 0.6 s of signals since $f_s = 100$ Hz) does not improve the accuracy of ArVE$_d$ since the EKF converges from the initial samples. For that reason, on the following we use 60 samples to calculate $\boldsymbol{r}_0$ for the initialization of the EKF of ArVE$_d$.

According to the errors shown in Figure 4.6, ArVE$_d$ outperforms in the evaluated cases

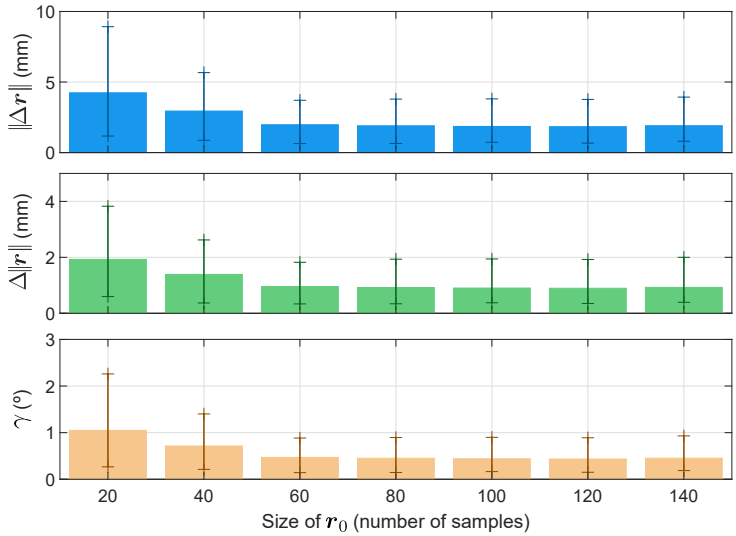


**Figure 4.6:** Errors with their corresponding ranges of values in the estimation of $\boldsymbol{r}$ with ArVE$_d$ over the 10 second-experiment with the different $\boldsymbol{r}_0$ considered. The Euclidean norm of the vector difference, $\|\Delta \boldsymbol{r}\|$, is depicted with blue bars, the difference between norms, $\Delta\|\boldsymbol{r}\|$, with green bars and the deviation angle $\gamma$ in orange bars. Each bar corresponds to the average error of the 100 tests carried out with this number of initial samples and the vertical lines depict the range of these errors.

our proposal of MrVS in a sliding window. This improvement in accuracy is due to the fact that ArVE$_d$ has no problems with the singular points of the signal as happens with MrVS. Despite the inaccurate estimations of MrVS near the instants when $\boldsymbol{\omega}$ is negligible, its estimations are accurate in the remaining time intervals.

### 4.2.4 Results on variable IMU-joint vectors

We simulate the STA of the real scenario as variations in $\boldsymbol{r}$ that imitate the translation of the IMU with respect to the fixed COR. The variation of $\boldsymbol{r}$ over time is presented as a sinusoidal signal of frequency 1 Hz and amplitude 20 mm in $r_x$ and $r_z$, and 5 mm in $r_y$, components previously shown in Figure 4.3. We set this frequency of the translational STA to make it similar to the frequency of motion of the pendulum, as suggested in [Cam13], and the amplitude values are also set according to the results in the same work. Since IMUs are taped to the body, lateral motions over the $y$-axis are restricted, whereas the muscle contractions entail translations in the $x$-and $z$-axis. In this case, we compare ArVE$_d$ with ArVE to evaluate the influence of the new parameter of adjustment introduced in ArVE$_d$ on the accuracy of this proposal. Figure 4.7 depicts in black these components of the variable $\boldsymbol{r}$ vector used as ground truth over the test, together with the components of the variable $\boldsymbol{r}$ using ArVE and ArVE$_d$.

Figure 4.7 shows that ArVE$_d$ and ArVE adapt to most of changes of $\boldsymbol{r}$ over time. Thus, both methods provide adaptability to a variable $\boldsymbol{r}$. Besides, according to these results,

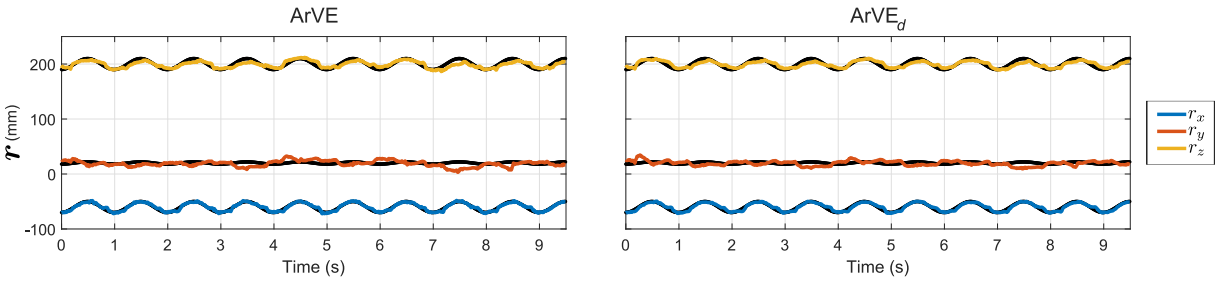


**Figure 4.7:** Coordinates of $\boldsymbol{r}$ over the test. The ground truth is depicted in black and the estimated $r_x$, $r_y$ and $r_z$ in blue, red and yellow, respectively. We estimate $\boldsymbol{r}$ using ArVE and ArVE$_d$, and their results correspond to the images presented on the left and on the right, respectively.

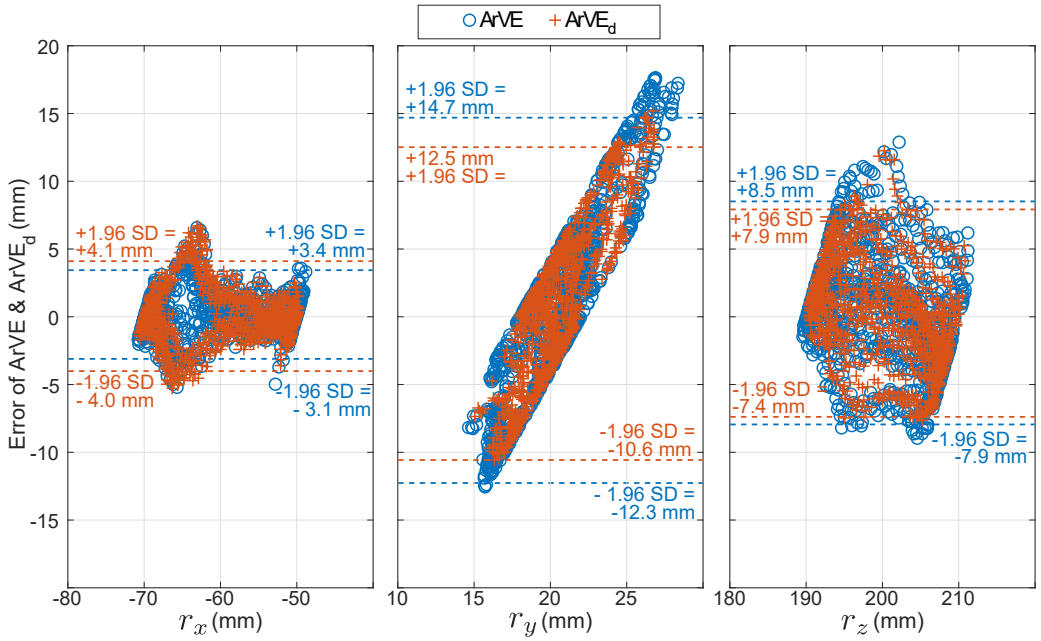


**Figure 4.8:** Bland-Altman plot with the comparison of ArVE$_d$ and ArVE. The dotted lines point out the confidence interval in which the 95 % of the errors obtained with each methods are contained, so these lines correspond with the value of 1.96 times the standard deviation (SD).

estimations using ArVE$_d$ are closer to the ground truth, with an improvement of 7 % compared to the results obtained by using ArVE. In this way, ArVE$_d$ outperforms ArVE through the adjustment of the noise parameters of $\dot{\boldsymbol{r}}$ in the EKF. Both methods are also evaluated by means of a Bland-Altman plot compared with the ground truth in Figure 4.8.

As shown in Figure 4.8, errors in the estimation of $r_x$ and $r_z$ are similar using ArVE$_d$ and ArVE. They are in the approximate range of $\pm 4$ mm for $r_x$ and $\pm 8$ mm for $r_z$. Conversely, there are differences in accuracy estimating $r_y$. The improvement in this coordinate is specially remarkable in the error dispersion, lowered 2 mm in each upper-and lower-bounds. The results may not be as good with $r_y$ because its range of variation is at the noise level in the filter, so none of these methods adapts to its variations.

These simulations are closer to the real scenario, where $\boldsymbol{r}$ changes due to STA, so we use the simulated data to evaluate the three methods, whose results are shown in Table 4.1. In this case, MrVS estimates a unique $\boldsymbol{r}$, constant for the complete test, whereas ArVE$_d$ and ArVE adapt to the variable vector, obtaining an instantaneous vector per sample.

**Table 4.1:** Errors in the determination of $\boldsymbol{r}$ with inertial methods with an average $\boldsymbol{r} = [200, 20, -60]^\top$.

| | $\|\Delta\boldsymbol{r}\|$ mm | $\Delta\|\boldsymbol{r}\|$ mm | $\gamma\,^\circ$ |
|---|---|---|---|
| ArVE$_d$ | $\mathbf{6.8 \pm 3.9}$ | $\mathbf{3.4 \pm 2.4}$ | $\mathbf{1.6 \pm 0.9}$ |
| ArVE | $7.3 \pm 4.6$ | $3.8 \pm 2.8$ | $1.7 \pm 1.1$ |
| MrVS | $14.4 \pm 3.8$ | $5.7 \pm 4.9$ | $3.5 \pm 0.7$ |

The $\|\Delta\boldsymbol{r}\|$ error shows the highest improvement, from 14.4 mm using MrVS, to 6.8 mm using ArVE$_d$, lowering errors more than a 50 %. This error decreases more than the difference of norms $\Delta\|\boldsymbol{r}\|$ and the angle $\gamma$ because the distance vector is affected by $\Delta\|\boldsymbol{r}\|$ and $\gamma$, and both errors are smaller using ArVE$_d$. According to these results, ArVE$_d$ is the method that best adapts to a variable $\boldsymbol{r}$, which justifies our proposal for improvement by introducing the derivative of $\boldsymbol{r}$ in the estate vector.

It is noticeable that the errors of using ArVE$_d$ in simulations that include the simulated effect of the translational STA are similar to those presented in [Fri18a], but they do not consider the three components of the IMU-joint vector in the reported errors. So, even if we cannot compare directly our results, we can conclude that our algorithm is at least as accurate as the methods in the literature. Furthermore, ArVE$_d$ only needs the initial data during 0.6 s to initialize the algorithm and we avoid the low-pass filtering of the IMU signals and the analytic derivation of the measured turn rate $\boldsymbol{\omega}_I$, used in other works as [Cra16, Cra17, Fri18a, Fri18b].

Finally, Figure 4.9 depicts the estimated COR in the simulations of the variable $\boldsymbol{r}$ using ArVE$_d$ and, drawn in red, its actual position in two different planes. According to these results, the relative errors depend on the component of $\boldsymbol{r}$, being larger for the $y$-axis and the smallest variation on the $x$-axis. But it is worth highlighting that 93 % of the COR estimated by ArVE$_d$ are in a sphere with a radius of 6 mm. This estimated radius is approximately a fifth of the hip joint radius, commonly included in the range of 25 mm to 30 mm according to [Cal16].

## 4.3 Experiments on the real scenario

We study now the performance of ArVE$_d$ on a real scenario. We obtain the COR of the hip of five volunteers with respect to one IMU, using the inertial-based systems

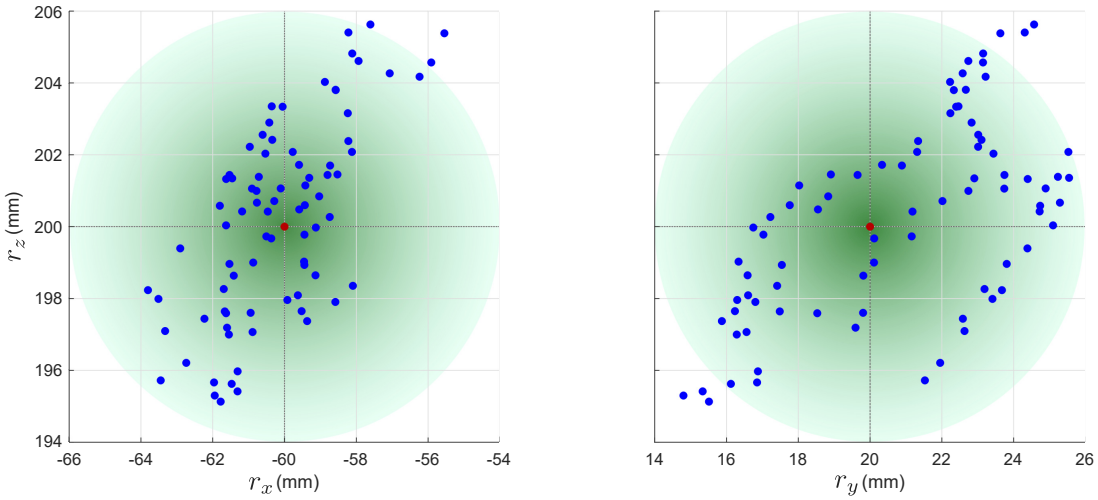


**Figure 4.9:** Projection of the points estimated by ArVE$_d$ in planes XZ, depicted in the image on the left, and YZ, in the image on the right, over one second of the experiment. The estimated points are depicted in blue and the ground truth in red.

and an optical system at the same time. We compare ArVE$_d$ and our implementation of [Cra16], MrVS, with the optical method introduced in [De 14]. We use this method because it aims to obtain a variable $\boldsymbol{r}$.

### 4.3.1 Experimental setup

Five volunteers with a height of $165 \pm 8$ cm participate in this study. During the experiments, they repeat 10 times the hip circles motion depicted in Figure 4.10 a), being equipped with one IMU placed on the thigh and four optical markers located around the IMU, as shown in Figure 4.10 b). We choose this motion to ensure the presence of a unique COR at each time instant instead of an axis of rotation, so our system has a unique solution, that is the searched COR. The concerns about estimations of axes using (4.1) are more detailed in [Cra18]. The motion of hip circles is performed maintaining both legs straightened, one foot is placed on the floor while the other leg performs circles from the hip. To do this exercise, the stability of the volunteers is important to keep the hip still, so their backs rest on a stable surface and we ensure that their motions are according to the requirements for these experiments. We eliminate the first and last signal segments of 1.5 s long of tests to remove movements other than hip circles.

As in the measurement campaign of Chapter 3, we recorded the real scenario data in the DLR during the research stay. The inertial sensor is the *MTw Awinda* from *Xsens* [Xse20] and the optical system consists in the Vicon equipment [Vic20] together with the method proposed in [De 14] to estimate CORs. Section 1.3 includes more details of the equipment. Both inertial and optical measurements are recorded at a

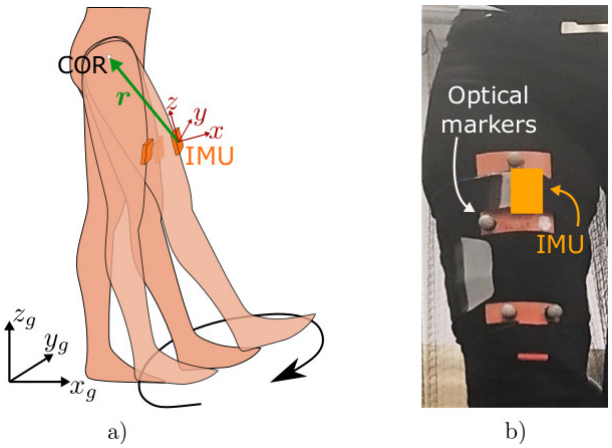


**Figure 4.10:** Experimental setup. a) Illustration of the movement performed by the volunteer in order to calibrate her/his hip. The COR, the IMU, its reference system and the global frame are shown. b) Picture of the mounting board with the IMU together with the four optical markers on the thigh of the volunteer.

sampling rate of 100 Hz. We synchronize both systems with an initial motion of flex-extension of the hip and the following detection of the maximum position and null turn rate measured with the optical system and the IMU, respectively, in the signals measured during calibration movement. In the definition of the mounting board, we ensure that its axes are aligned with the axes of the IMU and its location center is placed at the IMU accelerometer. Using the spatial location and position of the mounting board in the reference system of the Vicon, we translate the estimations of our reference IMU-joint vector $\mathbf{v}$ into the IMU system. We use the method proposed in [De 14] because it is aimed at estimating an adaptive $\mathbf{v}$, although we finally obtain an average vector for the complete test to improve its accuracy and eliminate the dependence with the number of samples considered for each estimation.

We obtain the location of the mounting board in which the IMU is placed, set at the location of the accelerometer in the device, its orientation and the position of each marker from the optical system. Since the IMU is aligned with the mounting board, we consider the data from the mounting board as the orientation and location of the IMU.

Besides, the covariance parameters are estimated as follows: we use the measurements of a static IMU to calculate the standard deviation needed to obtain the covariance matrix of the measurement noise; we estimate the estimation-error covariance matrix and the covariance matrix of the process using the reference data of one subject and adapting them to the best performance of ArVE$_d$, and we use these parameters for all the other subjects.

### 4.3.2 Metrics and errors

As optical methods are commonly used as baseline because they provide a high accuracy, we compare the outputs from both, ArVE$_d$ and our implementation of MrVS, with the results obtained trough the measurements from the optical system. We evaluate those methods with the same metrics that we used in the experiments on simulations to study the different sources of errors, described in section 4.2.2. In this case, our reference to determine the errors of ArVE$_d$ and MrVS is the **v** vector, obtained with the optical system and translated into the IMU system.

### 4.3.3 Evaluation of the adaptive r on human joints

On the real scenario of human hips, we have a reference **v** from the optical system, depicted in gray in Figure 4.11. We use this reference to evaluate the estimations of the variable $\boldsymbol{r}$ adapted to these changes caused by the STA using ArVE$_d$ and the average $\boldsymbol{r}$ for the complete test with MrVS. Figure 4.11 shows that results from both adaptive algorithms, ArVE$_d$ and the optical system, experience periodic changes caused by the STA in legs during the experiment. This is coherent with the exercise since it consists in repetitions of the circles performed from the hip.

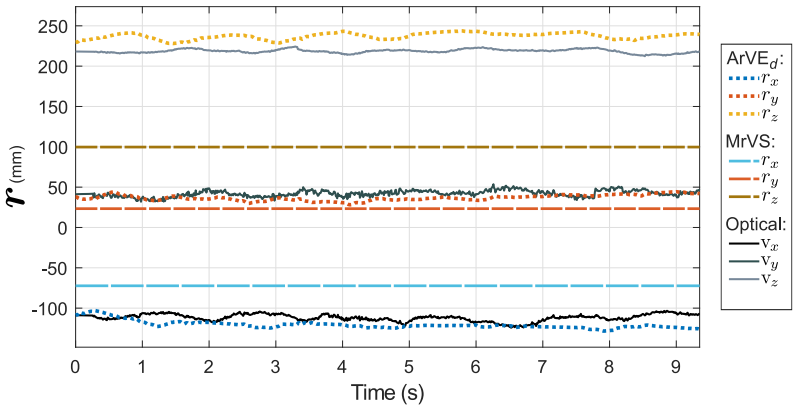


**Figure 4.11:** IMU-joint vector obtained with ArVE$_d$, depicted in blue, red and yellow dotted lines; with MrVS, presented in cyan, red and mustard stripes; and with the visual-based method, black and gray depicted in continuous lines.

Figure 4.12 depicts the norm of the difference vector $\|\Delta\boldsymbol{r}\|$, the difference of norms $\Delta\|\boldsymbol{r}\|$ and the deviation angle $\gamma$ of the estimations of ArVE$_d$ and MrVS with respect to **v** in the case of each evaluated volunteer. According to this figure, the errors obtained with ArVE$_d$ are similar for all volunteers and MrVS provides errors with great variability, so the accuracy of MrVS depends more on the volunteer. Also, these results show the decrement of $\|\Delta\boldsymbol{r}\|$ and $\Delta\|\boldsymbol{r}\|$ errors using ArVE$_d$ versus using MrVS in all cases and the deviation angle is similar in most cases around 5 ° with both methods, so the adaptive

method is the most accurate. The differences in the average values of those errors are also consistent with this affirmation.

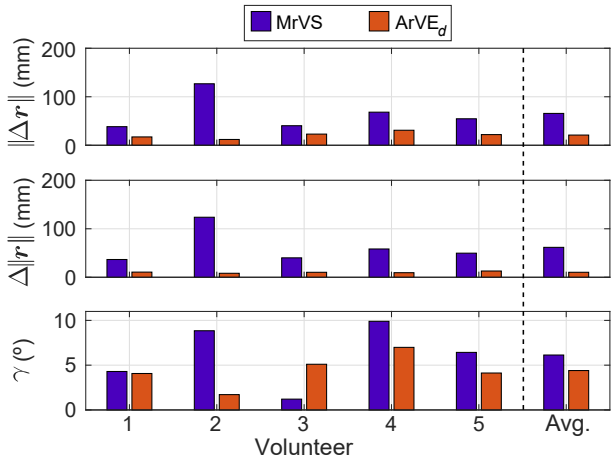


**Figure 4.12:** Errors obtained for each evaluated volunteer with MrVS and ArVE$_d$ compared with $\mathbf{v}$. The average values are also included with the label Avg.

Table 4.2 shows the values of the errors depicted in Figure 4.12 together with the norm of their corresponding reference vector $\mathbf{v}$. Differences exist between the metrics of both methods, being specially noticeable with respect to the difference between modulus $\Delta\|\boldsymbol{r}\|$ that decreases from 62 mm (28.0 %) until 10 mm (4.5 %).

**Table 4.2:** Average differences between ArVE$_d$ and MrVS compared with the optical method for the five volunteers, together with the average (Avg.) values.

| Volunteer | $\|\mathbf{v}\|$ mm | Method | $\|\Delta\boldsymbol{r}\|$ mm | $\Delta\|\boldsymbol{r}\|$ mm | $\gamma$ ° |
|---|---|---|---|---|---|
| 1 | $166 \pm 1$ | ArVE$_d$ | $17 \pm 5$ | $11 \pm 6$ | $4 \pm 2$ |
| | | MrVS | $38 \pm 1$ | $37 \pm 1$ | $4 \pm 1$ |
| 2 | $249 \pm 4$ | ArVE$_d$ | $12 \pm 2$ | $8 \pm 4$ | $2 \pm 1$ |
| | | MrVS | $126 \pm 3$ | $124 \pm 4$ | $9 \pm 1$ |
| 3 | $228 \pm 1$ | ArVE$_d$ | $23 \pm 6$ | $10 \pm 7$ | $5 \pm 1$ |
| | | MrVS | $40 \pm 1$ | $40 \pm 1$ | $1 \pm 1$ |
| 4 | $235 \pm 2$ | ArVE$_d$ | $31 \pm 3$ | $9 \pm 6$ | $7 \pm 1$ |
| | | MrVS | $68 \pm 3$ | $58 \pm 2$ | $10 \pm 2$ |
| 5 | $226 \pm 2$ | ArVE$_d$ | $22 \pm 5$ | $13 \pm 7$ | $4 \pm 1$ |
| | | MrVS | $55 \pm 2$ | $50 \pm 2$ | $6 \pm 1$ |
| Avg. | $221 \pm 2$ | ArVE$_d$ | $21 \pm 2$ | $10 \pm 3$ | $4 \pm 1$ |
| | | MrVS | $65 \pm 1$ | $62 \pm 1$ | $6 \pm 1$ |

The variation between the different errors used to evaluate MrVS is worth highlighting. The average deviation angle $\gamma$ versus $\mathbf{v}$ is only around 6 °, but the error in the estimated norm $\Delta\|\boldsymbol{r}\|$ is 62 mm, that is a 30 % of the norm of $\mathbf{v}$. This variation is a consequence of

errors in the estimation of the angular acceleration $\dot{\boldsymbol{\omega}}$, since these estimations contain the propagation of errors in the measurements of turn rate $\boldsymbol{\omega}$. It only affects the norm since during the derivation the direction of this vector does not change.

According to Table 4.2, we achieve a decrease in $\|\Delta \boldsymbol{r}\|$ larger than a 60 % with ArVE$_d$ compared to using MrVS. ArVE$_d$ outperforms MrVS also in experiments on the real scenario. In addition, the $\|\Delta \boldsymbol{r}\|$ difference is in most of volunteers under the upper limit, achieving accurate results, and the averaged accuracy is 9.5 % of the average norm of $\mathbf{v}$, which is lower than the upper limit.

Our adaptation of MrVS obtaining an average $\boldsymbol{r}$ for the complete test entails $\|\Delta \boldsymbol{r}\|$ differences of 65 mm, meaning a 29 % of relative error. Therefore, this method is not accurate enough to be used in the estimation of CORs with a low speed in limbs with STA. Differences are larger than the reported in the previous studies that use MrVS because the conditions of the evaluated tests are different, as in [Cra17]. In particular, the authors evaluate the arm and the experiments are based on two perpendicular linear motions, as crosses, with a maximum turn rate of 1.6 rad/s. However, our experiments are based on circular trajectories of the evaluated leg with an average turn rate of $0.8 \pm 0.1$ rad/s. This is worth highlighting since some of the leg exercises that may be prescribed to improve hip mobility include circular components, while not as many consider two perpendicular linear movements in a row. The speed difference is important, as it is stated in [Cra16], because errors are larger in the experiments carried out at a lower speed.

Furthermore, ArVE$_d$ is able to be implemented in real-time since it obtains one vector $\boldsymbol{r}$ per sample and only requires of the first 0.6 s of tests for the initialization. The algorithms are programmed in MATLAB R2019b, running in a personal computer (processor i7-8700 at 3.2 GHz, RAM memory 16 GB). In this platform, the average time for the execution of a sample with ArVE$_d$ is 0.03 ms. As the sampling rate is 100 Hz the available time for processing a sample is 10 ms. Since the execution time of a sample, i.e. the time to obtain one vector $\boldsymbol{r}$, is far lower than the sampling period, we consider that ArVE$_d$ is suitable for real-time applications, such as monitoring of rehabilitation exercises where null acceleration points exist (as in the orientation estimation of lower limbs presented in [Lin13] or [Bon15]). These results of accuracy prove the usability of ArVE$_d$ as an alternative to the optical methods, being adapted to the human lower-limb scenario when the joint is constraint to be fixed.

## 4.4 Conclusions

A novel adaptive method for IMU-joint vector determination is proposed and validated in this chapter using synthetic and real data from a hip. The method, called

ArVE$_d$, uses raw data from an IMU to determine in real-time the COR of fixed joints with respect to the IMU location at each time instant.

With the synthetic data, ArVE$_d$ achieves an accuracy higher than 1 % of length and 1 ° of deviation when the IMU-joint vector is constant and shows adaptability to variable vectors with an error around 3 % of length and 1 ° of deviation. This scenario of variable vector is in which the IMU undergoes from translational movements caused by STA apart from the main rotations. Besides, ArVE$_d$ has also been compared with our implementation of one state-of-the-art algorithm that we have called MrVS [Cra16] in this thesis. In all cases, the proposed ArVE$_d$ outperforms MrVS decreasing its errors around 50 %. The accuracy of ArVE$_d$ is 10 % when is tested on real volunteers performing standardized and repetitive exercises. In this case, the reference has been obtained with an optical system. Thus, ArVE$_d$ can be considered as an alternative to estimate the IMU-joint vector, obtaining a precise COR, suitable for monitoring rehabilitation therapies that imply the motion of ball joints, as shoulders or hips.

The initial results of this chapter are reported in two conference publications [Gar20a, Gar20b] and the ArVE$_d$ model is published in a journal paper [Gar21c].

# Chapter 5

# Physical Therapy Monitoring Database

One of the main limitations in the development of inertial algorithms is the lack of available data. In the proposal of new methods for human motion analysis, reference values are crucial. Besides, for a human monitoring based on the recognition or evaluation of exercises, the development of novel algorithms requires the information about the performed activity. In this way, each study of this field has to complete an initial step of a measurement campaign focused on its own particular objective. With the generation of unique data, the comparison of methods gets more complicated than if having a common database due to possible unfair situations. So the lack of publicly available data of human motions properly labeled and with a reference from a highly accurate system limits the development of new proposals and the comparison to find the most suitable one.

This chapter introduces the PHYTMO (from PHYsical Therapy MOnitoring) database, which aims to contribute to the research of the monitoring and evaluation of the performance of prescribed physical therapy exercises through inertial wearable sensors. The objective is to contribute in two areas: the analysis of techniques for the identification and evaluation of exercises using inertial sensors and the validation of inertial sensor-based algorithms for human motion analysis. The database contains data from physical therapies recorded with inertial sensors, including information from an optical reference system. For the development of robust and generalizable algorithms, a large amount of annotated data are required, and the subjects variability is also important. In this way, this database includes enough data for developing ML-based algorithms, as those proposed in the literature [Bev18, Gig14].

PHYTMO includes data of the performance of 6 exercises and 3 gait variations commonly prescribed in physical therapies. Data are recorded with four IMUs placed on arms or legs, according to the performed exercise. Data also include the position and orientation of IMUs in the 3D-space during the performance of the 6 exercises measured with an optical system. Data of each exercise are divided into two kind of

series, which consist of correctly and wrongly performed exercises. A total amount of 30 volunteers with variability in age and morphology performed these exercises, what makes it possible to study the differences between kinematic parameters that can occur in the execution of exercises at different ages. The anonymous subjects can be easily associated with their anthropometric information for this purpose. Furthermore, the data are labeled for the identification of each exercise separately, annotating its correct or incorrect performance.

In addition, this database can be very useful to train algorithms developed for human kinetic analysis. Using these data, IMU-based algorithms for kinetic parameter estimation can be developed or analyzed, as different proposals found in the literature [Lin13, M B16, All17b, Mul17c]. This application is especially noteworthy because PHYTMO includes data from IMUs together with reference data from an accurate optical system, related to the 6 exercises based on repetitions of motions. Therefore, this database can be used to check different proposals using the same data, facilitating a fair comparison between algorithms. PHYTMO is already publicly available in Zenodo [Gar21a].

## 5.1 Methods

### 5.1.1 Participants and ethical requirements

Thirty volunteers enrolled in the study: 13 women and 17 men. Table 5.1 shows their anthropometric information together with their age, sex (masculine, M, or feminine, F) and their identifier (Id) in the database. Volunteers are separated by their age range in order to ease the analysis of different aged population. These ranges are clustered by decade, so range A includes volunteers aged between 20 and 29 years old, B between 30 and 39, C between 40 and 49, D between 50 and 59 and E between 60 and 69. Table 5.1 also includes the volunteers' motor conditions that may have influenced in their movements. All volunteers were healthy and robust and only three of them reported pain during the motion, although they were able to perform all the evaluated exercises.

The study was carried out in the framework of FrailCheck project (SBPLY/17/180501/000392), following all the COVID-19 guidelines and recommendations. Volunteers wore masks during the exercises performance, which should be taken into consideration in the motion analysis because of possible early fatigue even in healthy volunteers. Guadalajara University Hospital approved the study protocol (Institutional Review Board No. 2018.22.PR, protocol version V.1. dated 21/12/2020, see Appendix B), and all participants signed a written informed consent.

**Table 5.1:** Anthropometric data, age and sex of volunteers. M and F stand for masculine and feminine, respectively.

| Range | Id | Age (years) | Height (cm) | Weight (kg) | Sex (M/F) | Motor conditions |
|---|---|---|---|---|---|---|
| A | A01 | 22 | 165 | 58 | F | Not reported |
| | A02 | 26 | 167 | 64 | F | Not reported |
| | A03 | 25 | 166 | 56 | F | Not reported |
| | A04 | 23 | 180 | 72 | M | Not reported |
| | A05 | 22 | 185 | 71 | M | Not reported |
| | A06 | 26 | 171 | 72 | M | Not reported |
| | A07 | 25 | 175 | 78 | M | Not reported |
| | A08 | 22 | 175 | 72 | M | Not reported |
| | A09 | 23 | 175 | 60 | M | Not reported |
| | A10 | 25 | 167 | 65 | M | Not reported |
| B | B01 | 30 | 179 | 76 | M | Not reported |
| | B02 | 34 | 185 | 84 | M | Not reported |
| | B03 | 39 | 161 | 51 | F | Not reported |
| | B04 | 31 | 164 | 58 | F | Not reported |
| | B05 | 38 | 176 | 59 | M | Not reported |
| C | C01 | 49 | 166 | 66 | F | Not reported |
| | C02 | 46 | 178 | 69 | M | Not reported |
| | C03 | 42 | 172 | 93 | M | Not reported |
| | C04 | 44 | 170 | 75 | F | Not reported |
| | C05 | 48 | 167 | 62 | F | Not reported |
| D | D01 | 50 | 168 | 72 | M | Not reported |
| | D02 | 56 | 172 | 85 | M | Not reported |
| | D03 | 51 | 154 | 67 | F | Not reported |
| | D04 | 54 | 160 | 62 | F | Not reported |
| | D05 | 55 | 165 | 75 | M | Pain in the right shoulder |
| E | E01 | 63 | 186 | 87 | M | Not reported |
| | E02 | 60 | 157 | 56 | F | Not reported |
| | E03 | 60 | 158 | 76 | F | Pain in the right shoulder and right knee |
| | E04 | 68 | 161 | 63 | M | Pain in the right shoulder |
| | E05 | 64 | 168 | 70 | F | Not reported |

### 5.1.2 Acquisition setup

The PHYTMO data set includes data recorded with four IMUs and an accurate optical system. These data were recorded in the Motion Capture Laboratory of the University of Alcala using the *NGIMU* [xio21] IMUs (*X-io Technology*, Bristol, UK) and the *OptiTrack* [Opt20] system (NaturalPoint Inc). Wearable sensors include 3-axis gyroscope, accelerometer and magnetometer, with a range of 2000 °/s, 16 g and 1300 $\mu$T, respectively. These are common IMUs resolution values used for human motion monitoring, such as the popular *XSENS* sensors [Luo20]. Their sample rate was set to 100 Hz for the gyroscopes and accelerometers and to 20 Hz for the magnetometers in the reported data. The IMUs stored the recorded data on an SD card and as each volunteer finished performing the designed set of exercises, we downloaded the data to the computer for further data processing. They have a size of $56 \times 39 \times 18$ mm with a weight of 46 g, what makes them practical for wearing during the performance of exercises. Each IMU was mounted on an *ad-hoc* structure (mounting board) for its placing at the limbs.

Regarding the optical system, it is based on infrared light-emitting cameras situated in the capture room that identify the position of reflective markers placed on the subject anatomic landmarks and on the IMU structure. The optical system recorded the motions of the volunteers and the devices they wore along the data collection. We used the *OptiTrack* system, which consisted of eight depth *Prime 13* cameras with a resolution of 1.3 MP and a frame rate of 240 fps. We used this system with the *Motive 2.2.0* software to calibrate it before each use, to set the cameras rate to 100 Hz and to define the skeletons and objects corresponding to the IMU mounting boards to be recorded.

### 5.1.3 Acquisition protocol

The volunteer recordings were made in a continuous session on the day each volunteer was available and the individual session lasted an average of two hours. At the beginning of each day recordings, we set the coordinates origin of the optical system on the floor and always in the same point, so optical measurements are always referred to the same origin. We established the initial orientation of the IMU mounting board in the optical system placing this board on the floor, so in this orientation the rotation angles are equal to zero. The IMU $Y_I$-axis was parallel to the mounting board Z-axis and the IMU $Z_I$-axis was parallel to the board Y-axis, so the IMU $X_I$-axis was anti-parallel to the board X-axis, as depicted in Figure 5.1-left.

The four IMUs were placed at the upper-or lower-limbs, according to the performed exercises, with their $X_I$-axis pointing to the ceiling, as the reference systems shown in Figure 5.1-right. On the volunteers' lower-limbs, the IMUs were placed on the anterior surface, so when volunteers were standing, the $Z_I$-axis was perpendicular to the

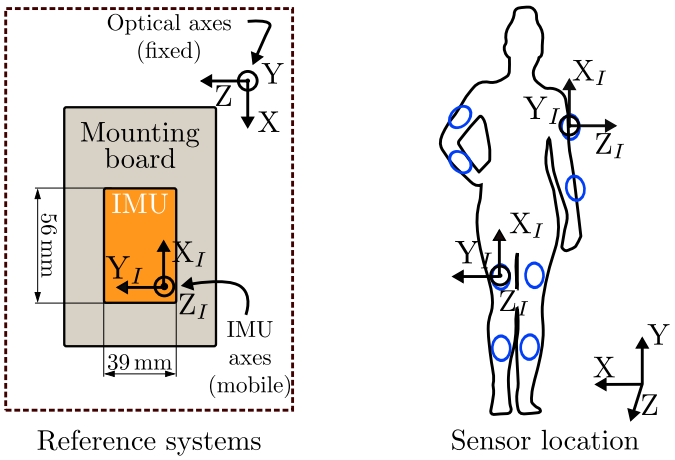


**Figure 5.1:** Axes of the optical and inertial systems and location of the IMUs on the lower-and upper-limbs. The picture on the left is a schema of the zenithal view of the IMU structure for the definition of its original orientation. The axes of the IMU and the optical systems are also depicted in the picture on the right, with the $X_I$-axes pointing to the ceiling in this position of the standing person. This picture also shows the axes of the optical system, where the XZ plane is parallel to the floor plane and the Y-axis points to the ceiling. The approximate location of IMUs (*Lshin*, *Lthigh*, *Rshin*, *Rthigh*, *Larm*, *Lforearm*, *Rarm* and *Rforearm*) are highlighted in blue in the picture. The silhouette graphic is from Vecteezy [Vec22].

coronal plane of their bodies and the $Y_I$-axis was perpendicular to their sagittal plane (Figure 5.1-right depicts these positions). On their upper-limbs, IMUs were placed on the exterior lateral position. In this case, when the volunteers' hands pointed to the floor, the $Y_I$-axis was perpendicular to the volunteers' coronal plane and the $Z_I$-axis was perpendicular to their sagittal plane. We chose these locations on the body for the easiness of placing sensors. Each IMU has an identifier with format *Xsegment*, where *X* refers to its position, left ("L") or right ("R"), being *segment* "thigh" or "shin", referring to the segment of the lower-limb the IMU was placed on, or "arm" or "forearm" for the upper-limb.

We synchronized the four IMUs through the identification of significant events in specific motions at the beginning of each recording. For the synchronization of the leg exercises, volunteers performed the three motions depicted in Figure 5.2, which consisted in: keeping the leg straight, two hip flex-extensions with the right leg to synchronize the two IMUs on this leg (Rshin and Rthigh), two hip flex-extensions with the left leg to synchronize the other two IMUs (Lshin and Lthigh), and two knee bending with both feet together in order to synchronize both legs by the detection of peaks in the signals of turn rate recorded by Lshin and Rshin. Data of arm exercises included two repetitions of straight arms elevation maintaining both hands together during the motion.

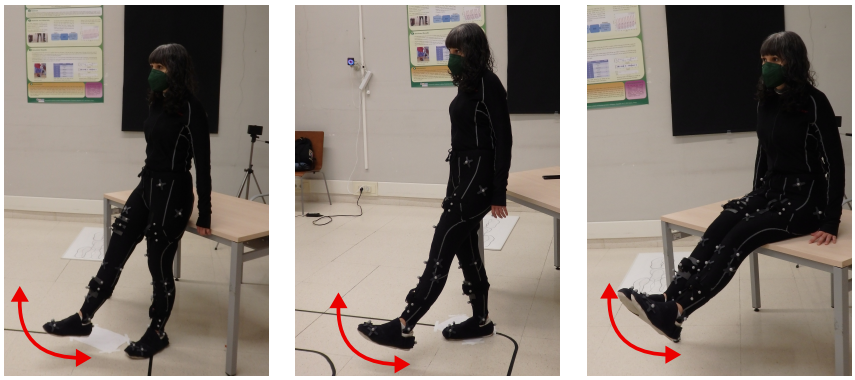

Rshin+Rthigh Lshin+Lhigh Lshin+Rshin

**Figure 5.2:** Data synchronization movements for the leg exercises. The labels under the pictures refer to the IMUs that are synchronized with each specific motion. The volunteer in the pictures has granted permission to publish.

After the synchronization phase, volunteers performed the different exercises or gait variations, commonly prescribed in a specific way in physical therapies. These particular movements have been chosen as part of a physical exercise routine prescribed for elderly people to maintain their functional capacity [Cas19]. The exercises can be divided into two groups of three exercises: focused on the lower-limbs and on the upper-limbs. Table 5.1.3 lists all the exercises and gait variations carried out by the volunteers, and describes the correct way to perform them. Before the motion recording, an initial description of the exercises set was explained by one of the authors of the study, who also performed each motion as demonstration. Besides the correct performance of the exercises, volunteers made them wrongly, receiving no instructions in this case. However, most of volunteers performed the wrong repetitions of the exercises in similar way, so we also report the most common deviations during the wrong performances in Table 5.1.3. The quality of the performance was evaluated by an expert person, who indicated how the proper exercises had to be done and labeled the exercises as correctly or wrongly performed. We only consider one kind of wrong gait for the three variations (GAT, GIS and GHT) during which volunteers walk freely but pretending to be tired, dragging their feet on the floor. Figure 5.3 shows pictures of all these evaluated exercises properly performed.

**Table 5.2:** Exercises included in the database together with the description of their correct and wrong performance.

| Exercise | Correct execution | Wrong execution |
|---|---|---|
| Knee flex-extension (KFE) | Sat on a stable surface, from the initial position of 90° of knee flexion, keeping the left leg still the right one moves in the sagittal plane extending the knee until its maximum. This variation is labeled as KFER. After all repetitions moving the right leg, this one remains still and the left one moves (KFEL). Number of repetitions: $10 - 20$. | • Deviations from the sagittal plane<br>• Focusing the motion on the thigh<br>• Moving both legs instead of only one of them |
| Squats (SQT) | From standing position, volunteers make the exercise sitting on a chair, avoiding the lateral bending of knees or hip, and when touching the chair they stand up again. Number of repetitions: $8 - 15$. | • Seating on the chair<br>• Without touching the chair<br>• Supporting their weight with their hands during the sitting or standing |
| Hip abduction (HAA) | Standing up, keeping the left leg still the right one moves upwards to the exterior side in the volunteer's frontal plane, remaining straight. This variation is labeled as HAAR. After all repetitions moving the right leg, the right leg remains still and the left moves (HAAL). Number of repetitions: $10 - 20$. | • Deviations from the frontal plane<br>• Bending the knee during the execution<br>• Lack of motion control |
| Gait (GAT) | Volunteers walk freely in the room. Number of repetitions $> 20$. | • Dragging the feet |
| Gait describing $\infty$ (GIS) | Volunteers walk around two objects on the floor, describing a trajectory similar to the infinity symbol ($\infty$). Number of repetitions $> 20$. | • Dragging the feet<br>• Without following the trajectory (GAT) |

| | | |
|---|---|---|
| Gait with heel-tiptoe (GHT) | During walking, volunteers place first the heel on the floor and then they raise into their tiptoe. Keeping their weight into their tiptoe, they place the other heel on the floor and repeat the motion. Number of repetitions $> 20$. | • Walking without the heel-tiptoe motion (GAT) |
| Elbow flex-extension (EFE) | Both arms move from the straight position to the maximum flexion of elbows in the sagittal plane, keeping the shoulders still. Number of repetitions: $10 - 20$. | • Moving only one arm<br>• Focusing the force on the back<br>• Deviating the motion from the sagittal plane |
| Extension of arms over head (EAH) | With both hands together, arms, as straight as possible, make a arch until reaching the maximum elevation of hands. Number of repetitions: $10 - 20$. | • Making the force with only one arm<br>• Not raising the arms over the head<br>• Separating both hands |
| Squeezing (SQZ) | Using a clothing and keeping arms straight forward, wrists move anti-symmetrically squeezing the clothing. Number of repetitions: $10 - 20$. | • Moving only one wrist<br>• Turning wrists in other directions |

The number of repetitions varies according to the age of volunteers, being the volunteers included in A and B ranges who performed the highest amount of repetitions. Volunteers repeated each exercise series four times. Two of these series consisted in the corresponding exercises properly performed and, in the other two series, the exercises were wrongly done.

### 5.1.4 Calibration of legs

In the human motion analysis field, it is common to use the information of the joints location or orientation [Lin13, M B16, All17b, Xu18]. Thus, PHYTMO also includes

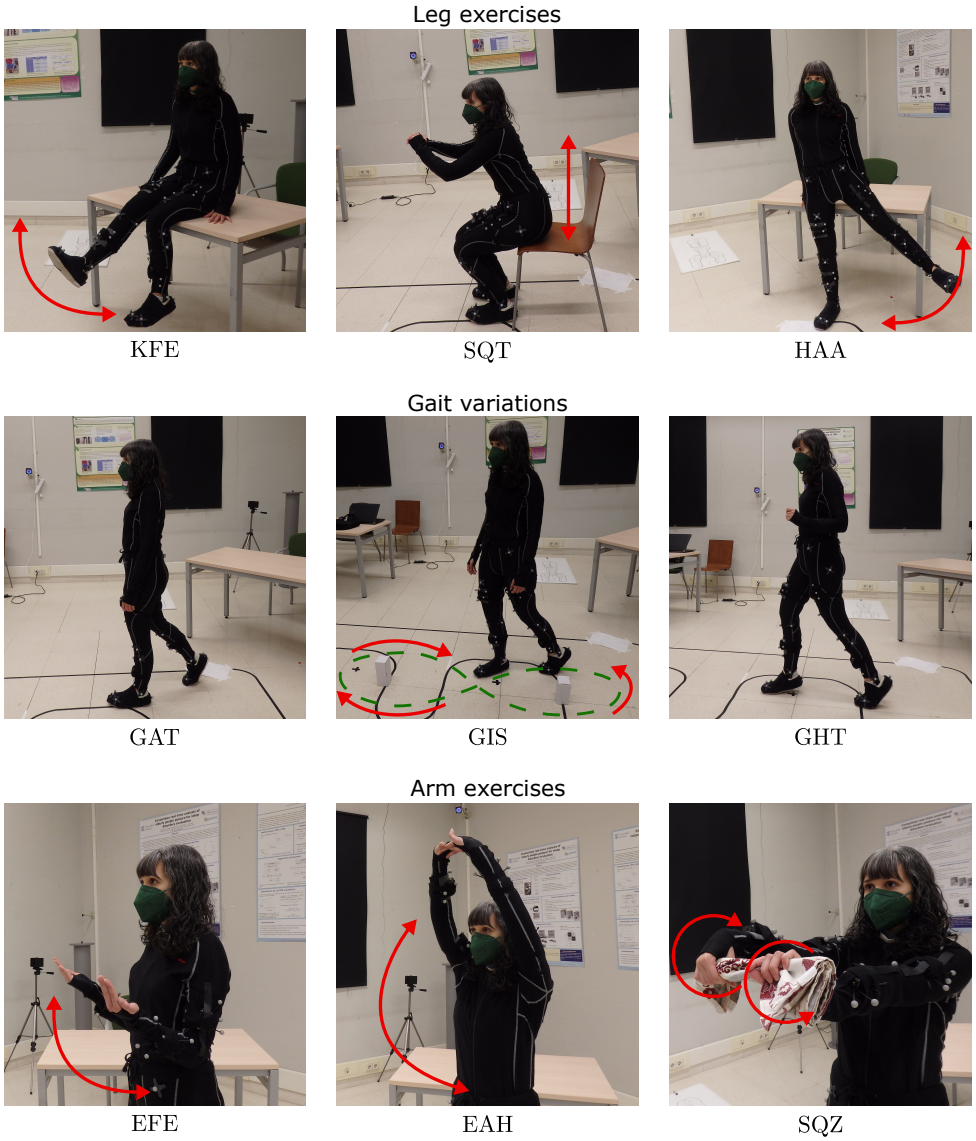


**Figure 5.3:** Exercises considered in this study performed by one of the volunteers. The first row includes knee flex-extension (KFE), squats (SQT) and hip abduction (HAA). The middle row contains natural gait (GAT), gait describing the infinity symbol (∞) in the trajectory (GIS) and heel-tiptoe gait (GHT). The last row presents elbow flex-extension (EFE), extension of arms over head (EAH) and squeezing (SQZ). PHYTMO includes the inertial data during all these exercises and the reference from a three-dimensional optical system of the leg and arm exercises (first and last rows). The volunteer in the pictures has granted permission to publish.

three motions for the calibration of joints. The volunteers performed the following three motions in order to have information to calibrate their lower-limbs:

- Hip circles: standing, keeping the hip still and maintaining the legs completely straight, the volunteers performed circles with one leg (see Hip COR in Figure 5.4). With this motion, the COR can be estimated using algorithms as different works propose [Cra17, Gar21c, Fri18a].

- Hip frontal flex-extensions: standing, keeping the hip still and maintaining the legs completely straight, the volunteers moved this leg in a forward-backwards motion (see Hip axis ⊥ sagittal in Figure 5.4). With this motion, the axis perpendicular to the sagittal plane can be determined using different methods in the literature [See12, Cra18].

- Knee frontal flex-extensions: sat on a stable surface, the volunteers moved the shin of one leg from its knee in a forward-backwards motion with a low range of motion, around 30 °, keeping the knee still (see Knee axis in Figure 5.4). With this motion, the location of the axis can be determined using some proposed methods [Cra18, Fri18a, See12].

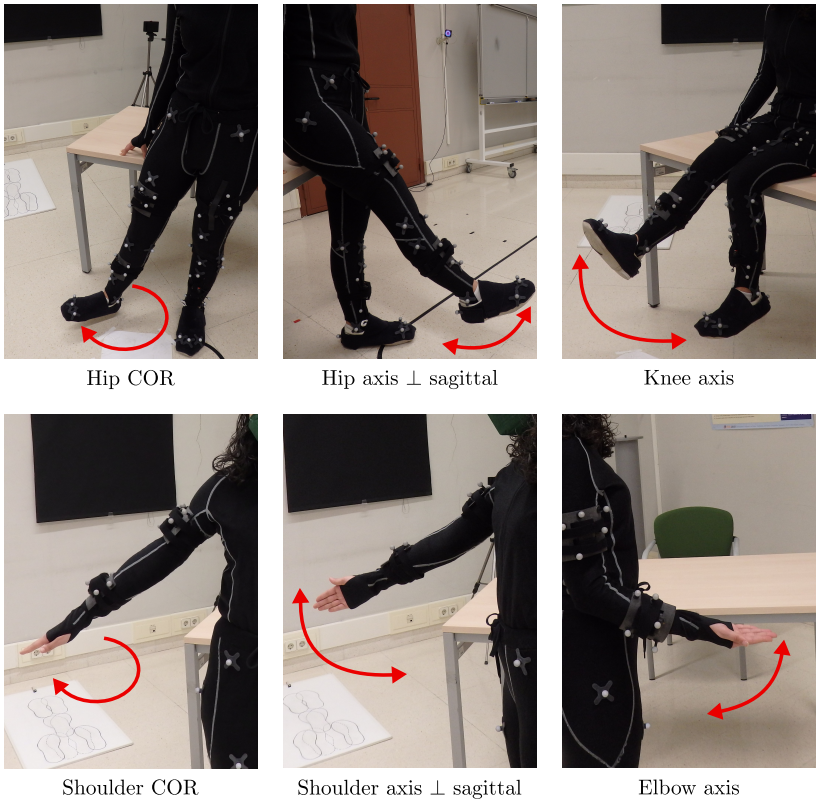


**Figure 5.4:** Motions performed for the calibration of the sensors with respect to the location and orientation of the CORs and AORs of leg joints. Hip COR is the motion performed in order to determine the COR of hips, Hip axis ⊥ sagittal corresponds to the movements carried out to calibrate the hip axis perpendicular to the sagittal plane of the body and Knee axis is the motion that allows us to locate the knee axis and its orientation.

Similar motions were performed in order to calibrate the volunteers' upper-limbs, so the aforementioned methods, which are suggested for the inertial calibration of lower-limbs, can also be applied in this scenario. In this case, volunteers performed the following three motions:

- Shoulder circles:keeping the shoulder still and one arm completely straight, the

volunteers performed circles with this arm (see Shoulder COR in Figure 5.4).

- Shoulder frontal flex-extensions: keeping the shoulder still and maintaining one arm completely straight, the volunteers moved it in a forward-backwards motion (see Shoulder axis $\perp$ sagittal in Figure 5.4).

- Elbow frontal flex-extensions: keeping the elbow still and the hand in the supine position, the volunteers moved one forearm from its elbow in a forward-backwards motion with a low range of motion, around 60 ° (see Elbow axis in Figure 5.4).

### 5.1.5 Data processing

As previously mentioned, we synchronized the four IMUs through the identification of significant events in the recorded signals during specific motions at the beginning of each recording. We used *MATLAB R2020b* [Mat20] to manually select the time instants of negligible turn rate recorded with each sensor in order to set the initial time of each signal. We exported the data of each sensor separately in CSV format. More information about the name and organization of data is provided in the following section.

With respect to the optical system data, we used the *Motive 2.2.0* software [Nat20] to fill gaps caused by occlusions during the data recording, so we provide the raw and interpolated optical data. Firstly, we corrected the mislabeled markers in their current location. Secondly, we interpolated using the *Model based* option, which uses the information of the visible markers of an object to infer the trajectory of the others. Finally, we used the *Cubic* interpolation in order to fill the information of markers in which the previous interpolation technique did not work because less than three markers of an object were seen. This technique uses a cubic spline to fill the missing data.

## 5.2 Data Records

### 5.2.1 Raw data

All raw data files exported from both inertial and optical systems were stored as CSV files and have been uploaded to Zenodo [Zen20]. A total of 7 076 files are available with DOI `10.5281/zenodo.5052756`. Files are called with the nomenclature *GNNEEELP_S*, where *G* refers to the letter of the range of age, so it is "A", "B", "C", "D" or "E" (see Table 5.1); *NN* is number of identification of the volunteer, which is associated to the ranges of age, varies from "01" to "10"; *EEE* indicates the type of exercise (KFE, HAA, SQT, EAH, EFE or SQZ) or gait variation (GAT, GIS or GHT); *L* is the leg with the ex-

ercise is performed, so this letter is only included in the KFE and HAA exercises and it can be "L" or "R"; *P* is a label that indicates the evaluation of the exercise performance, which takes the "0" value when the file contains the correctly performed exercise and "1" when exercises are wrongly performed; and finally, *S* indicates the index of the series, being "1" for the first recorded series and "2" for the second one. In this way, if the third (03) recorded volunteer aged between 41 and 50 years old (C) performs the knee flex-extension (KFE) of the right leg (R) following the prescriptions of the exercise (0) in the first series (1), the corresponding file is called "C03KFER0_1.csv".

The main directory includes three folders called "inertial", "optical raw" and "optical interp", which contain the data recorded with the IMUs and with the optical system, respectively. The "raw" and the "interp" folders contain the raw and interpolated data, respectively. The data organization is different for the inertial and for the optical data, so they are separately explained bellow.

On the one hand, the "inertial" folder is divided into two directories which refer to the two possible group of limbs, that is "upper" or "lower". The corresponding internal structure is schematized in Figure 5.5 and detailed in the following. Each limb directory contains five folders ("A", "B", "C", "D" and "E"), corresponding to each age group of volunteers. The age group folders contain one directory for each limb segment, which follows the names given to the IMUs. Thus, there are four directories for the lower-limbs ("Lshin", "Lthig", "Rshin" and "Rthigh") and other four for the upper-limbs ("Lforearm", "Larm", "Rforearm" and "Rarm").

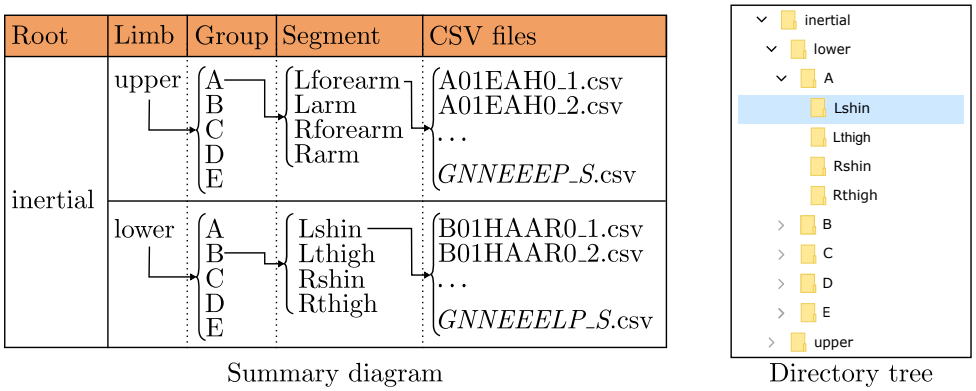


**Figure 5.5:** Data organization at the inertial folders. The upper and lower folders are included in the "inertial" directory. The "upper" and "lower" terms refer to the upper-and lower-limbs. The five groups correspond to the five age groups in which volunteers are organized. The segment folders are called according to the body side in which the IMUs are placed (left-L or right-R), and the corresponding limb segment. Finally, the CSV files follow the *GNNEEELP_S* nomenclature (*G*: range of age of the volunteer, *NN*: number of its identification, *EEE*: type of exercise, *L*: leg that moves, only in KFE and HAA exercises, *P*: evaluation of the exercise performance and *S*: index of the series).

On the other hand, the other two folders, "optical raw" and "optical interp", con-

tain two directories: "biomech_model" and "rigid_bodies", whose internal structure is schematized in Figure 5.6. The data of the markers placed directly on the body of each subject are contained in the "biomech_model" folder and the data of the IMU mounting boards are located in the "rigid_bodies" folder. Thus, "biomech_model" has only one folder, called "lower" to indicate that it corresponds to the lower-limbs, and this folder contains the five directories of each age group. Conversely, the "rigid_bodies" folder is divided into the two directories "upper" and "lower", with the corresponding age group folders (see Figure 5.6). Since the optical system includes the orientation and location of all the recorded objects in only one file, these data are not organized in segment folders but are included directly in the age group directories.

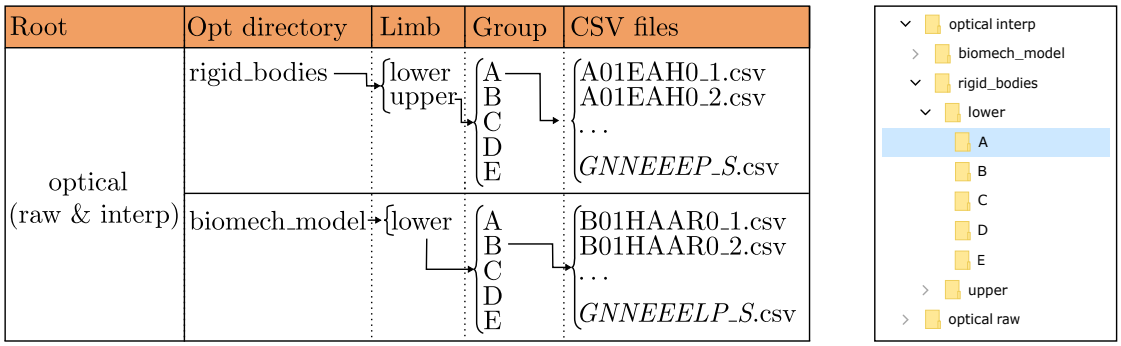


**Figure 5.6:** Data organization at the optical folders. The upper and lower folders are included in the "optical raw" and "optical interpolated" directories. The "upper" and "lower" terms refer to the upper-and lower-limbs. The five groups correspond to the five age groups in which volunteers are organized. Finally, the CSV files follow the *GNNEEELP_S* nomenclature (*G*: range of age of the volunteer, *NN*: number of its identification, *EEE*: type of exercise, *L*: leg that moves, only in KFE and HAA exercises, *P*: evaluation of the exercise performance and *S*: index of the series). The names of the files with interpolated data follow the same nomenclature and have "_interp" at the end.

Inertial systems, whose final CSV files organization is indicated in Figure 5.5, measure the turn rate, linear acceleration and magnetic field with the timestamp. This information is labeled in the inertial files as "Time (s)", "GyroscopeA (deg/s)", "AccelerometerA (g)" and "MagnetometerA (uT)", where "A" refers to the corresponding measurement axis (X, Y or Z). The information given by each sensor is detailed in Table 5.3.

Additionally, we provide the reference data of the optical system during the six repetitive exercises, i.e. the orientation and location in the 3D space of the IMU mounting boards. These files include three rows for the explanation of the recorded data. The first row indicates if the information corresponds to an IMU mounting board (Rigid Body) or to a marker (Rigid Body Marker). The second row contains the name of the corresponding Rigid Body. We defined four rigid bodies, named "shin" and "thigh" for the structures placed at the right side of the body and "shin2" and "thigh2" for the ones on the left side. The same mounting structures were used on legs and arms,

**Table 5.3:** Label of columns in the CSV files together with their units and description.

| | Column label | Unit | Description |
|---|---|---|---|
| Inertial | Time | s | Time since the turn on of the device until the recording of each sample |
| | Gyroscope | °/s | Turn rate. Divided into three coordinates: X, Y and Z, which correspond to the vertical, lateral and anterior directions. |
| | Accelerometer | g | Linear acceleration with the influence of the gravity force. Divided into three coordinates: X, Y and Z, which correspond to the vertical, lateral and anterior directions. |
| | Magnetometer | $\mu$T | 3D magnetic field. Divided into three coordinates: X, Y and Z, which correspond to the vertical, lateral and anterior directions. |
| Optical | OBJ/position | m | Position in/into the 3D space of the IMU object. Divided in three columns: X, Y and Z |
| | OBJ/orientation | N/A | Components of the orientation quaternion of the IMU object in the 3D space. Divided in four columns: X, Y, Z and W |
| | SKT/position | m | Position in the 3D space of the skeleton segment. Divided in three columns: X, Y and Z |
| | SKT/orientation | N/A | Components of the orientation quaternion of the joint in the 3D space. Divided in four columns: X, Y, Z and W |

placing always the "shin" named structures on the shin or forearm, and the "thigh" on the thigh or arm, according to the recorded exercise. In the Rigid Body Marker

case, the second row indicates the number of marker as "Rigid Body: MarkerNum", e.g. "shin:Marker1" corresponds to the marker labeled as "1" by the optical system that is part of the Rigid Body "shin". Finally, the third row distinguishes between the Rotation and Position information. The Rotation of the Rigid Bodies with respect to their initial position (see Figure 5.1) is provided in quaternions (note that markers do not have rotation information). The Position of the Rigid Bodies and the Rigid Body Markers, referred to the coordinates origin of the optical system, have magnitude of meters, as detailed in the "OBJ/position" and "OBJ/orientation" rows in Table 5.3.

PHYTMO also includes an extra file of the biomechanical model during the calibration of the lower-limbs of volunteers. In this way, we provide relevant anthropometric information that can be needed or used in the development of IMU-based algorithms for motion monitoring, as previous works propose [Lin13, M B16, All17b, Xu18]. The data of the lower-limb segments are indicated with the label "Bone" and when the data are referred to the position of markers, the corresponding label is "Bone Marker" . We use the Rizzoli Lower Body Markerset [Lea07], so the markers are called according to its protocol. The position of the Bones and the Bone Markers is measured in meters, as detailed in the "SKT/position" and "SKT/orientation" rows in Table 5.3. The names of skeletons are the group and identifier of the volunteer, as *GNN*, following the rules of the previously explained for the *GNNEEELP_S* nomenclature.

As an example, one representation of the inertial data during an exercise performed by one of the volunteers is depicted in Figure 5.7. We show the signals obtained with the tri-axial gyroscope, accelerometer and magnetometer of *Lshin* during the KFEL exercise when it is correctly performed and when the volunteer performed it wrongly.

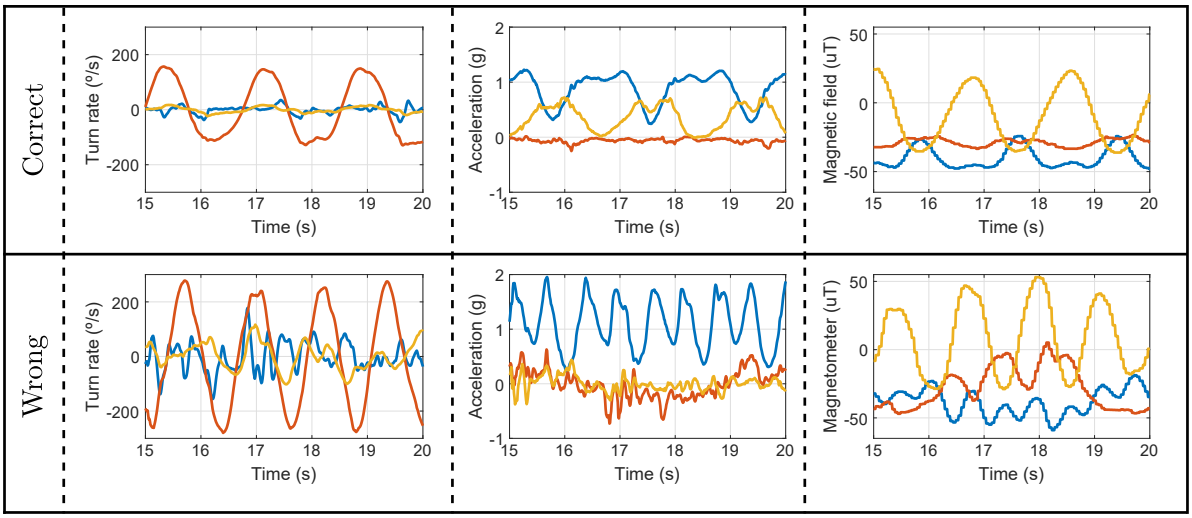


**Figure 5.7:** Signals from the gyroscope, accelerometer and magnetometer of *Lshin* during the KFEL exercise performed by volunteer A02. The corresponding files are "A02KFEL0_2.csv" and "A02KFEL1_1.csv", which are located at the "Lshin" folder.

Figure 5.7 shows that the correctly and wrongly performed exercises are alike, follow-

ing approximately similar patterns. However, the former is regular, the nine signals have similar amplitude in repetitions, whereas the latter shows changes between repetitions. Also, differences in the repetition duration and the magnitude of the signals can be observed. The features of these signals are studied in the following section in order to quantify these differences in performance.

### 5.2.2 Processed data

The files from the inertial system are provided in raw format, synchronized as previously explained. These signals contain relevant information for discerning the two kinds of performance of exercises: correct and wrong. One possible approach to extract information from the inertial system signals is to split them into repetitions of the exercises and analyze different features as the average, standard deviation, maximum and minimum of these segments.

One example of this analysis is represented in Figure 5.8, which shows some features of the three signals obtained with the accelerometer in *Lshin* through *boxplots*. Boxplots are standardized for displaying features using five numbers: minimum, maximum (both excluding the outliers), median, first quartile and third quartile. The outliers are also commonly depicted beyond the maximum and minimum. Thus, the boxplots in Figure 5.8 depict the quartiles and outliers of four features extracted from the acceleration signal of each repetition of the KFEL exercise correctly and wrongly performed by A02. The features analyzed with these boxplots are the average, standard deviation, maximum and minimum.

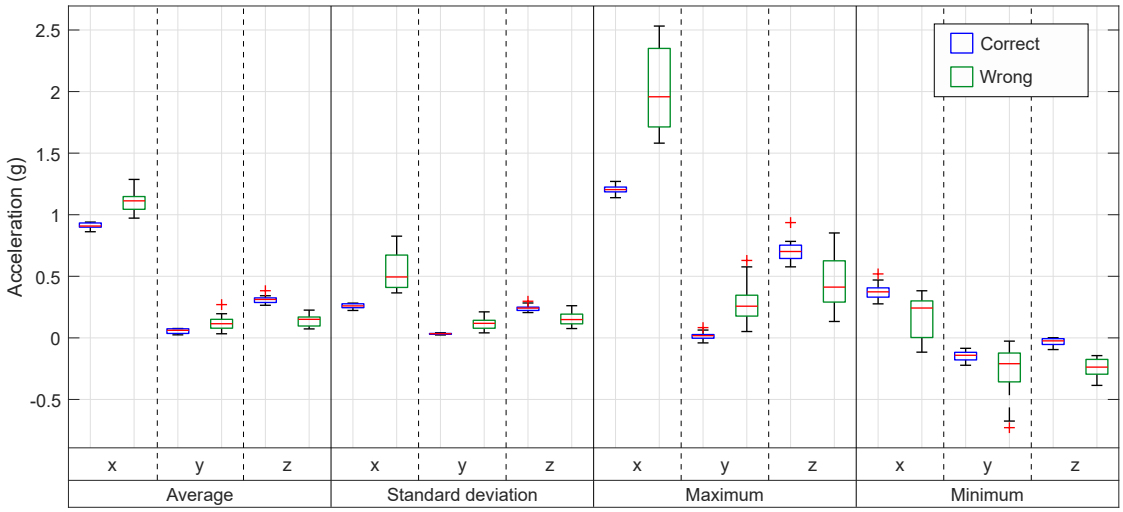


**Figure 5.8:** Boxplots of the mean, standard deviation, maximum and minimum of the acceleration measured by *Lshin* during the KFEL exercise performed by volunteer A02.

Figure 5.8 also shows the features of the correct exercises and the wrong ones. In this way, we can do not only a comparison between the two kinds of performance, but

also study the dynamics during both performances. The correct exercises show a low dispersion of data, with smaller boxes than those which correspond to the wrong performance. That is consistent with the signals depicted in Figure 5.7, which have similar amplitudes in the correct performance and high differences in its wrong performance. Furthermore, the median commonly differs between the two kinds of performance. Thus, the differences among these data make possible the classification between a correctly and wrongly performed exercise.

## 5.3 Technical Validation

### 5.3.1 Sensor placement

Volunteers wore tight and sporty clothing for the experiments in order to prevent sensor movement and limitations in the exercises performance. As described in the Methods (see Methods/Participants and Figure 5.3), the wearable sensors were placed on the legs or arms, according to the recording of an upper-or lower-limb exercise, and always with the $X_I$-axis pointed to the ceiling when volunteers were standing up. Sensors and optical markers were placed by the same two researchers to ensure consistency. It is also worth highlighting that previous to each recording, the optical system was calibrated, obtaining an error lower than 1 mm in all cases.

### 5.3.2 Missing data

Optical systems commonly loose data because of occlusions. We provide the raw and the filled data, in which we interpolate the missing data, in order to ease its use. The raw data include a 6.9 % of occlusions and we reduce until a 1.3 % of them when the data were interpolated. The interpolated files still have some missing data due to occlusions larger than 2 seconds in the raw data that were not accurately interpolated, as happened during the performance of the SQT exercise by some subjects who accidentally covered one or two IMUs during the exercise performance. We provide those files in which the data of some mounting boards are recorded as Rigid Bodies and other are missed. The recorded boards are given raw and interpolated along the complete recording.

When there were recording problems with the inertial system, we removed the erroneous data in PHYTMO (5 %). As a consequence, some volunteers have less recorded exercises.

## 5.4 Usage Notes

Different studies in the literature show that IMUs are valid for human motion monitoring, for the description of movements and for their evaluation. To ensure the usability of this database, the provided files are in CSV format, so they can be easily imported into Python or MATLAB.

This work contributes to the human motion analysis field by overcoming the lack of available data to compare algorithms. The validation of the proposals is so far performed on different data obtained for each of the studies. This difference makes it impossible to draw a fair comparison between them and, sometimes, not even the same metrics are available to compare them. This database helps to the development of new alternatives for motion analysis, by using the inertial data provided, and to their validation by using the reference data from the optical system. In this way, these data contribute to assess the strengths and limitations of various proposals. In addition, data are provided so that the research process does not require a previous step of collecting volunteers and recording movements in motion capture laboratories, and the data can be used directly.

Python tools are available, specifically for the analysis of the gait variations, which can be processed with GaityPy, which are Python functions to read accelerometry data and estimate gait features (`https://pypi.org/project/gaitpy/`). MATLAB also have tools for human motion analysis: the Kinematic and Inverse Dynamics toolbox (`https://www.mathworks.com/matlabcentral/fileexchange/72863-forward-and-inverse-kinematics`) can be used to study human kinematics and dynamics, and the Inertial Measurement Unit position calculator (`https://www.mathworks.com/matlabcentral/fileexchange/25730-inertial-measurement-unit-position-calculator`) can be applied for calculating the body's trajectory, velocity and attitude using data from an IMU as input.

Additionally, the presented IMU data can be used in OpenSim [Ope20], a freely available tool for musculoskeletal modeling and dynamic simulation of motions. Specifically, OpenSim has a workflow called OpenSense (`https://simtk-confluence.stanford.edu/display/OpenSim/OpenSense+-+Kinematics+with+IMU+Data`) that details the corresponding data processing to simulate the kinematics of the body using the measurements of IMUs.

This database contributes in other human monitoring fields different from the motion analysis. The data include different exercises and subject variability, which are also labeled for different classification applications. Some of these classifications can be human activity recognition, motion evaluation, or optimization of localization and number of sensors.

Finally, we help to its usability with the publication of the *features_extraction* function, developed for MATLAB in any of its version. This function splits signals using a sliding window, returning its segments, and extract signal features, in the time and frequency domain, based on prior studies of the literature [Zha20b, Pre20, Kia17, Bav19, Per19]. This function needs at least three signals from one triaxial sensor to extract their features, a window size in number of samples and a window shift that defines the distance between consecutive windows. The returning features are divided into the time and frequency domains. The time domain features are: mean of each signal, maximum of each signal, minimum of each signal, mean of the absolute value of each signal, standard deviation of each signal, variance of each signal, mean absolute deviation of each signal, root mean square of each signal, mean over the three axes of each sensor, average standard deviation over each three axes, skewness of each signal, average skewness over each three axes, kurtosis of each signal, average kurtosis over each three axes, 25, 50 and 75 quartiles of each signal, power of each signal, correlation between the three axes, correlation of each axis and the vector norm and entropy of each signal. The frequency domain features are always for each signal and they are the following: energy, absolute value of the maximum FFT coefficient, absolute value of the minimum FFT coefficient, maximum FFT coefficient, mean FFT coefficient, median FFT coefficient, discrete cosine transform and spectral entropy. Finally, a box plot of the selected features and sensor is depicted to ease the analysis of data in PHYTMO.

## 5.5 Conclusions

This data descriptor contributes to the research of the monitoring and evaluation of the performance of prescribed physical therapy exercises through inertial wearable sensors. PHYTMO is created for its use in the development of novel algorithms for human motion analysis, where is a lack of common data to validate and compare algorithms. Using these data, IMU-based algorithms for kinetic parameter estimation can be developed or analyzed, as different proposals found in the literature [Lin12, M B16, All17b, Mul17c]. This application is feasible because PHYTMO include data from IMUs together with reference data from an accurate optical system, related to the 6 exercises based on repetitions of motions. Therefore, this database can be used to check different proposals using the same data, facilitating a fair comparison among algorithms.

Furthermore, PHYTMO can be used for human motion monitoring, including the identification and assessment of a known set of prescribed exercises. The database includes enough variable data for developing ML-based algorithms, as those proposed in the literature [Bev18, Gig14].

The database presented in this chapter, PHYTMO, as far as we know, is the first data-

base with these characteristics. Its data are publicly available at Zenodo [Gar21a] together with a MATLAB function to increase its usability. In addition, the associated data descriptor is currently under review [Gar22a].

# Chapter 6

# Prescribed Motions Recognition and Evaluation

Motion analysis algorithms aim at estimating kinematic parameters of the motion. Alternatively, if the aim is to obtain a qualitative description of the movement performed, other algorithms are used, such as classifications based on ML methods.

The second research goal of this thesis is to investigate and implement ML algorithms for the recognition and evaluation of prescribed motions. The main aim is that this complete characterization of motions is based only on IMUs so we obtain objective information about their performance without limitations associated to other technological solutions.

Our approach is focused on home-based supervision systems, sometimes called virtual coaches, which are becoming increasingly important. These virtual coaches contribute to patients' adherence to physical treatments based on exercises [Kyr20b, Pal16], which is crucial to obtain the benefits of those long-term therapies. Inescapably, virtual coaches rely on the development of technological solutions to achieve those three objectives: to analyze the motions, to monitor the physical activity and to provide feedback to patients. The technological solutions have to be portable and everywhere usable in order to avoid the limitation of its use in controlled environments and increase their availability. We consider that virtual coaches based on IMUs fulfill all these requirements.

There are several proposals for the sport motion recognition using IMUs, most of them based on ML algorithms. IMUs and ML algorithms have been jointly applied to recognize fitness exercises [Pre20], swimming, tennis or basketball [Zha20b], among others [Cus19]. However, fewer proposals exist for the recognition of motions during the rehabilitation process. Besides the recognition, another problem related with the monitoring of physical routines is the evaluation of the exercises. This evaluation classifies exercises between correct or wrong performances and, in some works, different errors

in performance are evaluated. But these works use different ML algorithms for evaluating the performance of particular known exercises individually [Gig14, Hua16a, Bev18, Whe16, Gar21b]. These individual evaluation implies the classifier knowledge of the exercise to be evaluated, without requiring its previous recognition.

However, during a remote physical therapy, we do not have such information, and from a practical point of view, not only different exercises are carried out, but also they can be correctly and wrongly performed. Then, we have to consider both tasks (recognition and evaluation), that can be carried out separately or as a single task including the whole characterization of the performed exercises. As a consequence, both get more complicated. On the one hand, including correct and wrong performances of the exercises implies that their recognition entails a higher variability than if only accurate performances are taken into account. On the other hand, the evaluation of exercises relies on the correct recognition of motions. An error in the first stage will condition the result of the evaluation. If we combine both stages it results in an increase of the number of data classes, since they do not only include the kind of motions, but also their correctness. In conclusion, the complete characterization of exercises in prescribed routines is a complex task to study. To the best of our knowledge, no previous works deal with the whole exercises characterization as a single classification problem.

In this chapter, we analyze the problem of exercises characterization, recognizing and evaluating them, with the aim of establishing a first approach for its remote monitoring. We focus on eight upper-and lower-limb exercises included in a multidisciplinary routine found in the literature [Cas19], although it can be extrapolated to any exercise routine. The main objective is to characterize these exercises using inertial data from four IMUs placed on the person upper-and lower-limbs, in order to determine which one is being carried out and whether it is correctly or wrongly performed. The inertial data used are the previously introduced in Chapter 5, which are publicly available at Zenodo [Gar21a]. We evaluate several proposals by using the processed data from IMUs as inputs for six different ML algorithms [Bis06]: SVM, DT, RF, KNN, Extreme Learning Machines (ELM) and MLP.

Our main contribution is the proposal and validation of complete methods that cover the recognition of physical exercises considering also the quality in their performance. We evaluate the proposals with different ML algorithms and determine the most suitable one. In this way, we provide insights for the basis of exercises characterization by using ML algorithms.

## 6.1 Methods

The main goal of our proposal is to determine which exercise is carried out by a person in a therapeutic session and whether it is being performed according to its prescription (correct performance - C) or not (wrong performance - W). We refer to the process of determining the exercise as *recognition*, whereas the *evaluation* corresponds to the performance assessment, as correct (C) or wrong (W). Thus, our proposals both recognize and evaluate the exercises by measuring the turn rate and acceleration with four IMUs placed on the body of volunteers.

We detail three different approaches in section 6.1.1. We relate the formal classification problem with the objective of exercises characterization in section 6.1.2 and we provide a brief explanation of the ML algorithms used in this chapter in section 6.1.3.

### 6.1.1 Proposals for the exercises recognition and evaluation

Simultaneous exercise recognition and evaluation is a complex problem to solve. To deal with this issue, we propose three different approaches with the only *prior* knowledge of the type of exercises included in the dataset. Since the applied ML approaches are highly non-linear, the three proposals have to be characterized because they are not expected to be equivalent. These proposals are explained in the following:

- The first proposal, called "ReEv", makes the recognition and evaluation in one single step providing as outputs the type of exercise and its correctness. Its working scheme is shown in Figure 6.1. In this way, with one single classification process we obtain the complete characterization of the performed exercise. However, the number of classes doubles because we have the correct and wrong performance of exercises. That increment of classes complicates the classification task and, as a consequence, is expected to increase the error rates.

- From a practical point of view, we can assume that the recognition of exercises is relevant only if they are correctly performed. Therefore, the characterization of motions, i.e. determining the motion angles or the number of repetitions, is specially interesting in the correct repetitions. On the contrary, the wrongly performed exercises are required to be detected in order to get information about the correct comprehension of the description of exercises. The wrongly performed exercises of lower-or upper-limbs drive to quite similar features, easy to confuse even by humans, what reduce the accuracy rates. Our second approach, called "ReC-W", tries to surpass this issue by eliminating of the recognition process the wrongly performed exercises.

The main difference of ReC-W with respect to the first proposal, ReEv, is that ReC-W considers all wrongly performed exercises as two kind of motions, those performed with the upper-limbs and those performed with the lower-limbs. So this method only recognizes the correctly performed exercises, but assigns the generic labels, WU and WL (Wrong Upper-limbs, Wrong Low-limbs), to the wrong performances, as depicted in Figure 6.1.

- The last proposal, called "1Re-2Ev", divides the complete process of determining the kind of exercise and its performance quality into two different stages of classification. It is based on the hypothesis that separating the recognition and the evaluation into two different stages, both classifications would improve their accuracy rates. This would be a consequence of three different facts: *1)* the reduction of the number of classes; *2)* the increase of variability of each class in the recognition (by the mix of correct and wrong classes); and *3)* the simplification of the evaluation of each exercise separately after its previous recognition.

  Then, we separate both classifications as follows: the initial stage consists in a multi-class classification for the recognition of the exercise; and the second stage evaluates the recognized exercise making a binary classification, as schematized in Figure 6.1.

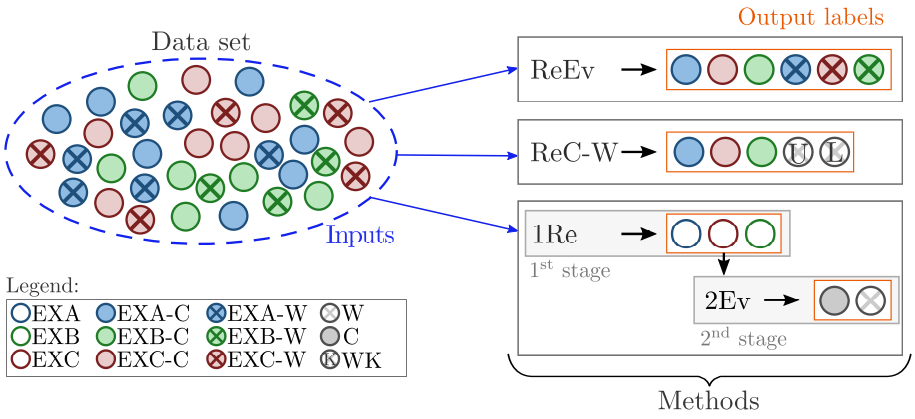


**Figure 6.1:** Scheme of the different classification approaches for the recognition and evaluation of exercises used in this study: ReEv, ReC-W and 1Re-2Ev. The scheme shows three different exercises, used as example: exercise A (EXA), exercise B (EXB) and exercise C (EXC); including also their correct (-C) and wrong (-W) performance label. Labels correct (C) and wrong (W) after the recognition of exercises are grey depicted, similar to the wrong label which specifies the kind of limb moved, called WK. In this label, K changes according to the limbs moved during the exercises, being WU when it refers to upper-limb exercises and WL when it does to lower-limb exercises.

### 6.1.2 Classification problem

Formally, we consider a set of input-output pairs $\mathcal{D} = \{(\mathbf{x}_i, y_i)\}_{i=1}^{N}$ where $\mathbf{x}_i \in \mathbb{R}^n$ are the $N$ samples of the input feature space obtained from the IMU signals recorded during the exercises and $y_i \in \mathcal{C} = \{C_j \mid 1 \leq j \leq J\}$ are the class to which these features correspond. The number of classes $J \in \mathbb{N}$ depend on each proposal. ML classifiers look for a decision function $f$:

$$\begin{aligned} f &: \mathbb{R}^n \to \mathcal{C} \\ \mathbf{x} &\mapsto y = f(\mathbf{x}, \omega) \end{aligned} \tag{6.1}$$

which given a sample, that in this chapter contains features from IMU signals, determines the output class, i.e. the one that includes the kind of exercise and its performance correctness.

The so-called parametric ML methods are characterized by a set of parameters $\omega$. During the training process, the ML classifier finds the parameters $\omega$ that best fit the given training data set. The aim of these methods is to find a function $f$ capable of generalizing its good accuracy to the given new data, which corresponds in this study to a person motion features recorded by the IMUs.

### 6.1.3 ML algorithms evaluated

We evaluate the performance of the following ML algorithms: SVM, RF, KNN, ELM, MLP and DT, which are explained in depth in Appendix A.4. All of them are supervised methods which require a labeled data set to be trained. We choose SVM, RF, KNN and the two neural networks, MPL and ELM, because they are the most promising algorithms for the sport monitoring and performance evaluation [Cam18] and recognition [Cus19]. Besides, we include DT as baseline method which is expected to present overfitting and be overcome, at least, by RF, an ensemble method of DT.

SVMs are classifiers which look for the maximum separation among different classes, i.e. their decision function is a separation hyperplane that maximally separates samples from different classes [Sch18]. Usually, SVMs apply appropriate non-linear maps to the input space $\phi\colon \mathbb{R}^N \to \mathbb{R}^p$ in order to guarantee that the transformed samples are more likely to be linearly separable in a higher-dimension feature space $\mathbb{R}^p$. This is the so-called *kernel trick*, which we employ to improve the performance of the classifier.

DTs are non-parametric methods based on simple decision rules inferred from data features [Bre01], but their overfitting problem is widely known. RFs are ensemble learning methods that construct $T$ classification decision trees to predict the outputs [Bre01]. They fix the characteristic overfitting problem of individual DT.

RF is one of the most accurate classification algorithms, with good scalable properties:

it efficiently deals with large amount of data and multiple input variables without consuming lot of resources such as memory. RFs are trained by the bootstrap aggregating technique [Bre96], selecting random feature trees during the training process.

KNN classification is a non-parametric ML method which finds a group of $k$ objects in the training set which are the closest to the test object [Sha08]. Frequently, it uses the Euclidean distance, weighting the importance of each feature, which is the distance used in this study. The assignment of a specific class is based on the predominance of a particular class in its neighborhood. The $k$ parameter specifies the size of the neighborhood, which votes for labeling the input data.

MLPs are a kind of feed-forward Artificial Neural Network (ANN) organized as a set of sequentially interconnected layers [Kub99, Bis95]. Each layer is fully connected, which means that all neurons of a layer have links to the neurons in the previous one, through which they receive information, emulating the synaptic links of the human brain. Links have associated weights that adjust the propagation of the information to the output. MLP has a high capacity of generalization, but suffers from overfitting if the number of layers, or neurons in each layer, is not well chosen. During the training process, the different algorithms search the best combination of link weights in order to optimize a goodness-of-fit function. The sequential network topology benefits the efficiency of the optimization methods. Optimization methods such as the backpropagation algorithm combined with the Levenberg-Marquardt algorithm [Lev44, Mar63] are possible due to this topology. In this thesis, both methods have been used for training the MLP.

ELM is a special kind of multi-layer perceptron, with one single hidden layer, characterized by being trained with a method computationally faster than the traditional backpropagation method [Hua06, Hua11]. The ELM training process randomly chooses the link weights of the hidden neurons, that frequently follows a uniform probability distribution. The weights of the links that connect the hidden layer to the output are computed establishing a linear least-squares problem which is solved calculating a fast pseudo-inverse, which considerably reduce the computation time during the training. ELMs have less capacity of generalization than MLPs, but suffer less overfitting during the training. The number of neurons of the hidden layer is the only hyperparameter to be determined.

## 6.2 Experimental protocol

The data consist in the dataset PHYTMO, presented in Chapter 5, which is summarized here for clarity. These data were recorded by inertial sensors placed on the volunteers' bodies while they performed the exercises commonly found in physical therapies. In this section, we detail the study population, the sensory system and the studied exer-

cises.

### 6.2.1 Study Population

Thirty volunteers participated in this study, 13 of them were women and the other 17 were men, whose anthropometric details, age and sex are in Table 5.1. They were all healthy people aged between 22 and 70 years old. In average, they were $169.1 \pm 7.9$ cm tall and had a weight of $69.5 \pm 10.3$ kg. In this way, we evaluate the proposed methods in a set of volunteers with variability in their age and anthropometric measures. Guadalajara University Hospital approved the study protocol (Institutional Review Board No.2018.22.PR, protocol version V.1. dated 21/12/2020), and a written informed consent was obtained from all participants. The approval from the Ethics Committee is in Appendix B.

### 6.2.2 Sensory system

During the performance of the physical routine, volunteers' motions were recorded with four IMUs. We used the commercial IMUs called *NGIMU*, by *X-io Technology* [xio21], which has a size of $56 \times 39 \times 18$ mm, what makes them practical for wearing during the performance of the studied motions. These IMUs include a 3-axis gyroscope, accelerometer and magnetometer, which have a range of $2000\,^\circ/s$ , 16 g and 1300 $\mu$T, respectively. In this work, we only use the gyroscope and the accelerometer that have a 16-bit resolution, and a maximum sample rate of 400 Hz. For the experiments, these devices measure the turn rate and specific force in each axis (six signals) during the exercises performance at a sample rate of 100 Hz. The signals of each device are stored into one micro SD card and processed off-line. However, the *NGIMU* has wireless communication what would meet the requirements of virtual coaching.

The experiments were carried out in the MoCap laboratory of the University of Alcalá. This environment is controlled and volunteers were recorded one at a time. IMUs were placed on the volunteers' thighs and shins during lower-limb exercises and on arms and forearms during upper-limb exercises. We used Velcro straps to secure the attachment of the sensors, while ensuring that their placement and tightness did not affect their freedom of movement. On the lower-limbs, we placed IMUs in the anterior surface of their limbs and, on the upper-limbs, IMUs were placed on the exterior lateral location, as Figure 6.2 shows. In all cases, the orientation of IMUs is the same, with the X-axis pointing to the ceiling when volunteers kept standing with their arms along their bodies and their hands pointing to the floor, see Figure 5.1. We selected those sensors location on the body because of the easiness of their placing.

Our proposals rely on maintaining this location of IMUs because the training data only

covers this configuration. As a consequence, following applications of these methods are limited to data obtained using the same IMU locations on the body.

**Figure 6.2:** IMUs placed at the right lower-limb and at the right upper-limb, marked with red circles. On the left limbs, there are two more IMUs at similar placements than in the right upper-and lower-limbs, respectively. Passive reflector sensors, which are commonly used to obtain optical reference data in biomechanical studies as in [Gar21c], are also shown. However, the optical data are not used in this study.

### 6.2.3 Experimental tests: exercises

A set of eight exercises were carried out by the volunteers, which are focused on the lower-or upper-limbs. Since two of them divides into their performance with the corresponding side of the body, right (R) of left (L), we study 10 types of exercises. These exercises consist in repetitive motions, commonly prescribed to older adults, that have to be performed in a specific way. In this study, volunteers mimicked the instructions found in [Cas19] in order to perform the exercises explained in the following. First, they carried out a set of lower-limbs exercises:

- Knee flex-extension (KFL/R): seated on a stable surface, from the initial position of 90° of knee flexion, keeping the left leg still, the right one moved until its extension and returned to knee flexion. After all repetitions moving the right leg, the right leg remained still and the left one moved, as shown in Figure 6.3-KFL/R.
- Squats (SQT): from standing position, volunteers made the motion of sitting on a chair and, when touching the chair with their back thighs, they stood up again. This exercise is depicted in Figure 6.3-SQT.
- Hip abduction (HAL/R): standing up, keeping the left leg still, the right one moved doing an abduction-abduction with the leg straight, as Figure 6.3 schematizes. After all repetitions moving the right leg, the right leg remained still and the left one moved.

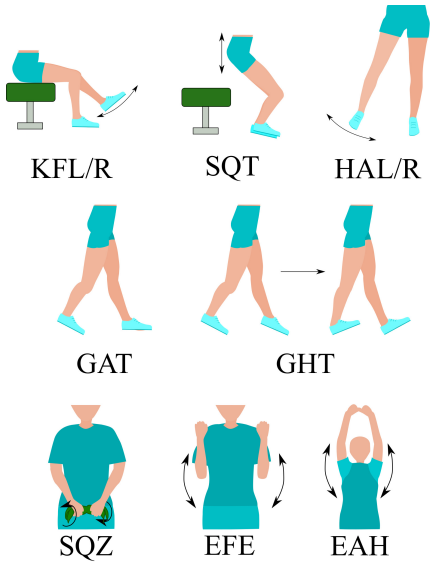


**Figure 6.3:** Exercises considered in this study, based on [Cas19]. The first row includes knee flex-extension (KFL/R), squats (SQT) and hip abduction (HAL/R). The row below contains natural gait (GAT) and heel-tiptoe gait (GHT). Finally, the column in the right shows squeezing (SQZ), elbow flex-extension (EFE) and extension of arms over head (EAH).

Besides these exercises of legs, we studied different variations of gait (see second row of Figure 6.3). We consider the gait variations as leg exercises because IMUs were placed on the volunteers' lower-limbs during their execution, even though they are more complex. Volunteers performed two gait variations:

- Gait (GAT): volunteers walked freely in the room.
- Gait with heel-tiptoe (GHT): during walking, volunteers placed first the heel on the floor and then they stood on tiptoe. Keeping their weight on their tiptoe, they placed the other heel on the floor and repeated the motion.

Furthermore, volunteers performed the following exercises of the upper-limbs, which are depicted in the third row of Figure 6.3:

- Squeezing (SQZ): using a clothing and keeping arms straight forward, wrists moved anti-symmetrically squeezing the clothing.
- Elbow flex-extension (EFE): both arms moved from the straight position to the maximum bending of elbows, keeping the shoulders still.
- Extension of arms over head (EAH): with both hands together, arms, as straight as possible, made an arch until reaching the maximum elevation of hands.

Volunteers repeated each motion between 10 and 20 times, according to their age, except for the squats. The squats were repeated only between 7 and 15 times to prevent

a wrong performance of the exercises caused by physical fatigue, as observed during the experiments with more repetitions. Volunteers performed four times each exercise series. Two of these series consisted in the corresponding repetitions properly done; and the other two series were wrongly performed, with a total motion freedom to modify the original exercise. The last two series are the ones labeled as wrong. More details about the exercises performance and their possible wrong executions are given in Table 5.1.3. Since volunteers made various motions for the wrong performances, data of this wrong exercises include a high variability. The gait exercises are an exception since we consider only one kind of wrongly gait variation, in which volunteers walked freely mimicking a tired gait or joint locking. So, gait divides into three variations: correct GAT, wrong GAT and GHT.

## 6.3 Data analysis

Figure 6.4 depicts the overview of the data analysis for the exercises recognition and evaluation using signals from four IMUs. The four dotted rectangles refer to the following sections: section 6.3.1 details the signal segmentation and feature extraction; section 6.3.2 defines the classes for each proposed method; section 6.3.3 introduces the optimization parameters or configuration for the ML algorithms; and section 6.3.4 describes the metrics used to evaluate the proposals.

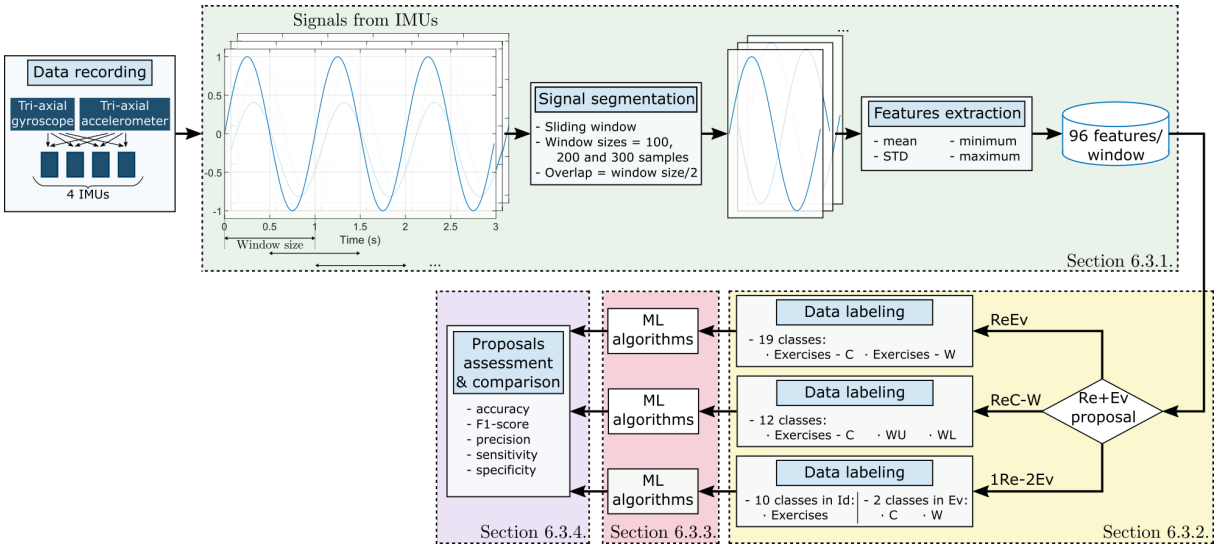


**Figure 6.4:** Flowchart of the data analysis. Using the IMU signals, we split them in windows and extract, from each one, its mean, average, minimum and maximum. Then, we label the data according to the corresponding proposal. The labeled data are the inputs in the ML algorithms, which are then assessed using five metrics. Each process box, squared with dashed lines, indicates the corresponding section of this document in which this process is detailed.

### 6.3.1 Signal processing

In this study, we use a sliding window to segment the raw IMU signals, as depicted in the green rectangle of Figure 6.4. Three window sizes are analysed: 100, 200 and 300 samples, which correspond to windows of 1 s, 2 s and 3 s, respectively. We limit the window size to 300 samples in order to find a balance between the algorithms' performance and the possible motions included in one single window. The larger the window, the more likely to mix different motions in them. Also, according to [Ban14b], the interval 1 s-2 s was proved to provide the best trade-off between recognition speed and accuracy when a high variety of features is employed. We limit the interval to 3 s because we use simple features in our analysis and they proved a direct relation between the features and the window size. In all cases, the overlap between consecutive windows is set to 50 % of the window size. We use four time-domain features commonly found in the literature: mean, standard deviation, maximum and minimum of signals over each axis. Since motions were recorded with four IMUs that record six signals each, the data set includes 96 features per window.

### 6.3.2 Data Labeling

The proposals are based on supervised algorithms, that require the labeling of samples for their training. To achieve a proper implementation of ML algorithms, in this step we ensure that labels are correctly associated to the corresponding classes and the number of data per label are balanced. We manually selected the beginning and the end of each exercise series and we associated the corresponding label to each group of features. We know the exercise performed and its quality by the design of the experiments and their supervision, as explained in section 6.2.3. However, the separation of the data between the different classes depends on the proposed method, since their output labels differ. It implies that the data labeling depends on the proposal and, more specifically, on the definitions of the classes into which the data are to be divided, as shown in the yellow rectangle of Figure 6.4. In the following, we explain this labeling process together with the labels assigned to each data class.

#### ReEv

In this proposal, labels include information of the kind of exercise and whether the exercise is correctly or wrongly performed, e.g. the EAH exercise, divides into EAH-C and EAH-W, which correspond to its correct and wrong performances. The only exercise that does not include the performance information is GHT because its wrong performance is included in the wrong performance of normal gait, so it is considered as the wrong GAT exercise. We study eight exercises, and two of them are divided into

the right or left sides of performance. As ReEv separately considers their correct and wrong performances, this proposal includes 19 classes, 9 kinds of exercises with their correct and wrong performance, and GHT.

#### ReC-W

The labels of the second proposal for the properly performed motions include the information about which exercise is being carried out. On the contrary, the wrong performances of the exercises are considered as only two kind of motions, those performed with the upper-limbs, labeled as WU, and those performed with the lower-limbs, labeled as WL. In this way, this proposal contains 12 classes (10 kinds of exercises, WU and WL).

Another main difference with the other two proposals is that in the design of ReC-W, we establish the number of samples in WU and WL (it means that we do not use the total number of samples, but we establish a quantity of them in order to ensure balance and variability). The other two methods include in their wrong-labeled classes those number of samples in which each exercise is wrongly performed because it is already balanced with the correct-labeled classes. In ReC-W, the number of samples in WU and WL has to ensure that the training set of the ML algorithms includes a high variability of wrongly performed motions so the test set can be properly classified. To do so, we separately double the number of samples in the largest class of the upper-and lower-limb exercises to establish the number of samples in WU and WL.

#### 1Re-2Ev

Since this proposal consists of two classification stages, we separate the labels depending on the objective of each stage. In the recognition stage, labels correspond to the kind of exercise, so we have 10 classes, whereas in the evaluation stage, the two possible labels indicate only if the classification is correctly (C) or wrongly (W) performed.

### 6.3.3 Classifier Training and Validation

After the extraction of the features and the labeling of associated windows, we trained the algorithms detailed in Section 6.1.3. For the optimization of hyperparameters, we split data into training set and validation set. The training set includes the data of twenty-four volunteers, the validation set includes the data of five volunteers. In this way, we have one volunteer left in order to test the algorithms through a LOSO cross-validation [Arl10], as explained in the following section. We study these algorithms using the Matlab R2020b software as follows:

- We evaluate SVMs with three different kernel mappings: linear ($SVM_L$), polynomial ($SVM_P$) and Gaussian ($SVM_G$).
- We optimize the minimum leaf size of DT.
- We validate the number of neighbors in KNN, analyzing from 1 to 20 of them and selecting the one that obtains the highest accuracy in the validation test.
- In MLP, we set the number of hidden layers to 1 since we do not observe any improvement of performance using more than one. We set the number of neurons as the average of the number of inputs (which is always 96 features), being the outputs the number of classes identified by the proposals, according to [Muk18].
- Since ELM is a fast algorithm, we validate the number of neurons from 10 to 1000 neurons and select the number that reports the highest accuracy.

### 6.3.4 Proposals Assessment

The proposals are evaluated with a LOSO cross-validation, using the data of each volunteer as test data set, so the training-test process is carried out 30 times, one for each volunteer. This is the most robust type of cross-validation in studies that involve human subjects, because it allows the subject-to-subject variability and avoids the autocorrelation in time series data obtained with one subject. It is also a more demanding cross-validation method than k-fold or random cross validation, so its results are expected to be worse than with those last types of cross-validation.

The assessment of the proposals is carried out in terms of the average metrics for the thirty volunteers. This is the final step, highlighted with a purple rectangle in Figure 6.4. The metrics considered operate separately for each class, which correspond to the kind of exercise and its performance quality. In this way, the positives ($P$) of a class are their number of sample, and the negatives ($N$) are the samples that correspond to the rest of classes. Positives are divided into true positives ($TP$) and false positives ($FP$) according to whether the samples really belong to the recognized class or they are misclassified, respectively. Negatives are also divided intro true negatives ($TN$) and false negatives ($FN$). $TN$ are those samples which do not belong to the considered class whereas $FN$ refer to the samples which really are members of the considered class but they are wrongly classified.

We study the proposals in terms of their accuracy (6.2), which measure the percentage of cases that the model has correctly predicted, although it must be combined with other different metrics for a meaningful analysis of the model. We also use the precision (6.3) to measure the quality in the detection of each class; sensitivity (6.4) to determine the effectiveness in the identification of each class; the F1-score (6.5) that

combines those two previous metrics assuming that both of them are equally important; and finally the specificity (6.6) relates to the model's ability to correctly classify a sample that does not correspond to a class in this way, so it measures the ability to detect negative labels.

$$\text{acc}\,(\%) = \frac{TP + TN}{P + N} \cdot 100 \tag{6.2}$$

$$\text{prec}\,(\%) = \frac{TP}{TP + FP} \cdot 100 \tag{6.3}$$

$$\text{sens}\,(\%) = \frac{TP}{TP + FN} \cdot 100 \tag{6.4}$$

$$\text{F1}\,(\%) = \frac{2\,TP}{2\,TP + FP + FN} \cdot 100 \tag{6.5}$$

$$\text{spec}\,(\%) = \frac{TN}{TN + FP} \cdot 100 \tag{6.6}$$

We study the average values for all classes and volunteers. In order to provide an in-depth study on the results, including the differences in the identification quality of each class, we also analyze the confusion matrices.

## 6.4 Experimental results

In this section, we describe and discuss the results of the proposals for the recognition and evaluation of exercises. We initially analyze the best window lengths and ML algorithms for the proposals in section 6.4.1. Then, we separately provide a detailed study of the three proposals. Section 6.4.2 contains the results obtained using ReEv, combining both classifications in one single step. Section 6.4.3 includes the results of ReC-W, which recognizes the correctly performed exercises and labels the wrong performances as WU or WL, depending on whether the motions are performed with the upper-or lower-limbs. Section 6.4.4 details the results of 1Re-2Ev, the two-stage method that firstly recognizes the exercises and secondly evaluates them. Finally, section 6.4.5 provides a comparison of the three proposals.

### 6.4.1 Windows length analysis and ML algorithms performance

In order to analyze the most suitable window length for the proposals and the best ML algorithm, we separately study the metrics with each proposal. For the case of ReEv, we provide in Table 6.1 its resultant accuracy, F1-score, precision, sensitivity

and specificity, using the three window sizes of 100, 200 and 300 samples. The first column for each window size shows the accuracy of each method, which in most of cases is about 80 %. As expected, the method that obtains the lowest metrics is DT, which is used as baseline, resulting in an accuracy lower than the 80 % with all the window sizes. This poor results are mainly caused by its common overfitting problem. Conversely, the two best algorithms are $SVM_L$ and RF.

**Table 6.1:** Classification results obtained with ReEv expressed in terms of accuracy, F1-score, precision, sensitivity and specificity. The first row specifies the window size for the signals cutting to obtain those metrics. The highest metrics of the two best methods are in bold and green, and the lowest metrics are in red color.

| | Window size = 100 samples | | | | | Window size = 200 samples | | | | | Window size = 300 samples | | | | |
|---|---|---|---|---|---|---|---|---|---|---|---|---|---|---|---|
| | acc (%) | F1 (%) | prec (%) | sens (%) | spec (%) | acc (%) | F1 (%) | prec (%) | sens (%) | spec (%) | acc (%) | F1 (%) | prec (%) | sens (%) | spec (%) |
| $SVM_G$ | 82.0 | 82.0 | 81.8 | 82.6 | 99.0 | 85.8 | 86.2 | 85.3 | 86.2 | 99.2 | 87.4 | 87.9 | 86.8 | 88.4 | 99.3 |
| **$SVM_L$** | **83.5** | **84.0** | **83.9** | **83.9** | **99.1** | **87.4** | **88.1** | **87.7** | **88.6** | **99.3** | **88.3** | **89.8** | **88.6** | **89.2** | **99.4** |
| $SVM_P$ | 82.7 | 82.6 | 82.6 | 83.0 | 99.0 | 86.1 | 86.9 | 86.3 | 87.6 | 99.2 | 87.5 | 88.3 | 87.6 | 88.7 | 99.3 |
| **RF** | **83.6** | **83.1** | **83.7** | **83.6** | **99.1** | **86.3** | **86.5** | **86.7** | **87.0** | **99.2** | **88.4** | **88.8** | **88.7** | **89.4** | **99.4** |
| KNN | 77.1 | 77.2 | 77.5 | 76.6 | 98.7 | 80.6 | 81.3 | 81.4 | 80.8 | 98.9 | 84.1 | 85.1 | 84.9 | 84.8 | 99.1 |
| ELM | 82.1 | 81.5 | 82.2 | 80.4 | 99.0 | 85.0 | 84.5 | 85.2 | 85.0 | 99.2 | 88.0 | 88.2 | 87.8 | 88.5 | 99.3 |
| MLP | 81.2 | 81.1 | 81.7 | 80.1 | 99.0 | 81.7 | 83.0 | 81.0 | 82.7 | 99.0 | 81.9 | 84.2 | 81.6 | 83.5 | 99.0 |
| DT | 69.3 | 69.7 | 70.0 | 69.2 | 98.3 | 72.8 | 72.9 | 73.7 | 73.9 | 98.5 | 75.5 | 75.5 | 76.2 | 76.3 | 98.6 |

We focus on $SVM_L$ to study the best window size because it gives the highest metrics in most cases. All its metrics improve with the enlargement of the window size from 100 to 300 samples. The accuracy increases from 83.5 % to 88.3 %, the F1-score from 84.0 % to 88.1 %, the precision from 83.9 % to 88.6 % and the sensitivity from 83.9 % to 89.2 %. So the most suitable window size is 300 samples. Conversely, specificity is above 99 % with all the ML methods and windows sizes, so this metric cannot be the criteria to choose the best proposal. This specificity value is due to the fact that the number of false positives of a single class is highly lower than its number of true negatives, which are the addition of the other correctly labeled exercises.

For the case of ReC-W, Table 6.2 shows its metrics. The best algorithms are $SVM_L$ and RF, whose results are written in green bold, and the worst is DT, whose results are highlighted in red. As in the previous method, the algorithm that obtains the best metrics is $SVM_L$, which range between 87.2 % and 99.2 %, improving with the window lengthening. Using $SVM_L$ the best metrics are obtained with a window size of 300 samples, it reaches an accuracy of 91.4 %, being the rest metrics about 90.7 %.

Finally, we analyze the results of 1Re-2Ev. Since this method divides the recognition and the evaluation of exercises into two different classifications, we study their results separately. Firstly, we evaluate the initial stage, the exercise recognition, in which each class collects the correct and wrong performances of the corresponding exercises. Secondly, we focus on the last stage, the exercise evaluation, whose inputs are the recognized exercises of the previous stage and classifies these exercises between correct or wrong.

Table 6.3 shows the resultant metrics of the recognition stage. The two best algorithms,

**Table 6.2:** Classification results obtained with ReC-W expressed in terms of accuracy, F1-score, precision, sensitivity and specificity. The first row specifies the window size for the signals cutting to obtain those metrics. The highest metrics of the two best methods are in bold and green, and the lowest metrics are in red color.

| | Window size = 100 samples | | | | | Window size = 200 samples | | | | | Window size = 300 samples | | | | |
|---|---|---|---|---|---|---|---|---|---|---|---|---|---|---|---|
| | acc (%) | F1 (%) | prec (%) | sens (%) | spec (%) | acc (%) | F1 (%) | prec (%) | sens (%) | spec (%) | acc (%) | F1 (%) | prec (%) | sens (%) | spec (%) |
| $SVM_G$ | 86.3 | 85.6 | 84.4 | 90.4 | 98.7 | 86.7 | 88.1 | 84.5 | 91.0 | 98.8 | 88.4 | 89.9 | 84.8 | 92.1 | 99.0 |
| **$SVM_L$** | **87.2** | **88.2** | **88.5** | **89.1** | **98.8** | **89.9** | **90.9** | **90.0** | **91.7** | **99.1** | **91.4** | **92.6** | **90.7** | **92.9** | **99.2** |
| $SVM_P$ | 85.8 | 85.9 | 84.8 | 88.6 | 98.7 | 88.1 | 89.6 | 87.5 | 91.6 | 98.9 | 89.3 | **89.9** | 87.4 | **92.4** | **99.1** |
| **RF** | **87.0** | **87.3** | **87.5** | **89.5** | **98.8** | **89.5** | **90.0** | **89.6** | **92.1** | **99.0** | **89.4** | 89.8 | **88.7** | 92.3 | **99.1** |
| KNN | 80.6 | 82.3 | 83.4 | 82.4 | 98.2 | 84.5 | 86.7 | 87.1 | 85.7 | 98.5 | 85.8 | 87.5 | 88.0 | 86.5 | 98.7 |
| ELM | 86.0 | 87.7 | 89.8 | 85.7 | 98.7 | 88.8 | 90.4 | 91.6 | 89.5 | 98.9 | 89.4 | 90.3 | 91.5 | 90.2 | 99.0 |
| MLP | 85.4 | 85.9 | 86.9 | 85.7 | 98.6 | 85.0 | 87.7 | 86.9 | 87.0 | 98.6 | 85.1 | 88.7 | 86.7 | 87.1 | 98.7 |
| DT | 75.7 | 77.0 | 76.4 | 79.5 | 97.7 | 79.1 | 80.1 | 79.6 | 82.1 | 98.0 | 77.2 | 77.6 | 76.6 | 80.5 | 98.0 |

printed its metrics in bold green, are SVM with the Gaussian and the polynomial kernels. These configurations obtain results above 95.2 % with all the window sizes. The kernel difference with respect to the previous methods is noteworthy. It means that gathering the correct and wrong performance of each exercise into one class, what implies an increment of variability in each class, the data distribution in the classes changes and their best separation is no longer with a linear hyperplane. The increase in variability also makes more difficult the generalization of the exercise recognition with RF, whose metrics are no longer included between the best ones. The worst algorithm is DT again, written in red in Table 6.3, as expected because of its results in the previous proposals.

**Table 6.3:** Classification results obtained in the first stage of 1Re-2Ev expressed in terms of accuracy, F1-score, precision, sensitivity and specificity. The first row specifies the window size for the signals cutting to obtain those metrics. The highest metrics of the two best methods are in bold green and the lowest metrics are in red.

| | Window size = 100 samples | | | | | Window size = 200 samples | | | | | Window size = 300 samples | | | | |
|---|---|---|---|---|---|---|---|---|---|---|---|---|---|---|---|
| | acc (%) | F1 (%) | prec (%) | sens (%) | spec (%) | acc (%) | F1 (%) | prec (%) | sens (%) | spec (%) | acc (%) | F1 (%) | prec (%) | sens (%) | spec (%) |
| **$SVM_G$** | **95.4** | **95.6** | **95.1** | **92.1** | **99.5** | **95.9** | **96.1** | **95.6** | **96.2** | **99.5** | **96.2** | **96.4** | **96.0** | **95.7** | **99.6** |
| $SVM_L$ | 94.8 | 94.8 | 94.7 | 92.0 | 99.4 | **95.8** | **95.8** | **95.7** | **95.5** | **99.5** | 96.0 | 96.0 | 95.9 | **95.8** | 99.6 |
| **$SVM_P$** | **95.2** | **95.1** | **95.0** | **92.6** | **99.5** | **95.8** | **95.8** | **95.7** | **95.0** | **99.5** | **96.1** | **96.1** | **96.0** | 94.8 | **99.6** |
| RF | 93.8 | 93.8 | 93.6 | 91.5 | 99.3 | 94.6 | 94.6 | 94.4 | 93.3 | 99.4 | 95.1 | 95.2 | 94.8 | 94.4 | 99.5 |
| KNN | 92.0 | 92.2 | 92.2 | 88.5 | 99.1 | 92.8 | 92.9 | 93.0 | 90.9 | 99.2 | 94.4 | 94.9 | 94.7 | 92.7 | 99.4 |
| ELM | 93.4 | 93.2 | 93.0 | 90.3 | 99.3 | 95.4 | 95.5 | 95.2 | 93.8 | 99.5 | 95.8 | 95.6 | 95.5 | 95.1 | 99.5 |
| MLP | 94.3 | 94.4 | 94.3 | 90.5 | 99.4 | 94.9 | 94.9 | 94.8 | 93.9 | 99.4 | 95.5 | 95.7 | 95.3 | 94.9 | 99.5 |
| DT | 87.5 | 87.9 | 87.7 | 84.4 | 98.6 | 89.8 | 89.9 | 89.8 | 87.4 | 98.8 | 89.9 | 89.8 | 89.9 | 87.9 | 98.9 |

With regard to the windows length, even though 1Re-2Ev provides a high accuracy with all the window sizes, using windows of 300 samples only improves 1 % the results obtained with the smallest size. However, this method allows us to determine the type of exercise being performed with good metrics by using the smallest window (100 samples). In this way, the most appropriate window size of 1Re-2Ev will be given either by the system requirements or by the second stage of the method.

In the exercises evaluation, carried out after their recognition, we focus on the accuracy as main metric and on the F1-score since it combines the precision and sensitivity. Table 6.4 shows these metrics for each of the evaluated exercises with the considered

ML algorithms.

**Table 6.4:** Classification results obtained in the second stage of 1Re-2Ev expressed in terms of accuracy, F1-score, precision, sensitivity and specificity. The first row specifies the window size for the signals cutting to obtain those metrics. The highest metrics of the two best methods are in bold green and the lowest metrics are in red.

Window size = 100 samples

| | EAH | | EFE | | SQZ | | GAT | | HAL | | HAR | | KFL | | KFR | | SQT | |
|---|---|---|---|---|---|---|---|---|---|---|---|---|---|---|---|---|---|---|
| | acc (%) | F1 (%) | acc (%) | F1 (%) | acc (%) | F1 (%) | acc (%) | F1 (%) | acc (%) | F1 (%) | acc (%) | F1 (%) | acc (%) | F1 (%) | acc (%) | F1 (%) | acc (%) | F1 (%) |
| **SVM G** | **94.8** | **94.7** | **94.2** | **94.3** | **87.3** | **85.8** | **87.7** | **82.9** | **93.4** | **92.8** | **88.2** | **87.9** | **95.9** | **95.8** | 93.7 | 93.5 | 81.2 | 78.9 |
| **SVM L** | 90.8 | 90.6 | 87.9 | 87.6 | 82.8 | 80.5 | **87.2** | **83.1** | **95.6** | **95.4** | **88.9** | **88.7** | 95.8 | 95.6 | **97.9** | **97.7** | **84.9** | **83.4** |
| SVM P | 91.9 | 91.7 | 93.6 | 93.5 | 83.8 | 83.3 | 86.3 | 80.6 | 92.5 | 91.8 | 86.5 | 85.5 | **97.2** | **97.1** | **95.2** | **95.0** | 80.1 | 78.7 |
| RF | **94.0** | **93.9** | **94.0** | **93.7** | **84.7** | **82.4** | 85.8 | 81.9 | 94.0 | 94.2 | 85.5 | 84.1 | 95.9 | 95.7 | 94.0 | 92.4 | **81.6** | **79.7** |
| KNN | 87.5 | 87.4 | 89.0 | 88.5 | 78.2 | 77.0 | 78.7 | 73.3 | 88.4 | 87.7 | 82.6 | 81.8 | 86.4 | 85.8 | 84.3 | 83.4 | 75.2 | 73.0 |
| ELM | 79.9 | 79.4 | 72.7 | 73.7 | 71.2 | 69.0 | 79.6 | 74.5 | 82.5 | 83.2 | 77.8 | 76.4 | 81.2 | 80.3 | 78.3 | 77.2 | 72.3 | 69.7 |
| MLP | 90.0 | 89.6 | 88.1 | 87.9 | 83.7 | 82.7 | 85.7 | 82.0 | **93.4** | 92.6 | 87.2 | 85.8 | 95.7 | 95.6 | 92.2 | 91.6 | 82.7 | 81.5 |
| DT | 84.9 | 84.6 | 87.4 | 88.4 | 74.3 | 72.1 | 79.5 | 74.5 | 87.2 | 86.3 | 75.7 | 74.6 | 85.2 | 84.6 | 82.5 | 80.6 | 70.5 | 68.3 |

Window size = 200 samples

| | EAH | | EFE | | SQZ | | GAT | | HAL | | HAR | | KFL | | KFR | | SQT | |
|---|---|---|---|---|---|---|---|---|---|---|---|---|---|---|---|---|---|---|
| | acc (%) | F1 (%) | acc (%) | F1 (%) | acc (%) | F1 (%) | acc (%) | F1 (%) | acc (%) | F1 (%) | acc (%) | F1 (%) | acc (%) | F1 (%) | acc (%) | F1 (%) | acc (%) | F1 (%) |
| **SVM G** | **98.4** | **98.4** | **97.8** | **97.7** | **90.6** | **89.5** | 89.7 | 85.8 | **97.5** | **97.4** | 92.4 | 91.8 | **100.0** | **100.0** | **98.1** | **98.1** | **92.2** | **91.8** |
| SVM L | 96.6 | 96.5 | 94.2 | 93.9 | 87.8 | 7.5 | **91.4** | **89.0** | 95.0 | 95.1 | **94.0** | **94.3** | **100.0** | **100.0** | **98.7** | **98.7** | 88.2 | 87.0 |
| **SVM P** | **98.4** | **98.4** | 95.6 | 95.5 | **90.9** | **90.2** | **90.4** | **87.4** | 96.7 | 96.5 | 93.1 | **93.0** | **100.0** | **100.0** | 95.6 | 95.5 | **90.9** | **90.2** |
| RF | **98.7** | **98.7** | **96.0** | **95.9** | 87.1 | 86.5 | 90.0 | 86.9 | 95.9 | 95.8 | **93.6** | 92.3 | 99.1 | 99.0 | 95.5 | 94.7 | 86.8 | 86.7 |
| KNN | 93.0 | 92.8 | 94.6 | 94.3 | 83.4 | 83.4 | 82.7 | 78.3 | 95.3 | 95.1 | 90.6 | 89.1 | 94.8 | 94.6 | 88.6 | 88.2 | 79.6 | 78.5 |
| ELM | 84.2 | 84.1 | 79.6 | 78.6 | 71.0 | 71.4 | 84.8 | 80.4 | 88.8 | 88.6 | 79.4 | 80.3 | 87.7 | 87.5 | 80.2 | 78.7 | 76.1 | 74.7 |
| MLP | 95.8 | 95.7 | 93.2 | 93.4 | 83.9 | 82.6 | 87.6 | 84.1 | **98.7** | **98.6** | 89.8 | 88.5 | 98.8 | 98.7 | 95.5 | 95.3 | 85.8 | 84.2 |
| DT | 90.0 | 89.8 | 93.2 | 93.5 | 80.6 | 79.1 | 76.6 | 73.0 | 83.7 | 84.2 | 83.9 | 83.7 | 93.4 | 93.1 | 82.7 | 82.2 | 72.1 | 69.6 |

Window size = 300 samples

| | EAH | | EFE | | SQZ | | GAT | | HAL | | HAR | | KFL | | KFR | | SQT | |
|---|---|---|---|---|---|---|---|---|---|---|---|---|---|---|---|---|---|---|
| | acc (%) | F1 (%) | acc (%) | F1 (%) | acc (%) | F1 (%) | acc (%) | F1 (%) | acc (%) | F1 (%) | acc (%) | F1 (%) | acc (%) | F1 (%) | acc (%) | F1 (%) | acc (%) | F1 (%) |
| **SVMG** | **100.0** | **100.0** | **100.0** | **100.0** | **96.3** | **96.0** | 91.3 | 88.0 | **100.0** | **100.0** | 92.4 | 91.9 | **100.0** | **100.0** | 99.3 | 99.3 | **95.1** | **94.8** |
| **SVM L** | **100.0** | **100.0** | 99.1 | 99.0 | 90.1 | 88.8 | **92.5** | **90.5** | 96.8 | 96.6 | **95.6** | **95.5** | **100.0** | **100.0** | **100.0** | **100.0** | **97.0** | **97.3** |
| **SVM P** | **100.0** | **100.0** | **100.0** | **100.0** | 92.4 | 92.0 | **93.6** | **92.2** | 99.0 | 99.0 | 92.9 | 91.8 | **100.0** | **100.0** | **99.8** | **99.8** | 94.0 | 93.5 |
| RF | **100.0** | **100.0** | **100.0** | **100.0** | **94.4** | **94.0** | 89.0 | 86.3 | 98.8 | 98.8 | **93.5** | **92.8** | 99.3 | 99.3 | 98.2 | 98.4 | 92.1 | 91.5 |
| KNN | 96.9 | 96.8 | 97.6 | 97.4 | 82.9 | 82.9 | 84.4 | 80.4 | 95.1 | 95.2 | 82.4 | 83.4 | 98.4 | 98.3 | 96.7 | 96.6 | 87.9 | 87.2 |
| ELM | 86.1 | 86.0 | 81.0 | 80.5 | 73.9 | 74.6 | 85.2 | 81.5 | 85.0 | 84.3 | 78.5 | 78.4 | 86.9 | 86.2 | 78.2 | 77.1 | 76.6 | 74.9 |
| MLP | **100.0** | **100.0** | 98.1 | 98.0 | 86.9 | 87.2 | 90.3 | 86.7 | **100.0** | **100.0** | 90.9 | 89.9 | 98.3 | 98.2 | 99.4 | 99.3 | 93.0 | 92.6 |
| DT | 93.9 | 93.7 | 88.1 | 87.6 | 84.9 | 83.1 | 77.1 | 73.5 | 87.5 | 87.0 | 84.8 | 83.1 | 95.0 | 94.8 | 86.5 | 86.6 | 75.9 | 73.7 |

Contrary to the results in the exercises recognition, in the evaluation stage, the metrics noticeably improve with the window lengthening. With the lowest windows, most algorithms achieve an accuracy between 90 % and 95 %, whereas with the largest ones, most algorithms show an accuracy above 95 %, reaching even some perfect classifications. Because of these results, the optimal window size for 1Re-2Ev is 300 samples, despite of the stage can be performed with smallest windows.

The worst algorithm with this approach differs from the other two proposed approaches. In this case, the ELM results in the poorest metrics, which are marked in red in Table 6.4. As in the case of DT, the main reason is its limited capacity of generalization.

The best results obtained with the 300-sample windows, marked in green in Table 6.4, are achieved with different variations of the SVM, whose results are shown in Figure 6.5 in order to ease their interpretation. Specifically, the Gaussian kernel, the one presented in blue, is the most suitable for the three window sizes, overcoming the other methods, in most of cases. However, this two-stage approach allows us to use a different algorithm depending on the recognized exercise. It is interesting because $SVM_G$ is in most cases the best algorithm, as seen in Figure 6.5, but there are three exercises in

which another kernel overcomes its accuracy. It is the case of he GAT, HAR and SQT exercises, whose evaluation is better with a linear kernel than with a Gaussian one.

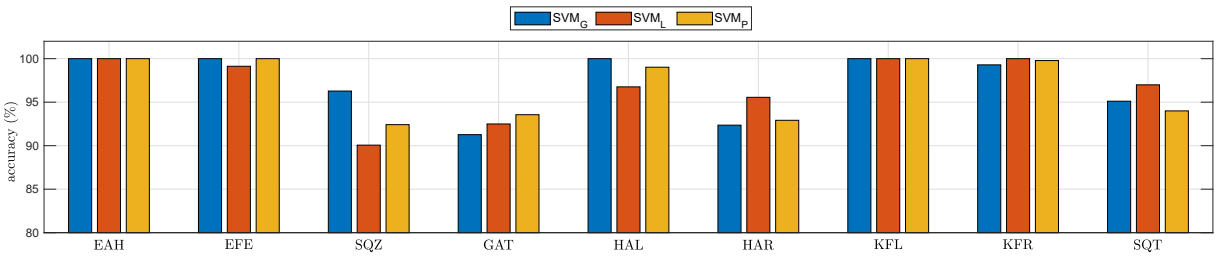


**Figure 6.5:** Accuracy of the different variations of SVM with the 300-sample windows, separated by the exercises. The interval zooms in the interesting area in order to ease the comparison of the different algorithms performances. We depict $SVM_G$ in blue, $SVM_L$ in red and $SVM_P$ in yellow.

Although the larger the window size, the better results, it is convenient to analyze whether a longer length could result in a significant improvement of the metrics. To do so, we study the metrics improvement with each window size enlargement. Using ReEv with $SVM_L$, its metrics improve around 4 % with the first lengthening, changing the window size from 100 samples to 200 samples, see Table 6.1. With the second lengthening, from 200 samples to 300 samples, metrics improve only around 1 %. The same differences in the improvement of metrics can be found in the results of the other three methods, included in Table 6.2, Table 6.3 and Table 6.4. According to the methods' metrics, enlarging the window size from 100 samples to 200 samples, we obtain the highest improvement. Then, we can conclude that windows above 300 samples will not significantly improve these results. In addition, we can consider 3 seconds (i.e. 300 samples) as the window size limit to avoid that several movements occur in the same window or are performed differently. Although increasing the window may be beneficial in terms of the evaluated metrics, temporal resolution of the execution of the exercises can be lost.

In [Pre20], they propose the use of 6 s windows, obtaining a similar accuracy as this thesis. Notice that the size of the window is the half. In this way, our signal processing includes less data so it is simpler. Conversely, we use an overlap of 50 % instead of 10 %, so we analyze each 1.5 s, whereas they provide information each second.

### 6.4.2 ReEv: recognition and evaluation in a single step

ReEv is the method with the most complex classification because it combines in a single step the complete characterization of the exercises. The best configuration of ReEv, using $SVM_L$ and windows of 300 samples, gives an accuracy, F1-score, precision and sensitivity between 88.3 % and 89.8 %, see Table 6.1. These metrics imply that we obtain

adequate results considering that we simplify the exercise characterization procedure to a single classification of nineteen classes with high variability.

In order to analyze in-depth the origin of errors and which are eliminated with the window lengthening, we study the average confusion matrix of the method that reports the best metrics, $SVM_L$. Figure 6.6 shows these average confusion matrices using a window size of 100 and 300 samples, respectively. The first quadrant of both matrices includes the lowest amount of errors, so among the correct exercises properly evaluated, the $SVM_L$ rarely misrecognizes the exercises. The main error in this recognition is between the two kinds of gait, GAT, the normal and GHT, the heel-toe gaits, as marked with the green square in Figure 6.6. These errors are a consequence of that GAT and GHT can seem similar exercises during some intervals of the motion.

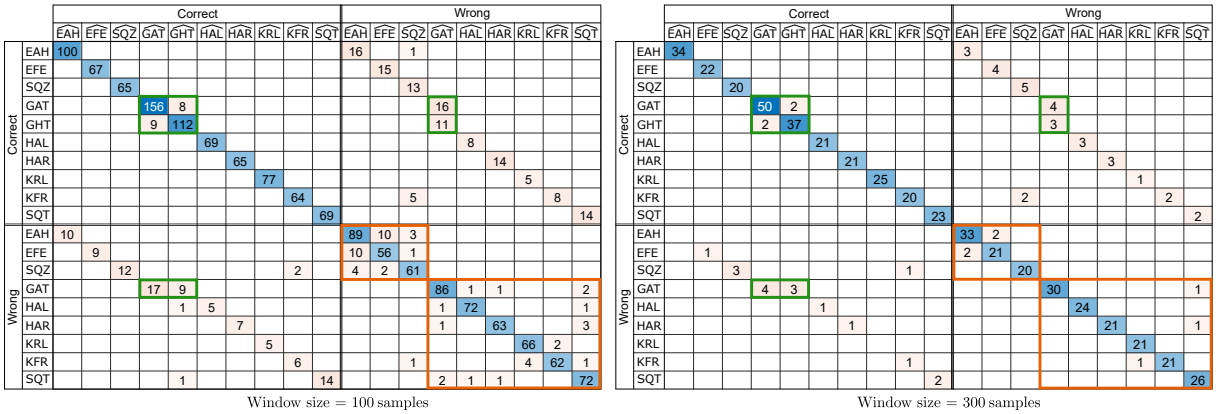


**Figure 6.6:** Average confusion matrix for the 30 volunteers using ReEv with $SVM_L$ and a window size of 100 and 300 samples (left and right respectively). Columns include the predicted classes, which are pointed out with a ˆ over their labels; and rows contain the actual classes. Double lines divide the correctly and wrongly performed exercises. The blue highlighted cells correspond to the average number of correct classifications and the cream colored ones indicate the misclassifications.

The second and third quadrants with a window size of 100 samples contain the highest number of errors. Their distribution is specially noteworthy since they form an almost diagonal line with the cells of misclassifications that correspond to each kind of exercise labeled as wrong whereas it is correct and the opposite. Again, the only exceptions are the highly related kinds of gait, GAT and GHT, which are marked with two green rectangles in Figure 6.6. In this way, errors by ReEv do not combine misrecognitions of exercises with their incorrect evaluations, but they can be divided into these two sources of error. Most of the errors of these quadrants are mainly caused by the incorrect evaluations of the exercises as correct or wrong. These errors are still present when the window lengthens to 300 samples, however, they are diminished and some of them are even eliminated. Thus, the evaluation of exercises requires a higher window size than the recognition of the correctly performed exercises.

It is worth highlighting that the errors from the evaluation as wrong of correctly performed exercises (32 misclassifications) double the errors from the evaluation as correct of wrongly performed exercises (17 misclassifications). It means that classifiers detect as wrong performance those exercises that due to the variability of volunteers some correctly exercises are labeled as wrong. The main reason of this error is the high amount of classes considered in this classification with respect to the amount of data, so each class includes so little variability that slight variations of the prescribed motions are classified as wrong performances.

The fourth quadrant using window sizes of 100 samples also has a great amount of errors. As hypothesized, wrongly performed exercises with the upper-or lower-limbs can be similar and, as consequence, they are misidentified. The errors distribution shows that the misrecognitions are more common in the upper-limb exercises than in the lower-limb ones. This difference occurs because during the execution of upper-limb exercises, both arms can freely move in the 3D-space whereas in the lower-limb exercises the volunteers posture does not allow as much freedom of movement. For example, if they are seated for the KFL exercise, the posture is different if they are walking, so the accelerometer measurements are clearly different and even if both exercises are wrongly performed, their measurements differ. This change in the posture is also the reason why the methods do not mix up the wrong upper-and lower-limb exercises. In this way, the errors in the recognition of wrong exercises can be divided according to if they are lower-or upper-limb exercises, which are the orange squared cells in Fig 6.6, fourth quadrant. These errors decreases using windows with 300 samples instead of 100 samples, but they maintain a similar distribution. Increasing the window size, wrongly performed exercises seem to be better identified. However, this reduction is mainly caused by the decrease of samples when increasing the window size, so a solution to this source of error is still needed. Thus, these results justify the next method, ReC-W, that groups the upper-and lower-limb wrongly performed exercises.

### 6.4.3 ReC-W: recognition of correct exercises and detection of the wrong ones

ReC-W simplifies ReEv in the respect that the first one only recognizes the correctly performed exercises or just distinguishes them from poorly executed ones. ReC-W overcomes the limitation of ReEv in the recognition of wrong exercises by reducing the number of classes that include wrong performance of motions to only two: WU and WL. In this way, using $SVM_L$ and a window size of 300 samples, ReC-W reaches accuracy, F1-score, precision and sensitivity metrics between 90.7 % and 92.9 %, see Table 6.2. According to these metrics, ReC-W proves to be a competitive method for the combination of the exercises recognition and evaluation tasks although it loses the

information related to which exercise has been wrongly performed.

Figure 6.7 depicts the confusion matrix obtained with the best method and configuration: $SVM_L$ and a window size of 300 samples. This confusion matrix shows that the recognition of correctly performed exercises is almost perfect, remaining the previous errors in gait types recognition, whose classification is marked in green. The division between upper-and lower-limb wrongly performed exercises, shown in the fourth quadrant of Figure 6.7, has only one misrecognition out of 220 samples.

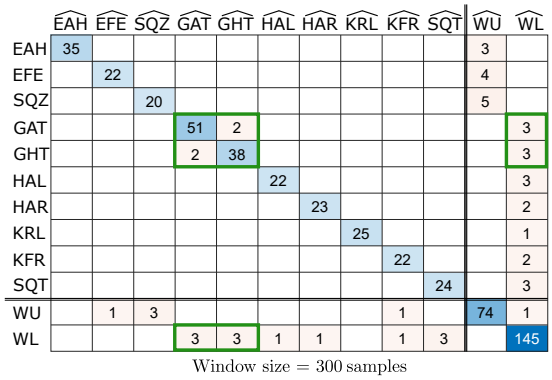


**Figure 6.7:** Average confusion matrix for the 30 volunteers using ReC-W with $SVM_L$ and a window size of 300 samples. Columns divide the predicted classes, which are pointed out with a ˆ over their labels; and rows divide the actual classes. Double lines divide the correctly and wrongly performed exercises.

In this way, by gathering the wrong performed exercises in WU and WL, the only source of error still present in ReC-W is the one from the performance evaluation. That is the main reason why the metrics are improved with respect to the previous proposal, ReEv, as we will discuss in-depth in section 6.4.5.

ReC-W is a promising approach with good metrics in the detection and evaluation of exercises, but it comes at a cost. We cannot obtain information about how the different wrong exercises are performed using ReC-W because all of them are gathered. As a consequence, the potential feedback of a combination of recognition and evaluation would be simpler than if we also knew which exercise is being performed wrongly. However, for applications aimed to count and characterize only the correct performances, this method has proven to be suitable.

### 6.4.4 1Re-2Ev: recognition of exercises, followed by their evaluation

1Re-2Ev simplifies the characterization of exercises by splitting it into two classification stages, starting with the exercises recognition and ending with its subsequent evaluation. We individually evaluate the results of each stage of this method: first, the ones corresponding to the exercises recognition and then, those results obtained

during the exercises evaluation. With regard to its metrics, with the exception of DT, most algorithms achieve accuracy, F1-score, precision, sensitivity and specificity above 90 % even with the smallest window, see Table 6.3. It implies that the recognition of the exercises, even combining their correct and wrong performance is highly accurate. The main reason is that 1Re-2Ev considers a lower number of classes with a high number of samples per class than the previous methods, so these data have a high variability in the training data. In this way, the distribution of the test data set, that belongs to a completely new volunteer, is more likely to be similar to the training data than when using less data per class.

We use a window size of 300 samples with the $SVM_G$ to obtain the confusion matrix shown in Figure 6.8. As in the results of the previous proposals, most errors of 1Re-2Ev are located in the upper-limb exercises and in gait variations. It is consistent with the previous statements about the influence of the posture in the recognition results.

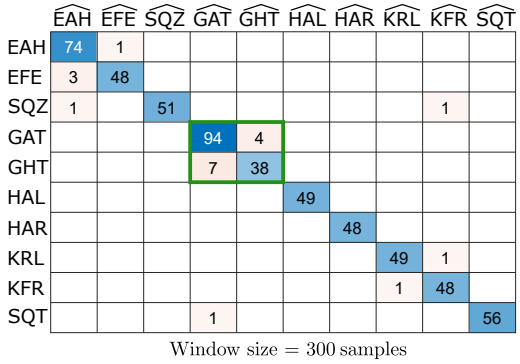


**Figure 6.8:** Average confusion matrix in the exercise recognition stage of 1Re-2Ev with $SVM_G$ and a window size of 300 samples. Columns divide the predicted classes, which are pointed out with a ˆ over their labels; and rows divide the actual classes.

The results of this recognition stage, shown in Table 6.3, are comparable to the state-of-the-art methods for exercises recognition. For example, Zhao and Chen obtained an average accuracy of 96 % in the recognition of four basketball motions using four IMUs on the upper-limbs [Zha20b]. As in that reference, the best accuracy is obtained by using SVMs. Even if these motions are more complex than the one studied in this thesis, they use a four-fold cross-validation method, which is expected to give higher metrics than using a LOSO cross-validation, as the one used in this study. Similar accuracy is reported in [Pre20], where four fitness exercises are recognized within a continuous workout using five IMUs placed on the lower back, the upper-and lower-limbs of one side of the body. They report an accuracy between 94 % and 99 %, a precision between 89 % and 94 %, and a sensitivity between 79 % and 97 %, which are specially interesting because they recognize the transition intervals when no exercise is being performed. However, the fourteen participants in that study correctly performed all the evaluated motions. In our work we consider a higher motion variety. Finally, in [Bav19], they use only one IMU placed on the arm for the motion monitoring. They obtain an ac-

curacy about the 90 % using a ten-fold cross-validation that decreases to a maximum of 80 % when they use a LOSO cross-validation and RF. In this way, our exercise recognition obtains better metrics, mainly because we use four IMUs instead of one. We obtain competitive metrics in relation to the results in the literature, with an average about 96 % in the exercises recognition. In addition, we study and recognize a higher number of exercises, which include their correct and wrong performances.

For the exercises evaluation after their recognition, we initially analyze only the results of $SVM_G$. This algorithm provides an average accuracy and F1-score of 97.17 % and 96.67 %, respectively, see Table 6.4. Furthermore, adapting the most suitable ML algorithm for each exercise, the average accuracy and F1-score increase around 1 %, being 98.06 % and 97.89 %, respectively. It implies that the exercise evaluation obtains excelent metrics, close to perfect classifications, even including the initial error in the exercise recognition.

The results of the second stage, shown in Table 6.4, are comparable to the ones reported in the literature about exercises evaluation. The 90 % accuracy, using RF for the lunge evaluation in [Whe16] and the 89 % accuracy using SVM for the single-leg squats exercises evaluation in [Kia17] are consistent with the results obtained in this chapter in the squat exercise, which is the most similar motion evaluated. For this exercise, we obtain slightly better accuracy, around 95 % with all SVMs configurations and 92 % with RF.

In the studies focused on the individual evaluation of multiple exercises, results are similar. The logistic regression in [Gig14] achieved a maximum accuracy of 83 % on binary exercise evaluation of seven lower-limb exercises. In the exercises evaluation of [Hua16a], the reported maximum accuracy was 97 %. These results are clearly comparable to the obtained in the lower-limb exercises evaluation in this chapter, which provide an accuracy above 95 %.

The results of the upper-limbs exercises are also comparable to those obtained in the literature. In [Per19], the fusion of two IMUs and sEMG sensors obtain an accuracy about 92 %. In this way, we obtain similar metrics in the exercises evaluation, although our classification is binary between correct and wrong, but we use less types of sensors. Similarly, in [Gar21b], the authors found an accuracy between $98 - 99$ % including both upper-and lower-limb exercises. These results are slightly better than the ones reported in this chapter. However, the random cross-validation used in the previous work, is less demanding and the exercise evaluation is simpler when we have a previous knowledge about the exercise that is executed.

In order to compare the results of gait evaluation in [Alc17] and our results, we consider that the wrongly performed gait is similar to an unhealthy gait. Therefore, our results, with an accuracy of 94 %, are in the same range of the results shown in [Alc17]. However, they obtain an accuracy of 100 % with LDA and NB by using more than four features to characterize the motions. Then, these results imply that the gait evaluation

requires more features than the evaluation of other exercises to improve the obtained metrics.

In previous works [Gar21b], we also evaluated two kinds of gait, classifying as correct and wrong, with results around 98 %. However, in this chapter we obtain an accuracy of 93.6 % and an accuracy of 92.2 %. The increment of errors in the evaluation of gait can be derived from the including of GHT gait variation, which entails a higher variability of motions similar to gait. Also, in [Gar21b] we used a random cross-validation with 10 iterations, whereas in this work we use LOSO cross-validation, so metrics are expected to decrease.

Finally, the differences of methods' performance between exercises are noteworthy. The evaluation of the simplest exercises achieves the best metrics. That is the case of EFE, EAH, HAL, KFL and KFR. The evaluation of these exercises produces an accuracy and a F1-score above 99 %. HAR is not included between them probably because of a bias generated by the order of the exercises in the experiments. During the firsts wrong repetitions of HAR, volunteers performed motions close to GAT or SQT, which were corrected by the time they did HAL. On the contrary, the evaluation of the most complex exercises, SQZ, GAT and SQT, has an accuracy and a F1-score between the 93 % and the 97 %. That is related to the easiness of separating between the correct and wrong performances of the simplest exercises, whose features clearly differ between a correct and a wrong performance. In the complex motions, features are more diverse and, as a consequence, they are closer in both performances than in simple motions.

### 6.4.5 Comparison between the proposed methods

One of the most noteworthy similarities between the proposals is that SVM is the ML algorithm that provides the highest metrics in all of them, closely followed by RF. This algorithm is the most suitable one for the recognition and evaluation of the exercises studied in this chapter. The difference between the proposals is the kernel used. The linear one is the most appropriate for ReEv, ReC-W and the first stage of 1Re-2Ev, see Table 6.1, Table 6.2 and Table 6.3 whereas in the second stage of 1Re-2Ev the Gaussian and polynomial kernels provide better results, see Table 6.4.

Another interesting similarity is that the optimal window size is also common for all the proposals. The highest metrics are reported with the 3-second windows (300 samples).

Comparing the results of ReEv and ReC-W, shown in Table 6.1 and Table 6.2 respectively, we can see that, as expected, ReC-W overcomes the initial proposal. Focusing on the best algorithm, $SMV_L$, with the largest window size, its accuracy, F1-score, precision and sensitivity increase a 3 % with this change of approach in the classification,

exceeding all of them the 90 %. Conversely, the specificity remains almost similar but decreases with ReC-W for two reasons that can be seen in the confusion matrix of this method (see Figure 6.7). Firstly, the number of *TN* decreases for WU and WL, since they are the largest classes. WU and WL correspond to the last rows and columns in Figure 6.7, so their true negatives are the first quadrant and the other corresponding class, i.e. WU for WL and the opposite. Secondly, their *FP* increase because these errors correspond to the exercise evaluation, which correspond to the second and third quadrants in Figure 6.7 and, as seen also in the results of ReEv, are the most frequent errors. In this way, errors in the recognition of wrongly performed exercises are eliminated using ReC-W. Not only the recognition of wrong exercises improves, but also the number of properly evaluated motions increases by decreasing the number of correct exercises labeled as wrong. We measure this improvement in terms of the F1-score of the WU and WL classes in ReC-W, compared to those classes of wrongly performed motions when using ReEv. Both the F1-scores of WU and WL are of 91 % versus the average F1-score of the upper-and lower-limb related motions, which are 84 % and 89 %, respectively. So the increment of variability of motions in the WU and WL classes by using ReC-W decrease the evaluation errors, compared to the results obtained when identifying separately the wrongly performed exercises, as made with ReEv.

With regard to the comparison of ReEv and the first stage of 1Re-2Ev, we focus on the misrecognition errors shown in Figure 6.6-right, resultant of ReEv using a window size of 300 samples, and the one in Figure 6.8, that includes the results of the recognition stage of 1Re-2Ev. In Figure 6.6-right, the misidentifiations of ReEv are in the first and fourth quadrants and also in the second and third quadrants but only in these cells which do not belong to the main diagonal, e.g. when in the third quadrant GĤT is recognized instead of GAT. They sum a total of 20 misrecognitions by ReEv. Conversely, the first stage of 1Re-2Ev confuse 19 samples. That means a slight reduction of errors by the division of classifications caused by the aforementioned reduction of classes and increment of data variability in each of them.

These results in exercises recognition are not comparable to those of ReC-W because the recognition of ReC-W only includes the correctly performed motions so it is not the same input data and neither the same output information. ReC-W overcomes the errors of ReEv in the recognition of wrongly performed errors and improve its performance in the exercises evaluation. However, ReC-W only allows us to know if an exercise is wrongly performed, whereas ReEv and 1Re-2Ev give enough information to relate the wrong exercises with their characterization.

With respect to the exercise evaluation, in the second stage of 1Re-2Ev, most metrics are above 95 % (see Table 6.4), which implies that 1Re-2Ev presents the lowest errors in the evaluation of exercises. This means that by separating both classifications, 1Re-2Ev overcomes the limitations related to the exercise evaluation of ReEv and ReC-W. This

improvement in comparison with ReEv is caused by lowering the number of classes, whereas in comparison with ReC-W is a consequence of the reduction of variability in the wrong classes of each exercise.

In this way, 1Re-2Ev overcomes ReEv and ReC-W because of two main reasons: *1)* the recognition metrics are better than ReEv and similar to ReC-W but gives more information since it also recognizes the wrong exercises and *2)* it provides the highest metrics in the exercise evaluation. Also, this proposal includes the flexibility of tuning the algorithm for the exercise evaluation in its second stage, in order to optimize its results according to the recognized exercise.

One can argue that 4 features per signal and window (96 per window combining all sensors) are not enough to obtain the best performance of the ML algorithms. In fact, one of the alternatives to improve the obtained results is to increase the number of features. However, the features used in this work allow us to compare the proposals for the exercises recognition and evaluation, and to establish the most suitable approach for this complex task. In addition, we obtain high metrics with an accuracy about 91.4 % with two of the proposed methods. These metrics prove that both proposals are comparable with the state-of-the-art methods even when they combine both tasks, recognition and evaluation of exercises, whereas in the literature these tasks are separately addressed.

Furthermore, the high metrics given by the three methods with such a variability of volunteers entail that the they adapt to different population. The main reason is that the design of motions is similar for all ages, so their correct performance is similar independently of the subject and they only show variations that are already in the analyzed database. In this way, the proposals are robust to changes in the motions caused by age.

## 6.5 Conclusions

This chapter proposes several approaches to automatically recognize and evaluate exercises included in a physical routine aimed for maintaining older adults health status, what can prevent the onset of frailty. Our work contributes to the development of virtual coaches that help achieve healthy aging by supporting regular daily exercise, improving adherence to the physical routine and monitoring it. With the proposals, we demonstrate the feasibility of the characterization of this routine performance, which may become a reality in the near future.

For this complex task, we have proposed three alternatives: 1) identifying and evaluating in a single stage (ReEv); 2) identifying only the correct exercises (ReC-W) in a sigle stage, and 3) identifying in a first stage and then evaluating in a second one

whether the exercise is well or poorly performed (1Re-2Ev). These proposals have been evaluated in a set of 30 volunteers between 20 and 70 years old, with different ML algorithms. The metrics used to evaluate the proposals prove that the one-stage classification approaches are less suitable than the two-stage one. Combining the recognition and evaluation in a single classification problem, ReEv and ReC-W obtain an accuracy of 88 % and 91 %, depending on whether or not the classification of the wrong executions is performed. Conversely, the initial recognition followed by the exercises evaluation of 1Re-2Ev, gives an accuracy around 95 %, even with the error propagation from the first stage. 1Re-2Ev is also interesting since we prove that different exercises are evaluated better with different ML algorithms, and this approach allow us to assign the most suitable classifier to each performed exercise, after it has been recognized.

Another main difference between the one-and two-stage methods is that, even SVM is the most suitable algorithm in all the studied cases, the most suitable kernel differs between proposals. In the ReEv and ReC-W, $SVM_L$ overcomes the other methods, whereas in 1Re-2Ev, $SVM_G$ and $SVM_P$ provide the best results.

We also find that the recognition of correct motions is less demanding than their evaluation, i.e. in the evaluation, parameters as the window size are more relevant to obtain better results than in the exercises recognition. These results are due to the differences in posture of the volunteers and, as a consequence, of the sensors placed on their limbs. It helps to recognize the exercises but not to evaluate them. The most complex exercises, as GAT and SQZ, reported the worst metrics in their recognition and evaluation, so richer features should be used to improve their characterization.

The initial results of this chapter are reported in two conference papers [Gar21b, Gar21d] and the final results are in a paper under review [Gar22b].

# Chapter 7

# Conclusions and Future Works

We close this work in this chapter in which we summarize the conclusions from the thesis. First, we gather the main learnings from this thesis. Then, we finish our work with different topics that may be of interest for future work in this inertial motion monitoring field.

## 7.1 Conclusions

The main research objective of this thesis was human motion monitoring by using inertial sensors. This work contributes to inertial monitoring systems by studying the determination of the anatomical parameters using IMUs. In this way, we overcome the previous limitation related to the need of external systems for this anatomical calibration and ensure that inertial kinematic analysis methods are based solely on IMUs.

This thesis proposes an IMU-based method for leg characterization based on the determination of the null acceleration point in their rotation centers and axes. The method uses just one IMU per joint to obtain a complete characterization of joints and is adapted to slow movements by a signal processing method. Furthermore, since anatomical joints can be related through trigonometric relationships, we can achieve a complete leg characterization that includes the locations of joints and the segment lengths, parameters commonly required by motion capture analysis algorithms. The method provides the highest accuracy by using the lowest cutoff frequency tested due to the slowness in leg movements needed to ensure fixed joints. In average, our method shows an error of 8 % in the determination of leg joint centers and axes, and of 4 % in the leg length estimation. Moreover, it can be concluded that the characterization of the lower-limbs depends on the performed exercises, being the circle, knee bending and pendulum exercises the motions that provide the highest accuracy.

In this thesis, we also prove that IMU-based calibration of joints can adapt to soft tissue

artifacts (STA) scenarios as an alternative approach to the common least squares or gradient descent algorithms. To do so, we propose an algorithm called ArVE$_d$ based on an extended Kalman filter that uses raw data from one IMU to estimate the location of fixed joints. ArVE$_d$ determines the location of joints when STA occurs by assuming a fixed center of rotation location in joints. This method adapts to the simulated STA with errors around the 3 % in the estimation of varying IMU-joint vectors, with only a 1 ° of deviation with respect to the reference positioning vector. We validate the results by ArVE$_d$ on the real scenario using an optical system. In this way, we prove that ArVE$_d$ is also suitable for the real scenario since it decreases the error of assuming a fixed IMU-joint vector around a 50 % compared with published works.

Furthermore, we identify and cover an important lack of public data for the comparison of methods and the validation of new proposals. Also, since the tendency of the new proposals is to be based on ML methods more than on the classical Kalman filters, more public data are needed for training the algorithms. For that reason, we design and provide a database with 30 volunteers performing 6 exercises and 3 gait variations for the development of new motion monitoring proposals. The database include inertial data and optical reference. Thus, we conclude that it meets the needs for the development of new algorithms and the comparison of the existent ones. Moreover, data are labeled according to the performed motion and its quality so it can also be used to produce algorithms aimed at obtaining qualitative information about motions.

With regard to obtaining qualitative information about the exercises performed in a physical therapy, IMUs also prove to be appropriate for their complete characterization. We study and perform the recognition and evaluation of motions, considering both of them as a unique complex task, since they appear combined in a remote monitoring of physical therapies. To do so, we propose three different methods based on ML techniques that recognize and evaluate motions in a single stage or in two of them. We prove that the three proposals are suitable with an accuracy, F1-score, precision and sensitivity over 88.3 % in the worst scenario. It is noteworthy since we evaluate 30 people of different ages and anatomic dimensions, so the proposals are adequate for the monitoring of diverse population. The method composed of an initial stage of exercise recognition followed by its evaluation is the most promising, with metrics over 95.7 % in recognition and over 92.2 % in evaluation. Our results show that the recognition stage is less demanding than the evaluation one due to the influence of the posture in the accelerometer data. It allows an easier recognition of motions between the correct performances. Besides, the study of the source of errors shows that most of the misclassifications occur in the distinction of the type of exercises when they are wrongly performed as this classification requires the definition of too many classes. The main reason is the high variability of classes and the similarity between wrongly performances of different exercises. Finally, regarding the ML algorithms, SVM is the most suitable algorithm in all the proposed methods.

In conclusion, it is worth highlighting that the study carried out of the exercises monitoring results in the contribution for a future development of virtual coaches. In this way, this thesis covers its initial objectives.

## 7.2 Future Works

As can be derived from the work developed and their contributions, there has been progress in the motion monitoring field, but there is still room for improvement. We now discuss some of the future lines that may be of interest in the research topic of this work.

First of all, for the inertial personalized calibration of limbs, we think is necessary to adapt the proposals to mobile CORs and AORs. One of the limitations of the proposal is that we assume the existence of a COR with null acceleration, which occurs in some physical exercises, but there are others that do not present this characteristic. That algorithm generalization would make the algorithms suitable for a higher variability of motions, such as gait or running analysis. We are working on the adaptation of ArVE$_d$ to be applied to motions in which CORs do not show a negligible linear acceleration, such as gait or running analysis. Nevertheless, ArVE$_d$ can be used in a previous calibration step to obtain an average IMU-joint vector for off-line applications. Moreover, the integration of these calibration algorithms with those algorithms aimed at obtaining kinematic parameters should be studied. In this way, no specific *prior* motions would be required and the algorithms would be more practical than the proposals for their use in remote monitoring systems.

With regard to the recognition and evaluation of motions, the reduction of the number of sensors should be studied in order to make a more user-friendly system. More variability of motions and people could be included to adapt the algorithms to different physical therapies. The evaluated algorithms should be assessed with that increment of variability. It could be suitable to explore other algorithms already proposed in the literature, such as deep learning algorithms, or increase the number of features used as inputs in the ML algorithms.

Also related with the generalization of algorithms, more subjects should be studied. We focus on a healthy variability of subjects, so we exclude people with motion related diseases. An extension of this work is to assess whether it is necessary to adapt the algorithms when a disease occurs. If the answer is affirmative, personalized algorithms would be necessary to be evaluated. For example, semi-supervised ML algorithms for the automatic learning of personal features.

The objective of this work is based only on inertial sensors for the motion monitoring. In the future, physiological measurements as the muscle response by sEMG could be

integrated in the monitoring system to provide more enlightening information about the performance of motions. That information could be specially important for rehabilitation purposes.

Finally, the algorithms could be adapted for their use on portable systems, e.g. smartphones, wirelessly connected to IMUs. It would allow to provide real-time feedback in rehabilitation therapies.

# Appendix A

# Mathematical Background

This section describes the notation and main mathematical background used in this thesis.

## A.1 Notation

We work with column vectors in the Euclidean vector space $\mathbb{R}^3$ with their components ordered as $(x, y, z)$. Cases where a column vector is required are indicated through the transpose operator using the superscript $(\cdot)^\top$, and the same operator is used for transposed matrices. Vectors are presented with bold lower-scripts as $\boldsymbol{\omega}$. We use Latin scripts for the linear magnitudes, as $\boldsymbol{a}$ to present the linear acceleration, and Greek scripts for the angular ones, such as $\boldsymbol{\omega}$ to notate the turn rate. Points are represented with Latin upper-case scripts, such as O. Italic upper-case scripts denote matrices, as $C$. Scalars are written with lower-case scripts, such as $d$, using upper-case subscripts in case of it is needed an indication of the body that the scalar is related ($d_S$). If scalars are vector components, we use lower-case scripts with $x$, $y$ or $z$ subscripts, e.g., $\omega_x$. We use "r" as subscript to note reference values, such as $\boldsymbol{r}_r$. When denotation of the coordinate system in which a magnitude is presented is needed, we use the subscript $_g$ for the global inertial system. Measurements obtained from IMUs in their coordinate system are written using $I$ as subscript, i.e. $\boldsymbol{\omega}_I$. Since we use Bayesian filters with a estimation step followed by an update step, we distinguish the estimated parameters with a circumflex accent, as $\hat{x}$. The circumflex accent also points out the estimated classes by the ML-based classifiers. The temporal index is $k$, used as a superscript. Thus, superscript $k-1$ denotes that it corresponds to the previous state, i.e., $x^{k-1}$. We present differentiation respect to time of each parameter $x$ as $\dot{x}$, and its second-order derivative as $\ddot{x}$, being $x$ a scalar, vector or matrix, according to the case. The operator $\|\cdot\|$ refers to the Euclidean norm.

## A.2 Singular Value Decomposition

Let $M \in \mathcal{M}_{m,n}(\mathbb{R})$ be a $m \times n$ matrix in the real field. The matrix $M^T M$ is a positive semi-definite symmetric squared matrix:

- As $(M^T M)^T = M^T (M^T)^T = M^T M$, the matrix $M^T M$ is symmetric.
- $M^T M$ is positive semi-definite:

$$x^T M^T M x = (x^T M^T)(Mx) = (Mx)^T Mx = \|Mx\|^2 \geq 0 \tag{A.1}$$

The matrix $M^T M$ is a diagonalizable matrix whose eigenvalues are all non-negative real values $\{\lambda_i \geq 0\}$. Ordering these eigenvalues $\{\lambda_1 \geq \lambda_2 \geq \cdots \lambda_n \geq 0\}$, the $\sigma_i = \sqrt{\lambda_i}$ is called the $i$th singular value of the matrix $M$. The matrix $M^T M$ and its eigenvalues fulfill Theorem A.1, whose proof are in [Ban14a].

**Theorem A.1.** *Let the $\{\lambda_1 \geq \cdots \geq \lambda_r > \lambda_{r+1} = \cdots \lambda_n = 0\}$ be the eigenvalues of the matrix $M^T M$, where the first r eigenvalues are positive and the rest are null eigenvalues. Let the set $\{v_i \in \mathbb{R}^n \mid 0 \leq i \leq n\}$ be a basis of $\mathbb{R}^n$ where the $v_i$ are the eigenvectors of $M^T M$. Then:*

- *The set $\{Mv_1, \cdots, Mv_r\}$ is orthogonal and $\|Mv_i\| = \sqrt{\lambda_i} = \sigma_i$.*
- *The set $\{\frac{Mv_1}{\sigma_1}, \cdots, \frac{Mv_r}{\sigma_r}\}$ is orthonormal basis of the column space $\mathrm{Col}(M)$.*
- *The set $\{Mv_{r+1}, \cdots, Mv_n\}$ is an orthonormal basis of the null space $\mathrm{Nul}(M)$.*
- *$\mathrm{rank}(M) = r$ which means that the rank of M is equal to the number of positive singular values.*

According to Theorem A.1, matrix $M$ can be factorized as follows:

$$M = USV^\top, \tag{A.2}$$

where $U \in \mathcal{M}_{m,m}(\mathbb{R})$ and $V \in \mathcal{M}_{n,n}(\mathbb{R})$ are orthogonal matrices which contain the left and right singular vectors of $M$. Matrix $S \in \mathcal{M}_{n,n}(\mathbb{R})$ is formed by the singular values of $M$ in descending order.

This decomposition can be applied to look for the linear subspace which best represents the variability of the inputs with the smallest amount of features, as in principal component analysis (PCA). PCA computes the SVD and vanishes the less important singular values. The vector spaces associated with the principal components are then used for reducing the number of input variables.

In some cases, SVD is applied with the contrary objective, selecting the smallest eigenvalue that determine the null space of $M$, where the uncertainty occurs. Since the eigenvalues are in descending order, the singular vector of our interest is the last column of $V$, in the following called $\mathbf{v}$. This singular vector $\mathbf{v}$ defines the direction of the subspace of solutions of $M$, that is the direction of the axis over the rotation is carried out. This implies that $\mathbf{v}$ is the director vector of the axis of rotation.

## A.3 Bayesian filters: the filtering problem

The problem formulation of Bayesian filters, such as KFs, consists in the identification of the desirable estimations using a series of measurements observed over time containing statistical noise and different inaccuracies [Sim06]. The common application of these filters is depicted in Fig. A.1, in which a physical system is driven by a set of external inputs or controls and its outputs are the external measurements or observations. These inputs and observations form the knowledge on the system's behavior and both convey errors and uncertainties, named the measurement and the system errors.

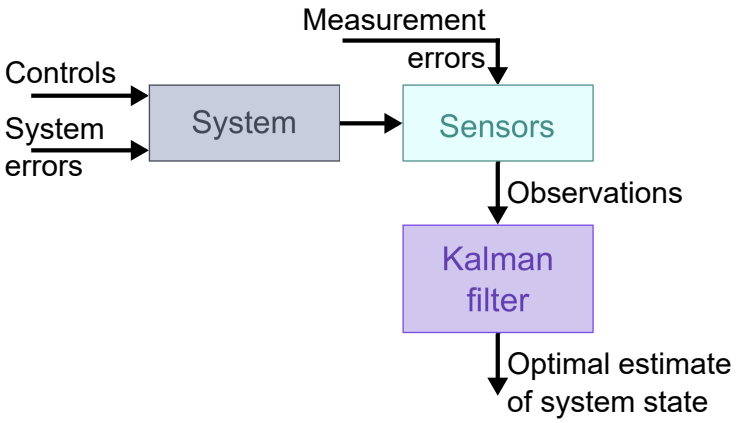


**Figure A.1:** Problem formulation for Bayesian filtering.

On the basis of the control inputs and observations, filters obtain an estimate of the system's state that optimizes a given criteria.

### A.3.1 Kalman filter (KF)

The KF is a sensor fusion technique that estimates the states of a linear system through the minimization of the variance of the estimation error [Sim06]. KFs use a series of measurements observed over time and their statistical noise to produce estimates of unknown variables. KFs are defined for processes that can be described as linear sys-

tems by using the following equations of state (A.3) and observation (A.4):

$$\boldsymbol{x}^k = A\boldsymbol{x}^{k-1} + B\mathbf{u}^{k-1} + \mathbf{w}^{k-1} \tag{A.3}$$

$$\boldsymbol{z}^k = C\boldsymbol{x}^k + \mathbf{v}^k, \tag{A.4}$$

where $A$, $B$ and $C$ are matrices, $k$ is the time index, $\boldsymbol{x}$ is the system state, $\boldsymbol{u}$ is the known input to the system, $\boldsymbol{z}$ is the measured output and $\mathbf{w}$ and $\mathbf{v}$ are the noise associated to the state and measurements, respectively. Noises are assumed to be Gaussian and temporally uncorrelated. The quantities are notated as vectors since they usually contain more than one element. The common problem is that $\boldsymbol{x}$ contains the state of the system, but it cannot be directly measured. Instead, we measure $\boldsymbol{z}$, which is a function of $\boldsymbol{x}$ with the influence of noise $\mathbf{v}$. The average value of the process noise $\mathbf{w}$ and the measurement noise $\mathbf{v}$ are assumed to be zero. Then, the noise covariance matrices $Q$ and $R$ are defined in each time $k$ as:

$$\begin{aligned} Q &= \mathrm{E}[\mathbf{w}^k[\mathbf{w}^k]^\top] \\ R &= \mathrm{E}[\mathbf{v}^k[\mathbf{v}^k]^\top], \end{aligned} \tag{A.5}$$

where $\mathrm{E}[\cdot]$ denotes the expected operator.

KFs include two steps, estimation and correction, after the initialization. The initial state $\boldsymbol{x}^0$ is a vector with known mean $\boldsymbol{\mu}^0 = \mathrm{E}[\boldsymbol{x}^0]$ and covariance $P_x^0 = \mathrm{E}[(\boldsymbol{x}^0 - \boldsymbol{\mu}^0)(\boldsymbol{x}^0 - \boldsymbol{\mu}^0)^\top]$. After that, the first step includes the estimation of the state vector $\hat{x}^k$ and the *a priori* estimation error covariance $\hat{P}^k$. To do so, KFs rely on the estimation based on the previous time step, working as an iterative algorithm. This step is defined by the following equations:

$$\hat{\boldsymbol{x}}^k = A\boldsymbol{x}^{k-1} + B\mathbf{u}^{k-1} \tag{A.6}$$

and

$$\hat{P}_x^k = AP_x^{k-1}A^\top + Q \tag{A.7}$$

Then, the update step is performed only when $\boldsymbol{z}^k$ observations are available. The *a posteriori* covariance matrix can be computed as:

$$P_x^k = \hat{P}_x^k - A_x P^{k-1} C^\top R^{-1} C P_x^{k-1} A^\top. \tag{A.8}$$

Let be $K^k$ the *Kalman gain*, that minimizes the error covariance $\hat{P}_x^k$ for the *a posteriori* state estimate $\hat{\boldsymbol{x}}^k$, defined as follows:

$$K^k = \hat{P}_x^k C^\top \left( C\hat{P}_x^k C^\top + R \right)^{-1}. \tag{A.9}$$

Eventually, the corrected estimation can be calculated using (A.10).

$$\boldsymbol{x}^k = \hat{\boldsymbol{x}}^k + K^k \left( \boldsymbol{z}^k - C\hat{\boldsymbol{x}}^k \right) \tag{A.10}$$

The residual $\boldsymbol{z}^k - C\hat{\boldsymbol{x}}^k$ is called *innovation*, which indicates the discrepancy between the predicted state $\hat{\boldsymbol{x}}^k$ and the actual measurement $\boldsymbol{z}^k$. The closer it is to zero, the more similar are the prediction and the measurement.

### A.3.2 Extended Kalman filter (EKF)

KFs are only applicable to linear systems. However, they have been generalized to non-linear systems trough EKFs [Sim06].

In this case, we define the following nonlinear system:

$$\begin{cases} \boldsymbol{x}^k = f(\boldsymbol{x}^{k-1}) + \mathbf{w}^{k-1} \\ \boldsymbol{z}^k = h(\boldsymbol{x}^k) + \mathbf{v}^k \end{cases}. \tag{A.11}$$

Assuming the non-linearities in the dynamic and the observation model are smooth, we can expand $f$ and $h$ in Taylor series and approximate in this way the next estimate of the state vector $\boldsymbol{x}^k$as follows:

$$\begin{cases} \boldsymbol{x}^k \approx \hat{\boldsymbol{x}}^k + A\left(\boldsymbol{x}^{k-1} - \hat{\boldsymbol{x}}^{k-1}\right) + Q \\ \boldsymbol{z}^k \approx \hat{\boldsymbol{z}}^k + H\left(\boldsymbol{x}^k - \hat{\boldsymbol{x}}^k\right) + R \end{cases}. \tag{A.12}$$

Thus, the state prediction equations are:

$$\begin{aligned} \boldsymbol{x}^k &= f\left(\boldsymbol{x}^{k-1}, \mathbf{w} = \mathbf{0}\right) \\ \hat{P}_x^k &= A P_x^{k-1} A^\top + Q \end{aligned}, \tag{A.13}$$

and the measurement update equations:

$$\begin{aligned} P_y &= H\hat{P}^k H^\top + R \\ K^k &= \hat{P}_x^k H^\top \left(P_y\right)^{-1} \\ \boldsymbol{x}^k &= \hat{\boldsymbol{x}}^k + K^k\left(\boldsymbol{z}^k + h\left(\hat{\boldsymbol{x}}^k, \mathbf{v} = \mathbf{0}\right)\right) \\ P_x^k &= \left(I + K^k C\right)\hat{P}_x^k \end{aligned}, \tag{A.14}$$

where $P_y$ is an intermediate noise covariance matrix.

However, this approximation can introduce large errors in the true posterior mean and covariance of the variable, which may lead even to the divergence of the filter. One of the possible solutions is using the UKF, explained in the following section.

### A.3.3 Unscented Kalman filter (UKF)

UKFs address the approximation issues of EKFs. In this case, the state vector distribution, still Gaussian, is represented as a set of sample points, called *sigma points* [Sim06]. Sigma points capture the actual mean and covariance of the Gaussian random variables and are obtained through the *unscented* transform (UT).

The UT is a method for calculating the statistics of a random variable that suffers a non-linear transformation. It considers the propagation of a random vector $\boldsymbol{x}$ of dimension L with mean $\boldsymbol{\mu}_x$ and covariance $P$ through a non linear function $\boldsymbol{z} = h(\boldsymbol{x})$. To calculate the statistics of $\boldsymbol{z}$, UTs form a matrix $\mathcal{X}$ of $2L+1$ sigma vectors $\boldsymbol{\mathcal{X}}_i$ as follows:

$$\begin{cases} \boldsymbol{\mathcal{X}}_0 = \boldsymbol{\mu}_x \\ \boldsymbol{\mathcal{X}}_{1,\mathrm{L}} = \boldsymbol{\mu}_x + \sqrt{\mathrm{L}+\lambda P} \\ \boldsymbol{\mathcal{X}}_{\mathrm{L}+1,2\mathrm{L}} = \boldsymbol{\mu}_x - \sqrt{\mathrm{L}+\lambda P} \end{cases}, \tag{A.15}$$

where $\lambda = \alpha^2(\mathrm{L}+\kappa) - \mathrm{L}$ is the scaling parameter that considers the spread of the sigma points through $\alpha$ and a secondary scaling parameter $\kappa$, commonly set to $3-\mathrm{L}$, obtained as $\alpha^2(\mathrm{L}+\kappa) - \mathrm{L}$. These sigma points are propagated through the nonlinear function $h$:

$$\mathcal{Z}_i = h(\mathcal{X}_i), \tag{A.16}$$

where $i$ denotes the $i$th column of matrices. The mean and covariance of $\boldsymbol{z}$, $\boldsymbol{\mu}_z$, are then approximated through a weighted sample mean and covariance of the posterior sigma points $\mathcal{Z}$ as follows:

$$\begin{aligned} \boldsymbol{\mu}_z &\approx \sum_{i=0}^{2L} \mathrm{W}_i^{(m)} \mathcal{Z}_i \\ P_z &\approx \sum_{i=0}^{2L} \mathrm{W}_i^{(c)} \left(\mathcal{Z}_i - \boldsymbol{\mu}_z\right)\left(\mathcal{Z}_i - \boldsymbol{\mu}_z\right)^\top \end{aligned}, \tag{A.17}$$

whose weights $\mathrm{W}_i$ are obtained as:

$$\begin{cases} \mathrm{W}_0^{(m)} = \dfrac{\lambda}{\mathrm{L}+\lambda} \\ \mathrm{W}_0^{(c)} = \dfrac{\lambda}{\mathrm{L}+\lambda} + 1 - \alpha^2\beta \\ \mathrm{W}_i^{(m)} = \mathrm{W}_i^{(c)} = \dfrac{\lambda}{2(\mathrm{L}+\lambda)} \qquad \text{for } i = 1,\ldots,2\mathrm{L}, \end{cases}, \tag{A.18}$$

being $\beta$ the parameter that incorporates *prior* knowledge of the distribution of $\boldsymbol{x}$, set to $\beta = 2$ for Gaussian distributions.

UKFs are an extension of UTs to the recursive estimation where the UT is applied to the augmented state vector $\boldsymbol{x}_a^k = \left[(\boldsymbol{x}^k)^\top (\mathbf{v}^k)^\top (\mathbf{n}^k)^\top\right]^\top$ that include the state and noise variables. The UKF initialization is similar than in the general KFs but considering the state and noise variables in the state vector:

$$\hat{\boldsymbol{x}}_a^0 = E\left[\boldsymbol{x}_{\boldsymbol{a}}^{\mathbf{0}}\right] = \left[(\boldsymbol{x}^0)^\top \mathbf{0}^\top \mathbf{0}^\top\right]^\top \tag{A.19}$$

$$P_{xa}^0 = E\left[\left(\boldsymbol{x}_a^0 - \hat{\boldsymbol{x}}_a^0\right)\left(\boldsymbol{x}_a^0 - \hat{\boldsymbol{x}}_a^0\right)^\top\right] = \begin{pmatrix} P^0 & 0 & 0 \\ 0 & R^v & 0 \\ 0 & 0 & R^n \end{pmatrix}. \tag{A.20}$$

Then, the sigma points at each time $k$ are calculated as:

$$\mathcal{X}_a^{k-1} = \left[\hat{\boldsymbol{x}}_a^{k-1} \quad \hat{\boldsymbol{x}}_a^{k-1} + \sqrt{\mathrm{L} + \lambda P} \quad \hat{\boldsymbol{x}}_a^{k-1} - \sqrt{\mathrm{L} + \lambda P}\right]. \tag{A.21}$$

The estimation stage equations are:

$$\begin{aligned}
\mathcal{X}^k &= f\left(\mathcal{X}_x^{k-1}, \mathbf{u}, \mathcal{X}_v^k\right) \\
\hat{\boldsymbol{\mu}}_x &= \sum_{i=0}^{2L} \mathrm{W}_i^{(m)} \mathcal{X}_i^k \\
\hat{P}_x^k &= \sum_{i=0}^{2L} \mathrm{W}_i^{(c)} \left(\mathcal{X}_i^k - \hat{\boldsymbol{\mu}}_x\right)\left(\mathcal{X}_i^k - \hat{\boldsymbol{\mu}}_x\right)^\top
\end{aligned}, \tag{A.22}$$

and the update equations are:

$$\begin{aligned}
\mathcal{Z}^k &= h\left(\mathcal{X}_x^k, \mathcal{X}_n^k\right) \\
\boldsymbol{\mu}_z^k &= \sum_{i=0}^{2L} \mathrm{W}_i^{(m)} \mathcal{Z}_i^k \\
P_z^k &= \sum_{i=0}^{2L} \mathrm{W}_i^{(c)} \left(\mathcal{Z}_i^k - \hat{\boldsymbol{\mu}}_z\right)\left(\mathcal{Z}_i^k - \hat{\boldsymbol{\mu}}_z\right)^\top \\
P_{xz}^k &= \sum_{i=0}^{2L} \mathrm{W}_i^{(c)} \left(\mathcal{X}_i^k - \hat{\boldsymbol{\mu}}_x\right)\left(\mathcal{Z}_i^k - \hat{\boldsymbol{\mu}}_z\right)^\top, \\
K^k &= P_{xz}^k \left(P_z^k\right)^{-1} \\
\hat{\boldsymbol{x}}^k &= \boldsymbol{\mu}_x^k + K^k\left(\boldsymbol{z}^k - \boldsymbol{\mu}_z^k\right) \\
P_x^k &= \hat{P}_x^k - K^k P_z^k \left(K^k\right)^\top
\end{aligned} \tag{A.23}$$

where $\mathcal{X}_a = \left[\mathcal{X}_x^\top \; \mathcal{X}_v^\top \; \mathcal{X}_n^\top\right]^\top$ and $R^v$ is the process-noise covariance matrix and $R^n$ is the measurement-noise covariance matrix.

## A.4 Data Science algorithms

Data science is a multidisciplinary field that aims to extract knowledge from data [Bis06]. It gathers methods and theoretical basis from mathematics, statistics, computer science, domain knowledge and information science. One of the main methodologies in data science is ML, which is the study of computer algorithms that improve through their own experience. These algorithms include several proposals based on the creation of models from known data to infer information about it or new data. The main key is to create generic models for a great amount of data from a smaller database. These algorithms can be divided into three types according to their approach and the

type of data they use as input and output: supervised, unsupervised and reinforcement learning.

Supervised learning algorithms infer mathematical models from a set of data, called training data, that include inputs and the searched outputs. Through iterative optimization of an objective function, these algorithms learn a function that models the data in some extent. This function is then used to predict the outputs associated with the new data whose outputs are unknown for the algorithm. Models can be used for active learning, that is to label new data points with the desired outputs, classification, which consist in finding the corresponding label between a small set of labels for some data, or regression, where the set of labels include any numerical value within a range.

Unsupervised learning algorithms consider data which do not contain the outputs, so only the inputs are known. These algorithms find the structure in the data, finding similarities. One of the main applications of unsupervised learning is in the field of statistics summarizing and explaining data features.

Semi-supervised learning combines both supervised and unsupervised learning, since some of the training examples are not labeled.

Reinforcement learning works in environments to maximize some notion of cumulative reward. These algorithms do not assume knowledge of an exact mathematical model and are used when exact models are not feasible. Some autonomous vehicles and machines that learn how to play a game against humans use these kind of learning.

In this work, we use the supervised learning algorithms because we work with labeled data. In the following sections, we explain the different algorithms applied in this work. For ease the exposition, in the following we assume just two classes $y = 0, 1$.

### A.4.1 Support Vector Machines

The performance of SVM is based on optimizing the distance between samples from different classes. The classification function for a linearly separable dataset is a separating hyperplane $f(x)$ that passes through the middle of the two classes [Sch18]. The decision function of SVMs is the hyperplane that maximize the margin between classes, which is the shortest distance between the closest data points of each class to the hyperplane. Given a labeled training data set $\{(\mathbf{x}_i, y_i)\}_{i=1}^{N}$ where $\mathbf{x}_i \in \Re^N$ are the features and $y_i \in \mathcal{C} = \{C_j \mid 1 \leq j \leq J\}$ are its labels. Also given a non-linear mapping $\psi(\cdot) : \Re^N \to \Re^p$ where $(N << p)$, SVMs:

$$\begin{aligned} &\min_{\mathbf{w},b,\epsilon} \tfrac{1}{2}\|\mathbf{w}\| + C\sum_{i=1}^{N} \epsilon_k \\ &y_j\left(\mathbf{w}\,\psi(\mathbf{x}_i) + b\right) + \epsilon_i - 1 \geq 0 \qquad i = 1, \ldots, n \\ &\epsilon_i \geq 0, \end{aligned} \tag{A.24}$$

where $\mathbf{w}$ and $b$ define a separating hyperplane in $\Re^N$ and $\epsilon_k$ are positive slack variables that ensure the optimal hyperplane despite of the permitted errors.

In this way, using the cost function (A.24) minimize the committed errors with the term $\sum_{i=1}^{N} \epsilon_k$, whereas minimizes the Euclidean norm of the model weights $\|\mathbf{w}\|$, which is equivalent to maximize the margin that separates classes. The regularization hyperparameter C controls the generalization capability of the classifier, which must be usually tuned by the user.

A correct choice of the non-linear mapping $\psi : \Re^N \rightarrow \Re^p$ increases the likelihood of the transformed samples to be linearly separable. The problem giving by (A.24) is solved by the following decision function for any test sample $\mathbf{x}_* \in \Re^N$:

$$f(\mathbf{x}_*) = \text{sgn}\left(\sum_{k=1}^{n} y_i \alpha_i K(\mathbf{x}_i, \mathbf{x}_*) + b\right) \tag{A.25}$$

where $\alpha_i$ are the Lagrange multipliers corresponding to the constraints of the primal problem (A.24). The *support vectors* (SVs) are those training samples $\mathbf{x}_i$ with a non-zero Lagrange multiplier. The function $K(\mathbf{x}_i, \mathbf{x}_*)$ is the scalar product of the higher-order space $\Re^p$. The bias term $b$ is defined as:

$$b = \frac{1}{m} \sum_{k=1}^{m} \left(y_i - \mathbf{w}\, \psi(\mathbf{x}_i)\right), \tag{A.26}$$

being $m$ the number of *unbounded* Lagrange multipliers and $\mathbf{w} = \sum_{i=1}^{n} y_i \alpha_i \psi(\mathbf{x}_i)$.

SVMs offers the best generalization ability in classification performance in both training and new data.

### A.4.2 Decision Trees and Random Forest

Random forests are an ensemble learning method that constructs $T$ classification decision trees at training time to predict the searched outputs. A decision tree is a binary recursive partitioning procedure [Wu09], constructed using a directed graph $G = (V, E), E \subset V^2$, with set of nodes $V$ split into three disjoint sets $V = D \cup C \cup T$ decision and terminal nodes [Kam18]. These algorithms base on choosing a variable at each node that best splits the training data set.

Classification trees use Gini *impurity* to measure the likelihood of mislabel a sample if this one is randomly labeled. The Gini rule measures impurity of a node $V$ as

$$G(t) = 1 - p(V)^2 - (1 - p(V))^2 \tag{A.27}$$

where $p(V)$ is the relative frequency of class 1 in the node and the gain generated by a split of the parent node P into left and right branches $L$ and $R$ is

$$I(P) = G(P) - qG(L) - (1 - q)G(R), \tag{A.28}$$

being $q$ the fraction of instances going left.

The best split is the one that provides the higher information gain $I(P)$. Thus, the next branch split is made with the variable which results into a higher $I(P)$ and this process is repeated for each node until the tree is completed.

Decision trees tend to learn highly irregular patterns, overfitting the training sets. Random forests correct the problem of overfitting associated with decision trees through bagging. Each tree $t$ is grown on a different bootstrap sample (explain that is the subset of samples) which contains a random set of points from the original training data set. Besides, bagging at each node of the tree $t$, $r$ features are selected from the $R$ original features. In this way, bagging increases stability of the original decision trees and the random feature selection enhances the robustness of this algorithm. The class assigned to each sample is the most voted by the $T$ trees, as:

$$y' = \text{argmax}_v \sum_{(\mathbf{x}_i, y_i) \in D_z} I(v = y_i), \tag{A.29}$$

where $v$ is a class label, $y_i$ is the class label for the $k$th nearest neighbors, and $I(\cdot)$ is a function that returns the value 1 if the argument is true and 0 otherwise.

### A.4.3 K-Nearest Neighbor

KNN classification finds a group of $k$ objects in the training set that are closest to the test object [Sha08]. The assignment of a label bases on the predominance of a particular class in this neighborhood. To classify new data, the distance of each sample to the labeled objects from the training set is computed, its *k nearest neighbors* are identified and their class labels are assigned to the test sample.

Once the nearest-neighbor list is obtained, the test sample is classified based on the majority class of its nearest neighbors using (A.29).

### A.4.4 Multi-Layer Perceptron

MLPs are a class of ANN that consists of an input layer, a number of hidden layers and an output layer, all of which are composed by a number of processing units called *neurons*[Hay98, Bis95]. All these neurons are connected to other neurons in the next layer by means of weighted links. The values of the weights are related to the ability of the MLP to learn about the problem from the training data, which has to be sufficiently large. During the raining process, the values of these weights are assigned, which are aimed at minimizing the error between the MLP output and the expected value of the training set.

The input data for the MLP consist of a number of samples $\{(\mathbf{x}_i \in \Re^n)\}_{i=1}^N$, where the input vectors $\mathbf{x}_i = [x_{i,1}, \ldots, x_{i,n}]$. Once a MLP is trained, it is able to generate an estimated output $\hat{y}_i \in \mathcal{C} = \{C_j \mid 1 \leq j \leq J\}$, where $j$ are the possible labels of data. The relationship between output $\hat{y}$ and a generic input $\mathbf{x} = [x_1, \ldots, x_n]$ of a neuron is:

$$\hat{y} = \phi\left(\sum_{j=1}^{n} w_j x_j - b\right), \tag{A.30}$$

where $x_j$ are the input signals, $w_j$ is the weight associated with the $j$th input, $b$ is the bias term and $\phi$ is the transfer function, which is commonly the logistic function:

$$\phi(x) = \frac{1}{1+e^{-x}}. \tag{A.31}$$

### A.4.5 Extreme Learning Machines

ELMs are a fast training method for ANN that can be applied to feed-forward perceptron structures [Hua11]. These are characterized for setting the network weights of the first layer randomly, and then obtaining the pseudo-inverse of the hidden-layer output matrix. This pseudo-inverse is used to obtain the weights of the output layer that best fit the training data labels.

Considering a training set $\{(\mathbf{x}_i, y_i)\}_{i=1}^N$ where $\mathbf{x}_i \in \Re^N$ are the features and $y_i \in \mathcal{C} = \{C_j \mid 1 \leq j \leq J\}$, an activation function $g(x)$ and a given number of hidden nodes $\hat{N}$, which has to be set before the raining, ELM applies the following steps:

1. Random assignation of input weighs $\mathbf{w_i}$ and bias $b_i$, where $i = 1, \ldots, \hat{N}$, with a uniform probability distribution in $[-1, 1]$.

2. Calculation of the hidden-layer output matrix $\mathbf{H}$, which is defined as:

$$\mathbf{H} = \begin{bmatrix} g(\mathbf{w}_1\mathbf{x}_1 + b_1) & \cdots & g(\mathbf{w}_{\hat{N}}\mathbf{x}_1 + b_{\hat{N}}) \\ \vdots & \ddots & \vdots \\ g(\mathbf{w}_1\mathbf{x}_N + b_1) & \cdots & g(\mathbf{w}_{\hat{N}}\mathbf{x}_N + b_{\hat{N}}) \end{bmatrix} \tag{A.32}$$

3. Obtaining the output weight vector $\beta$ as:

$$\beta = \mathbf{BT}, \tag{A.33}$$

   where $\mathbf{B}$ is the Moore-Penrose pseudo-inverse of the matrix $\mathbf{H}$ and $\mathbf{T} = [y_1, \ldots, y_N]^\top$ is the training vector of labels.

This method present the great advantage of being extremely fast and their results are competitive versus other approaches, such as SVM or multi-layer perceptrons.

# Appendix B

# Ethics committees approvals

This chapter includes the approvals by two different Ethics Committees of the experiments carried out in order to develop this thesis. First, the report of the Ethics Committee for drug research of the Guadalajara health area, and second, the favorable report of the animal experimentation research Ethics Committee of the University of Alcalá. Both documents are written in Spanish because the evaluation committees are from Spanish entities.

Hospital Universitario de Guadalajara
C/ Donantes de Sangre S/N- 19002
Guadalajara-ESPAÑA
Teléfono 949 20 92 44 Fax 949 20 92 16
Mail: secretaria.ceim.gaigu@sescam.jccm.es

**DICTAMEN DEL COMITÉ DE ÉTICA DE LA INVESTIGACIÓN DEL MEDICAMENTO DEL ÁREA DE SALUD DE GUADALAJARA (CEIm)**

D. Gabriel de Arriba de la Fuente, Secretario Técnico del Comité de Ética de la Investigación del Área de Salud de Guadalajara, Sescam

**C E R T I F I C A:**

Que este Comité, en calidad de CEIm implicado, ha evaluado la documentación del estudio adicional consistente en la ***validación de una herramienta para la evaluación de ejercicios físicos pautados en adultos mayores***, perteneciente al estudio:

**Ref CEIm: *2018.22.PR FRAILCHECK.***
**TÍTULO: "Diseño y desarrollo de un sistema de detección y análisis de la actividad física y pautas de comportamiento para ayuda al diagnóstico de la fragilidad".**
**CÓDIGO DE PROTOCOLO: Referencia SBPLY/17/180501/000392.**
**PROMOTOR: Financiado por la Junta de Comunidades de Castilla La Mancha.**
**INVESTIGADOR PRINCIPAL: Dr. Juan Jesús García Domínguez, Catedrático. del Departamento de Electrónica de la Universidad de Alcalá.**

Los documentos presentados y evaluados son:

- ***Protocolo Versión protocolo V.1. Fecha 21/12/2020.***
- ***Hoja de Información al Paciente y Consentimiento Informado V.1: Fecha 21/12/2020.***

Universidad de Alcalá

Comité de Ética de la Investigación y de Experimentación Animal

(A rellenar por la Secretaría)
**Cód. CEI**: CEID/2021/5/125

## COMITÉ DE ÉTICA DE LA INVESTIGACIÓN Y DE EXPERIMENTACIÓN ANIMAL DE LA UNIVERSIDAD DE ALCALÁ

## INFORME



El Comité de Ética de la Investigación y de Experimentación Animal de la Universidad de Alcalá ha evaluado el proyecto de tesis doctoral titulado ***"Validación de una herramienta para el seguimiento de ejercicios físicos pautados en adultos mayores.",*** presentado por Dª Sara García de la Villa, adscrita al Departamento de Electrónica de esta Universidad.

Analizados los extremos acreditados en el expediente, el Comité considera que el proyecto de tesis doctoral y el procedimiento evaluado son correctos desde el punto de vista ético y metodológico, y por lo tanto da su informe FAVORABLE.

Y para que conste, se firma este informe en Alcalá de Henares, a 29 de septiembre de 2021.

F. Javier de la Mata de la Mata
Presidente del CEI y EA

# Bibliography


[Abb17] R. Abbasi-Kesbi, A. Nikfarjam, H. Memarzadeh-Tehran. 'A patient-centric sensory system for in-home rehabilitation'. *IEEE Sensors Journal*. 17 (2), pp. 524–533, 2017.
doi:10.1109/JSEN.2016.2631464

[Abb18] R. Abbasi-Kesbi, A. Nikfarjam. 'A Miniature Sensor System for Precise Hand Position Monitoring'. *IEEE Sensors Journal*. 18 (6), pp. 2577–2584, 2018.
doi:10.1109/JSEN.2018.2795751

[Acc18] K. Açıcı, Ç.B. Erdaş, T. Aşuroğlu, H. Oğul. 'HANDY: A benchmark dataset for context-awareness via wrist-worn motion sensors'. *Data*. 3 (3), pp. 1–11, 2018.
doi:10.3390/data3030024

[Alc17] J.C. Alcaraz, S. Moghaddamnia, J. Peissig. 'Mobile quantification and therapy course tracking for gait rehabilitation'. In *International Conference on Digital Signal Processing, DSP*, vol. 2017-Augus (2017) .
doi:10.1109/ICDSP.2017.8096106

[Ali17] A. Alizadegan, S. Behzadipour. 'Shoulder and elbow joint angle estimation for upper limb rehabilitation tasks using low-cost inertial and optical sensors'. *Journal of Mechanics in Medicine and Biology*. 17 (2), 2017.
doi:10.1142/S0219519417500312

[All17a] M. Allen, Q. Zhong, N. Kirsch, A. Dani, W.W. Clark, N. Sharma. 'A nonlinear dynamics-based estimator for functional electrical stimulation: Preliminary results from lower-leg extension experiments'. *IEEE Transactions on Neural Systems and Rehabilitation Engineering*. 25 (12), pp. 2365–2374, 2017.
doi:10.1109/TNSRE.2017.2748420

[All17b] E. Allseits, J. Lučarević, R. Gailey, V. Agrawal, I. Gaunaurd, C. Bennett. 'The development and concurrent validity of a real-time algorithm for temporal gait analysis using inertial measurement units'. *Journal of Biomechanics*. 55,

pp. 27–33, apr 2017.
doi:10.1016/j.jbiomech.2017.02.016

[All18] E. Allseits, K.J. Kim, C. Bennett, R. Gailey, I. Gaunaurd, V. Agrawal. 'A novel method for estimating knee angle using two leg-mounted gyroscopes for continuous monitoring with mobile health devices'. *Sensors (Switzerland)*. 18 (9), 2018.
doi:10.3390/s18092759

[Alv17] D. Alvarado, L. Corona, S. Muñoz, J. Aquino. 'Sensorial system for obtaining the angles of the human movement in the coronal and sagittal anatomical planes'. *Lecture Notes in Computer Science (including subseries Lecture Notes in Artificial Intelligence and Lecture Notes in Bioinformatics)*. 10061 LNAI, pp. 535–547, 2017.
doi:10.1007/978-3-319-62434-1_43

[Ar14] I. Ar, Y.S. Akgul. 'A computerized recognition system for the home-based physiotherapy exercises using an RGBD camera'. *IEEE Transactions on Neural Systems and Rehabilitation Engineering*. 22 (6), pp. 1160–1171, nov 2014.
doi:10.1109/TNSRE.2014.2326254

[Arl10] S. Arlot, A. Celisse. 'A survey of cross-validation procedures for model selection *'. *Statistics Surveys*. 4, pp. 40–79, 2010.
doi:10.1214/09-SS054

[Atr18] A. Atrsaei, H. Salarieh, A. Alasty, M. Abediny. 'Human Arm Motion Tracking by Inertial/Magnetic Sensors Using Unscented Kalman Filter and Relative Motion Constraint'. *Journal of Intelligent and Robotic Systems: Theory and Applications*. 90 (1-2), pp. 161–170, 2018.
doi:10.1007/s10846-017-0645-z

[Ban14a] S. Banerjee, A. Roy. *Linear algebra and matrix analysis for statistics*, vol. 181 (Crc Press Boca Raton, FL, USA:, 2014).

[Ban14b] O. Banos, J.M. Galvez, M. Damas, H. Pomares, I. Rojas. 'Window size impact in human activity recognition'. *Sensors*. 14 (4), pp. 6474–6499, 2014.

[Bav19] L. Bavan, K. Surmacz, D. Beard, S. Mellon, J. Rees. 'Adherence monitoring of rehabilitation exercise with inertial sensors: A clinical validation study'. *Gait & posture*. 70, pp. 211–217, 2019.

[Ben11] J.A. Bennett, K. Winters-Stone. 'Motivating older adults to exercise: what works?' *Age and Ageing*. 40 (2), pp. 148–149, mar 2011.
doi:10.1093/AGEING/AFQ182

[Bev18] A. Bevilacqua, B. Huang, R. Argent, B. Caulfield, T. Kechadi. 'Automatic classification of knee rehabilitation exercises using a single inertial sensor: A case study'. In *2018 IEEE 15th International conference on wearable and implantable Body Sensor Networks (BSN)* (2018) pp. 21–24.

[Bis95] C.M. Bishop, *et al. Neural networks for pattern recognition* (Oxford university press, 1995).

[Bis06] C.M. Bishop. *Pattern Recognition and Machine Learning* (Springer Cham, Switzerland, 2006).

[Bon15] V. Bonnet, V. Joukov, D. Kulić, P. Fraisse, N. Ramdani, G. Venture. 'Monitoring of hip and knee joint angles using a single inertial measurement unit during lower limb rehabilitation'. *IEEE Sensors journal*. 16 (6), pp. 1557–1564, 2015.

[Bre96] L. Breiman. 'Bagging predictors'. *Machine learning*. 24 (2), pp. 123–140, 1996.

[Bre01] L. Breiman. 'Random forests'. *Machine learning*. 45 (1), pp. 5–32, 2001.

[But19] H.T. Butt, M. Pancholi, M. Musahl, P. Murthy, M.A. Sanchez, D. Stricker. 'Inertial Motion Capture Using Adaptive Sensor Fusion and Joint Angle Drift Correction'. In *FUSION 2019 - 22nd International Conference on Information Fusion* (2019) .
https://www.scopus.com/inward/record.uri?eid=2-s2.0-85081786670&partnerID=40&md5=87eacff2db2c6f07efc23a4c71634453

[But21] H.T. Butt, B. Taetz, M. Musahl, M.A. Sanchez, P. Murthy, D. Stricker. 'Magnetometer robust deep human pose regression with uncertainty prediction using sparse body worn magnetic inertial measurement units'. *IEEE Access*. 9, pp. 36657–36673, 2021.
doi:10.1109/ACCESS.2021.3062545

[Cal16] D. Calin, D. Tarniţă, D. Popa, D. Calafeteanu, D. Tarnita. 'Virtual Model and Simulation of the Normal and Affected Human Hip Joint'. *Applied Mechanics and Materials*. 823 (January), pp. 167–172, 2016.
doi:10.4028/www.scientific.net/amm.823.167

[Cam13] V. Camomilla, A. Cereatti, L. Chèze, A. Cappozzo. 'A hip joint kinematics driven model for the generation of realistic thigh soft tissue artefacts'. *Journal of biomechanics*. 46 (3), pp. 625–630, 2013.

[Cam18] V. Camomilla, E. Bergamini, S. Fantozzi, G. Vannozzi. 'Trends supporting the in-field use of wearable inertial sensors for sport performance evaluation: A systematic review'. *Sensors*. 18 (3), p. 873, 2018.

[Cas19] A. Casas-Herrero, I. Anton-Rodrigo, F. Zambom-Ferraresi, M.L.S. de Asteasu, N. Martinez-Velilla, J. Elexpuru-Estomba, I. Marin-Epelde, F. Ramon-Espinoza, R. Petidier-Torregrosa, J.L. Sanchez-Sanchez, *et al.* 'Effect of a multicomponent exercise programme (VIVIFRAIL) on functional capacity in frail community elders with cognitive decline: study protocol for a randomized multicentre control trial'. *Trials*. 20 (1), p. 362, 2019.

[Cer03] P. Cerveri, A. Pedotti, G. Ferrigno. 'Robust recovery of human motion from video using Kalman filters and virtual humans'. *Human movement science*. 22 (3), pp. 377–404, 2003.

[Che14] L. Chèze. *Kinematic Analysis of Human Movement* (2014).

[Che20] Y. Chen, C. Fu, W.S.W. Leung, L. Shi. 'Drift-Free and Self-Aligned IMU-Based Human Gait Tracking System with Augmented Precision and Robustness'. *IEEE Robotics and Automation Letters*. 5 (3), pp. 4671–4678, 2020. doi:10.1109/LRA.2020.3002203

[Cho18] S. Choi, Y.B. Shin, S.Y. Kim, J. Kim. 'A novel sensor-based assessment of lower limb spasticity in children with cerebral palsy'. *Journal of NeuroEngineering and Rehabilitation*. 15 (1), 2018. doi:10.1186/s12984-018-0388-5

[Com15] P. Comfort, P.A. Jones, L.C. Smith, L. Herrington. 'Joint kinetics and kinematics during common lower limb rehabilitation exercises'. *Journal of Athletic Training*. 50 (10), pp. 1011–1018, 2015. doi:10.4085/1062-6050-50.9.05

[Con21] J. Conte Alcaraz, S. Moghaddamnia, J. Peissig. 'Efficiency of deep neural networks for joint angle modeling in digital gait assessment'. *Eurasip Journal on Advances in Signal Processing*. 2021 (1), 2021. doi:10.1186/s13634-020-00715-1

[Cra16] M. Crabolu, D. Pani, L. Raffo, A. Cereatti. 'Estimation of the center of rotation using wearable magneto-inertial sensors'. *Journal of Biomechanics*. 49 (16), pp. 3928–3933, 2016. doi:10.1016/j.jbiomech.2016.11.046

[Cra17] M. Crabolu, D. Pani, L. Raffo, M. Conti, P. Crivelli, A. Cereatti. 'In vivo estimation of the shoulder joint center of rotation using magneto-inertial sensors: MRI-based accuracy and repeatability assessment'. *BioMedical Engineering Online*. 16 (1), pp. 1–18, 2017. doi:10.1186/s12938-017-0324-0

[Cra18] M. Crabolu, D. Pani, L. Raffo, M. Conti, A. Cereatti. 'Functional estimation of bony segment lengths using magneto-inertial sensing: Application to the humerus'. *PLoS ONE*. 13 (9), pp. 1–11, 2018.
doi:10.1371/journal.pone.0203861

[Cus19] E.E. Cust, A.J. Sweeting, K. Ball, S. Robertson. 'Machine and deep learning for sport-specific movement recognition: a systematic review of model development and performance'. *Journal of sports sciences*. 37 (5), pp. 568–600, 2019.

[Cut08] A.G. Cutti, A. Giovanardi, L. Rocchi, A. Davalli, R. Sacchetti. 'Ambulatory measurement of shoulder and elbow kinematics through inertial and magnetic sensors'. *Medical & biological engineering & computing*. 46 (2), pp. 169–178, 2008.

[De 14] H. De Rosario, Á. Page, V. Mata. 'Point of optimal kinematic error: Improvement of the instantaneous helical pivot method for locating centers of rotation'. *Journal of Biomechanics*. 47 (7), pp. 1742–1747, 2014.
doi:10.1016/j.jbiomech.2014.02.003

[Dia19] E.M. Diaz, D.B. Ahmed, S. Kaiser. 'A Review of Indoor Localization Methods Based on Inertial Sensors'. In *Geographical and Fingerprinting Data to Create Systems for Indoor Positioning and Indoor/Outdoor Navigation*pp. 311–333 (Elsevier, 2019).

[Din20] Z. Ding, C. Yang, J. Ma, J.G. Wei, F. Jiang. 'The online estimation of the joint angle based on the gravity acceleration using the accelerometer and gyroscope in the wireless networks'. *Multimedia Tools and Applications*. 79 (23-24), pp. 16265–16279, 2020.
doi:10.1007/s11042-019-07911-8

[Dom19] M.F. Domingues, C. Tavares, V. Rosa, L. Pereira, N. Alberto, P. Andre, P. Antunes, A. Radwan. 'Wearable eHealth System for Physical Rehabilitation: Ankle Plantar-Dorsi-Flexion Monitoring'. In *2019 IEEE Global Communications Conference (GLOBECOM)* (IEEE, 2019) pp. 1–6.
doi:10.1109/GLOBECOM38437.2019.9014293

[Dor19] E. Dorschky, M. Nitschke, A.K. Seifer, A.J. van den Bogert, B.M. Eskofier. 'Estimation of gait kinematics and kinetics from inertial sensor data using optimal control of musculoskeletal models'. *Journal of Biomechanics*. 95, 2019.
doi:10.1016/j.jbiomech.2019.07.022

[Dor20] E. Dorschky, M. Nitschke, C.F. Martindale, A.J. van den Bogert, A.D. Koelewijn, B.M. Eskofier. 'CNN-Based Estimation of Sagittal Plane Walking and Running Biomechanics From Measured and Simulated Inertial Sensor Data'. *Frontiers in Bioengineering and Biotechnology*. 8, 2020.
doi:10.3389/fbioe.2020.00604

[Dua20] Y. Duan, X. Zhang, Z. Li. 'A new quaternion-based kalman filter for human body motion tracking using the second estimator of the optimal quaternion algorithm and the joint angle constraint method with inertial and magnetic sensors'. *Sensors (Switzerland)*. 20 (21), pp. 1–19, 2020.
doi:10.3390/s20216018

[Ehr06] R.M. Ehrig, W.R. Taylor, G.N. Duda, M.O. Heller. 'A survey of formal methods for determining the centre of rotation of ball joints'. *Journal of biomechanics*. 39 (15), pp. 2798–2809, 2006.

[El 15] M. El-Gohary, J. McNames. 'Human joint angle estimation with inertial sensors and validation with a robot arm'. *IEEE Transactions on Biomedical Engineering*. 62 (7), pp. 1759–1767, 2015.

[Fal20] M. Falbriard, F. Meyer, B. Mariani, G.P. Millet, K. Aminian. 'Drift-Free Foot Orientation Estimation in Running Using Wearable IMU'. *Frontiers in Bioengineering and Biotechnology*. 8, 2020.
doi:10.3389/fbioe.2020.00065

[Fas18] B. Fasel, J. Sporri, J. Chardonnens, J. Kroll, E. Muller, K. Aminian. 'Joint Inertial Sensor Orientation Drift Reduction for Highly Dynamic Movements'. *IEEE Journal of Biomedical and Health Informatics*. 22 (1), pp. 77–86, 2018.
doi:10.1109/JBHI.2017.2659758

[Fav09] J. Favre, R. Aissaoui, B.M. Jolles, J.A. de Guise, K. Aminian. 'Functional calibration procedure for 3D knee joint angle description using inertial sensors'. *Journal of biomechanics*. 42 (14), pp. 2330–2335, 2009.

[Fei21] F. Fei, S. Xian, X. Xie, C. Wu, D. Yang, K. Yin, G. Zhang. 'Development of a wearable glove system with multiple sensors for hand kinematics assessment'. *Micromachines*. 12 (4), 2021.
doi:10.3390/mi12040362

[Fig20] J. Figueiredo, S.P. Carvalho, J.P. Vilas-Boas, L.M. Gonçalves, J.C. Moreno, C.P. Santos. 'Wearable inertial sensor system towards daily human kinematic gait analysis: Benchmarking analysis to MVN BIOMECH'. *Sensors (Switzerland)*. 20 (8), 2020.
doi:10.3390/s20082185

[Fin19] S. Finocchietti, M. Gori, A. Souza Oliveira. 'Kinematic Profile of Visually Impaired Football Players During Specific Sports Actions'. *Scientific Reports*. 9 (1), pp. 1–8, dec 2019.
doi:10.1038/s41598-019-47162-z

[Fou17] H. Fourati, N. Manamanni, L. Afilal, Y. Handrich. *Rigid body motion capturing by means of a wearable inertial and magnetic MEMS sensor assembly-from reconstitution of the posture toward dead reckoning: An application in bio-logging* (2017).
doi:10.1201/b14970

[Fra19] M.S. Fragala, E.L. Cadore, S. Dorgo, M. Izquierdo, W.J. Kraemer, M.D. Peterson, E.D. Ryan. 'Resistance Training for Older Adults'. *Journal of Strength and Conditioning Research*. 33 (8), pp. 2019–2052, aug 2019.
doi:10.1519/JSC.0000000000003230

[Fri14] N. Friedman, J.B. Rowe, D.J. Reinkensmeyer, M. Bachman. 'The manumeter: A wearable device for monitoring daily use of the wrist and fingers'. *IEEE Journal of Biomedical and Health Informatics*. 18 (6), pp. 2168–2194, 2014.
doi:10.1109/JBHI.2014.2329841

[Fri18a] E. Frick, S. Rahmatalla. 'Joint center estimation using single-frame optimization: Part 1: Numerical simulation'. *Sensors (Switzerland)*. 18 (4), pp. 1–17, 2018.
doi:10.3390/s18041089

[Fri18b] E. Frick, S. Rahmatalla. 'Joint center estimation using single-frame optimization: Part 2: Experimentation'. *Sensors (Switzerland)*. 18 (8), pp. 1–22, 2018.
doi:10.3390/s18082563

[Gar18] S. García de Villa, J.J. García Domínguez, A. Jiménez Martín, A. Page del Pozo. 'Estimación de centros y ejes de rotación mediante sensores inerciales'. In *XXV Annual Seminar on Automation, Industrial Electronics and Instrumentation 2018 - Proceedings* (2018) pp. 379–398.

[Gar19] S. García de Villa, E. Munoz Diaz, D. Bousdar Ahmed, A. Jiménez Martín, J.J. García Domínguez. 'IMU-based Characterization of the Leg for the Implementation of Biomechanical Models'. In *International Conference on Indoor Positioning and Indoor Navigation - Proceedings* (2019) .

[Gar20a] S. García de Villa, A. Jiménez Martín, J.J. García Domínguez. 'Adaptive IMU-based Calibration of the Center ofJoints for Movement Analysis: One Case Study'. In *IEEE International Symposium on Medical Measurements and Applications* (2020) pp. 1–10.

[Gar20b] S. García de Villa, A. Jiménez Martín, J.J. García Domínguez. 'Calibración adaptativa de los centros articulares para el análisis de movimientos con IMUs'. In *27 Seminario Anual de Automática, Electrónica Industrial e Instrumentación - Libro de actas* (2020) .

[Gar21a] S. García-de-Villa, A. Jiménez-Martín, J.J. García-Domínguez. 'A database of physical therapy exercises with variability of execution collected by wearable sensors', 7 2021.
doi:10.5281/ZENODO.5052756

[Gar21b] S. García-de-Villa, A. Martínez Parra, A. Jiménez Martín, J.J. García Domínguez, D. Casillas-Perez. 'ML algorithms for the assessment of prescribed physical exercises'. In *2021 IEEE International Symposium on Medical Measurements and Applications (MeMeA)* (2021) pp. 1–6.
doi:10.1109/MeMeA52024.2021.9478725

[Gar21c] S. García-de-Villa, A. Jiménez-Martín, J.J. García-Domínguez. 'Novel IMU-based Adaptive Estimator of the Center of Rotation of Joints for Movement Analysis'. *IEEE Transactions on Instrumentation and Measurement*, 2021.

[Gar21d] S. García de Villa, A. Martínez Parra, A. Jiménez Martín, J.J. García Domínguez, D. Casillas-Pérez. 'Evaluación de ejercicios físicos pautados mediante algoritmos de Machine Learning'. In *28 Seminario Anual de Automática, Electrónica Industrial e Instrumentación - Libro de actas* (2021) .

[Gar22a] S. García-de-Villa, A. Jiménez-Martín, J.J. García-Domínguez. 'A database of physical therapy exercises with variability of execution collected by wearable sensors - Under review'. *Scientific Data*, 2022.

[Gar22b] S. García-de-Villa, A. Jiménez-Martín, J.J. García-Domínguez, D. Casillas-Pérez. 'Simultaneous Exercise Recognition and Evaluation in Prescribed Routines: Approach to Virtual Coaches - Under review'. *Expert Systems with Applications*, 2022.

[Gho20] M. Gholami, C. Napier, C. Menon. 'Estimating lower extremity running gait kinematics with a single accelerometer: A deep learning approach'. *Sensors (Switzerland)*. 20 (10), 2020.
doi:10.3390/s20102939

[Gig14] O.M. Giggins, K.T. Sweeney, B. Caulfield. 'Rehabilitation exercise assessment using inertial sensors: a cross-sectional analytical study'. *Journal of neuroengineering and rehabilitation*. 11 (1), p. 158, 2014.

[Hay98] S. Haykin. 'Neural Networks: A Comprehensive Foundation Subsequent Edition. Prentice Hall PTR, Upper Saddle River, NJ, United States', 1998.

[Her21] V. Hernandez, D. Dadkhah, V. Babakeshizadeh, D. Kulić. 'Lower body kinematics estimation from wearable sensors for walking and running: A deep learning approach'. *Gait & posture*. 83, pp. 185–193, jan 2021. doi:10.1016/j.gaitpost.2020.10.026

[Hua00] C. Huang. 'On definitions of pitches and the finite screw system for displacing a line'. In *Proceedings of a symposium commemorating the legacy, works and life of Sir Robert Stawell Ball upon the 100th anniversary of A Treatise on the Theory of Screws. Cambridge: University of Cambridge* (2000) .

[Hua06] G.B. Huang, Q.Y. Zhu, C.K. Siew. 'Extreme learning machine: theory and applications'. *Neurocomputing*. 70 (1-3), pp. 489–501, 2006.

[Hua11] G.B. Huang, H. Zhou, X. Ding, R. Zhang. 'Extreme learning machine for regression and multiclass classification'. *IEEE Transactions on Systems, Man, and Cybernetics, Part B (Cybernetics)*. 42 (2), pp. 513–529, 2011.

[Hua16a] B. Huang, O. Giggins, T. Kechadi, B. Caulfield. 'The limb movement analysis of rehabilitation exercises using wearable inertial sensors'. In *2016 38th Annual International Conference of the IEEE Engineering in Medicine and Biology Society (EMBC)* (2016) pp. 4686–4689.

[Hua16b] B. Huang, O. Giggins, T. Kechadi, B. Caulfield. 'The Limb Movement Analysis of Rehabilitation Exercises using Wearable Inertial Sensors'. pp. 4686–4689, 2016.

[Izq18] M. Izquierdo Redín. 'Exercise as therapeutic agent to improve intrinsic capacity in older adults'. pp. 17–23, 2018.

[Izq20] M. Izquierdo, J.E. Morley, A. Lucia. 'Exercise in people over 85', feb 2020. doi:10.1136/bmj.m402

[Izq21] M. Izquierdo, R.A. Merchant, J.E. Morley, S.D. Anker, I. Aprahamian, H. Arai, M. Aubertin-Leheudre, R. Bernabei, E.L. Cadore, M. Cesari, L.K. Chen, P. de Souto Barreto, G. Duque, L. Ferrucci, R.A. Fielding, A. García-Hermoso, L.M. Gutiérrez-Robledo, S.D.R. Harridge, B. Kirk, S. Kritchevsky, F. Landi, N. Lazarus, F.C. Martin, E. Marzetti, M. Pahor, R. Ramírez-Vélez, L. Rodriguez-Mañas, Y. Rolland, J.G. Ruiz, O. Theou, D.T. Villareal, D.L. Waters, C.W. Won, J. Woo, B. Vellas, M.F. Singh. 'International Exercise Recommendations in Older Adults (ICFSR): Expert Consensus Guidelines'. *The journal of nutrition, health & aging 2021*. 25 (7), pp. 824–853, 2021.

[Jar19] N.J. Jarque-Bou, M. Vergara, J.L. Sancho-Bru, V. Gracia-Ibáñez, A. Roda-Sales. 'A calibrated database of kinematics and EMG of the forearm and

hand during activities of daily living'. *Scientific Data*. 6 (1), pp. 1–11, dec 2019.
doi:10.1038/s41597-019-0285-1

[Jou18] V. Joukov, V. Bonnet, M. Karg, G. Venture, D. Kulić. 'Rhythmic Extended Kalman Filter for Gait Rehabilitation Motion Estimation and Segmentation'. *IEEE Transactions on Neural Systems and Rehabilitation Engineering*. 26 (2), pp. 407–418, feb 2018.
doi:10.1109/TNSRE.2017.2659730

[Jou19] V. Joukov, J.S. Lin, D. Kulic. 'Closed-chain pose estimation from wearable sensors'. In *IEEE-RAS International Conference on Humanoid Robots*, vol. 2019-Octob (2019) pp. 594–600.
doi:10.1109/Humanoids43949.2019.9035015

[Jou20] V. Joukov, J. Cesic, K. Westermann, I. Markovic, I. Petrovic, D. Kulic. 'Estimation and Observability Analysis of Human Motion on Lie Groups'. *IEEE Transactions on Cybernetics*. 50 (3), pp. 1321–1332, 2020.
doi:10.1109/TCYB.2019.2933390

[Kam18] B. Kamiński, M. Jakubczyk, P. Szufel. 'A framework for sensitivity analysis of decision trees'. *Central European journal of operations research*. 26 (1), pp. 135–159, 2018.

[Kay17] J. Kaye. 'Making Pervasive Computing Technology Pervasive for Health & Wellness in Aging'. *Public Policy & Aging Report*. 27 (2), pp. 53–61, may 2017.
doi:10.1093/ppar/prx005

[Kia16] R. Kianifar, A. Lee, S. Raina, D. Kulic. 'Classification of squat quality with inertial measurement units in the single leg squat mobility test'. *Proceedings of the Annual International Conference of the IEEE Engineering in Medicine and Biology Society, EMBS*. 2016-Octob, pp. 6273–6276, 2016.
doi:10.1109/EMBC.2016.7592162

[Kia17] R. Kianifar, A. Lee, S. Raina, D. Kulic. 'Automated Assessment of Dynamic Knee Valgus and Risk of Knee Injury during the Single Leg Squat'. *IEEE Journal of Translational Engineering in Health and Medicine*. 5 (June), 2017.
doi:10.1109/JTEHM.2017.2736559

[Kit19] K. Kitano, A. Ito, N. Tsujiuchi. 'Hand Motion Measurement using Inertial Sensor System and Accurate Improvement by Extended Kalman Filter'. In *Proceedings of the Annual International Conference of the IEEE Engineering in*

*Medicine and Biology Society, EMBS* (2019) pp. 6405–6408.
doi:10.1109/EMBC.2019.8856462

[Kom19a] K. Komukai, R. Ohmura. 'Optimizing of the Number and Placements of Wearable IMUs for Automatic Rehabilitation Recording'. pp. 3–15 (2019).
doi:10.1007/978-3-030-13001-5_1

[Kom19b] K. Komukai, R. Ohmura. 'Optimizing of the Number and Placements of Wearable IMUs for Automatic Rehabilitation Recording'. In *Human Activity Sensing*pp. 3–15 (Springer, 2019).

[Kub99] M. Kubat. 'Neural networks: a comprehensive foundation by Simon Haykin, Macmillan, 1994, ISBN 0-02-352781-7.' *The Knowledge Engineering Review*. 13 (4), pp. 409–412, 1999.

[Kum18] S. Kumar, K. Gopinath, L. Rocchi, P.T. Sukumar, S. Kulkarni, J. Sampath. 'Towards a portable human gait analysis & monitoring system'. In *2018 International Conference on Signals and Systems, ICSigSys 2018 - Proceedings* (2018) pp. 174–180.
doi:10.1109/ICSIGSYS.2018.8372660

[Kwo19] B. Kwolek, A. Michalczuk, T. Krzeszowski, A. Switonski, H. Josinski, K. Wojciechowski. 'Calibrated and synchronized multi-view video and motion capture dataset for evaluation of gait recognition'. *Multimedia Tools and Applications*. 78 (22), pp. 32437–32465, nov 2019.
doi:10.1007/s11042-019-07945-y

[Kyr20a] S. Kyriazakos, H. Schlieter, K. Gand, M. Caprino, M. Corbo, P. Tropea, E. Judica, I. Sterpi, S. Busnatu, P. Philipp, J. Rovira, A. Martínez, M. Lange, I. Gabilondo, R. Del Pino, J. Carlos Gomez-Esteban, L. Pannese, M. Bøttcher, V. Lynggaard. 'A Novel Virtual Coaching System Based on Personalized Clinical Pathways for Rehabilitation of Older Adults-Requirements and Implementation Plan of the vCare Project'. *Frontiers in Digital Health | www.frontiersin.org*. 2, p. 546562, 2020.
doi:10.3389/fdgth.2020.546562

[Kyr20b] S. Kyriazakos, H. Schlieter, K. Gand, M. Caprino, M. Corbo, P. Tropea, E. Judica, I. Sterpi, S. Busnatu, P. Philipp, J. Rovira, A. Martínez, M. Lange, I. Gabilondo, R.D. Pino, J.C. Gomez-Esteban, L. Pannese, M. Bøttcher, V. Lynggaard. 'A Novel Virtual Coaching System Based on Personalized Clinical Pathways for Rehabilitation of Older Adults-Requirements and Implementation Plan of the vCare Project'. *Frontiers in Digital Health | www.frontiersin.org*. 2, p. 546562, 2020.
doi:10.3389/fdgth.2020.546562

[Lai17] D. Laidig, T. Seel. 'Deriving kinematic quantities from accelerometer readings for assessment of functional upper limb motions'. *Current Directions in Biomedical Engineering*. 3 (2), pp. 573–576, 2017.
doi:10.1515/cdbme-2017-0119

[Lea07] A. Leardini, Z. Sawacha, G. Paolini, S. Ingrosso, R. Nativo, M.G. Benedetti. 'A new anatomically based protocol for gait analysis in children'. *Gait and Posture*. 26, pp. 560–571, 10 2007.
doi:10.1016/j.gaitpost.2006.12.018

[Lee21] T. Lee, I. Kim, S.H. Lee. 'Estimation of the continuous walking angle of knee and ankle (Talocrural joint, subtalar joint) of a lower-limb exoskeleton robot using a neural network'. *Sensors*. 21 (8), 2021.
doi:10.3390/s21082807

[Len19] T. Lencioni, I. Carpinella, M. Rabuffetti, A. Marzegan, M. Ferrarin. 'Human kinematic, kinetic and EMG data during different walking and stair ascending and descending tasks'. *Scientific Data*. 6 (1), 2019.
doi:10.1038/s41597-019-0323-z

[Lev44] K. Levenberg. 'A method for the solution of certain non-linear problems in least squares'. *Quarterly of applied mathematics*. 2 (2), pp. 164–168, 1944.

[Lia21] F.Y. Liang, F. Gao, W.H. Liao. 'Synergy-based knee angle estimation using kinematics of thigh'. *Gait and Posture*. 89, pp. 25–30, 2021.
doi:10.1016/j.gaitpost.2021.06.015

[Lig20] G. Ligorio, E. Bergamini, L. Truppa, M. Guaitolini, M. Raggi, A. Mannini, A.M. Sabatini, G. Vannozzi, P. Garofalo. 'A Wearable Magnetometer-Free Motion Capture System: Innovative Solutions for Real-World Applications'. *IEEE Sensors Journal*. 20 (15), pp. 8844–8857, 2020.
doi:10.1109/JSEN.2020.2983695

[Lim20] H. Lim, B. Kim, S. Park. 'Prediction of lower limb kinetics and kinematics during walking by a single IMU on the lower back using machine learning'. *Sensors (Switzerland)*. 20 (1), 2020.
doi:10.3390/s20010130

[Lin12] J.F. Lin, D. Kulić. 'Human pose recovery using wireless inertial measurement units'. *Physiological Measurement*. 33 (12), pp. 2099–2115, 2012.
doi:10.1088/0967-3334/33/12/2099

[Lin13] J.S. Lin, D. Kulic. 'Human pose recovery for rehabilitation using ambulatory sensors'. In *Proceedings of the Annual International Conference of the IEEE*

*Engineering in Medicine and Biology Society, EMBS* (2013) pp. 4799–4802.
doi:10.1109/EMBC.2013.6610621

[Liu10] K. Liu, Y. Inoue, K. Shibata. 'Visual and quantitative analysis of lower limb 3D gait posture using accelerometers and magnetometers'. In *2010 IEEE International Conference on Mechatronics and Automation, ICMA 2010* (2010) pp. 1420–1425.
doi:10.1109/ICMA.2010.5589037

[Liu20] S.Q. Liu, J.C. Zhang, R. Zhu. 'A Wearable Human Motion Tracking Device Using Micro Flow Sensor Incorporating a Micro Accelerometer'. *IEEE Transactions on Biomedical Engineering*. 67 (4), pp. 940–948, 2020.
doi:10.1109/TBME.2019.2924689

[Llo15] R. Lloréns, E. Noé, C. Colomer, M. Alcañiz. 'Effectiveness, usability, and cost-benefit of a virtual reality-based telerehabilitation program for balance recovery after stroke: A randomized controlled trial'. *Archives of Physical Medicine and Rehabilitation*. 96 (3), pp. 418–425.e2, 2015.
doi:10.1016/j.apmr.2014.10.019

[Lop16] I.H. Lopez-Nava, M.M. Angelica. 'Wearable Inertial Sensors for Human Motion Analysis: A review'. *IEEE Sensors Journal*. PP (99), 2016.
doi:10.1109/JSEN.2016.2609392

[Luo20] Y. Luo, S.M. Coppola, P.C. Dixon, S. Li, J.T. Dennerlein, B. Hu. 'A database of human gait performance on irregular and uneven surfaces collected by wearable sensors'. *Scientific data*. 7 (1), pp. 1–9, 2020.

[M B16] M. M. B. Morrow, B. Lowndes, E. Fortune, K.R. Kaufman, S. Hallbeck, D. Robert, E. Patricia. 'Validation of inertial measurement units for upper body kinematics'. *Journal of Applied Biomechanics*, 2016.
http://dx.doi.org/10.1123/jab.2016-0120

[Man17] M. Mancini, M. El-Gohary, S. Pearson, J. McNames, H. Schlueter, J.G. Nutt, L.A. King, F. B Horak. 'Continuous Monitoring of Turning in Parkinson's disease: Rehabiliation Potential'. *NeuroRehabilitation*. 37 (1), pp. 783–790, 2017.
doi:10.3233/NRE-151236.Continuous

[Mar63] D.W. Marquardt. 'An algorithm for least-squares estimation of nonlinear parameters'. *Journal of the society for Industrial and Applied Mathematics*. 11 (2), pp. 431–441, 1963.

[Mat20] MathWorks. 'MathWorks - Makers of MATLAB and Simulink - MATLAB & Simulink'. "*https://in.mathworks.com/* Last visit: 2020-06-12", 2020. https://in.mathworks.com/

[May20] D. Mayorca-Torres, J.C. Caicedo-Eraso, D.H. Peluffo-Ordóñez. 'Knee joint angle measuring portable embedded system based on inertial measurement units for gait analysis'. *International Journal on Advanced Science, Engineering and Information Technology*. 10 (2), pp. 430–437, 2020. doi:10.18517/ijaseit.10.2.10814

[McG13] R.S. McGinnis, N.C. Perkins. 'Inertial sensor based method for identifying spherical joint center of rotation'. *Journal of Biomechanics*. 46 (14), pp. 2546–2549, 2013.

[McG18] T. McGrath, R. Fineman, L. Stirling. 'An auto-calibrating knee flexion-extension axis estimator using principal component analysis with inertial sensors'. *Sensors (Switzerland)*. 18 (6), 2018. doi:10.3390/s18061882

[Men19] L. Meng, B. Li, C. Childs, A. Buis, F. He, D. Ming. 'Effect of walking variations on complementary filter based inertial data fusion for ankle angle measurement'. In *2019 IEEE International Conference on Computational Intelligence and Virtual Environments for Measurement Systems and Applications, CIVEMSA 2019 - Proceedings* (2019) . doi:10.1109/CIVEMSA45640.2019.9071595

[Mol18] M. Molnar, M. Kok, T. Engel, H. Kaplick, F. Mayer, T. Seel. 'A Method for Lower Back Motion Assessment Using Wearable 6D Inertial Sensors'. In *2018 21st International Conference on Information Fusion, FUSION 2018* (2018) pp. 799–806. doi:10.23919/ICIF.2018.8455828

[Muk18] S. Mukhopadhyay. *Deep Learning and Neural Networks* (Apress, 2018). doi:10.1007/978-1-4842-3450-1_5

[Mul17a] P. Müller, M.A. Bégin, T. Schauer, T. Seel. 'Alignment-Free , Self-Calibrating Elbow Angles Measurement Using Inertial Sensors'. *IEEE Journal of Biomedical and Health Informatics*. 21 (2), pp. 312–319, 2017.

[Mul17b] P. Muller, M.A. Begin, T. Schauer, T. Seel. 'Alignment-Free, Self-Calibrating Elbow Angles Measurement Using Inertial Sensors'. *IEEE Journal of Biomedical and Health Informatics*. 21 (2), pp. 312–319, 2017. doi:10.1109/JBHI.2016.2639537

[Mul17c] P. Müller, M.A.S.T. Bégin, T. Seel. 'Alignment-Free , Self-Calibrating Elbow Angles Measurement Using Inertial Sensors'. *IEEE Journal of Biomedical and Health Informatics*. 21 (2), pp. 312–319, 2017.
doi:10.1109/JBHI.2016.2639537

[Mun20a] M. Mundt, A. Koeppe, F. Bamer, S. David, B. Markert. 'Artificial neural networks in motion analysis—applications of unsupervised and heuristic feature selection techniques'. *Sensors (Switzerland)*. 20 (16), pp. 1–15, 2020.
doi:10.3390/s20164581

[Mun20b] M. Mundt, A. Koeppe, S. David, T. Witter, F. Bamer, W. Potthast, B. Markert. 'Estimation of Gait Mechanics Based on Simulated and Measured IMU Data Using an Artificial Neural Network'. *Frontiers in Bioengineering and Biotechnology*. 8, 2020.
doi:10.3389/fbioe.2020.00041

[Mun20c] M. Mundt, W. Thomsen, T. Witter, A. Koeppe, S. David, F. Bamer, W. Potthast, B. Markert. 'Prediction of lower limb joint angles and moments during gait using artificial neural networks'. *Medical and Biological Engineering and Computing*. 58 (1), pp. 211–225, 2020.
doi:10.1007/s11517-019-02061-3

[Mun21] M. Mundt, W.R. Johnson, W. Potthast, B. Markert, A. Mian, J. Alderson. 'A Comparison of Three Neural Network Approaches for Estimating Joint Angles and Moments from Inertial Measurement Units'. *Sensors (Basel, Switzerland)*. 21 (13), 2021.
doi:10.3390/s21134535

[Nag21] D. Nagaraj, R. Dobinson, D. Werth. 'Towards kinematically constrained real time human pose estimation using sparse IMUs'. In *CEUR Workshop Proceedings*, vol. 2846 (2021) .
https://www.scopus.com/inward/record.uri?eid=2-s2.0-85104619159&partnerID=40&md5=4b999a00afd4661c76d11667c385fa81

[Nat20] NaturalPoint. 'Data Editing - NaturalPoint Product Documentation, see 2.2'. "*https://v22.wiki.optitrack.com/* Last visit: 2020-06-12", 2020.
https://v22.wiki.optitrack.com/index.php?title=Data_Editing#Fill_Gaps

[Naz21a] M. Nazarahari, H. Rouhani. 'A Full-State Robust Extended Kalman Filter for Orientation Tracking during Long-Duration Dynamic Tasks Using Magnetic and Inertial Measurement Units'. *IEEE Transactions on Neural Systems*

*and Rehabilitation Engineering*. 29, pp. 1280–1289, 2021.
doi:10.1109/TNSRE.2021.3093006

[Naz21b] M. Nazarahari, H. Rouhani. 'Adaptive Gain Regulation of Sensor Fusion Algorithms for Orientation Estimation with Magnetic and Inertial Measurement Units'. *IEEE Transactions on Instrumentation and Measurement*. 70, 2021.
doi:10.1109/TIM.2020.3033077

[Ols17] F. Olsson, K. Halvorsen. 'Experimental evaluation of joint position estimation using inertial sensors'. *20th International Conference on Information Fusion, Fusion 2017 - Proceedings*, 2017.
doi:10.23919/ICIF.2017.8009669

[Ope20] OpenSim. 'OpenSim'. *https://opensim.stanford.edu/* Last visit: 2020-05-23, 2020.
https://opensim.stanford.edu/

[Opt20] OptiTrack. 'OptiTrack - Motive - Optical motion capture software'. *https://optitrack.com/software/motive/* Last visit: 2020-06-05, 2020.
https://optitrack.com/software/motive/

[Pal16] C. Palazzo, E. Klinger, V. Dorner, A. Kadri, O. Thierry, Y. Boumenir, W. Martin, S. Poiraudeau, I. Ville. 'Barriers to home-based exercise program adherence with chronic low back pain: Patient expectations regarding new technologies'. *Annals of physical and rehabilitation medicine*. 59 (2), pp. 107–113, 2016.

[Pat18] P.N. Pathirana, M.S. Karunarathne, G.L. Williams, P.T. Nam, H. Durrant-Whyte. 'Robust and Accurate Capture of Human Joint Pose Using an Inertial Sensor'. *IEEE Journal of Translational Engineering in Health and Medicine*. 6, 2018.
doi:10.1109/JTEHM.2018.2877980

[Pen55] R. Penrose. 'A generalized inverse for matrices'. *Mathematical Proceedings of the Cambridge Philosophical Society*. 51 (3), p. 406–413, 1955.
doi:10.1017/S0305004100030401

[Per19] A. Pereira, D. Folgado, R. Cotrim, I. Sousa. 'Physiotherapy Exercises Evaluation using a Combined Approach based on sEMG and Wearable Inertial Sensors.' In *BIOSIGNALS* (2019) pp. 73–82.

[Pre20] E. Preatoni, S. Nodari, N.F. Lopomo. 'Supervised Machine Learning Applied to Wearable Sensor Data Can Accurately Classify Functional Fitness

Exercises Within a Continuous Workout'. *Frontiers in Bioengineering and Biotechnology*. 8, 2020.
doi:10.3389/fbioe.2020.00664

[Rap21] E. Rapp, S. Shin, W. Thomsen, R. Ferber, E. Halilaj. 'Estimation of kinematics from inertial measurement units using a combined deep learning and optimization framework'. *Journal of Biomechanics*. 116, 2021.
doi:10.1016/j.jbiomech.2021.110229

[Rei12] A. Reiss, D. Stricker. 'Creating and benchmarking a new dataset for physical activity monitoring'. *ACM International Conference Proceeding Series*. (February), 2012.
doi:10.1145/2413097.2413148

[Rod19] A. Roda-Sales, M. Vergara, J.L. Sancho-Bru, V. Gracia-Ibáñez, N.J. Jarque-Bou. 'Human hand kinematic data during feeding and cooking tasks'. *Scientific Data*. 6 (1), pp. 1–10, sep 2019.
doi:10.1038/s41597-019-0175-6

[Sah19] S. Sahinovic, A. Dzebo, B.C. Ustundag, E. Golubovic, T. Uzunovic. 'An Open and Extensible Data Acquisition and Processing Platform for Rehabilitation Applications'. In *Lecture Notes in Networks and Systems*, vol. 59pp. 394–406 (Springer, 2019).
doi:10.1007/978-3-030-02574-8_32

[Sai20] A. Saito, S. Kizawa, Y. Kobayashi, K. Miyawaki. 'Pose estimation by extended Kalman filter using noise covariance matrices based on sensor output'. *ROBOMECH Journal*. 7 (1), 2020.
doi:10.1186/s40648-020-00185-y

[Sal20] S. Salehi, D. Stricker. 'Validation of a low-cost inertial exercise tracker'. In *SENSORNETS 2020 - Proceedings of the 9th International Conference on Sensor Networks* (2020) pp. 97–104.
https://www.scopus.com/inward/record.uri?eid=2-s2.0-85082994867&partnerID=40&md5=3ae65ab6d7a95250747e78c8a65240d1

[Sau18] A. Saudabayev, Z. Rysbek, R. Khassenova, H.A. Varol. 'Human grasping database for activities of daily living with depth, color and kinematic data streams'. *Scientific data*. 5 (1), pp. 1–13, 2018.

[Sch18] B. Scholkopf, A.J. Smola. *Learning with kernels: support vector machines, regularization, optimization, and beyond* (Adaptive Computation and Machine Learning series, 2018).

[See12] T. Seel, T. Schauer. 'Joint Axis and Position Estimation from Inertial Measurement Data by Exploiting Kinematic Constraints'. *2012 IEEE International Conference on Control Applications (CCA)*. pp. 0–4, 2012.

[See14] T. Seel, J. Raisch, T. Schauer. 'IMU-Based joint angle measurement for gait analysis'. *Sensors*. pp. 6891–6909, 2014.
doi:10.3390/s140406891

[Sha08] G. Shakhnarovich, T. Darrell, P. Indyk. 'Nearest-neighbor methods in learning and vision'. *IEEE Trans. Neural Networks*. 19 (2), p. 377, 2008.

[Sha17] B.S.M. Sharma, S. Vidhya, N. Kumar. 'System for measurement of joint range of motion using inertial sensors'. *Biomedical Research (India)*. 28 (8), pp. 3699–3704, 2017.
https://www.scopus.com/inward/record.uri?eid=2-s2.0-85019569908&partnerID=40&md5=e7a2eefbcff26188bf8dd2b6550d867c

[Sha21] M. Sharifi Renani, A.M. Eustace, C.A. Myers, C.W. Clary. 'The use of synthetic IMU signals in the training of deep learning models significantly improves the accuracy of joint kinematic predictions'. *Sensors*. 21 (17), 2021.
doi:10.3390/s21175876

[Sim06] D. Simon. *Optimal state estimation: Kalman, H infinity, and nonlinear approaches* (John Wiley & Sons, 2006).

[Sou19] P. de Souto Barreto, Y. Rolland, B. Vellas, M. Maltais. 'Association of long-term exercise training with risk of falls, fractures, hospitalizations, and mortality in older adults: a systematic review and meta-analysis'. *JAMA internal medicine*. 179 (3), pp. 394–405, 2019.

[Suc57] E.A. Suchman, B.S. Phillips, G.F. Streib. 'An Analysis of the Validity of Health Questionnaires'. *Social Forces*. 36, 1957.
https://heinonline.org/HOL/Page?handle=hein.journals/josf36{&}id=239{&}div={&}collection=

[Sy21a] L. Sy, M. Raitor, M.D. Rosario, H. Khamis, L. Kark, N.H. Lovell, S.J. Redmond. 'Estimating Lower Limb Kinematics Using a Reduced Wearable Sensor Count'. *IEEE Transactions on Biomedical Engineering*. 68 (4), pp. 1293–1304, 2021.
doi:10.1109/TBME.2020.3026464

[Sy21b] L.W. Sy, N.H. Lovell, S.J. Redmond. 'Estimating Lower Body Kinematics Using a Lie Group Constrained Extended Kalman Filter and Reduced IMU Count'. *IEEE Sensors Journal*. 21 (18), pp. 20969–20979, 2021.
doi:10.1109/JSEN.2021.3096078

[Szc21] A. Szczęsna, M. Błaszczyszyn, M. Pawlyta. 'Optical motion capture dataset of selected techniques in beginner and advanced Kyokushin karate athletes'. *Scientific Data*. 8 (1), pp. 2–8, 2021.
doi:10.1038/s41597-021-00801-5

[Tha21] L.K. Tham, N.A.A. Osman, M.A. Kouzbary, K. Aminian. 'Biomechanical Ambulatory Assessment of 3D Knee Angle Using Novel Inertial Sensor-Based Technique'. *IEEE Access*. 9, pp. 36559–36570, 2021.
doi:10.1109/ACCESS.2021.3062978

[Tit04] D. Titterton, , J. Weston. *Strapdown inertial navigation technology*, vol. 17 (IET, 2004).

[Vak18] A. Vakanski, H.P. Jun, D. Paul, R. Baker. 'A data set of human body movements for physical rehabilitation exercises'. *Data*. 3 (1), 2018.
doi:10.3390/data3010002

[Vec22] Vecteezy. 'Free Vector Art'. *https://www.vecteezy.com/* Last visit: 2022-01-15, 2022.
https://www.vecteezy.com/

[Vic20] Vicon. 'Vicon Motion Capture'. *https://www.vicon.com/* Last visit: 2020-01-28, 2020.
https://www.vicon.com/

[Vie17] A. Vienne, R.P. Barrois, S. Buffat, D. Ricard, P.P. Vidal. 'Inertial sensors to assess gait quality in patients with neurological disorders: A systematic review of technical and analytical challenges'. *Frontiers in Psychology*. 8 (MAY), pp. 1–12, 2017.
doi:10.3389/fpsyg.2017.00817

[Vig19] R.M. Viglialoro, S. Condino, G. Turini, M. Carbone, V. Ferrari, M. Gesi. 'Review of the augmented reality systems for shoulder rehabilitation'. *Information (Switzerland)*. 10 (5), pp. 1–14, 2019.
doi:10.3390/info10050154

[Vil17] E. Villeneuve, W. Harwin, W. Holderbaum, B. Janko, R.S. Sherratt. 'Reconstruction of angular kinematics from wrist-worn inertial sensor data for smart home healthcare'. *IEEE Access*. 5, pp. 2351–2363, 2017.
doi:10.1109/ACCESS.2016.2640559

[W B13] T. W. Buford, M. D. Roberts, T. S. Church. 'Towards Exercise as Personzalized Medicine'. *Sports Med.* 34 (3), pp. 157–165, 2013.
doi:10.1007/s40279-013-0018-0.

[Wan17] Q. Wang, P. Markopoulos, B. Yu, W. Chen. 'Interactive wearable systems for upper body rehabilitation : a systematic review'. pp. 1–21, 2017.
doi:10.1186/s12984-017-0229-y

[Wat21] A. Watson, A. Lyubovsky, K. Koltermann, G. Zhou. 'Magneto: Joint angle analysis using an electromagnet-based sensing method'. In *Proceedings of the 20th International Conference on Information Processing in Sensor Networks, IPSN 2021 (co-located with CPS-IoT Week 2021)* (2021) pp. 1–14.
doi:10.1145/3412382.3458253

[Wey20] I. Weygers, M. Kok, H. De Vroey, T. Verbeerst, M. Versteyhe, H. Hallez, K. Claeys. 'Drift-Free Inertial Sensor-Based Joint Kinematics for Long-Term Arbitrary Movements'. *IEEE Sensors Journal*. 20 (14), pp. 7969–7979, 2020.
doi:10.1109/jsen.2020.2982459

[Whe16] D. Whelan, M. O'Reilly, T. Ward, E. Delahunt, B. Caulfield. 'Evaluating performance of the lunge exercise with multiple and individual inertial measurement units'. In *Pervasive Health 2016: 10th EAI International Conference on Pervasive Computing Technologies for Healthcare, Cancun, Mexico, 16-19 May 2016* (2016) .

[Wou19] F.J. Wouda, M. Giuberti, N. Rudigkeit, B.J. van Beijnum, M. Poel, P.H. Veltink. 'Time coherent full-body poses estimated using only five inertial sensors: Deep versus shallow learning'. *Sensors (Switzerland)*. 19 (17), 2019.
doi:10.3390/s19173716

[Wu09] X. Wu, V. Kumar. *The top ten algorithms in data mining* (CRC press, 2009).

[xio21] xio. 'NGIMU – x-io Technologies'. *https://x-io.co.uk/ngimu/* Last visit: 2021-05-13, 2021.
https://x-io.co.uk/ngimu/

[Xse20] Xsens. 'Xsens Motion Tracking'. *https://www.xsens.com/* Last visit: 2020-01-15, 2020.
https://www.xsens.com/

[Xu17] B. Xu, L. Xu, H. Cai, L. Jiang, Y. Luo, Y. Gu. 'The design of an m-Health monitoring system based on a cloud computing platform'. *Enterprise Information Systems*. 11 (1), pp. 17–36, jan 2017.
doi:10.1080/17517575.2015.1053416

[Xu18] C. Xu, J. He, X. Zhang, C. Yao, P.H. Tseng. 'Geometrical kinematic modeling on human motion using method of multi-sensor fusion'. *Information Fusion*. 41, pp. 243–254, 2018.
doi:10.1016/j.inffus.2017.09.014

[Yan21] H. Yang, S. Liu, T. Luo, H. Liang, J. Zou, L. Zhao. 'Research on Human Motion Monitoring Method Based on Multi-Joint Constraint Filter Model'. *IEEE Sensors Journal*. 21 (9), pp. 10989–10999, 2021.
doi:10.1109/JSEN.2021.3062464

[Yin21] W. Yin, C. Reddy, Y. Zhou, X. Zhang. 'A Novel Application of Flexible Inertial Sensors for Ambulatory Measurement of Gait Kinematics'. *IEEE Transactions on Human-Machine Systems*. 51 (4), pp. 346–354, 2021.
doi:10.1109/THMS.2021.3086017

[Zab15] M. Zabat, N. Ouadahi, A. Youyou, A. Ababou, N. Ababou. 'Digital inclinometer for joint angles measurements with a real-time 3D-animation'. In *12th International Multi-Conference on Systems, Signals and Devices, SSD 2015* (2015) .
doi:10.1109/SSD.2015.7348258

[Zeh21] J.D. Zehr, L.M. Tennant, J.M. Buchman-Pearle, J.P. Callaghan. 'Reconstructing an accelerometer-based pelvis segment for three-dimensional kinematic analyses during laboratory simulated tasks with obstructed line-of-sight'. *Journal of Biomechanics*. 123, 2021.
doi:10.1016/j.jbiomech.2021.110512

[Zen20] Zenodo. 'Zenodo - Research. Shared.' *https://zenodo.org/* Last visit: 2020-06-15, 2020.
https://zenodo.org/

[Zha16] W. Zhang, M. Tomizuka, N. Byl. 'A Wireless Human Motion Monitoring System for Smart Rehabilitation', 2016.
doi:10.1115/1.4033949

[Zha20a] J. Zhao, G. Li. 'Study on real-time wearable sport health device based on body sensor networks'. *Computer Communications*. 154, pp. 40–47, mar 2020.
doi:10.1016/j.comcom.2020.02.045

[Zha20b] L. Zhao, W. Chen. 'Detection and recognition of human body posture in motion based on sensor technology'. *IEEJ Transactions on Electrical and Electronic Engineering*. 15 (5), pp. 766–770, 2020.

[Zhe21] Z. Zheng, H. Ma, W. Yan, H. Liu, Z. Yang. 'Training Data Selection and Optimal Sensor Placement for Deep-Learning-Based Sparse Inertial Sensor Human Posture Reconstruction'. *Entropy (Basel, Switzerland)*. 23 (5), may 2021.
doi:10.3390/e23050588

[Zih16] S. Zihajehzadeh, S. Member, E.J. Park, S. Member. 'A novel biomechanical model-aided IMU / UWB fusion for magnetometer-free lower body motion capture'. *IEEE Transactions on systems, man and cybernetics: systems*. pp. 1–12, 2016.